Competition of solvation and ionic aggregation in ionic-molecular systems of different nature : influence on transport properties

Dmytro Dudariev

Université Lille

Faculté des sciences et des technologies

Ecole Doctorale 104 – Sciences de la Matiére, du Rayonnement, et de l'Environment

Thèse de Doctorat

par

Dmytro DUDARIEV

pour l'obtention du titre de

Docteur de l'Université Lille

Discipline : Chimie physique, analytique et théorique

Compétition entre la solvatation et l'agrégation ionique dans des systèmes ioniques-solvant: influence sur les propriétés de transport

Date de soutenance: 03 Mars 2023

Oleg PREZHDO **Rapporteur**
Professeur, Université Southern California (Etats-Unis)

Ari Paavo SEITSONEN **Rapporteur**
Enseignant-Chercheur, (ENAC, ISAE), Université Pierre et Marie Curie

Abdenacer IDRISSI **Directeur de thèse**
Professeur, Université Lille

Oleg KALUGIN **Co-directeur de thèse**
Professeur, Université nationale de Kharkiv V. N. Karazine (Ukraine)

Pal JEDLOVSZKY **Examinateur**
Professeur,Université Eszterházy Károly University (Hongrie)

Fredric AFFOUARD **Examinateur**
Professeur, Université de Lille

François-Alexandre MIANNAY **Examinateur**
Maître de conférences, Université de Lille

Dietmar PASCHEK **Examinateur**
Docteur, Universität Rostock (Allemagne)

University of Lille

Faculty of Sciences and Technologies

Doctoral School 104 – Science of the Matter, of the Radiation, and of the Environment

Doctoral Thesis

by

Dmytro DUDARIEV

to obtain the degree of

Doctor of the University of Lille

Discipline: Physical, analytical and theoretical chemistry

Competition of solvation and ionic aggregation in ionic-molecular systems of different nature: influence on transport properties

Date of defense: 03 March 2023

Oleg PREZHDO *Professor, University of Southern California (USA)*	**Referee**
Ari Paavo SEITSONEN *Teacher-Researcher, (ENAC, ISAE), Pierre and Marie Curie University*	**Referee**
Abdenacer IDRISSI *Professor, University of Lille*	**Supervisor**
Oleg KALUGIN *Professor, V.N. Karazin Kharkiv National University (Ukraine)*	**Co-supervisor**
Pal JEDLOVSZKY *Professor, Eszterházy Károly University (Hungary)*	**Examiner**
Fredric AFFOUARD *Professor, University of Lille*	**Examiner**
François-Alexandre MIANNAY *Assistant professor, University of Lille*	**Examiner**
Dietmar PASCHEK *Doctor, Universität Rostock (Germany)*	**Examiner**

ACKNOWLEDGEMENTS

I would like to express my sincere gratitude to my supervisors, Profs. Abdenacer Idrissi and Oleg Kalugin, for their unwavering support, guidance and encouragement throughout my PhD journey. Without Nacer's tireless efforts and patience, my defense at the University of Lille would not have been possible. I am also deeply grateful to Oleg for introducing me to the scientific world and providing invaluable guidance and ideas throughout all the years of my PhD research.

I would also like to thank Profs. Oleg Prezhdo and Ari Paavo Seitsonen for their invaluable insights and feedback as my reviewers.

My research would not have been possible without the support of the Ukrainian government, who provided me with basic scholarships, as well as Erasmus+ and MobLilEx research mobility grants for the opportunity to perform my research in Lille I am also grateful to Université Côte d'Azur and University of Warsaw, and particularly Dr. Kamil Polok, for providing me with access to their computing clusters. I also wish to thank my alma mater, V.N. Karazin Kharkiv National University, and my native department of Inorganic Chemistry, for playing a significant role in shaping my academic carrier.

I am also grateful for the enormous assistance and valuable advice provided by my colleague Igor Vovchynsyi and my other colleagues, namely Yaroslav Kolesnik, Volodymyr Koverga, Oleksandr Korsun, and others for their valuable advices and suggestions during my PhD. I would also like to thank my friends Daria Stepaniuk, Yaroslav Filatov, Rostyslav Bardovskyi, Dmytro Strilets and many others for their support and encouragement.

My greatest thanks go to my family who always supported and cheered for me like no other, in spite of any difficulties. And to my significant other, Olena, without whom I would have not gone this far. Thank you for your love, faith and strength you gave me.

RÉSUMÉ

L'objectif de cette thèse est d'analyser la structure microscopique des mélanges de liquide avec des solvants utilisés comme électrolytes dans les dispositifs électrochimiques afin de caractériser l'effet de l'agrégation des ions sur les propriétés de transport de ces systèmes. En utilisant la simulation de dynamique moléculaire, les systèmes suivants ont été étudiés: (i) les solutions de hexafluorophosphate de lithium dans le mélange carbonate de diméthyle / carbonate d'éthylène (1:1), (ii) les solutions de tétrafluoroborate de spirobipyrrolidinium dans l'acétonitrile, et (iii) les mélanges de liquides ioniques (ILs) C_4mimX à température ambiante (X= BF_4^-, PF_6^-, TFO^-, $TFSI^-$) avec des solvants aprotiques dipolaires tels que l'acétonitrile, la γ-butyrolactone et le carbonate de propylène.

Pour tous les systèmes, l'analyse des agrégats a montré la formation d'un réseau ionique continu avec l'augmentation de la concentration de l'électrolyte. Ceci affecte significativement la diffusivité et la viscosité dans ces solutions.

L'analyse des polyèdres de Voronoi des mélanges ILs-solvants a montré qu'en dessous de la fraction molaire IL d'environ 0.2, les ions sont bien solv atés par les molécules de solvant, mais au-dessus de cette fraction molaire, ils commencent à former des paires de contact, tandis que les molécules de solvant, expulsées du voisinage des ions, s'autoassocient.

Mots clés : systèmes ioniques-moléculaires, structure locale, propriétés de transport, agrégation ionique, polyèdres de Voronoi.

ABSTRACT

The objective of this thesis is to analyze the microscopic structure of the series ion-molecular systems that widely used for practical electrochemistry and to characterize the effect of the ion aggregation on the transport properties of these systems. By using molecular dynamics simulation, the following systems were investigated: (i) the solutions of lithium hexafluorophosphate in dimethyl carbonate / ethylene carbonate mixture (1:1), (ii) the solutions of spirobipyrrolidinium tetrafluoroborate in acetonitrile, and (iii) the mixtures of room-temperature ionic liquids (ILs) C_4mimX (X= BF_4^-, PF_6^-, TFO^-, $TFSI^-$) with dipolar aprotic solvents such as acetonitrile, γ-butyrolactone and propylene carbonate.

For all the systems the aggregate analysis showed the formation of the ionic continuous network with the increase of electrolyte concentration. This affects significantly diffusivity and viscosity in these solutions.

Voronoi polyhedra analysis of ILs-solvent mixtures showed that below the IL mole fraction of about 0.2, the ions are well solvated by the solvent molecules, but above this mole fraction they start to form contact pairs, while the solvent molecules, expelled from the vicinity of the ions, self-associates.

Keywords: ionic-molecular systems, local structure, transport properties, ionic aggregation, Voronoi polyhedra.

Table of contents

List of abbreviations

SBP	1-1'-spirobipyrrolidinium
AN	acetonitrile
γ-BL	γ-butyrolactone
PC	propylene carbonate
IL	ionic liquid
C_4mim^+	1-*n*-butyl-3-methylimidazolium
TFO^-	trifluoromethylsulfonate
$TFSI^-$	bis(trifluoromethanesulfonyl)imide
PME	particle mesh Ewald
LJ	Lennard-Jones
GAFF	generalized AMBER force field
MD	molecular dynamics
RDF	radial distribution function
RCN	running coordination number
CIP	contact ion pair
SSIP	solvent shared ion pair
VP	Voronoi polyhedra

Chapter 1. General introduction

Ionic-molecular systems represent a huge interest for the researchers as new advanced systems with high performances for the electrochemical needs. There are many different types of such systems of different cation and solvent nature. At the same time, many of them have maximum on the conductivity-concentration curve that remains to be explained.

This chapter gives a brief introduction to such ionic-molecular systems, as well as an overview of the problem and possible theories that can explain such behavior.

Today the global electricity consumption is constantly rising, which is caused by technology development and the constantly rising state of the global economy.[1, 2] This have caused the growing demand for various energy storages, for which the advanced electrochemical systems with high performances are essential for proper and long-term functioning of these devices. Electrolyte systems with high electric conductivity and stability are required. At today's market there are numerous types of such systems that can fulfill these criteria.

Li-ion batteries are widely used when large energy density is needed,[3, 4] e.g., in portable electronics,[5] hybrid electric vehicles,[6, 7] etc. For these systems lithium salts are often mixed with alkylcarbonates such as ethylene, dimethyl, diethyl and ethyl-methyl carbonates,[8-11] which can optimize the operating temperature range and increase the conductivity of the Li^+.[12] As for the lithium salts themselves, there are several numerous candidates such as $LiBF_4$, $LiPF_6$, LiTFSI, LiTDI, $LiAsF_6$, CF_3SO_3Li, $LiClO_4$, etc.[6, 13-16] From practical point of view $LiPF_6$ dissolved in the binary mixture of two solvents usually used. One of the solvents is considered to play a role in dissociating the cations and anions via high dielectric constant whereas the other in improving ionic movement via its low viscosity: ethylene carbonate (EC) and dimethyl carbonate (DMC) are one of the common examples of such a mixture.[17]

During the last few decades electric double layer capacitors have shown themselves as promising charge storage devices too.[18-22] These types of systems have better power density, long cycle life compared to secondary batteries and also are safer in usage and Li-ion batteries.[23-26] Thus, such capacitors are often used in modern electric vehicles, smartphones, industrial power management, complex power systems, etc.[27-30] However, the widespread usage of these devices is hindered by their low energy density.[31] It is necessary to improve the energy density without sacrificing the high power density and long cycle life. Because the energy density is proportional to the square of the voltage, the organic electrolytes that have wide voltage window are used for high energy density applications.[32-34] Usually these electrolytes are dissolved in carbonate-based

organic solvents, e.g., acetonitrile (AN) or propylene carbonate (PC).[31, 34, 35] AN is electrochemically stabile and has high conductivity while PC has high flash point, but low conductivity. And among different salts tetraethylammonium tetrafluoroborate ($TEABF_4$) is the most common one.[36-38] However, this electrolyte has a significant drawback of limited solubility in organic solvents. 1,1'-spirobipyrrolidinium tetrafluoroborate ($SBPBF_4$), on the other hand, has low viscosity and high solubility in many organic solvents, as well as good electrochemical stability and high value of conductivity.[34, 39, 40]

Another type of systems that has been actively studied in recent decades along with traditional electrolyte ones is ionic liquids (ILs). They are known for a long time and gained mainstream popularity about 30 years ago. This was made possible by the commercial availability and the increased variability of the IL. The first applications of ILs were as solvents for chemical reactions,[41, 42] for catalysis with transition metals,[43] as a stationary phase in gas-liquid chromatography[44] and they are finding new improvements nowadays.[45-56] ILs, room-temperature ionic liquids, are molten salts usually composed of relatively large organic cations and organic or inorganic anions, where the ionic head groups (ammonium, imidazolium, sulfate, sulfonate etc.) are attached to non-polar (mostly alkyl) side chains which are liquid below 100 °C. Due to perspective properties such as nonvolatile, nonflammable, and nonexplosive, possess high chemical and thermal stability, large electrochemical potential window, high ionic conductivity, large liquid temperature range, negligibly low vapor pressure, ILs successfully used in many fields of science. The most studied application areas now are biological (antimicrobial ionic liquid-based materials[57-59] pharmaceutical (active medecine ingredients[60, 61]) chemical (molecular gas capture, such as H_2S, H_2, CO and CO_2,[62-66] functional materials,[67-71] lubricants[72, 73]) Because of unique properties of ILs one of their main applications is electrochemistry where they used as electrolytes in different energy storage devices such as batteries,[17] solar cells,[74-77] supercapacitors,[78-80] etc. The family of 1-alkyl-3-methylimdazolium (C_nmim^+) ILs with perfluorinated anions like tetrafluoroborate (BF_4^-),

hexafluorophosphate (PF_6^-), trifluoromethanesulfonate (TFO^-), bis(trifluoromethane)sulfonimide ($TFSI^-$) has proven to be good electrolytes for various electrochemical devices.[81-87] The stopping factor for widespread use of ILs is their high viscosity that is one of the reasons of low ion mobility. To overcome this problem the mixing of ILs with molecular solvents is usually made. Typical candidates for this purpose are AN,[88-91] PC,[92-94] γ-butyrolactone (γ-BL),[95-98] dimethyl sulfoxide (DMSO),[99, 100] etc.

As it was mentioned, all of these systems have a wide range of use for electrochemical applications for batteries, supercapacitors, solar cells, etc. For this purpose, electroconductivity remains a crucial property for the investigation. Lithium-type systems, alkylammonium electrolyte solutions and ILs with aprotic dipolar solvents – for all of them the electroconductivity has maximum at concentration of electrolyte.[91, 101-109] The traditional explanation for this phenomenon is the local structure changes in these systems (particularly, ion-ion and ion-solvent interactions) and the viscosity changes that both occurs at around the concentration where maximum of conductivity curve can be found.[110] Moreover, vibrational spectroscopic techniques and nuclear magnetic resonance (NMR) spectroscopy were used to analyze interactions in mixtures of imidazolium-based ILs with molecular solvents.[111-123] The findings indicate that noteworthy alterations in the vibration modes of C-H (or the ring of cations) and the ^1H chemical shift manifest at a certain IL concentration range where the conductivity undergoes changes. This phenomenon was linked to the adjustment, through modification of the mixture composition, of the equilibrium between different intercomponent interactions present in the mixtures, namely interionic (predominant at very high IL mole fractions), ion-solvent, and solvent-solvent interactions. Thus, the investigation of the microstructure of these systems remains a relevant task.

Theoretical approaches still cannot answer the question about these phenomena for solutions of different types. Especially considering the different nature of them: lithium and alkylammonium electrolytes are being solid salts

under normal conditions and never can be studied in their "pure" liquid form unlike ILs. Nevertheless, numerous studies (in particularly, for ILs-solvent mixtures) have been made during last 30 years to study the ionic association and solvation processes and their correlation with the transport properties in order to understand the reasoning of this behavior.[109, 124-129] One of the concepts that can describe the maximum on the conductivity-electrolyte concentration curve states that ion pairs and aggregates exist in such systems. Indeed, if the system consists predominantly (or only for neat ILs) of ions, the one should expect high conductivity in the solution, but that's not the case in real systems as was mentioned earlier. The interpretation with ion-pairing indication[110] or aggregates formation (triplets, quadruplets and higher)[130] can help to interpret this observation. In this case the effective concentration of charge carriers in solution – free ions – becomes lower with the increasing of the electrolyte concentration which lowers the electroconductivity as well comparing to diluted solution. Following this, the ion pairs do not contribute in the conductivity of the solution at all because of their neutral charge. But considering larger aggregates is a lot trickier. For instance, if triple ions are more likely to form in the solution than ion pairs, an increase in conductivity can be anticipated as they always possess a non-zero charge.[130-132] Also, the larger the aggregates in the solution, the lower the electroconductivity is. The overall structure and stability of the aggregates depend on the components of the solution itself, specifically, their interactions with each other and local structure as a result.[133]

Another possible approach is the free volume theory, which posits that the rate of molecular diffusion is determined by the quantity of unoccupied space between the particles within the solution.[134, 135]According to the free volume theory, total volume of a solution:

$$V_s = V_{occ} + V_f, \tag{2.1}$$

where V_{occ} is occupied volume, V_f is free volume.

The V_f is distributed locally into so-called voids or holes between molecules and ions. These holes can be formed from other smaller ones, they have irregular shape, size and location and formed by a particular molecular distribution. Voids are constantly changing in the solution due to the molecules and ions displacement. Free volume is closely linked to the transport properties such as viscosity and conductivity. Studying the free volume in IL and its potential impact on its physicochemical properties establishes a connection between the IL's structure and its suitability for a particular application.[136, 137]

In order to investigate these approaches a classical molecular dynamics (MD) simulation technique is proposed. It allows to obtain a wide spectrum of physicochemical, transport and structural properties of simulated systems, including the ones that cannot be directly obtained from the experimental data or easily interpreted.[138]

To investigate the local structure of the proposed systems, two methods have been suggested. The first one was studied by Bernardes and co-workers.[139-141] It is based on the distance criteria to observe the formation of the aggregates in the solution. This method enables not only qualitative verification of the formation of aggregates but also quantitative exploration of the process in terms of the probability distribution of aggregation sizes in the solution. More details regarding this method are provided in Chapter 2.

The second method involves the algorithm proposed by Ruocco et al.,[142] which generates a tessellation of the space without gaps or overlaps. This is achieved through Voronoi polyhedral (VP), which represent spatial points closer to one seed than to any other. The VP algorithm is based on a spatial set of seeds and can be used to investigate the local structure of the proposed systems. More details about this algorithm are provided in Chapter 2.

1.1. Organization of the thesis

In this thesis a set of classical MD simulations were performed to investigate the microscopic structure and transport properties of lithium (Li^+), 1-1'-spirobipyrrolidinium (SBP^+) and 1-methyl-3-butylimidazolium (C_4mim^+) with various anions, dissolved in aprotic dipolar solvents. The simulations utilized aggregation analysis and Voronoi polyhedra analysis to study the systems in detail.

Chapter 2 presents general computational details for MD simulations that were used in this study, as well as describes the properties analyzed in further Chapters.

Chapters 3, 4 and 5 provide a detailed MD simulation study of $LiPF_6$ in dimethyl carbonate (DMC) / ethylene carbonate (EC) mixture, $SBPBF_4$ in acetonitrile (AN) and the mixtures of room-temperature ionic liquids C_4mimX (X = BF_4^-, PF_6^-, TFO^-, $TFSI^-$) with dipolar aprotic solvents such as AN, γ-butyrolactone (γ-BL) and propylene carbonate (PC) respectively. The local environment, association analysis as well as transport properties were obtained, results were discussed in details in these three Chapters.

The local structure study via Voronoi polyhedra analysis for C_4mim^+ with various anions in aprotic molecular solvents were performed in the Chapter 6.

1.2. References for Chapter 1

(1) Gür, T. M. Review of electrical energy storage technologies, materials and systems: challenges and prospects for large-scale grid storage. *Energy & Environmental Science* **2018**, *11*, 2696-2767.
(2) Hossain, E.; Faruque, H.; Sunny, M.; Mohammad, N.; Nawar, N. A Comprehensive Review on Energy Storage Systems: Types, Comparison, Current Scenario, Applications, Barriers, and Potential Solutions, Policies, and Future Prospects. *Energies* **2020**, *13*, 3651-3651.
(3) Khomenko, V.; Raymundo-Piñero, E.; Béguin, F. High-energy density graphite/AC capacitor in organic electrolyte. *Journal of Power Sources* **2008**, *177*, 643-651.
(4) Tarascon, J. M.; Armand, M. Issues and challenges facing rechargeable lithium batteries. *Nature* **2001**, *414*, 359-367.
(5) Martha, S. K.; Dudney, N. J.; Kiggans, J. O.; Nanda, J. Electrochemical Stability of Carbon Fibers Compared to Aluminum as Current Collectors for Lithium-Ion Batteries. *Journal of The Electrochemical Society* **2012**, *159*, A1652-A1658.
(6) Karthikeyan, K.; Aravindan, V.; Lee, S. B.; Jang, I. C.; Lim, H. H.; Park, G. J.; Yoshio, M.; Lee, Y. S. A novel asymmetric hybrid supercapacitor based on Li_2FeSiO_4 and activated carbon electrodes. *Journal of Alloys and Compounds* **2010**, *504*, 224-227.
(7) Sato, N. Thermal behavior analysis of lithium-ion batteries for electric and hybrid vehicles. *Journal of Power Sources* **2001**, *99*, 70-77.
(8) Nitta, N.; Wu, F.; Lee, J. T.; Yushin, G. Li-ion battery materials: present and future. *Materials Today* **2015**, *18*, 252-264.
(9) Hajizadeh, A.; Shahalizade, T.; Riahifar, R.; Yaghmaee, M. S.; Raissi, B.; Gholam, S.; Aghaei, A.; Rahimisheikh, S.; Ghazvini, A. S. Electrophoretic deposition as a fabrication method for Li-ion battery electrodes and separators – A review. *Journal of Power Sources* **2022**, *535*, 231448-231448.
(10) Takamura, T. Trends in advanced batteries and key materials in the new century. *Solid State Ionics* **2002**, *152-153*, 19-34.
(11) Srour, H.; Rouault, H.; Santini, C. C. Novel Ionic Liquids Based Electrolytes for Secondary Lithium-Ion Batteries. *ECS Transactions* **2013**, *50*, 15-24.
(12) Aurbach, D.; Talyosef, Y.; Markovsky, B.; Markevich, E.; Zinigrad, E.; Asraf, L.; Gnanaraj, J. S.; Kim, H.-J. Design of electrolyte solutions for Li and Li-ion batteries: a review. *Electrochimica Acta* **2004**, *50*, 247-254.
(13) Xia, C.; Baek, B.; Xu, F.; Jung, C. Modification of electrolyte transport within the cathode for high-rate cycle performance of Li-ion battery. *Journal of Solid State Electrochemistry* **2013**, *17*, 2151-2156.
(14) Dougassa, Y. R.; Jacquemin, J.; El Ouatani, L.; Tessier, C.; Anouti, M. Viscosity and carbon dioxide solubility for LiPF6, LiTFSI, and LiFAP in alkyl carbonates: lithium salt nature and concentration effect. *The Journal of Physical Chemistry B* **2014**, *118*, 3973-3980.
(15) Miyoshi, S.; Nagano, H.; Fukuda, T.; Kurihara, T.; Watanabe, M.; Ida, S.; Ishihara, T. Dual-Carbon Battery Using High Concentration $LiPF_6$ in Dimethyl Carbonate (DMC) Electrolyte. *Journal of The Electrochemical Society* **2016**, *163*, A1206-A1213.
(16) Mercier-Guyon, B.; Chavillon, B.; Mayousse, E.; Le Comte, A.; Reynier, Y.; Barchasz, C. Influence of electrolyte composition on high energy lithium metal cells. *Solid State Ionics* **2020**, *350*, 115321-115321.
(17) Scrosati, B.; Garche, J. Lithium batteries: Status, prospects and future. *Journal of Power Sources* **2010**, *195*, 2419-2430.
(18) Kim, J.; Kim, Y.; Park, S.-J.; Jung, Y.; Kim, S. Preparation and electrochemical analysis of graphene nanosheets/nickel hydroxide composite electrodes containing carbon nanotubes. *Journal of Industrial and Engineering Chemistry* **2016**, *36*, 139-146.

(19) Park, S.-J.; Son, Y.-R.; Heo, Y.-J. Prospective Synthesis Approaches to Emerging Materials for Supercapacitor. In *Emerging Materials for Energy Conversion and Storage*, Elsevier, 2018; pp 185-208.
(20) Rebbani, A.; Bouattane, O.; Bahatti, L.; Zazoui, M. An Efficient Electric Charge Transfer Device for Intelligent Storage Units. *Open Journal of Energy Efficiency* **2014**, *03*, 50-63.
(21) Fernando, J. Electrical double-layer capacitors. In *Energy Storage Devices for Electronic Systems*, Nihal, K. Ed.; Murata Manufacturing Co, 2015; pp 149-186.
(22) Sharma, P.; Bhatti, T. S. A review on electrochemical double-layer capacitors. *Energy Conversion and Management* **2010**, *51*, 2901-2912.
(23) Zhang, Y.; Zhang, X.; Lang, X.; Zhang, Q. Study on the themodynamic properties and electrochemical performance of mixture electrolyte for supercapacitor composed of ionic liquid [BMIM][BF_4] and $SBPBF_4$/PC. *Ionics* **2021**, *27*, 4003-4011.
(24) Yu, J.; Xie, F.; Wu, Z.; Huang, T.; Wu, J.; Yan, D.; Huang, C.; Li, L. Flexible metallic fabric supercapacitor based on graphene/polyaniline composites. *Electrochimica Acta* **2018**, *259*, 968-974.
(25) Wang, Z.; Liu, C.; Shi, G.; Wang, G.; Zhang, H.; Zhang, Q.; Jiang, X.; Li, X.; Luo, F.; Hu, Y.; et al. Preparation and electrochemical properties of electrospun FeS/carbon nanofiber composites. *Ionics* **2020**, *26*, 3051-3060.
(26) Xia, L.; Yu, L.; Hu, D.; Chen, G. Z. Electrolytes for electrochemical energy storage. *Materials Chemistry Frontiers* **2017**, *1*, 584-618.
(27) Yu, X.; Ruan, D.; Wu, C.; Wang, J.; Shi, Z. Spiro-(1,1′)-bipyrrolidinium tetrafluoroborate salt as high voltage electrolyte for electric double layer capacitors. *Journal of Power Sources* **2014**, *265*, 309-316.
(28) Liu, W.; Yan, X.; Lang, J.; Xue, Q. Electrochemical behavior of graphene nanosheets in alkylimidazolium tetrafluoroborate ionic liquid electrolytes: influences of organic solvents and the alkyl chains. *Journal of Materials Chemistry* **2011**, *21*, 13205-13205.
(29) Pan, S.; Yao, M.; Zhang, J.; Li, B.; Xing, C.; Song, X.; Su, P.; Zhang, H. Recognition of Ionic Liquids as High-Voltage Electrolytes for Supercapacitors. *Frontiers in Chemistry* **2020**, *8*.
(30) Shi, M.-J.; Kou, S.-Z.; Shen, B.-S.; Lang, J.-W.; Yang, Z.; Yan, X.-B. Improving the performance of all-solid-state supercapacitors by modifying ionic liquid gel electrolytes with graphene nanosheets prepared by arc-discharge. *Chinese Chemical Letters* **2014**, *25*, 859-864.
(31) Burke, A. R&D considerations for the performance and application of electrochemical capacitors. *Electrochimica Acta* **2007**, *53*, 1083-1091.
(32) Béguin, F.; Presser, V.; Balducci, A.; Frackowiak, E. Carbons and Electrolytes for Advanced Supercapacitors. *Advanced Materials* **2014**, *26*, 2219-2251.
(33) Cheng, F.; Qiu, W.; Yang, X.; Gu, X.; Hou, W.; Lu, W. Ultrahigh-power supercapacitors from commercial activated carbon enabled by compositing with carbon nanomaterials. *Electrochimica Acta* **2022**, *403*, 139728-139728.
(34) Kim, M.; Kim, S. Electrochemical properties of non-aqueous electrolytes containing spiro-type ammonium salts. *Journal of Industrial and Engineering Chemistry* **2014**, *20*, 4447-4451.
(35) Perricone, E.; Chamas, M.; Leprêtre, J. C.; Judeinstein, P.; Azais, P.; Raymundo-Pinero, E.; Béguin, F.; Alloin, F. Safe and performant electrolytes for supercapacitor. Investigation of esters/carbonate mixtures. *Journal of Power Sources* **2013**, *239*, 217-224.
(36) Ding, M. S.; Xu, K.; Zheng, J. P.; Jow, T. R. γ-Butyrolactone-acetonitrile solution of triethylmethylammonium tetrafluoroborate as an electrolyte for double-layer capacitors. *Journal of Power Sources* **2004**, *138*, 340-350.
(37) Zhong, C.; Deng, Y.; Hu, W.; Qiao, J.; Zhang, L.; Zhang, J. A review of electrolyte materials and compositions for electrochemical supercapacitors. *Chemical Society Reviews* **2015**, *44*, 7484-7539.

(38) Tripathi, M.; Bobade, S. M.; Kumar, A. Preparation of polyvinylidene fluoride-co-hexafluoropropylene-based polymer gel electrolyte and its performance evaluation for application in EDLCs. *Bulletin of Materials Science* **2019**, *42*, 27-27.
(39) Krummacher, J.; Schütter, C.; Hess, L. H.; Balducci, A. Non-aqueous electrolytes for electrochemical capacitors. *Current Opinion in Electrochemistry* **2018**, *9*, 64-69.
(40) Chiba, K.; Ueda, T.; Yamaguchi, Y.; Oki, Y.; Saiki, F.; Naoi, K. Electrolyte Systems for High Withstand Voltage and Durability II. Alkylated Cyclic Carbonates for Electric Double-Layer Capacitors. *Journal of The Electrochemical Society* **2011**, *158*, A1320-A1320.
(41) Earle, M. J.; McCormac, P. B.; Seddon, K. R. Diels–Alder reactions in ionic liquids. *Green Chemistry* **1999**, *1*, 23-25.
(42) Fischer, T.; Sethi, A.; Welton, T.; Woolf, J. Diels-Alder reactions in room-temperature ionic liquids. *Tetrahedron Letters* **1999**, *40*, 793-796.
(43) Chauvin, Y.; Gilbert, B.; Guibard, I. Catalytic dimerization of alkenes by nickel complexes in organochloroaluminate molten salts. *Journal of the Chemical Society, Chemical Communications* **1990**, 1715-1715.
(44) Welton, T. Ionic liquids: a brief history. *Biophysical Reviews* **2018**, *10*, 691-706.
(45) Hallett, J. P.; Welton, T. Room-Temperature Ionic Liquids: Solvents for Synthesis and Catalysis. 2. *Chemical Reviews* **2011**, *111*, 3508-3576.
(46) Olivier-Bourbigou, H.; Magna, L.; Morvan, D. Ionic liquids and catalysis: Recent progress from knowledge to applications. *Applied Catalysis A: General* **2010**, *373*, 1-56.
(47) Khupse, N. D.; Kumar, A. The Cosolvent-Directed Diels–Alder Reaction in Ionic Liquids. *The Journal of Physical Chemistry A* **2011**, *115*, 10211-10217.
(48) Kumar, A.; Pawar, S. S. Converting exo-Selective Diels−Alder Reaction to endo-Selective in Chloroloaluminate Ionic Liquids. *The Journal of Organic Chemistry* **2004**, *69*, 1419-1420.
(49) Sheldon, R. Catalytic reactions in ionic liquids. *Chemical Communications* **2001**, 2399-2407.
(50) Chen, J.; Ren, Y.; Li, H.; Yang, W.; Wu, Q.; Zhao, Y.; Jiao, Q.; Lu, Y.; Shi, D. Structural Regulation of Magnetic Polymer Microsphere@Ionic Liquids with an Intermediate Protective Layer and Application as Core–Shell–Shell Catalysts with High Stability and Activity. *ACS Omega* **2020**, *5*, 23062-23069.
(51) Scholten, J. D.; Leal, B. C.; Dupont, J. Transition Metal Nanoparticle Catalysis in Ionic Liquids. *ACS Catalysis* **2012**, *2*, 184-200.
(52) Plechkova, N. V.; Seddon, K. R. Applications of ionic liquids in the chemical industry. *Chem. Soc. Rev.* **2008**, *37*, 123-150.
(53) Adamski, J.; Qadir, M. I.; Serna, J. P.; Bernardi, F.; Baptista, D. L.; Salles, B. R.; Novak, M. A.; Machado, G.; Dupont, J. Core–Shell Fe–Pt Nanoparticles in Ionic Liquids: Magnetic and Catalytic Properties. *The Journal of Physical Chemistry C* **2018**, *122*, 4641-4650.
(54) Poole, C. F.; Poole, S. K. Extraction of organic compounds with room temperature ionic liquids. *Journal of Chromatography A* **2010**, *1217*, 2268-2286.
(55) Mazzucotelli, M.; Bicchi, C.; Marengo, A.; Rubiolo, P.; Galli, S.; Anderson, J. L.; Sgorbini, B.; Cagliero, C. Ionic liquids as stationary phases for gas chromatography—Unusual selectivity of ionic liquids with a phosphonium cation and different anions in the flavor, fragrance and essential oil analyses. *Journal of Chromatography A* **2019**, *1583*, 124-135.
(56) Qiao, Y.; Ma, W.; Theyssen, N.; Chen, C.; Hou, Z. Temperature-Responsive Ionic Liquids: Fundamental Behaviors and Catalytic Applications. *Chemical Reviews* **2017**, *117*, 6881-6928.
(57) Nikfarjam, N.; Ghomi, M.; Agarwal, T.; Hassanpour, M.; Sharifi, E.; Khorsandi, D.; Ali Khan, M.; Rossi, F.; Rossetti, A.; Nazarzadeh Zare, E.; et al. Antimicrobial Ionic Liquid-Based Materials for Biomedical Applications. *Advanced Functional Materials* **2021**, *31*, 2104148-2104148.
(58) Pang, L. Q.; Zhong, L. J.; Zhou, H. F.; Wu, X. E.; Chen, X. D. Grafting of ionic liquids on stainless steel surface for antibacterial application. *Colloids and Surfaces B: Biointerfaces* **2015**, *126*, 162-168.

(59) Fallah, Z.; Zare, E. N.; Khan, M. A.; Iftekhar, S.; Ghomi, M.; Sharifi, E.; Tajbakhsh, M.; Nikfarjam, N.; Makvandi, P.; Lichtfouse, E.; et al. Ionic liquid-based antimicrobial materials for water treatment, air filtration, food packaging and anticorrosion coatings. *Advances in Colloid and Interface Science* **2021**, *294*, 102454-102454.
(60) Hough, W. L.; Smiglak, M.; Rodríguez, H.; Swatloski, R. P.; Spear, S. K.; Daly, D. T.; Pernak, J.; Grisel, J. E.; Carliss, R. D.; Soutullo, M. D.; et al. The third evolution of ionic liquids: active pharmaceutical ingredients. *New Journal of Chemistry* **2007**, *31*, 1429-1429.
(61) Petkovic, M.; Seddon, K. R.; Rebelo, L. P. N.; Silva Pereira, C. Ionic liquids: a pathway to environmental acceptability. *Chem. Soc. Rev.* **2011**, *40*, 1383-1403.
(62) Jia, X.; Hu, X.; Su, K.; Wang, W.; Du, C. Molecular screening of ionic liquids for CO_2 absorption and molecular dynamic simulation. *Open Chemistry* **2022**, *20*, 379-387.
(63) Abdi, J.; Hadipoor, M.; Esmaeili-Faraj, S. H.; Vaferi, B. A modeling approach for estimating hydrogen sulfide solubility in fifteen different imidazole-based ionic liquids. *Scientific Reports* **2022**, *12*, 4415-4415.
(64) Vijayraghavan, R.; Pas, S. J.; Izgorodina, E. I.; MacFarlane, D. R. Diamino protic ionic liquids for CO_2 capture. *Physical Chemistry Chemical Physics* **2013**, *15*, 19994-19994.
(65) MacDowell, N.; Florin, N.; Buchard, A.; Hallett, J.; Galindo, A.; Jackson, G.; Adjiman, C. S.; Williams, C. K.; Shah, N.; Fennell, P. An overview of CO_2 capture technologies. *Energy & Environmental Science* **2010**, *3*, 1645-1645.
(66) Anderson, J. L.; Dixon, J. K.; Brennecke, J. F. Solubility of CO_2, CH_4, C_2H_6, C_2H_4, O_2, and N_2 in 1-hexyl-3-methylpyridinium bis(trifluoromethylsulfonyl)imide: comparison to other ionic liquids. *Accounts of Chemical Research* **2007**, *40*, 1208-1216.
(67) Ghafoor, B.; Schrekker, H. S.; Amico, S. C. Multifunctional Characteristics of Carbon Fibers Modified with Imidazolium Ionic Liquids. *Molecules* **2022**, *27*, 7001-7001.
(68) Peng, K.; Wang, X.; Huang, Q.; Yang, Z.; Li, Y.; Chen, X. Molecular-Level Understanding of Structures and Dynamics of Imidazolium-Based Ionic Liquids around Single-Walled Carbon Nanotubes: Different Effects between Alkyl Chains of Cations and Nanotube Diameters. *The Journal of Physical Chemistry C* **2019**, *123*, 18932-18938.
(69) Ghazali-Esfahani, S.; Song, H.; Păunescu, E.; Bobbink, F. D.; Liu, H.; Fei, Z.; Laurenczy, G.; Bagherzadeh, M.; Yan, N.; Dyson, P. J. Cycloaddition of CO_2 to epoxides catalyzed by imidazolium-based polymeric ionic liquids. *Green Chemistry* **2013**, *15*, 1584-1584.
(70) Zhang, S.; Zhang, Q.; Zhang, Y.; Chen, Z.; Watanabe, M.; Deng, Y. Beyond solvents and electrolytes: Ionic liquids-based advanced functional materials. *Progress in Materials Science* **2016**, *77*, 80-124.
(71) Pei, Y.; Zhang, Y.; Ma, J.; Fan, M.; Zhang, S.; Wang, J. Ionic liquids for advanced materials. *Materials Today Nano* **2022**, *17*, 100159-100159.
(72) Jiang, H.; Yu, Y.; Tang, W.; Zhou, R.; Shi, W.; Bai, L. A molecular dynamics study on the lubrication performance of ionic liquids. *Journal of Materials Science* **2022**, *57*, 18874-18888.
(73) Zhou, Y.; Qu, J. Ionic Liquids as Lubricant Additives: A Review. *ACS Applied Materials & Interfaces* **2017**, *9*, 3209-3222.
(74) Grätzel, M. Conversion of sunlight to electric power by nanocrystalline dye-sensitized solar cells. *Journal of Photochemistry and Photobiology A: Chemistry* **2004**, *164*, 3-14.
(75) Ghosh, S.; Singh, T. Role of ionic liquids in organic-inorganic metal halide perovskite solar cells efficiency and stability. *Nano Energy* **2019**, *63*, 103828-103828.
(76) Reza Zolghadr, A.; Azari, N.; Heydari Dokoohaki, M. The use of 1-ethyl-3-methylimidazolium iodide ionic liquid in dye sensitized solar cells: A joint experimental and computational perspective. *Journal of Molecular Liquids* **2022**, *364*, 119982-119982.
(77) Chu, W.; Yang, J.; Jiang, Q.; Li, X.; Xin, J. Enhancement of photovoltaic performance of flexible perovskite solar cells by means of ionic liquid interface modification in a low temperature all solution process. *Applied Surface Science* **2018**, *440*, 1116-1122.

(78) Arkhipova, E. A.; Ivanov, A. S.; Maslakov, K. I.; Savilov, S. V.; Lunin, V. V. Effect of cation structure of tetraalkylammonium- and imidazolium-based ionic liquids on their conductivity. *Electrochimica Acta* **2019**, *297*, 842-849.
(79) Galiński, M.; Lewandowski, A.; Stępniak, I. Ionic liquids as electrolytes. *Electrochimica Acta* **2006**, *51*, 5567-5580.
(80) Dong, X.-L.; Wang, S.-Q.; He, B.; Li, W.-C. Highly sp2 hybridized and nitrogen, oxygen dual-doped nanoporous carbon network: Synthesis and application for ionic liquid supercapacitors. *Microporous and Mesoporous Materials* **2018**, *259*, 229-237.
(81) MacFarlane, D. R.; Tachikawa, N.; Forsyth, M.; Pringle, J. M.; Howlett, P. C.; Elliott, G. D.; Davis, J. H.; Watanabe, M.; Simon, P.; Angell, C. A. Energy applications of ionic liquids. *Energy Environ. Sci.* **2014**, *7*, 232-250.
(82) Yeletsky, P. M.; Lebedeva, M. V.; Yakovlev, V. A. Today's progress in the synthesis of porous carbons from biomass and their application for organic electrolyte and ionic liquid based supercapacitors. *Journal of Energy Storage* **2022**, *50*, 104225-104225.
(83) Patel, K. K.; Singhal, T.; Pandey, V.; Sumangala, T. P.; Sreekanth, M. S. Evolution and recent developments of high performance electrode material for supercapacitors: A review. *Journal of Energy Storage* **2021**, *44*, 103366-103366.
(84) Rizzuto, A. M.; Pennington, R. L.; Sienerth, K. D. Study of the BMIM-PF_6: Acetonitrile binary mixture as a solvent for electrochemical studies involving CO_2. *Electrochimica Acta* **2011**, *56*, 5003-5009.
(85) MacFarlane, D. R.; Forsyth, M.; Howlett, P. C.; Pringle, J. M.; Sun, J.; Annat, G.; Neil, W.; Izgorodina, E. I. Ionic Liquids in Electrochemical Devices and Processes: Managing Interfacial Electrochemistry. *Accounts of Chemical Research* **2007**, *40*, 1165-1173.
(86) Shiddiky, M. J. A.; Torriero, A. A. J. Application of ionic liquids in electrochemical sensing systems. *Biosensors and Bioelectronics* **2011**, *26*, 1775-1787.
(87) Zhumadilova Zh, O.; Utepov, T. E. Development of alloys on an iron basis. In *Conference Proceeding. TMS 2010 - 139th Annual Meeting and Exhibition; Seattle*, Seattle, 2010; Vol. 3, pp 753-758.
(88) Waliszewski, D.; Piekarski, H. Heat capacities of the mixtures of ionic liquids with acetonitrile. *The Journal of Chemical Thermodynamics* **2010**, *42*, 189-192.
(89) Zhang, Q.; Liu, X.; Yin, L.; Chen, P.; Wang, Y.; Yan, T. Electrochemical impedance spectroscopy on the capacitance of ionic liquid–acetonitrile electrolytes. *Electrochimica Acta* **2018**, *270*, 352-362.
(90) Zhuravlev, O. E. Effect of the Structure of Imidazolium Ionic Liquids on the Electrical Conductivity and Processes of Ionic Association in Acetonitrile Solutions. *Russian Journal of Physical Chemistry A* **2021**, *95*, 298-302.
(91) Kalugin, O. N.; Voroshylova, I. V.; Riabchunova, A. V.; Lukinova, E. V.; Chaban, V. V. Conductometric study of binary systems based on ionic liquids and acetonitrile in a wide concentration range. *Electrochimica Acta* **2013**, *105*, 188-199.
(92) Zhang, Q.-G.; Sun, S.-S.; Pitula, S.; Liu, Q.-S.; Welz-Biermann, U.; Zhang, J.-J. Electrical Conductivity of Solutions of Ionic Liquids with Methanol, Ethanol, Acetonitrile, and Propylene Carbonate. *Journal of Chemical & Engineering Data* **2011**, *56*, 4659-4664.
(93) Pohlmann, S.; Olyschläger, T.; Goodrich, P.; Vicente, J. A.; Jacquemin, J.; Balducci, A. Mixtures of Azepanium Based Ionic Liquids and Propylene Carbonate as High Voltage Electrolytes for Supercapacitors. *Electrochimica Acta* **2015**, *153*, 426-432.
(94) Pires, J.; Timperman, L.; Jacquemin, J.; Balducci, A.; Anouti, M. Density, conductivity, viscosity, and excess properties of (pyrrolidinium nitrate-based Protic Ionic Liquid+propylene carbonate) binary mixture. *The Journal of Chemical Thermodynamics* **2013**, *59*, 10-19.
(95) Borba, K. N.; Trombetta, F.; de Souza, R. F.; Martini, E. M. A. Stability of Al_2O_3/Al in ionic liquid $BMIMBF_4$/γ-butyrolactone electrolytes for use in electrolytic capacitors. *Ionics* **2017**, *23*, 1165-1171.

(96) Dagousset, L.; Nguyen, G. T. M.; Vidal, F.; Galindo, C.; Aubert, P.-H. Ionic liquids and γ-butyrolactone mixtures as electrolytes for supercapacitors operating over extended temperature ranges. *RSC Advances* **2015**, *5*, 13095-13101.
(97) Papović, S.; Gadžurić, S.; Bešter-Rogač, M.; Jović, B.; Vraneš, M. A systematic study on physicochemical and transport properties of imidazolium-based ionic liquids with γ-butyrolactone. *The Journal of Chemical Thermodynamics* **2018**, *116*, 330-340.
(98) Papović, S.; Vraneš, M.; Gadžurić, S. A comprehensive study of {γ-butyrolactone + 1-methyl-3-propylimidazolium bis(trifluoromethylsulfonyl)imide} binary mixtures. *The Journal of Chemical Thermodynamics* **2015**, *91*, 360-368.
(99) Ferreira, D. C.; Oliveira, M. L.; Bioni, T. A.; Nawaz, H.; King, A. W. T.; Kilpeläinen, I.; Hummel, M.; Sixta, H.; El Seoud, O. A. Binary mixtures of ionic liquids-DMSO as solvents for the dissolution and derivatization of cellulose: Effects of alkyl and alkoxy side chains. *Carbohydrate Polymers* **2019**, *212*, 206-214.
(100) Zheng, Y.-Z.; Zhou, Y.; Deng, G.; Yu, Z.-W. Hydrogen-bonding interactions between a nitrile-based functional ionic liquid and DMSO. *Journal of Molecular Structure* **2016**, *1124*, 207-215.
(101) Wu, X.; Gong, Y.; Xu, S.; Yan, Z.; Zhang, X.; Yang, S. Electrical Conductivity of Lithium Chloride, Lithium Bromide, and Lithium Iodide Electrolytes in Methanol, Water, and Their Binary Mixtures. *Journal of Chemical & Engineering Data* **2019**, *64*, 4319-4329.
(102) Gottwald, T.; Sedlaříková, M.; Vondrák, J. Conductivity of Inorganic Perchlorates Dissolved in Aprotic Solvents. *ECS Transactions* **2017**, *81*, 47-55.
(103) Berhaut, Christopher L.; Lemordant, D.; Porion, P.; Timperman, L.; Schmidt, G.; Anouti, M. Ionic association analysis of LiTDI, LiFSI and $LiPF_6$ in EC/DMC for better Li-ion battery performances. *RSC Advances* **2019**, *9*, 4599-4608.
(104) Jackson, N. M.; Payne, M. Functional Electrolytes for Use in Non-aqueous EDLCs. *ECS Transactions* **2008**, *16*, 139-149.
(105) Nguyen, H. V. T.; Kwak, K.; Lee, K.-K. 1,1-Dimethylpyrrolidinium tetrafluoroborate as novel salt for high-voltage electric double-layer capacitors. *Electrochimica Acta* **2019**, *299*, 98-106.
(106) Higashiya, S.; Devarajan, T. S.; Rane-Fondacaro, M. V.; Dangler, C.; Snyder, J.; Haldar, P. Synthesis of Oxygen-Containing Spirobipyrrolidinium Salts for High Conductivity Room Temperature Ionic Liquids. *Helvetica Chimica Acta* **2009**, *92*, 1600-1609.
(107) Zhang, Q.-Y.; Xie, P.; Wang, X.; Yu, X.-W.; Shi, Z.-Q.; Zhao, S.-H. Thermodynamic and transport properties of spiro-(1,1')-bipyrrolidinium tetrafluoroborate and acetonitrile mixtures: A molecular dynamics study. *Chinese Physics B* **2016**, *25*, 066102-066102.
(108) Stoppa, A.; Hunger, J.; Buchner, R. Conductivities of Binary Mixtures of Ionic Liquids with Polar Solvents. *Journal of Chemical & Engineering Data* **2009**, *54*, 472-479.
(109) Dorbritz, S.; Ruth, W.; Kragl, U. Investigation on Aggregate Formation of Ionic Liquids. *Advanced Synthesis & Catalysis* **2005**, *347*, 1273-1279.
(110) Marcus, Y.; Hefter, G. Ion Pairing. *Chemical Reviews* **2006**, *106*, 4585-4621.
(111) Kiefer, J. Vibrational Spectroscopy for Studying Hydrogen Bonding in Imidazolium Ionic Liquids and their Mixtures with Cosolvents. In *Hydrogen Bonding and Transfer in the Excited State*, John Wiley & Sons, Ltd, 2010; pp 341-352.
(112) Cha, S.; Ao, M.; Sung, W.; Moon, B.; Ahlstrom, B.; Johansson, P.; Ouchi, Y.; Kim, D. Structures of ionic liquid-water mixtures investigated by IR and NMR spectroscopy. *Physical Chemistry Chemical Physics* **2014**, *16*, 9591-9601.
(113) Takamuku, T.; Kyoshoin, Y.; Shimomura, T.; Kittaka, S.; Yamaguchi, T. Effect of Water on Structure of Hydrophilic Imidazolium-Based Ionic Liquid. *The Journal of Physical Chemistry B* **2009**, *113*, 10817-10824.
(114) Wang, H.; Wang, J.; Zhang, L. Temperature dependence of the microstructure of 1-butyl-3-methylimidazolium tetrafluoroborate in aqueous solution. *Vibrational Spectroscopy* **2013**, *68*, 20-28.

(115) Zhang, Q.-G.; Wang, N.-N.; Wang, S.-L.; Yu, Z.-W. Hydrogen Bonding Behaviors of Binary Systems Containing the Ionic Liquid 1-Butyl-3-methylimidazolium Trifluoroacetate and Water/Methanol. *The Journal of Physical Chemistry B* **2011**, *115*, 11127-11136.
(116) Zhang, Q.-G.; Wang, N.-N.; Yu, Z.-W. The Hydrogen Bonding Interactions between the Ionic Liquid 1-Ethyl-3-Methylimidazolium Ethyl Sulfate and Water. *The Journal of Physical Chemistry B* **2010**, *114*, 4747-4754.
(117) Zhang, L.; Xu, Z.; Wang, Y.; Li, H. Prediction of the solvation and structural properties of ionic liquids in water by two-dimensional correlation spectroscopy. *The Journal of Physical Chemistry B* **2008**, *112*, 6411-6419.
(118) Jeon, Y.; Sung, J.; Kim, D.; Seo, C.; Cheong, H.; Ouchi, Y.; Ozawa, R.; Hamaguchi, H.-o. Structural Change of 1-Butyl-3-methylimidazolium Tetrafluoroborate + Water Mixtures Studied by Infrared Vibrational Spectroscopy. *The Journal of Physical Chemistry B* **2008**, *112*, 923-928.
(119) Jeon, Y.; Sung, J.; Seo, C.; Lim, H.; Cheong, H.; Kang, M.; Moon, B.; Ouchi, Y.; Kim, D. Structures of Ionic Liquids with Different Anions Studied by Infrared Vibration Spectroscopy. *The Journal of Physical Chemistry B* **2008**, *112*, 4735-4740.
(120) Fazio, B.; Triolo, A.; Di Marco, G. Local organization of water and its effect on the structural heterogeneities in room-temperature ionic liquid/H_2O mixtures. *Journal of Raman Spectroscopy* **2008**, *39*, 233-237.
(121) Holomb, R.; Martinelli, A.; Albinsson, I.; Lassègues, J. C.; Johansson, P.; Jacobsson, P. Ionic liquid structure: the conformational isomerism in 1-butyl-3-methyl-imidazolium tetrafluoroborate ([bmim][BF_4]). *Journal of Raman Spectroscopy* **2008**, *39*, 793-805.
(122) Hatano, N.; Watanabe, M.; Takekiyo, T.; Abe, H.; Yoshimura, Y. Anomalous Conformational Change in 1-Butyl-3-methylimidazolium Tetrafluoroborate–D_2O Mixtures. *The Journal of Physical Chemistry A* **2012**, *116*, 1208-1212.
(123) Andanson, J. M.; Traïkia, M.; Husson, P. Ionic association and interactions in aqueous methylsulfate alkyl-imidazolium-based ionic liquids. *The Journal of Chemical Thermodynamics* **2014**, *77*, 214-221.
(124) Wang, Y.-L.; Li, B.; Sarman, S.; Mocci, F.; Lu, Z.-Y.; Yuan, J.; Laaksonen, A.; Fayer, M. D. Microstructural and Dynamical Heterogeneities in Ionic Liquids. *Chemical Reviews* **2020**, *120*, 5798-5877.
(125) Vovchynskyi, I. S.; Kolesnik, Y. V.; Filatov, Y. I.; Kalugin, O. N. Molecular modelling on solutions of 1-1′-spirobipirrolidinium tetrafluoroborate in acetonitrile. *Journal of Molecular Liquids* **2017**, *235*, 60-67.
(126) Hou, J.; Zhang, Z.; Madsen, L. A. Cation/Anion Associations in Ionic Liquids Modulated by Hydration and Ionic Medium. *The Journal of Physical Chemistry B* **2011**, *115*, 4576-4582.
(127) Krachkovskiy, S. A.; Bazak, J. D.; Fraser, S.; Halalay, I. C.; Goward, G. R. Determination of Mass Transfer Parameters and Ionic Association of $LiPF_6$: Organic Carbonates Solutions. *Journal of The Electrochemical Society* **2017**, *164*, A912-A916.
(128) Zhang, X.; Kuroda, D. G. An ab initio molecular dynamics study of the solvation structure and ultrafast dynamics of lithium salts in organic carbonates: A comparison between linear and cyclic carbonates. *J Chem Phys* **2019**, *150*, 184501.
(129) Bešter-Rogač, M.; Stoppa, A.; Hunger, J.; Hefter, G.; Buchner, R. Association of ionic liquids in solution: a combined dielectric and conductivity study of [bmim][Cl] in water and in acetonitrile. *Physical Chemistry Chemical Physics* **2011**, *13*, 17588-17588.
(130) MacFarlane, D. R.; Forsyth, M.; Izgorodina, E. I.; Abbott, A. P.; Annat, G.; Fraser, K. On the concept of ionicity in ionic liquids. *Physical Chemistry Chemical Physics* **2009**, *11*, 4962-4962.
(131) Zhang, Y.; Maginn, E. J. Direct Correlation between Ionic Liquid Transport Properties and Ion Pair Lifetimes: A Molecular Dynamics Study. *The Journal of Physical Chemistry Letters* **2015**, *6*, 700-705.

(132) Robinson, R. A.; Stokes, R. H. *Electrolyte Solutions: Second Revised Edition*; Courier Corporation, 2002.
(133) de Castro, C. A. N. Thermophysical properties of ionic liquids: Do we know how to measure them accurately? *Journal of Molecular Liquids* **2010**, *156*, 10-17.
(134) Ramesh, N.; Davis, P. K.; Zielinski, J. M.; Danner, R. P.; Duda, J. L. Application of free-volume theory to self diffusion of solvents in polymers below the glass transition temperature: A review. *Journal of Polymer Science Part B: Polymer Physics* **2011**, *49*, 1629-1644.
(135) Slattery, J. M.; Daguenet, C.; Dyson, P. J.; Schubert, T. J. S.; Krossing, I. How to Predict the Physical Properties of Ionic Liquids: A Volume-Based Approach. *Angewandte Chemie International Edition* **2007**, *46*, 5384-5388.
(136) Beichel, W.; Yu, Y.; Dlubek, G.; Krause-Rehberg, R.; Pionteck, J.; Pfefferkorn, D.; Bulut, S.; Bejan, D.; Friedrich, C.; Krossing, I. Free volume in ionic liquids: a connection of experimentally accessible observables from PALS and PVT experiments with the molecular structure from XRD data. *Physical Chemistry Chemical Physics* **2013**, *15*, 8821-8821.
(137) Brooks, N. J.; Castiglione, F.; Doherty, Cara M.; Dolan, A.; Hill, A. J.; Hunt, P. A.; Matthews, R. P.; Mauri, M.; Mele, A.; Simonutti, R.; et al. Linking the structures, free volumes, and properties of ionic liquid mixtures. *Chemical Science* **2017**, *8*, 6359-6374.
(138) Zahn, S.; Brehm, M.; Brüssel, M.; Hollóczki, O.; Kohagen, M.; Lehmann, S.; Malberg, F.; Pensado, A. S.; Schöppke, M.; Weber, H.; et al. Understanding ionic liquids from theoretical methods. *Journal of Molecular Liquids* **2014**, *192*, 71-76.
(139) Bernardes, C. E. S. AGGREGATES: Finding structures in simulation results of solutions. *Journal of Computational Chemistry* **2017**, *38*, 753-765.
(140) Bernardes, C. E. S.; Minas da Piedade, M. E.; Canongia Lopes, J. N. The Structure of Aqueous Solutions of a Hydrophilic Ionic Liquid: The Full Concentration Range of 1-Ethyl-3-methylimidazolium Ethylsulfate and Water. *The Journal of Physical Chemistry B* **2011**, *115*, 2067-2074.
(141) Simões, R. G.; Melo, P. L. T.; Bernardes, C. E. S.; Heilmann, M. T.; Emmerling, F.; Minas da Piedade, M. E. Linking Aggregation in Solution, Solvation, and Solubility of Simvastatin: An Experimental and MD Simulation Study. *Crystal Growth & Design* **2021**, *21*, 544-551.
(142) Ruocco, G.; Sampoli, M.; Vallauri, R. Analysis of the network topology in liquid water and hydrogen sulphide by computer simulation. *The Journal of Chemical Physics* **1992**, *96*, 6167-6176.

Chapter 2. Methodology and computational details

In this chapter all the details of molecular dynamics simulations are provided. Two approaches for microscopic structure investigations are presented: (i) in terms of radial distribution functions (RDF), running coordination numbers (RCN) and (ii) Voronoi polyhedra (VP) analysis. The former ones were used for the detailed description of ion subsystems in terms ion aggregates. Special attention was paid to the algorithm of calculation of transport properties: viscosity and diffusion.

2.1. Molecular dynamics methodology

MD simulations have been performed at the temperature of 298.15 K. To set the size of the cubic simulation box, a short (i.e., 1 ns) run has been performed on the isothermal-isobaric NPT ensemble at 1 bar. The compositions of each set of systems are given in respective Chapters.

All simulations have been carried out using the GROMACS 2019.4 software package.[1] The temperature and the pressure have been kept constant by means of the velocity-rescaling thermostat[2] with the relaxation time of 0.1 ps, and the Berendsen barostat[3] with the relaxation time of 0.5 ps, respectively. Equations of motion have been integrated using the leap-frog algorithm with a time-step of 0.5 fs. All interactions have been truncated to zero beyond the center-center cut-off distance of 1.2 nm. The long-range part of the electrostatic interaction has been accounted for by the particle mesh Ewald method,[4] while that of the Lennard-Jones interaction has been treated by the conventional shifted force technique. The Lennard-Jones parameters corresponding to unlike pairs of atoms have been calculated by the standard Lorentz-Berthelot combination rules.[5] After equilibrating the systems in the NPT ensemble, simulations of 10 ns have been performed in the NVT ensemble using the equilibrium density determined from the constant pressure run. All set of systems were simulated at least five times from new independent randomly created configuration. The last 1 ns of the trajectory of these simulations have then been used for the detailed structural analyses while full 10 ns trajectories were used for transport properties calculation.

2.2. Microscopic structure

2.2.1. Radial distribution function

A quantitative description of the structure of liquids can be made with the help of radial distribution function (RDF). As a result of the interaction of particles with each other, the position of each particle depends on the location of the others. The correlation between the mutual arrangement of particles is described by the RDF. It is a pair correlation function, which can show how the investigated system is packed with the particles.

A RDF specifies the probability of finding an observed particle at a certain distance from the reference particle for all directions, relative to the uniform density of the observed particle. This uniform density is the density of observed particles that would be present if they were uniformly distributed throughout the simulation cell. Thus, the value of the RDF larger than 1 indicates the higher probability of finding the observed particle at certain distance from reference particle than on average. The RDF usually determined as $g(r)$:[6]

$$g_{ij}(r) = \frac{N_{ij}(r)}{4\pi r^2 \Delta r} \frac{V}{N_j}, \tag{2.1}$$

where r is the distance between particles, $N_{ij}(r)$ is the average number of observed particles j in a sphere with a thickness Δr at the distance of r from the reference particle, N_j is the total number of particles j, V is the volume of the system.

The example of RDF is shown at Figure 2.1, from which several important observations can be made. At very small distances, the value of the $g(r)$ approaches zero, which indicates that the probability of finding a particle at that distance is very low due to the strong repulsive interactions between the particles. This behavior reflects the effective size or diameter of the atoms. Next, there are several peaks that show the most probable distances between observed and reference particles. Usually, the most probable distance between neighbor particles is of most interest. It is equal to the position of the first peak on the RDF. Also, shoulders can appear near the peaks as seen at the example. It indicates

additional probability of location of observed particles regarding to the reference one. In combination with the peaks itself the shoulders can usually give additional information about local organization in investigated systems. Also peaks and shoulders indicate such known “shells” of neighbors – a regions where the two types of particles investigated are packed in some order around each other. The border of such shells can be determined as the respective minimum on the RDF. The occurrence of peaks and shoulders at long range distances indicates a high degree ordering in the investigated system. Lastly, at the very long range every RDF becomes equal to the value of 1, which states for uniform or average density of the observed particle.

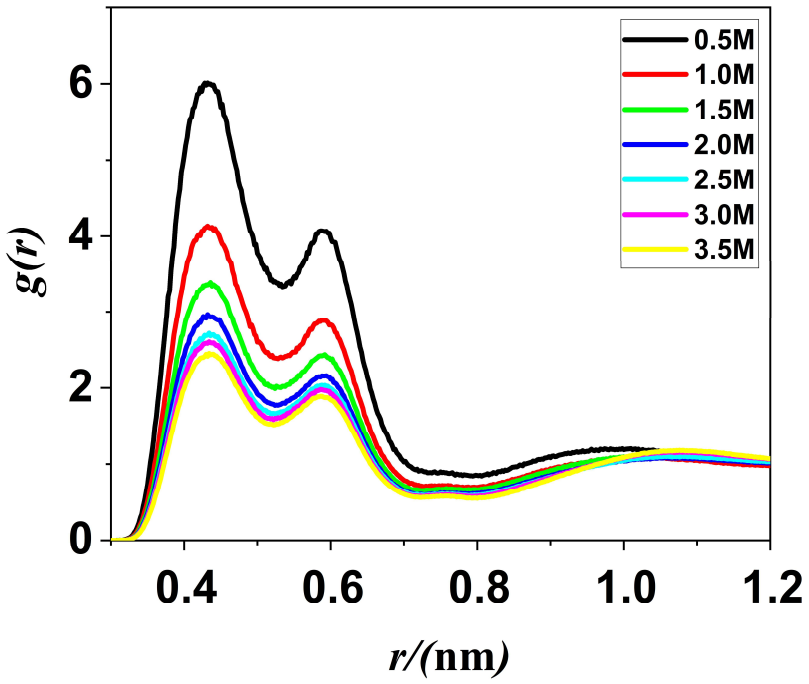

Figure 2.1. Example of cation-anion (N-F) radial distribution function at various molar concentrations of $SBPBF_4$ in AN mixture.

2.2.2. Running coordination number

One of the simplest characteristics of the structure in the liquid along with the RDF is running coordination number (RCN). A RCN shows how many observed particles can be found in certain range around the reference particle. It

can be obtained by integrating $g(r)$ in spherical coordinates to the distance *r*. Thus, the RCN can be determined as $n(r)$:[7, 8]

$$n_{ij}(r) = 4\pi\rho\int_0^r r^2 g_{ij}(r)\,dr. \qquad (2.2)$$

The example of the RCN is shown at Figure 2.2. The observations based on the running coordination number (RCN) heavily rely on the interpretation of the respective RDF due to their definition. The first coordination sphere is limited at the distance of the first minimum on the RDF. The plateaus (or soft incline) at the RCN curve in the same region show the stale composition of particles in the frame of that sphere.

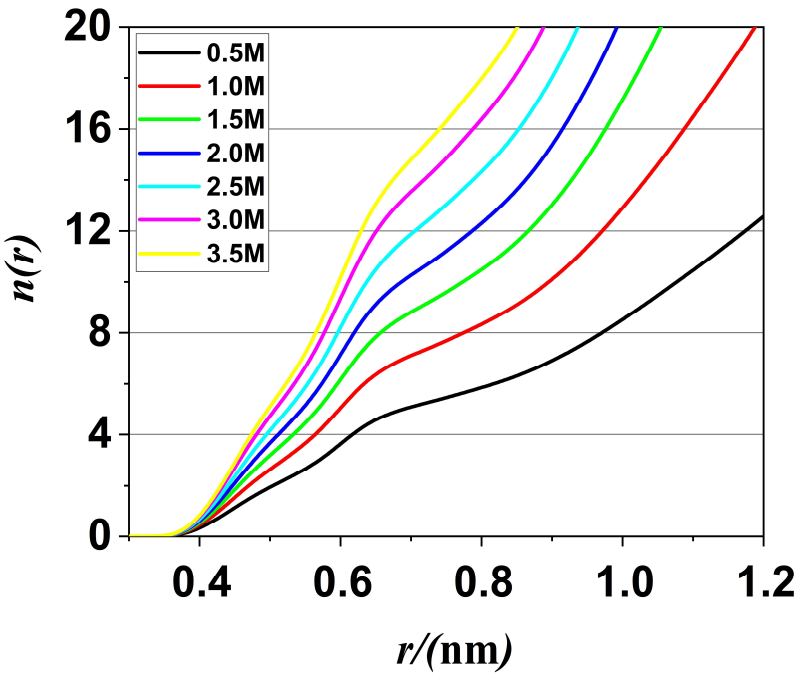

Figure 2.2. Example of cation-anion (N-F) running coordination numbers at various molar concentrations of $SBPBF_4$ in AN mixture.

2.2.3. Aggregate analysis

In order to study the association of ions one should to identify the criterion by which two ions can be considered as a part of one aggregate (or cluster, associate). Such a criterion was proposed in different works[9, 10] as the distance between coordination centers of respective ions. Thus, two ions were considered to belong to the same associate if their respective centers are located at the equal or lower distance that was chosen as a criterion from each other.[11]

After the definition of the criterion, the neighbor list of each cation and anion was determined for each configuration during the simulation at each timestep. The obtained neighbor list was later used to establish the connectivity between ions in the system. Important to note that mainly differently charged ions are coordinating around each other (anions around cations and vice versa). This means that the resulting clusters are constructed from the ions of altering charge that have the distance between them that fulfill the determined criterion.

Finally, the statistical analysis was applied to determine the characteristics of clusters. One of such statistical functions can be a size distribution of the aggregates $P(n)$. It shows the probability of finding an ion in an aggregate of size n:

$$P(n) = \frac{n\sum_{j=1}^{C} A_n(j)}{CN}, \tag{2.3}$$

where $A_n(j)$ is the number of aggregates of size n for a given configuration j, C is the total number of configurations acquired during the simulation, N is the total number of cations and anions combined in the simulation box.

The size distribution of the aggregates $P(n)$ is shown at Figure 2.3. From the graph, it is possible to observe the probability of cluster occurrence in the system for each cluster size. Expanding this picture to the whole concentration range can give the insight into the local organization of ionic subsystem and clusterization processes. In this case size clusters of 1 (isolated ions) and of

numbers close to *N* are the most interesting for the analysis. For example, the domination of clusters of size one can point out the domination of solvation effects over association in the system. If the concentration of ions will increase, the transition from small clusters to large aggregates can occur which specifies the change in the preferable interactions from solvation to the ionic association.

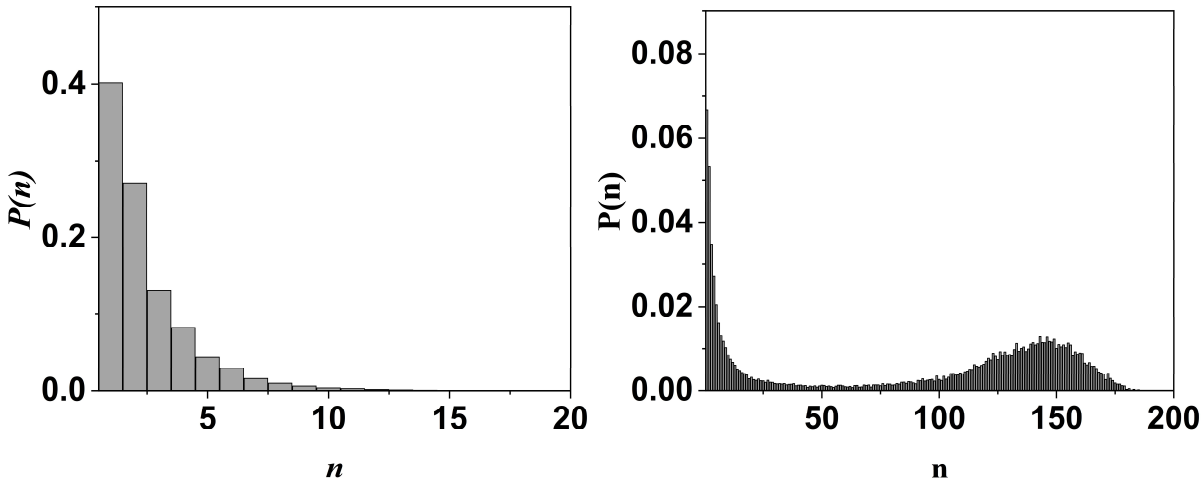

Figure 2.3. Example of probability distributions of aggregate sizes for 0.5 M (left) and 3.0 M (right) concentrations of $SBPBF_4$ in AN mixture with 0.53 nm as a distance criterion.

Aggregate analysis has been performed by AGGREGATES 3.2.0 software package.[12]

To better represent the results of the clusterization the average number of association $\bar{n}$ can be obtained. In general case, one can calculate it as follows:

$$\bar{n} = \sum_{i=1}^{N} n_i P_i(n). \qquad (2.4)$$

2.3. Transport properties

2.3.1. Diffusion coefficient

For microscopic analysis of the translational dynamics of particles in condensed systems, the autocorrelation function (ACF) of the linear velocity *v* of a particle $C_{vv}(t)$ is used:

$$C_{vv}(t) = \langle v(0)v(t) \rangle. \tag{2.5}$$

According to the ergodic hypothesis, the time average for the equilibrium system coincides with the ensemble average. For direct analysis and comparison of particle dynamics, it is more convenient to use the normalized ACF of linear velocity $\overline{C}_{vv}(t)$:

$$\overline{C}_{vv}(t) = \frac{C_{vv}(t)}{\langle v^2(0) \rangle}. \tag{2.6}$$

At the same time, for an equilibrium system, the average square of the speed of particles is related to their mass and average temperature by the ratio:

$$\langle v^2(0) \rangle = \frac{3k_B T}{m}. \tag{2.7}$$

The coefficient of translational self-diffusion of atoms (molecules, ions) in a liquid can be found using the Green-Kubo relation:

$$D = \frac{1}{3}\int_0^\infty C_{vv}(t)\,dt. \tag{2.8}$$

2.3.2. Viscosity

For the viscosity a nonequilibrium periodic perturbation method has been used.[13] To sum it up, molecular dynamic simulation is carried out in the 3D

periodic cell with the external force in x direction $a(z)$. According to the Navier-Stokes's equation:

$$\rho\frac{\partial u}{\partial t}+\rho(u\cdot\nabla)u=\rho a-\nabla p+\eta\nabla^2 u, \tag{2.10}$$

where u is the velocity of the liquid, p is pressure of the fluid, ρ is the density of the fluid, t is time, η is viscosity. Because force is applied only in the x direction, the velocity along y and z will be zero:

$$\rho\frac{\partial u_x(z)}{\partial t}=\rho a_x(z)+\eta\frac{\partial^2 u_x(z)}{\partial z^2}. \tag{2.11}$$

The velocity profile as well as acceleration should be periodic because of the periodic system in the simulations. Thus, the cosine function can be used for this purpose:

$$a_x(z)=\Lambda\cos(kz), \tag{2.12}$$

$$k=\frac{2\pi}{l_z}, \tag{2.13}$$

where l_z is the height of the box, Λ is the acceleration amplitude of the external force. The viscosity then can be obtained:

$$\eta=\frac{\Lambda}{V}\frac{\rho}{k^2}. \tag{2.14}$$

The measured viscosity greatly depends on the parameter Λ. To obtain the viscosity at zero acceleration few viscosities for different accelerations should be

obtained. Then plotting the viscosities versus the amplitudes allows to obtain shear viscosity for Λ=0 via extrapolation.

2.4. Voronoi analysis

In a three-dimensional space of seeds, the Voronoi polyhedral (VP) of a given seed is the locus of the spatial points that are closer to this seed than to any other one.[14, 15] Thus, by calculating the Voronoi tessellation, the space can be unambiguously divided between the seeds. This way, the VP of each seed corresponds to the volume element that belongs to this particular seed. In other words, the volume of a VP represents the space available around its central particle. Conversely, the reciprocal volume of a VP can be the measure of the local density around this particle. Further, considering that the vertices of the VP are the spatial points that are equally far from the four nearest seeds, they mark the centers of the largest spherical voids located between the particles.

In applying the Voronoi analysis for multi-atomic particles, such as the cations, anions, and solvent molecules in the mixtures considered here, the seeds are associated with chosen atoms of these particles.

In performing Voronoi analysis and determining the VP around representative sites of each component of the mixture, the algorithm proposed by Ruocco et al.[16] has been used. To calculate the volume of the VP of a given site, first the vertices pertaining to each face of the polyhedron have been determined and sorted according to their sequence along the perimeter of this face.[17] The VP faces have then been divided to elemental triangles, determined by their first, j^{th} and $(j+1)^{th}$ vertex, and the VP itself has been divided to elemental tetrahedra, one face of which is one of these elemental triangles, and the fourth vertex is the position of the atom around which the VP is centered.[17]

In this study, the following metric properties have been evaluated, X: the volume of the Voronoi polyhedra, V, the local density around the central particle, $\rho = 1/V$, and the radii of the spherical voids between the particles, R, simply as

the distances of the VP vertices from the central atom. For each of these metric quantities, the distribution was calculated, $P(X)$. Further, to characterize the change of the shape of these distributions with the mixture composition, the mean value was also evaluated, $\langle X \rangle$, standard deviation, ΔX, and skewness parameter, $m_{3/2}(X)$ of these quantities. The skewness parameter, characterizing the asymmetry of the distribution, is defined as:[18, 19]

$$m_{3/2} = \frac{M_3}{(M_2)^{3/2}}, \tag{2.14}$$

where M_n is the nth moment of the distribution. The value of this parameter helps to evaluate the asymmetry of the corresponding distribution. Thus, in the case of symmetric distribution, the value of the skewness parameter is unity, values below or above 1 indicate that the distribution extends more to lower (negative skew) or higher (positive skew) values.[18, 19] The composition dependence of these values can shed some additional light to the change of the local structure with the mixture composition. Indeed, in previous papers it was shown that the occurrence of a maximum of the standard deviation of the reciprocal volume as a function of either the temperature or the composition is a signature of large density fluctuation (i.e., occurrence of low and high density domains, where the local density around the particles that are located at the boundary of these domains is fluctuating more than those located at the core of them).[20-22]

Further, the analysis of the VP volume or density distribution when one of the two components (here the IL ions or the solvent) is disregarded in the analysis can provide some additional insight into the self-association of the like components in the mixtures.[17] This way, the VP volume distribution reflects the spatial distribution of the non-disregarded component only, and self-associates of the disregarded component appear as large voids in the analysis.[17] Thus, similarly to the case of one component systems with large density fluctuations,[23] the VP

volume distribution of the non-disregarded component becomes asymmetric, having large standard deviation and positive skewness values when the disregarded component exhibits considerable self-association.[17] For this reason, the distributions of the metric properties were calculated considered (i) taking all the components into account in the analysis, $P^T(X)$, (ii) taking only the cations and anions into account while disregarding the molecular solvent, $P^{CA}(X)$, and finally (iii) taking only the solvent molecules into account while disregarding the cations and anions, $P^S(X)$.

2.5. References for Chapter 2

(1) Abraham, M. J.; Murtola, T.; Schulz, R.; Páll, S.; Smith, J. C.; Hess, B.; Lindah, E. GROMACS: High performance molecular simulations through multi-level parallelism from laptops to supercomputers. *SoftwareX* **2015**, *1-2*, 19-25.
(2) Bussi, G.; Donadio, D.; Parrinello, M. Canonical sampling through velocity rescaling. *The Journal of Chemical Physics* **2007**, *126*, 014101.
(3) Berendsen, H. J. C.; Postma, J. P. M.; Van Gunsteren, W. F.; Dinola, A.; Haak, J. R. Molecular dynamics with coupling to an external bath. *The Journal of Chemical Physics* **1998**, *81*, 3684-3684.
(4) Essmann, U.; Perera, L.; Berkowitz, M. L.; Darden, T.; Lee, H.; Pedersen, L. G. A smooth particle mesh Ewald method. *The Journal of Chemical Physics* **1998**, *103*, 8577-8577.
(5) Allen, P.; Tildesley, D. J. *Computer simulation of liquids*; Clarendon Press, 1987.
(6) Frenkel, D.; Smit, B. *Understanding Molecular Simulation: From Algorithms to Applications*; Elsevier, 2001.
(7) Kondo, K.; Sano, M.; Hiwara, A.; Omi, T.; Fujita, M.; Kuwae, A.; Iida, M.; Mogi, K.; Yokoyama, H. Conductivity and Solvation of Li^+ Ions of $LiPF_6$ in Propylene Carbonate Solutions. *The Journal of Physical Chemistry B* **2000**, *104*, 5040-5044.
(8) Jorn, R.; Kumar, R.; Abraham, D. P.; Voth, G. A. Atomistic Modeling of the Electrode–Electrolyte Interface in Li-Ion Energy Storage Systems: Electrolyte Structuring. *The Journal of Physical Chemistry C* **2013**, *117*, 3747-3761.
(9) Bernardes, C. E. S.; Minas da Piedade, M. E.; Canongia Lopes, J. N. The Structure of Aqueous Solutions of a Hydrophilic Ionic Liquid: The Full Concentration Range of 1-Ethyl-3-methylimidazolium Ethylsulfate and Water. *The Journal of Physical Chemistry B* **2011**, *115*, 2067-2074.
(10) Hanke, C. G.; Lynden-Bell, R. M. A Simulation Study of Water−Dialkylimidazolium Ionic Liquid Mixtures. *The Journal of Physical Chemistry B* **2003**, *107*, 10873-10878.
(11) Marekha, B. A.; Kalugin, O. N.; Idrissi, A. Non-covalent interactions in ionic liquid ion pairs and ion pair dimers: a quantum chemical calculation analysis. *Physical Chemistry Chemical Physics* **2015**, *17*, 16846-16857.
(12) Bernardes, C. E. S. AGGREGATES: Finding structures in simulation results of solutions. *Journal of Computational Chemistry* **2017**, *38*, 753-765.
(13) Hess, B. Determining the shear viscosity of model liquids from molecular dynamics simulations. *The Journal of Chemical Physics* **2002**, *116*, 209-209.
(14) Voronoi, G. Nouvelles applications des paramètres continus à la théorie des formes quadratiques. Deuxième mémoire. Recherches sur les parallélloèdres primitifs. *Journal fur die Reine und Angewandte Mathematik* **1908**, *134*, 198-287.
(15) Okabe, A.; Boots, B.; Sugihara, K.; Chiu, S. N. *Spatial tessellations: concepts and applications of Voronoi diagrams, with a foreword by DG Kendall*; John Wiley & Sons, Ltd., 2000.
(16) Ruocco, G.; Sampoli, M.; Vallauri, R. Analysis of the network topology in liquid water and hydrogen sulphide by computer simulation. *The Journal of Chemical Physics* **1992**, *96*, 6167-6176.
(17) Idrissi, A.; Damay, P.; Yukichi, K.; Jedlovszky, P. Self-association of urea in aqueous solutions: A Voronoi polyhedron analysis study. *The Journal of Chemical Physics* **2008**, *129*, 164512.
(18) Montoro, J. C. G.; Abascal, J. L. F. The Voronoi polyhedra as tools for structure determination in simple disordered systems. *The Journal of Physical Chemistry* **1993**, *97*, 4211-4215.
(19) Gil Montoro, J. C.; Bresme, F.; Abascal, J. L. F. Ionic association in electrolyte solutions: A Voronoi polyhedra analysis. *The Journal of Chemical Physics* **1994**, *101*, 10892-10898.

(20) Idrissi, A.; Vyalov, I.; Damay, P.; Kiselev, M.; Puhovski, Y. P.; Jedlovszky, P. Local structure in sub- and supercritical CO_2: A Voronoi polyhedra analysis study. *Journal of Molecular Liquids* **2010**, *153*, 20-24.
(21) Idrissi, A.; Marekha, B.; Kiselev, M.; Jedlovszky, P. The local environment of the molecules in water-DMSO mixtures, as seen from computer simulations and Voronoi polyhedra analysis. *Physical chemistry chemical physics : PCCP* **2015**, *17*, 3470-3481.
(22) Idrissi, A.; Vyalov, I.; Kiselev, M.; Fedorov, M. V.; Jedlovszky, P. Heterogeneity of the Local Structure in Sub- and Supercritical Ammonia: A Voronoi Polyhedra Analysis. *The Journal of Physical Chemistry B* **2011**, *115*, 9646-9652.
(23) Zaninetti, L. The Voronoi tessellation generated from different distributions of seeds. *Physics Letters A* **1992**, *165*, 143-147.

Chapter 3. Microstructure and transport properties of lithium hexafluorophosphate in binary mixture of dimethyl carbonate with ethylene carbonate from molecular dynamics simulations

Explaining the reason behind the maximum on the conductivity dependence of the concentration of the electrolyte in solutions of Li^+ salts in many solvents is not an easy task. For this purpose, $LiPF_6$ in dimethyl carbonate (DMC) / ethylene carbonate (EC) (1:1) binary mixtures of five different concentrations have been studied with classical MD simulation method. The potential models for DMC and EC molecules were developed as the combination of two different force fields: OPLS-AA and GAFF in order to properly reproduce the diffusion coefficients of pure solvents. The structure has been analyzed in terms of RDFs and RCNs. The results show that Li^+ cation can form contact ion pairs (CIPs) and solvent shared ion pairs (SSIPs) in the solutions. The total coordination number of the cation remains the same at around 5.5-6.0 for all concentrations. EC molecules and PF_6^- anions are competing for the position in the first coordination shell of the cation. The aggregate analysis with two different set of criteria to take into account CIPs and SSIPs formation was performed. For them two different distances were used: minima on the RDFs and the minima on the second derivative of the RCNs. For the second set of criteria the massive aggregation was spotted from the concentration of 1.0 M and higher which in agreement with the experimental conductivity value. Also, the criteria to take SSIPs into account seem to overestimate the aggregation. The diffusion coefficients for all components of the solutions and viscosity of simulated systems were also obtained. The diffusion coefficients for all components are decreasing and viscosity values are non-linearly increasing with the salt concentration increase. These findings and the drastic viscosity increase at 1.0 M and at higher concentrations of $LiPF_6$ are in agreement with the experimental conductivity values.

3.1. Introduction

Lithium-ion batteries are widely used in various portable devices.[1-5] They were leading the technological revolution in the electrochemistry for the last decades. The combination of electrode materials, electrolyte solvents and, of course, salts can hugely impact the battery performance.[5-17] Practical electrolyte should be electrochemically stable, have high ionic conductivity, transference number, good electrochemical and thermal stability, low volatility, flammability, toxicity and be cheap in the production.[18]

Polar organic molecules such as dimethyl carbonate (DMC) and ethylene carbonate (EC) are one of the most common solvents in lithium batteries.[6, 19-21] Binary mixtures of solvents proved to be useful in improving electrolyte behavior for different temperatures and in optimizing electrochemical and physical properties.[22, 23] Electrolytes with EC known to form a stable solid electrolyte interface on anodes that can prevent electrolyte decomposition.[24] EC also has high dielectric constant and relative viscosity. That is why linear DMC with low viscosity and dielectric constant usually paired with the cyclic ester like EC: the overall viscosity of such mixture is lower than of pure EC, the mixture can still dissolve lithium salts because of high dielectric constant of EC and, most importantly, the ionic conductivity of such system improves.[25] As for the salt, $LiPF_6$ has a large dissociation degree in organic carbonate solvents, which results in an excellent ionic conductivity for the electrolyte.

Due to these reasons organic polar electrolytes was studied by variety techniques with the accent on electrochemical application. These studies include such methods as vibrational spectroscopy, X-ray diffraction,[26] photoelectron spectroscopy,[27, 28] neutron scattering,[29] NMR,[30] etc. Although as was mentioned the combination of $LiPF_6$ with carbonate solvents leads to better electroconductivities of such systems, one needs to choose the composition of the components attentively because the conductivity dependence has maximum on the concentration curve.[31-33] One of the most common commercial used solutions

of $LiPF_6$ in DMC/EC (1:1) binary has the peak electrical conductance at 1 M.[33, 34] This maximum usually explained via local structure changes in the solution,[35] although the literature data are of a qualitative nature without a detailed analysis of the contribution of ion aggregation to the formation of a maximum on the concentration curve of electrical conductivity.

In this Chapter, MD simulations are used to obtain microstructural and transport properties for $LiPF_6$ in DMC/EC (1:1) binary mixture of various salt concentration. In addition, the aggregate analysis has been performed to study the features of ionic clusterization in lithium salt solutions. The Chapter is organized as follows. In sec. 2 details of the details of molecular dynamics simulation and force field development for solvent molecules is provided. In sec. 3 the main results are showed and discussed further in the section. In sec. 4 the main conclusions are presented.

3.2. Methodology

3.2.1. Details of molecular dynamics simulation

MD simulations of the $LiPF_6$ and binary mixtures of DMC/EC (1:1) have been performed at five different compositions. To calculate the exact number of the ions and solvent molecules for the MD simulation from the molarities the experimental densities, ρ, of the $LiPF_6$ in DMC/EC (1:1) binary mixture were used.[36, 37] The number of the different particles in cubic box and molar concentration of the $LiPF_6$ in the simulated systems are collected in Table 3.1. The total number of Li^+ cations and PF_6^- anions were always equal to 100.

Two systems of pure solvents (DMC and EC) were also simulated (with the number of molecules of 500 for each). Pure EC system was simulated at the temperature of 313.15 K because at 298.15 K this solvent is solid substance.

All simulations were performed as described in Chapter 2.

Table 3.1. The composition of the simulated systems of $LiPF_6$ in DMC/EC (1:1) binary mixture.

$LiPF_6$ concentration	Number of Li^+	Number of PF_6^-	Number of DMC	Number of EC	ρ,[36, 37] g/cm^3
0.1 M			6707	6707	1.21
0.5 M			1318	1318	1.25
1.0 M	100	100	664	664	1.29
1.5 M			420	420	1.33
2.0 M			308	308	1.36

3.2.2. Force field refinement

The structure of the PF_6^- anion and DMC and EC solvent molecules along with the atomic labeling scheme is shown at Figure 3.1.

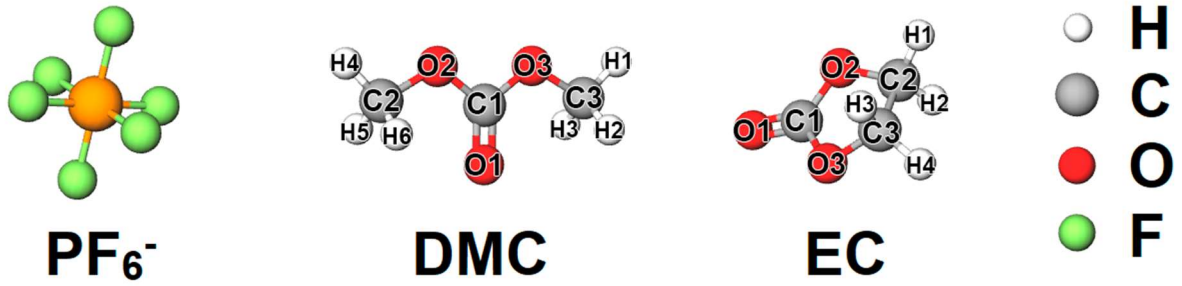

Figure 3.1. Structure of the PF_6^- anion and molecular solvents of DMC and EC. The labeling of solvent molecules used in potential models is also shown.

For the Li^+ the potential model directly from OPLS-AA[38] has been used.

For the PF_6^- anion the potential model from Canongia Lopes et al.[39] was taken.

As a first step the LigParGen[40] was used to develop Lennard-Jones (LJ) parameters, as well as bond, angle, and dihedral angle parameters based on the OPLS-AA[38, 41, 42] force field for both DMC and EC.

In current study according potential models have the following functional form of the total potential energy:

$$U_{tot} = \sum_{ij}^{bonds} \frac{k_{r,ij}}{2}\left(r_{ij} - r_{0,ij}\right)^2 + \sum_{ijk}^{angles} \frac{k_{\theta,ijk}}{2}\left(\theta_{ijk} - \theta_{0,ijk}\right)^2 + \sum_{ijkl}^{dihedral} \sum_{n=0}^{5} C_n \left(\cos\left(\psi_{ijkl}\right)\right)^n + \\ + \sum_{ijkl}^{improper} k_{\phi,ijkl}\left(1 + \cos\left(n\phi_{ijkl} - \phi_{s,ijkl}\right)\right) + \sum_{ij}^{nonbonded} \left(4\varepsilon_{ij}\left[\left(\frac{\sigma_{ij}}{r_{ij}}\right)^{12} - \left(\frac{\sigma_{ij}}{r_{ij}}\right)^{6}\right] + \frac{q_i q_j}{4\pi\varepsilon_0 r_{ij}} \right), \quad (3.1)$$

where k is the force constant for bond stretching (r), angle bending (θ), proper and improper dihedral (ϕ), respectively, ε and σ are the Lennard-Jones energy and the distance parameters, respectively, and q stands for the fractional charges of the interaction sites. For proper dihedral $\psi_{ijkl} = 180^o - \phi_{ijkl}$.

Optimization of the geometry and calculation of partial charges of atoms was carried out using the software package Gaussian16[43] at M062X-AUG\-cc-PVTZ level. The algorithm for calculating partial atomic charges according to Breneman was applied.[44, 45] The charges obtained are presented in the Table 3.2.

But the results for diffusion coefficients of these potential models in pure solvents are much lower than the experimental ones. For pure DMC diffusion coefficient, D, was equal to $1.5 \cdot 10^{-5}$ cm/s^2, for pure EC – $0.5 \cdot 10^{-5}$ cm/s^2. Experimental values are $2.6 \cdot 10^{-5}$ cm/s^2 (at 303 K) and $0.8 \cdot 10^{-5}$ cm/s^2 respectively.

In order to improve the results for the solvent potential models and to reproduce transport properties of pure molecular liquids the OPLS-AA models were modified. Lowering the effective molecule radius can improve the diffusion coefficients. Thus, the Lennard-Jones parameters of H atoms of DMC and EC were replaced with the GAFF force field ones.[46, 47] The GAFF ε parameter is almost two times lower than such of OPLS-AA force field. This approach can give transport properties closer to the experimental ones. The Lennard-Jones parameters and charges of the DMC and EC are shown in the Table 3.2.

Table 3.2. Charge distribution, q, Lennard-Jones parameters, σ and ε, intramolecular parameters, k_i, for DMC and EC. Asterisk represents the Lennard-Jones parameters of the GAFF for H atoms that replaced the original ones.

	DMC		EC	
Charge	q, e		q, e	
O^1	-0.597267		-0.563993	
O^{2-3}	-0.449998		-0.396963	
C^1	1.004995		0.878357	
C^{2-3}	0.098148		0.167807	
H^1	0.035715		0.035874	
H^2	0.035720		0.036100	
H^3	0.076551		0.035878	
H^4	0.035718		0.036096	
H^5	0.035717			
H^6	0.076551			
Atom	σ, nm	ε, kJ/mol	σ, nm	ε, kJ/mol
O^1	0.296	0.87864	0.296	0.87864
O^{2-3}	0.290	0.58576	0.290	0.58576
C^1	0.355	0.29288	0.355	0.29288
C^{2-3}	0.350	0.276144	0.350	0.276144
H^{1-4}			0.250 (0.2471)*	0.12552 (0.065693)*
H^{1-6}	0.250 (0.2471)*	0.12552 (0.065693)*		
Bond	r_0, nm	k_r, kJ/(mol·nm^2)	r_0, nm	k_r, kJ/(mol·nm^2)
C^1-O^1	0.1229	476976.0	0.1229	476976
C^1-O^{1-2}	0.1327	179075.2	0.1327	179075.2
C^2-C^3			0.1529	224262.4
C^2-O^2	0.141	267776.0	0.141	267776.0
C^3-O^3	0.141	267776.0	0.141	267776.0
C^2-H^{1-2}			0.109	284512.0
C^2-H^{1-3}	0.109	284512.0		
C^3-H^{3-4}			0.109	284512.0
C^3-H^{4-6}	0.109	284512.0		
Angle	θ_0, deg	k_θ, kJ/(mol·rad^2)	θ_0, deg	k_θ, kJ/(mol·rad^2)
O^1-C^1-O^{1-2}	123.4	694.544	123.4	694.544
C^1-O^2-C^2	116.9	694.544	116.9	694.544
C^1-O^3-C^3	116.9	694.544	116.9	694.544
C^2-C^3-O^3			109.5	418.4
C^3-C^2-O^3			109.5	418.4
C^2-C^3-H^{3-4}			110.7	313.8
C^3-C^2-H^{1-2}			110.7	313.8
O^2-C^1-O^3	118.18	584.923	118.18	584.923

Table 3.2 continued

O^2-C^2-H^{1-2}				109.5	292.88	
O^2-C^2-H^{1-3}	109.5	292.88				
O^3-C^3-H^{3-4}				109.5	292.88	
O^3-C^3-H^{4-6}	109.5	292.88				
H^1-C^2-H^2	107.8	276.144		107.8	276.144	
H^3-C^2-H^{1-2}	107.8	276.144				
H^3-C^3-H^4				107.8	276.144	
H^4-C^3-H^5	107.8	276.144				
H^6-C^3-H^{4-5}	107.8	276.144				
Improper	ϕ_s, deg	k_ϕ, kJ/mol	n	ϕ_s, deg	k_ϕ, kJ/mol	n
O^1-O^2-C^1-O^3	180.0	43.932	2			
O^3-C^1-O^1-O^2				180.0	43.932	2
Dihedral	C_0, kJ/mol	C_1, kJ/mol	C_2, kJ/mol	C_3, kJ/mol	C_4, kJ/mol	C_5, kJ/mol
			DMC			
C^1-O^2-C^2-H^{1-3}	0.414	1.243	0.0	-1.657	0.0	0.0
C^1-O^3-C^3-H^{4-6}	0.414	1.243	0.0	-1.657	0.0	0.0
O^1-C^1-O^2-C^2	21.439	0.0	-21.439	0.0	0.0	0.0
O^1-C^1-O^3-C^3	21.439	0.0	-21.439	0.0	0.0	0.0
C^2-O^2-C^1-O^3	31.206	-9.768	-21.439	0.0	0.0	0.0
C^3-O^3-C^1-O^2	31.206	-9.768	-21.439	0.0	0.0	0.0
			EC			
C^1-O^2-C^2-O^3	-2.197	5.201	0.527	-3.531	0.0	0.0
C^1-O^3-C^3-O^2	-2.197	5.201	0.527	-3.531	0.0	0.0
C^1-O^2-C^2-H^{1-2}	0.414	1.243	0.0	-1.657	0.0	0.0
C^1-O^3-C^3-H^{3-4}	0.414	1.243	0.0	-1.657	0.0	0.0
O^1-C^1-O^2-C^2	21.439	0.0	-21.439	0.0	0.0	0.0
O^1-C^1-O^3-C^3	21.439	0.0	-21.439	0.0	0.0	0.0
C^2-O^2-C^1-O^3	31.206	-9.768	-21.439	0.0	0.0	0.0
C^3-O^3-C^1-O^2	31.206	-9.768	-21.439	0.0	0.0	0.0
O^2-C^2-C^3-O^3	-1.151	1.151	0.0	0.0	0.0	0.0
O^2-C^2-C^3-H^{3-4}	0.979	2.937	0.0	-3.916	0.0	0.0
O^3-C^3-C^2-H^{1-2}	0.979	2.937	0.0	-3.916	0.0	0.0
H^{1-2}-C^2-C^3-H^{3-4}	0.628	1.883	0.0	-2.51	0.0	0.0

The obtained results for density, self-diffusion coefficient and enthalpy of vaporization for systems of pure solvents in the comparison with the experimental data are shown in the Table 3.3. For the potential models with the H parameters from GAFF the results are close to the experimental values. For further MD simulations these modified potential models were selected.

Table 3.3. Observed density, ρ, self-diffusion coefficient, D, and enthalpy of vaporization, ΔH_{vap}, and share viscosity, η, calculated at 298.15 K for DMC and at 313.15 K for EC in comparison with the results obtained through experimental measurements.

	DMC (298.15 K)		**EC** (313.15 K)	
Property	MD	Exp.	MD	Exp.
ρ, g/dm^3	1038	1057[48]	1294	1321[48]
D·10^5, cm^2/s	2.2	2.6[49,a]	0.6	0.8[49]
ΔH_{vap}, kJ/mol	35.5	38.0[50]	54.8	60[51]

a – for 303 K.

3.3. Results and discussion

3.3.1. Structural properties

Structural properties of $LiPF_6$ in DMC/EC (1:1) binary mixture were analyzed in terms of radial distribution functions (RDF) and running coordination numbers (RCN). For all RDFs the center atom P of anion as well as most electronegative atom of solvent (the carbonyl O atom for DMC and EC) has been chosen for the analysis.

The cation-anion RDFs for all systems are presented in Figure 3.2. Here similar curves for all of the concentrations of $LiPF_6$ in DMC/EC binary mixture can be seen. The first high sharp peak indicates a structured first coordination shell with maximum at approximately 0.34 nm. It corresponds to the classical MD simulation results with a polarizable force field of $LiPF_6$ in DMC/EC.[48] The small shoulder on all curves with its local maximum near 0.29 nm can be detected. This indicates the occurrence of different mutual cation-anion configuration at these Li-P distance values. The example of cation-anion relative disposition at these distances was obtained from GROMACS trajectory files via VMD program package[52] and shown at Figure 3.3. The first maximum of RDFs here (0.34 nm)

corresponds to the monodentate linkage of the anion to the cation when Li^+ is close to only one of the F atoms of anion. Thus, the local maximum of shoulder (0.29 nm) corresponds to the position of anion when Li^+ is close to two or even three F atoms of anion at the same time (bidentate and tridentate linkage respectively). The first minimum of RFDs is approximately at 0.45 nm.

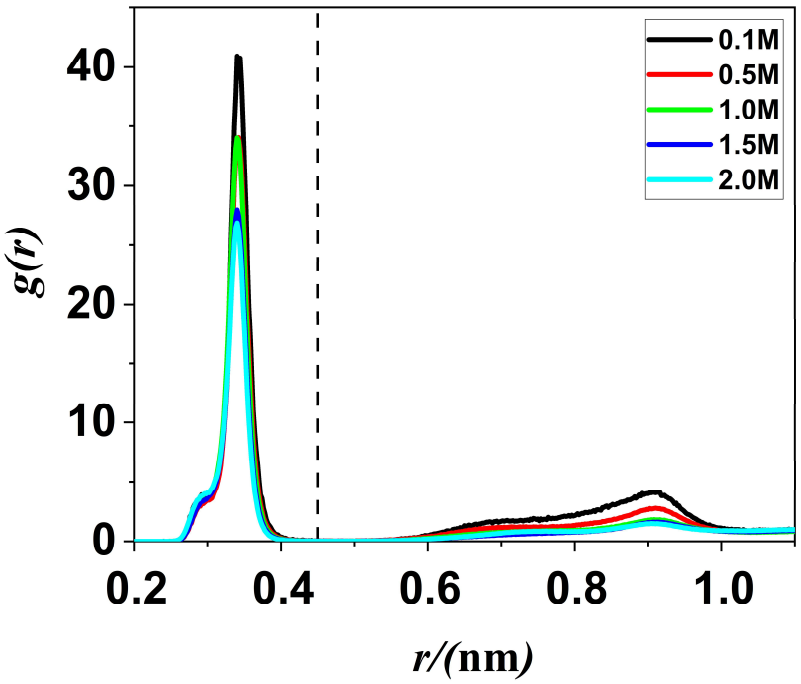

Figure 3.2. Cation-anion (Li-P) radial distribution functions at various molar concentrations of $LiPF_6$ in DMC/EC (1:1) binary mixture. The vertical dashed line corresponds to the first coordination shell.

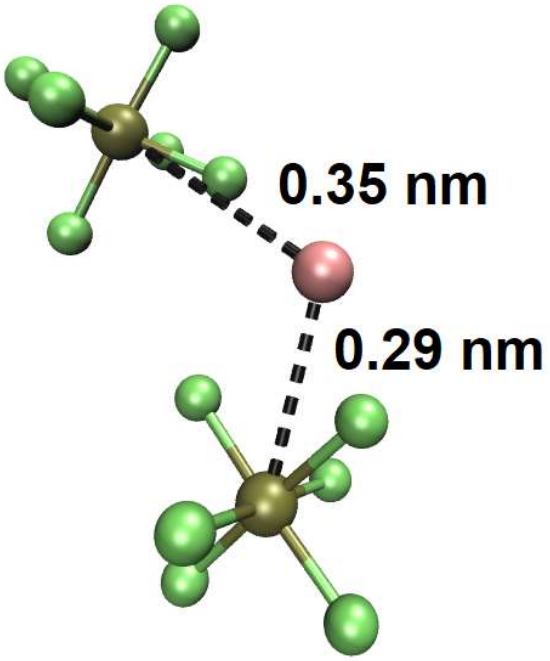

Figure 3.3. Example of $(Li(PF_6)_2)^-$ associate with monodentate (0.35 nm) and bidentate (0.29 nm) linkage of the anion to the cation. The respective Li-P distances are shown as well.

As was stated in the literature, contact ion pairs (CIP) and solvent shared ion-pair (SSIP) may occur in the solutions of lithium salts.[33, 53, 54]The latter are formed when the solvent molecule (DMC or EC for investigated solutions) is located between cation and anion. After the first minimum all of the RDFs have wide plateau until approximately 0.6 nm, and second maximum occurs only at 0.91 nm, second minimum – at 1.04 nm. The wide region, related to the formation of SSIPs, of uncertain position of PF_6^- anion relatively to Li^+ cation (0.6 nm – 1.0 nm on RDFs) can be explained with the packing of solvent molecules around the cation. It was proposed that solvent molecules are arranged around the Li^+ cation in a way that leaves large holes between them. The anions can penetrate into these empty spaces quite closely to the cation.[33, 53, 54] Similar phenomenon can be observed in our investigation. The example of such configuration if shown at Figure 3.4. The height of each peak at RDF decreases with the increase of the salt concentration.

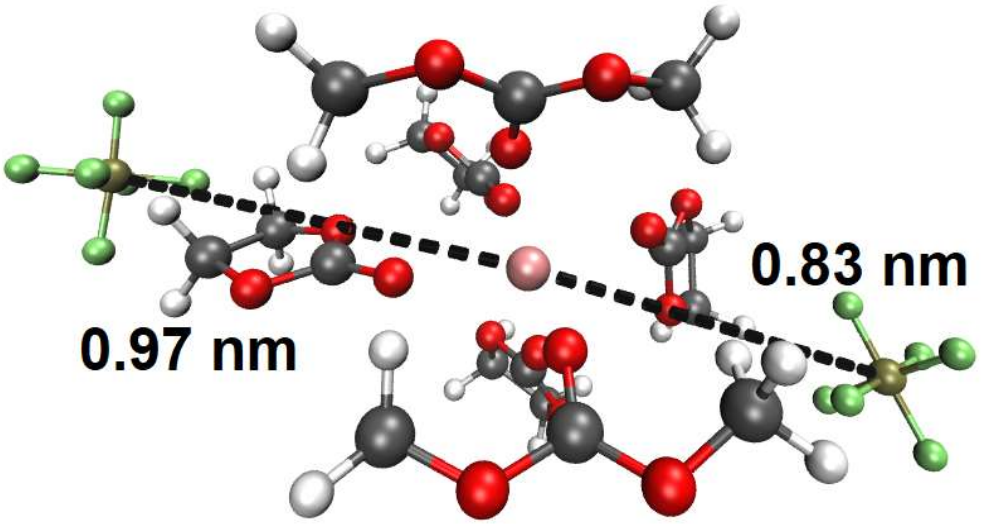

Figure 3.4. Example of cation coordination shell with two anions that formed solvent-shared pairs. The respective Li-P distances are shown as well.

To further prove this point, the RDFs between Li^+ and carbonyl O atoms of solvents DMC and EC for all concentrations were obtained (Figures 3.5. and 3.6.).

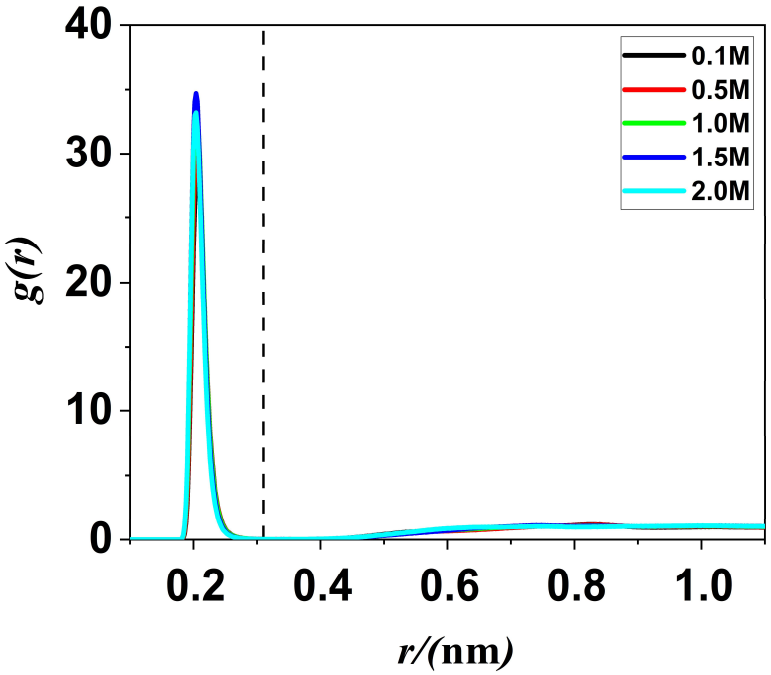

Figure 3.5. Cation-solvent ($Li\text{-}O_{DMC}$) radial distribution functions at various molar concentrations of $LiPF_6$ in DMC/EC (1:1) binary mixture. The vertical dashed line corresponds to the first solvation shell.

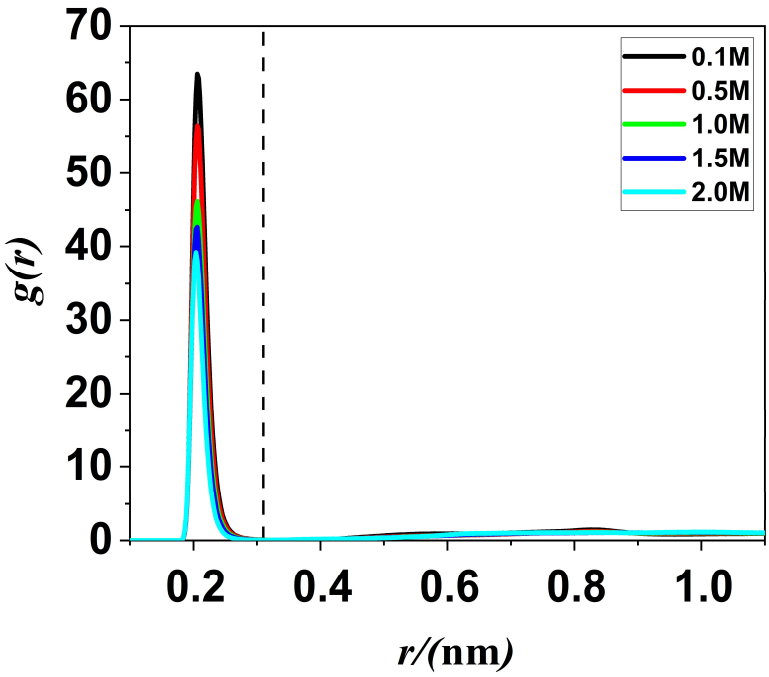

Figure 3.6. Cation-solvent (Li-O_{EC}) radial distribution functions at various molar concentrations of $LiPF_6$ in DMC/EC (1:1) binary mixture. The vertical dashed line corresponds to the first solvation shell.

All positions at curves are remained unchanged at different concentrations as with the cation-anion RDFs discussed earlier. Thin sharp first peaks without any shoulders at both cation-solvent RDFs can be observed that indicate the structured first solvation shell. The first maxima of RDFs are at approximately 0.20 nm as well as first minima at 0.31 nm for both solvents. This agrees well with time-of-flight neutron diffraction measurements for $LiPF_6$ in PC with Li-O peak at approximately 0.20 nm.[29] Similar peaks from MD simulations for lithium salts in DMC, EC or PC have value of 0.19-0.20 nm.[48, 55-58] The heights of the Li-O_{DMC} curves almost do not change with the concentration increase of the salt while Li-O_{EC} curves' heights become lower.

The RCNs for relative interactions of Li-P, Li-O_{DMC} and Li-O_{EC} are shown at Figures 3.7-3.9 respectively.

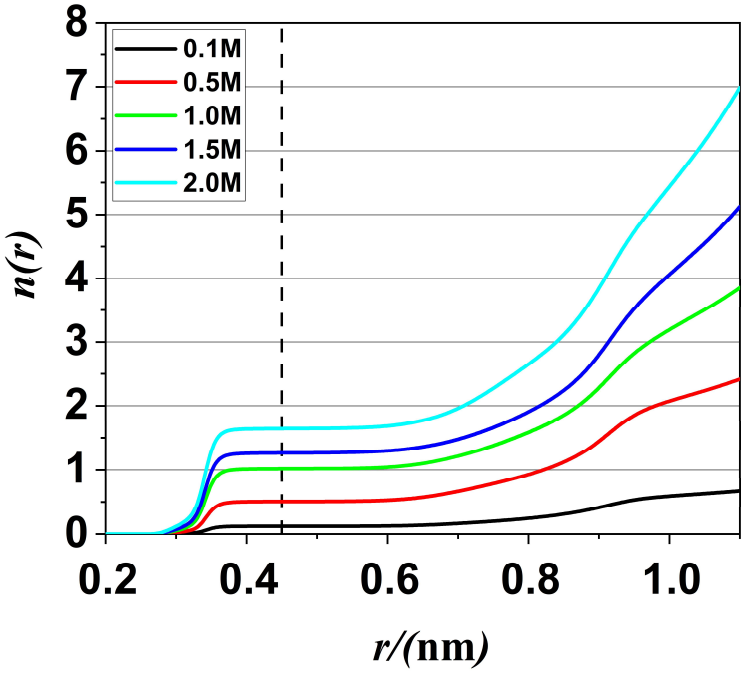

Figure 3.7. Cation-anion (Li-P) running coordination numbers at various molar concentrations of $LiPF_6$ in DMC/EC (1:1) binary mixture. The vertical dashed line corresponds to the first coordination shell.

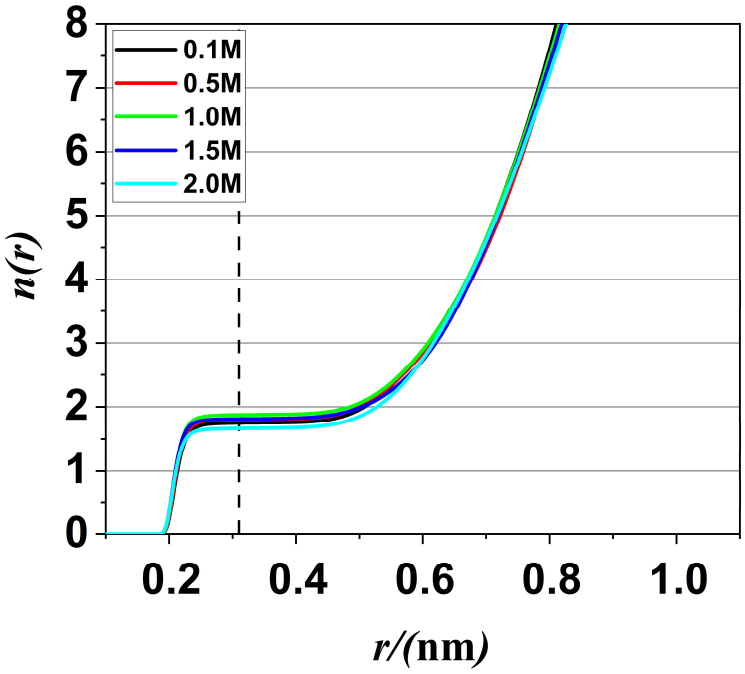

Figure 3.8. Cation-solvent (Li-O_{DMC}) running coordination numbers at various molar concentrations of $LiPF_6$ in DMC/EC (1:1) binary mixture. The vertical dashed line corresponds to the first solvation shell.

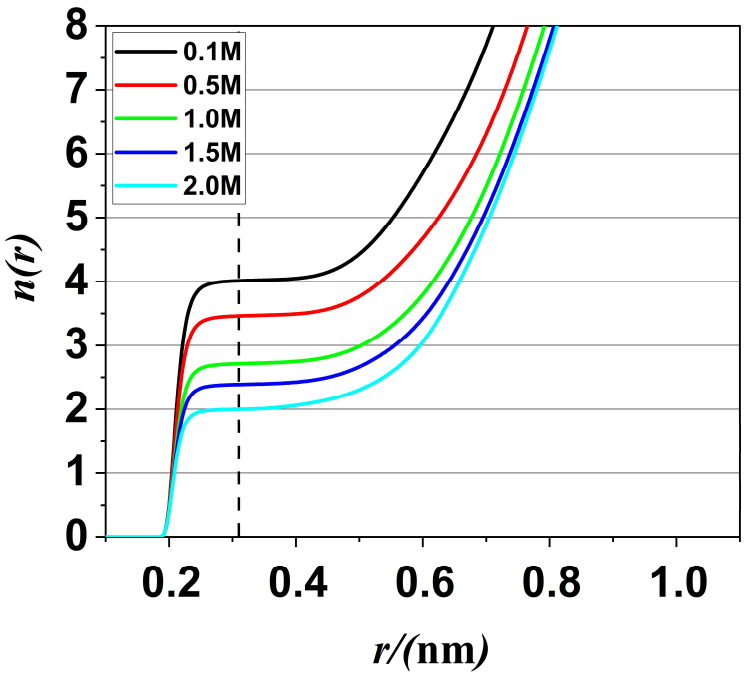

Figure 3.9. Cation-solvent (Li-O_{EC}) running coordination numbers at various molar concentrations of $LiPF_6$ in DMC/EC (1:1) binary mixture. The vertical dashed line corresponds to the first solvation shell.

It was expected that the coordination numbers for cation-solvent interaction will decrease while the cation-anion ones will increase with the increasing of the $LiPF_6$ concentration. The EC carbonyl O atoms are competing with the PF_6^- anions for the coordination with the Li^+ cation. But in the case of DMC its number is independent of the concentration of the salt. It remains ~1.8 for all systems while for Li-P it increases from 0.1 to 1.6 and for EC it decreases from 4 to 2 with the increasing of $LiPF_6$ concentration in DMC/EC binary mixture. This is caused by higher molecular dipole moment of EC comparing to DMC. Also, EC molecule is smaller and can be packed more efficiently in the Li^+ first coordination sphere than wide and linear DMC. The average total coordination number remains 5.5-6.0 regardless of the concentration. These results are in agreement with previous MD simulations.[59]

3.3.2. Aggregate analysis

To analyze the formation of the aggregates on the solution two distance criteria are proposed. The first is the first minimum in cation-anion RDF (0.45 nm, Figure 3.2) which indicates the first coordination sphere around the Li^+ cation. The second criterion was determined by the minimum at the second derivative of cation-anion RCN (0.35 nm, Figure 3.10). This value shows the distance at which the RCN curve comes into plateau regime at which the coordination number have almost no change at all. Further in the Chapter they will be referred to as the first set of criteria.

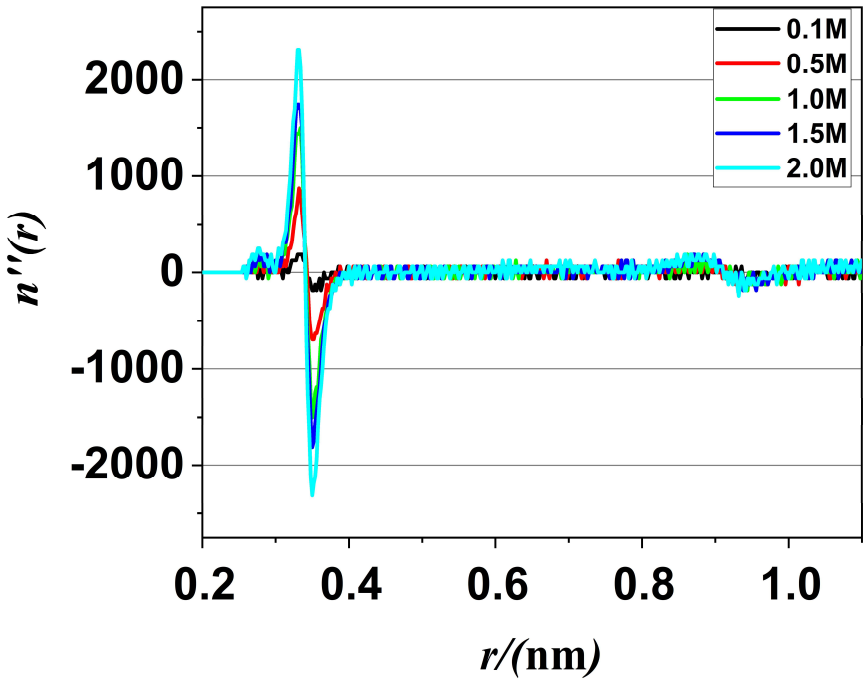

Figure 3.10. Second derivatives of cation-anion (Li-P) running coordination numbers at various molar concentrations of $LiPF_6$ in DMC/EC (1:1) binary mixture.

As mentioned in sec. 3.3.1, the Li^+ cation has very strong cation-solvent interaction to the point that EC and DMC molecules are dominating its first coordination sphere. Also, as were discussed, Li^+ cation can form SSIPs with anions. Thus, it is necessary to investigate this type of ion pairing in these systems.

For the second set of criteria the second minimum on cation-anion RDF (1.04 nm, Figure 3.2) was chosen as well as the second minimum on the second derivative of cation-anion RCN graphs (0.93 nm, Figure 3.10). Further in this Chapter they will be referred to as the second set of criteria. The results of the association analysis can be found in Figures 3.11 and 3.12.

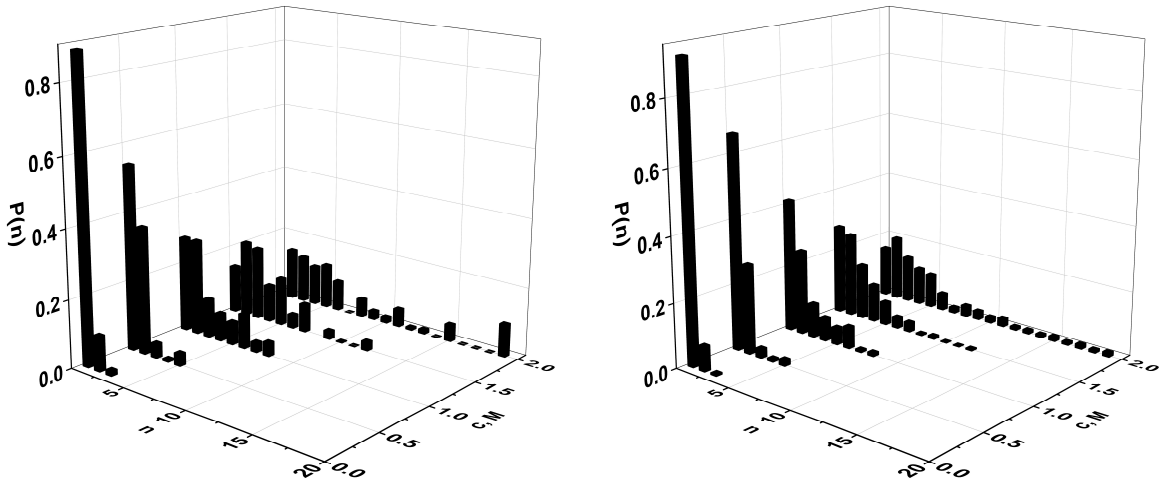

Figure 3.11. Probability distributions of aggregate sizes of the first set of criteria with respective first (left) and second (right) criterion at various molar concentrations of $LiPF_6$ in DMC/EC (1:1) binary mixture.

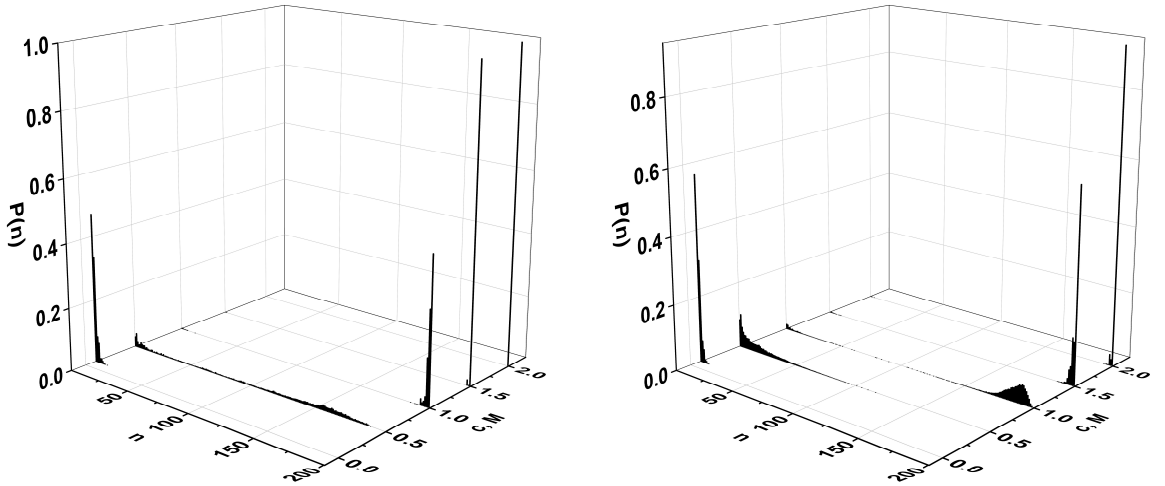

Figure 3.12. Probability distributions of aggregate sizes of the second set of criteria with respective first (left) and second (right) criterion at various molar concentrations of $LiPF_6$ in DMC/EC (1:1) binary mixture.

For the first set the results are pretty similar for both criteria chosen. The ions are mostly isolated from each other in 0.1 M solution of $LiPF_6$ in DMC/EC (1:1) binary mixture. With the increasing of the salt concentration, one can see that more and more aggregates of different sizes start to appear. Nevertheless, at the 2.0 M concentration still the size of biggest ionic associate is 19 for both criteria. This fact ones again proves the strong solvation effect comparing to the association which is still not dominant even at high concentrations of salt.

For the second set of criteria the ions mostly are isolated or are in small clusters in 0.1 M solution of $LiPF_6$ in DMC/EC (1:1) binary mixture. With the increasing of the salt concentration more and more aggregates of different sizes start to appear. For 0.5 M the so-called “transition” state appears for the first criterion that is defined by numerous aggregates of different sizes in solution at the same time. It indicates that the system will form a network of solvent-shared ion pairs with the further salt concentration increase. Indeed, at 1.0 M almost all of the ions are part of this aggregation network for both criteria. At 2.0 M all ions in the system are forming one large aggregate.

To illustrate the general result among all concentrations for both set of criteria the average number of associations were obtained (Figure 3.13). For the first set it can be seen that both criteria are similar in their values. Also, there are not any massive association processes indicated in the systems for all concentrations of $LiPF_6$. For the second set of criteria the massive aggregation can be seen beginning from the 1.0 M $LiPF_6$ concentration.

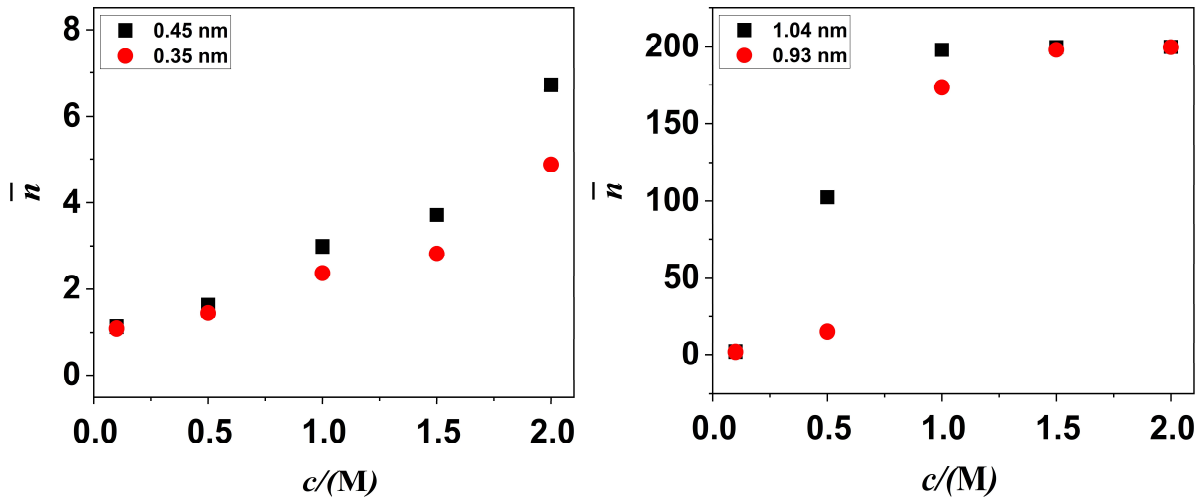

Figure 3.13. Average numbers of association of the second set of criteria with respective first (left) and second (right) criterion at various molar concentrations of $LiPF_6$ in DMC/EC (1:1) binary mixture.

The ionic conductivity is related to the effective concentration of the charge carriers in the solution according to the Nernst-Einstein relation.[60] The formation of CIPs and SSIPs in the solution and the formation of the ionic clusters as a result reduces the number of charge carriers and thus lowers conductivity. That is why the concentration at which the massive clusterization of ions in aggregate analysis occurs for the second set of criteria is close to the concentration at which the experimental conductivity has maximum at its curve.[33]

Also, it should be stated that the second set of criteria in the analysis overvalues the distance to take SSIPs into account as can be seen at Figure 3.12 and 3.13. If all (or almost all) the ions are part of one aggregate, the concentration of effective charge carriers should be very low, to the point where no conductivity should be observed.

3.3.3. Transport properties

The transport properties were studied in terms of diffusion coefficients of all the components of the $LiPF_6$ in DMC/EC binary mixture systems as well as their shear viscosity. The obtained values are presented at Figure 3.14.

Here it is seen the decreasing of all diffusion coefficients as the concentration of $LiPF_6$ increases from 0.1 M to 2.0 M. Also, it can be seen that diffusion coefficients of solvent molecules are approximately two times larger than of ions. The values of coefficients for both solvents are similar to each other with less solvated DMC being higher.

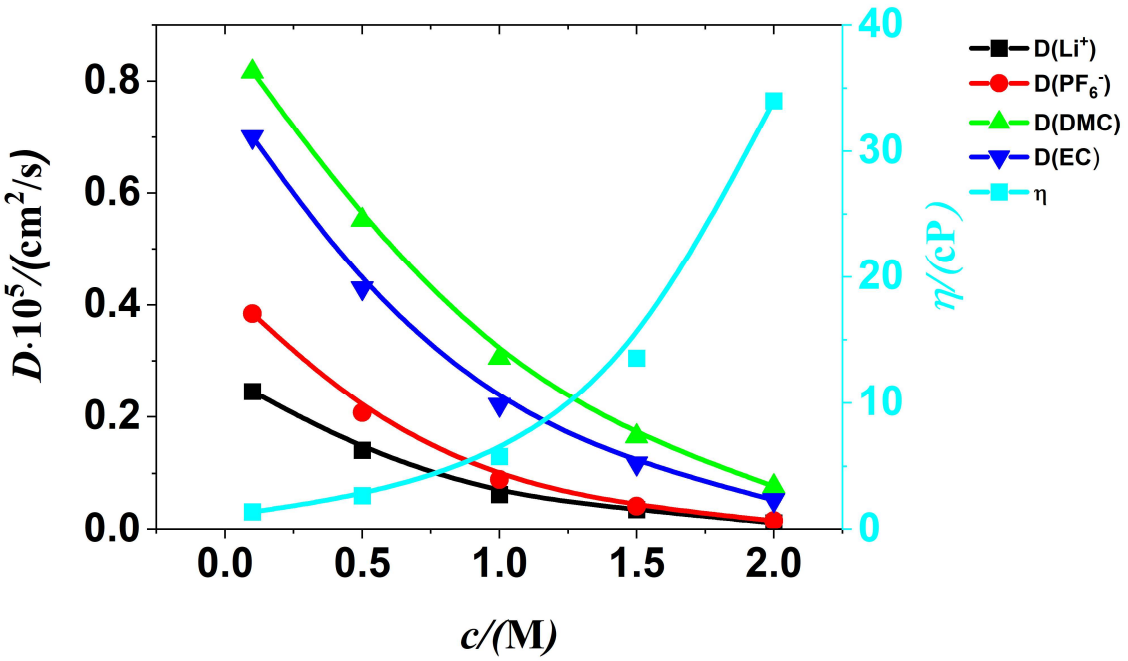

Figure 3.14. Diffusion coefficients for cation, anions and solvent molecules and viscosity values at various molar concentrations of $LiPF_6$ in DMC/EC (1:1) binary mixture.

Simultaneously, the viscosity of the system increases according to a non-linear dependence and at highest concentrations investigated it reaches rather huge values of ~35 cP. These results approve the appearing of the large cluster in the simulated system with the formation of SSIPs in solution beginning after the 1.0 M concentrations of $LiPF_6$ after which the viscosity is drastically changes.

Diffusion coefficients of ions is one of the factors that affects the electric conductivity as stated by Nernst-Einstein relation.[60] Diffusion coefficients decrease together with the drastic non-linear increase of the viscosity at nearly 1.0 M of $LiPF_6$ concentration confirms the presence of the maximum of experimental electroconductivity at this concentration value.[33]

3.4. Conclusions

In the present Chapter $LiPF_6$ in DMC/EC (1:1) binary mixture solutions of five different concentrations have been studied with classical MD simulation technique. The potential models for DMC and EC molecules were optimized in this work from the combination of two different force fields: OPLS-AA and GAFF in order to properly reproduce the transport properties of these solvents.

The structure has been analyzed in terms of cation-anion and cation-solvent RDFs and RCNs. The snapshot from the trajectory files of the simulation confirmed the RDF and RCN data and shoved that Li^+ cations tend to form contact ion pairs as well as solvent-shared ion pairs.

The RCNs showed that total coordination number of the cation for the first coordination sphere remains 5.5-6.0 for all concentrations. In particular, for DMC it remains ~1.8, while for EC it decreases from 4 to 2 and for PF_6^- anion it increases from 0.1 to 1.6 with the increasing of the salt concentration. This indicates that EC solvent and anions are competing for the position in first coordination sphere.

For the ionic aggregate analysis two set of criteria were proposed (based on the fact of formation of CIPs and SSIPs). For them two different distances were used: minima on the RDFs and the minima on the second derivative of the RCNs. As with the first set of criteria only small aggregates were spotted in the system, the previous statement was confirmed that $LiPF_6$ give preference to formation of solvent-shared ion pairs in DMC/EC (1:1) binary mixtures. The massive aggregation for the second set of criteria was spotted beginning from the concentration of 1.0 M for both criteria. The results for distances of minimum on the RDFs or minimum on the second derivative on the RCNs are not differ significantly. Also, the distances taken for the second set of criteria seem to overestimate the aggregation.

Lastly, the transport properties of simulated systems were obtained. The diffusion coefficients for all components are decreasing and viscosity values are

non-linearly increasing with the salt concentration increase. The drastic non-linear increase of the viscosity from nearly 1.0 M and for higher concentrations of $LiPF_6$ also occurs. These findings are consistent with the maximum of experimental electroconductivity at this concentration value.

3.5. References for Chapter 3

(1) Wang, Y.; Liu, B.; Li, Q.; Cartmell, S.; Ferrara, S.; Deng, Z. D.; Xiao, J. Lithium and lithium ion batteries for applications in microelectronic devices: A review. *Journal of Power Sources* **2015**, *286*, 330-345.
(2) Liu, J.; Liu Pacifi, J. Addressing the Grand Challenges in Energy Storage. *Advanced Functional Materials* **2013**, *23*, 924-928.
(3) Liang, Y.; Zhao, C. Z.; Yuan, H.; Chen, Y.; Zhang, W.; Huang, J. Q.; Yu, D.; Liu, Y.; Titirici, M. M.; Chueh, Y. L.; et al. A review of rechargeable batteries for portable electronic devices. *InfoMat* **2019**, *1*, 6-32.
(4) Chapter 2 - Characteristics of Batteries for Portable Devices. In *Batteries for Portable Devices*, Pistoia, G. Ed.; Elsevier Science B.V., 2005; pp 17-27.
(5) Pistoia, G. APPLICATIONS – PORTABLE | Portable Devices: Batteries. In *Encyclopedia of Electrochemical Power Sources*, Garche, J. Ed.; Elsevier, 2009; pp 29-38.
(6) Xu, K. Nonaqueous liquid electrolytes for lithium-based rechargeable batteries. *Chem Rev* **2004**, *104*, 4303-4417.
(7) Julien, C.; Mauger, A.; Vijh, A.; Zaghib, K. *Lithium Batteries: Science and Technology*; Springer Cham, 2016.
(8) Whittingham, M. S. Lithium batteries and cathode materials. *Chem Rev* **2004**, *104*, 4271-4301.
(9) Ye, X.; Wu, J.; Liang, J.; Sun, Y.; Ren, X.; Ouyang, X.; Wu, D.; Li, Y.; Zhang, L.; Hu, J.; et al. Locally Fluorinated Electrolyte Medium Layer for High-Performance Anode-Free Li-Metal Batteries. *ACS Appl Mater Interfaces* **2022**, *14*, 53788-53797.
(10) Nam, K. H.; Jeong, S.; Yu, B. C.; Choi, J. H.; Jeon, K. J.; Park, C. M. Li-Compound Anodes: A Classification for High-Performance Li-Ion Battery Anodes. *ACS Nano* **2022**, *16*, 13704-13714.
(11) Wu, F.; Yushin, G. Conversion cathodes for rechargeable lithium and lithium-ion batteries. *Energy & Environmental Science* **2017**, *10*, 435-459.
(12) Srivastava, N.; Singh, S. K.; Meghnani, D.; Mishra, R.; Tiwari, R. K.; Patel, A.; Tiwari, A.; Singh, R. K. Molybdenum-Doped Li/Mn-Rich Layered Transition Metal Oxide Cathode Material Li1.2Mn0.6Ni0.1Co0.1O2with High Specific Capacity and Improved Cyclic Stability for Rechargeable Li-Batteries. *ACS Applied Energy Materials* **2022**, *5*, 12183-12195.
(13) Rodrigues, M. T. F.; Babu, G.; Gullapalli, H.; Kalaga, K.; Sayed, F. N.; Kato, K.; Joyner, J.; Ajayan, P. M. A materials perspective on Li-ion batteries at extreme temperatures. *Nature Energy 2017 2:8* **2017**, *2*, 1-14.
(14) Luo, X.; Jiang, S.; Yan, X.; Chen, C.; Liu, S.; Zhan, S.; Zhang, L. Aminoalkyldisiloxane compound as efficient high-temperature electrolyte additive for LiMn2O4/graphite batteries. *Ionics* **2022**, *29*, 87-96.
(15) Lavi, O.; Luski, S.; Shpigel, N.; Menachem, C.; Pomerantz, Z.; Elias, Y.; Aurbach, D. Electrolyte Solutions for Rechargeable Li-Ion Batteries Based on Fluorinated Solvents. *ACS Applied Energy Materials* **2020**, *3*, 7485-7499.
(16) Kabra, V.; Birn, B.; Kamboj, I.; Augustyn, V.; Mukherjee, P. P. Mesoscale Machine Learning Analytics for Electrode Property Estimation. *Journal of Physical Chemistry C* **2022**, *126*, 14413-14429.
(17) Hu, M.; Pang, X.; Zhou, Z. Recent progress in high-voltage lithium ion batteries. *Journal of Power Sources* **2013**, *237*, 229-242.
(18) Choi, N. S.; Chen, Z.; Freunberger, S. A.; Ji, X.; Sun, Y. K.; Amine, K.; Yushin, G.; Nazar, L. F.; Cho, J.; Bruce, P. G. Challenges Facing Lithium Batteries and Electrical Double-Layer Capacitors. *Angewandte Chemie International Edition* **2012**, *51*, 9994-10024.

(19) Chen, X.; Zhang, X. Q.; Li, H. R.; Zhang, Q. Cation−Solvent, Cation−Anion, and Solvent−Solvent Interactions with Electrolyte Solvation in Lithium Batteries. *Batteries & Supercaps* **2019**, *2*, 128-131.
(20) Chen, X.; Yao, N.; Zeng, B. S.; Zhang, Q. Ion–solvent chemistry in lithium battery electrolytes: From mono-solvent to multi-solvent complexes. *Fundamental Research* **2021**, *1*, 393-398.
(21) Su, C. C.; He, M.; Amine, R.; Rojas, T.; Cheng, L.; Ngo, A. T.; Amine, K. Solvating power series of electrolyte solvents for lithium batteries. *Energy & Environmental Science* **2019**, *12*, 1249-1254.
(22) Ding, M. S.; Xu, K.; Zhang, S.; Jow, T. R. Liquid/Solid Phase Diagrams of Binary Carbonates for Lithium Batteries Part II. *Journal of The Electrochemical Society* **2001**, *148*, A299-A299.
(23) Klassen, B.; Aroca, R.; Nazri, M.; Nazri, G. A. Raman Spectra and Transport Properties of Lithium Perchlorate in Ethylene Carbonate Based Binary Solvent Systems for Lithium Batteries. *Journal of Physical Chemistry B* **1998**, *102*, 4795-4801.
(24) Wang, Y.; Balbuena, P. B. Theoretical studies on cosolvation of Li ion and solvent reductive decomposition in binary mixtures of aliphatic carbonates. *International Journal of Quantum Chemistry* **2005**, *102*, 724-733.
(25) Uchida, S.; Kiyobayashi, T. What differentiates the transport properties of lithium electrolyte in ethylene carbonate mixed with diethylcarbonate from those mixed with dimethylcarbonate? *Journal of Power Sources* **2021**, *511*, 230423-230423.
(26) Kimura, K.; Hayashi, K.; Kiuchi, H.; Morita, M.; Haruyama, J.; Otani, M.; Sakaebe, H.; Fujisaki, F.; Mori, K.; Yonemura, M.; et al. Structural Variation in Carbonate Electrolytes by the Addition of Li Salts Studied by X-Ray Total Scattering. *physica status solidi (b)* **2020**, *257*, 2000100-2000100.
(27) Schechter, A.; Aurbach, D.; Cohen, H. X-ray Photoelectron Spectroscopy Study of Surface Films Formed on Li Electrodes Freshly Prepared in Alkyl Carbonate Solutions. *Langmuir* **1999**, *15*, 3334-3342.
(28) Zhang, W.; Wang, Y.; Lan, X.; Huo, Y. Imidazolium-based ionic liquids as electrolyte additives for high-voltage Li-ion batteries. *Research on Chemical Intermediates* **2020**, *46*, 3007-3023.
(29) Kameda, Y.; Umebayashi, Y.; Takeuchi, M.; Wahab, M. A.; Fukuda, S.; Ishiguro, S.-i.; Sasaki, M.; Amo, Y.; Usuki, T. Solvation Structure of Li^+ in Concentrated $LiPF_6$ −Propylene Carbonate Solutions. *The Journal of Physical Chemistry B* **2007**, *111*, 6104-6109.
(30) Berhaut, C. L.; Porion, P.; Timperman, L.; Schmidt, G.; Lemordant, D.; Anouti, M. LiTDI as electrolyte salt for Li-ion batteries: transport properties in EC/DMC. *Electrochimica Acta* **2015**, *180*, 778-787.
(31) Wu, X.; Gong, Y.; Xu, S.; Yan, Z.; Zhang, X.; Yang, S. Electrical Conductivity of Lithium Chloride, Lithium Bromide, and Lithium Iodide Electrolytes in Methanol, Water, and Their Binary Mixtures. *Journal of Chemical & Engineering Data* **2019**, *64*, 4319-4329.
(32) Gottwald, T.; Sedlaříková, M.; Vondrák, J. Conductivity of Inorganic Perchlorates Dissolved in Aprotic Solvents. *ECS Transactions* **2017**, *81*, 47-55.
(33) Berhaut, Christopher L.; Lemordant, D.; Porion, P.; Timperman, L.; Schmidt, G.; Anouti, M. Ionic association analysis of LiTDI, LiFSI and $LiPF_6$ in EC/DMC for better Li-ion battery performances. *RSC Advances* **2019**, *9*, 4599-4608.
(34) Khomenko, V.; Raymundo-Piñero, E.; Béguin, F. High-energy density graphite/AC capacitor in organic electrolyte. *Journal of Power Sources* **2008**, *177*, 643-651.
(35) Marcus, Y.; Hefter, G. Ion Pairing. *Chemical Reviews* **2006**, *106*, 4585-4621.
(36) Han, S. A salient effect of density on the dynamics of nonaqueous electrolytes. *Scientific Reports* **2017**, *7*, 46718-46718.

(37) Uchida, S.; Kiyobayashi, T. How does the solvent composition influence the transport properties of electrolyte solutions? LiPF(6) and LiFSA in EC and DMC binary solvent. *Physical chemistry chemical physics : PCCP* **2021**, *23*, 10875-10887.
(38) Jorgensen, W. L.; Maxwell, D. S.; Tirado-Rives, J. Development and Testing of the OPLS All-Atom Force Field on Conformational Energetics and Properties of Organic Liquids. *Journal of the American Chemical Society* **1996**, *118*, 11225-11236.
(39) Canongia Lopes, J. N.; Deschamps, J.; Pádua, A. A. H. Modeling Ionic Liquids Using a Systematic All-Atom Force Field. *The Journal of Physical Chemistry B* **2004**, *108*, 2038-2047.
(40) Dodda, L. S.; Cabeza de Vaca, I.; Tirado-Rives, J.; Jorgensen, W. L. LigParGen web server: an automatic OPLS-AA parameter generator for organic ligands. *Nucleic Acids Research* **2017**, *45*, W331-W336.
(41) Damm, W.; Frontera, A.; Tirado-Rives, J.; Jorgensen, W. L. OPLS all-atom force field for carbohydrates. *Journal of Computational Chemistry* **1997**, *18*, 1955-1970.
(42) Allen, M. P.; Tildesley, D. J. *Computer Simulation of Liquids*; Oxford University Press, 2017.
(43) Frisch, M. J.; Trucks, G. W.; Schlegel, H. B.; Scuseria, G. E.; Robb, M. A.; Cheeseman, J. R.; Scalmani, G.; Barone, V.; Petersson, G. A.; Nakatsuji, H.; et al. Gaussian 16 Rev. C.01. Gaussian, Inc., Wallingford CT: 2016.
(44) Mulliken, R. S. Electronic Population Analysis on LCAO–MO Molecular Wave Functions. I. *The Journal of Chemical Physics* **1955**, *23*, 1833-1840.
(45) Breneman, C. M.; Wiberg, K. B. Determining atom-centered monopoles from molecular electrostatic potentials. The need for high sampling density in formamide conformational analysis. *Journal of Computational Chemistry* **1990**, *11*, 361-373.
(46) Wang, J.; Wang, W.; Kollman, P. A.; Case, D. A. Automatic atom type and bond type perception in molecular mechanical calculations. *Journal of Molecular Graphics and Modelling* **2006**, *25*, 247-260.
(47) Wang, J.; Wolf, R. M.; Caldwell, J. W.; Kollman, P. A.; Case, D. A. Development and testing of a general amber force field. *Journal of Computational Chemistry* **2004**, *25*, 1157-1174.
(48) Borodin, O.; Smith, G. D. Quantum Chemistry and Molecular Dynamics Simulation Study of Dimethyl Carbonate: Ethylene Carbonate Electrolytes Doped with $LiPF_6$. *The Journal of Physical Chemistry B* **2009**, *113*, 1763-1776.
(49) Hayamizu, K.; Aihara, Y.; Arai, S.; Martinez, C. G. Pulse-Gradient Spin-Echo (1)H, (7)Li, and (19)F NMR Diffusion and Ionic Conductivity Measurements of 14 Organic Electrolytes Containing LiN(SO2CF3)2. *J Phys Chem B* **1999**, *103*, 519-524.
(50) Kozlova, S. A.; Emel'yanenko, V. N.; Georgieva, M.; Verevkin, S. P.; Chernyak, Y.; Schäffner, B.; Börner, A. Vapour pressure and enthalpy of vaporization of aliphatic dialkyl carbonates. *The Journal of Chemical Thermodynamics* **2008**, *40*, 1136-1140.
(51) Verevkin, S. P.; Toktonov, A. V.; Chernyak, Y.; Schäffner, B.; Börner, A. Vapour pressure and enthalpy of vaporization of cyclic alkylene carbonates. *Fluid Phase Equilibria* **2008**, *268*, 1-6.
(52) Humphrey, W.; Dalke, A.; Schulten, K. VMD: Visual molecular dynamics. *Journal of Molecular Graphics* **1996**, *14*, 33-38.
(53) Gans, P.; Gill, J. B.; Longdon, P. J. Spectrochemistry of solutions. Part 21.—Inner- and outer-sphere complexes of lithium with thiocyanate in acetonitrile solutions. *Journal of the Chemical Society, Faraday Transactions 1: Physical Chemistry in Condensed Phases* **1989**, *85*, 1835-1839.
(54) Bachelin, M.; Gans, P.; Gill, J. B. Spectrochemistry of solutions. Part 24.—Li, Na, K and Bun4N thiocyanates in methanol: infrared spectroscopic evidence for ion pairing and hydrogen bonding. *Journal of the Chemical Society, Faraday Transactions* **1992**, *88*, 3327-3330.

(55) Ganesh, P.; Jiang, D.-e.; Kent, P. R. C. Accurate Static and Dynamic Properties of Liquid Electrolytes for Li-Ion Batteries from ab initio Molecular Dynamics. *The Journal of Physical Chemistry B* **2011**, *115*, 3085-3090.
(56) Yu, J.; Balbuena, P. B.; Budzien, J.; Leung, K. Hybrid DFT Functional-Based Static and Molecular Dynamics Studies of Excess Electron in Liquid Ethylene Carbonate. *Journal of The Electrochemical Society* **2011**, *158*, A400-A400.
(57) Takeuchi, M.; Matubayasi, N.; Kameda, Y.; Minofar, B.; Ishiguro, S.-i.; Umebayashi, Y. Free-Energy and Structural Analysis of Ion Solvation and Contact Ion-Pair Formation of Li^+ with BF_4^- and PF_6^- in Water and Carbonate Solvents. *The Journal of Physical Chemistry B* **2012**, *116*, 6476-6487.
(58) Dudariev, D.; Logacheva, K.; Kolesnik, Y.; Kalugin, O. Interparticle interactions and dynamics in BmimBF4 and LiBF4 solutions in propylene carbonate: MD simulation. *Kharkiv University Bulletin. Chemical Series* **2019**, 54-64.
(59) Tenney, C. M.; Cygan, R. T. Analysis of Molecular Clusters in Simulations of Lithium-Ion Battery Electrolytes. *The Journal of Physical Chemistry C* **2013**, *117*, 24673-24684.
(60) France-Lanord, A.; Grossman, J. C. Correlations from Ion Pairing and the Nernst-Einstein Equation. *Phys Rev Lett* **2019**, *122*, 136001.

Chapter 4. Microstructure and transport properties of 1-1'-spirobipyrrolidinium tetrafluoroborate in acetonitrile from molecular dynamics simulations

For the solutions of 1-1'-spirobipyrrolidinium tetrafluoroborate ($SBPBF_4$) in acetonitrile (AN) the maximum on conductivity concentration curve occurs at the concentration of salt at 2.0 M as was obtained the experimental data in the literature. Although this phenomenon is usually related to the ion association at a high electrolyte concentration, the detailed microscopic structure of the ion subsystem is not properly analyzed. Thus, in this Chapter $SBPBF_4$ in AN of seven different concentrations were studied with classical MD simulation technique. For this purpose, the cation full-atom potential model has been developed on the base of GROMOS force field. To account several existing conformers of the cation in the solution, the several iterations of MD simulations and charge unification for hydrogen atoms of SBP^+ were performed. The structure was studied in terms of RDFs and RCNs. The cation-anion (N-B) RDFs of mixtures of different concentrations shows the presence of two possible cation-anion relative disposition: axial (when the BF_4^- anion is close to the nitrogen atom of the cation) and equatorial (when BF_4^- anion is near one of the pyrrolidinium rings). The RCNs show that anions competing with the solvent molecules for the position in the first coordination shell around the cation: with the salt concentration increase the anion coordination number is increasing as well while the solvent coordination number is decreasing. Aggregate analysis with two different criteria (to take into account the equatorial anions and to not) confirmed the existence of ionic clusters in $SBPBF_4$ in AN solutions. The first criterion showed the presence of massive aggregates at 1.5 M and higher. For the second criterion the average number of association starts to increase at the same concentration values as the maximum on the experimental conductivity curve is located. This indicates that the second criterion is the correct choice for such an analysis. The transport properties were investigated via diffusion coefficients of solution components and viscosity of simulated systems. The diffusion coefficients for ions and solvent molecules are decreasing and viscosity values are non-linearly increasing with the increasing of the salt concentration. The obtained results and the fact that calculated viscosity values are drastically non-linearly increasing from the concentration 2.0 M of the $SBPBF_4$ are in agreement with the maximum of the experimental concentration conductivity curve.

4.1. Introduction

Electric double-layer capacitors (EDLCs) or supercapacitors were considered as one of the most promising energy storing devices recently.[1-7] Their main benefits are high power density, long lifetime (cycle time) and fast charge/discharge process. Also, EDLCs usually have up to 1000 times higher power density as well as better safety comparing to Li-ion batteries.[8-11] One of the main properties that determine the great performance of supercapacitors is conductance of the electrolyte. As a result, developing the new electrolyte systems with high conductance and wide operating temperature ranges remains the relevant task.

The development of such systems involves the use of electrolyte salts with large electrochemical stability windows. Typically, the acetonitrile (AN) is used as a solvent for such systems due to low viscosity and wide electrochemical window.[12, 13] As for the salt, ideally, it should have large electrochemical stability window, high ionic conductivity as well as ionic mobility and good solubility in organic solvents. Also, it should be inexpensive and environmentally friendly. The most common salt in practical usage is tetraethylammonium tetrafluoroborate ($TEABF_4$).[14-19] But one of the most favorable candidates among electrolytes that possess all of the above criteria is spiro-1,1'-bipyrrolidinium tetrafluoroborate ($SBPBF_4$) salt.[20-24] It has higher solubility in organic solvents as well as $SBPBF_4$ in AN solutions have a higher conductivity value comparing to $TEABF_4$.[20, 25, 26]

In published works it was proven that maximum of conductivity concentration dependence of electrolyte (or ionic liquids) in organic solvents exists.[25, 27, 28] This phenomenon was related to the viscosity increase in such systems.[29] It was also reported that it can be due to the formation of ion associates at a high electrolyte concentration.[30] Still, all literature does not provide a detailed analysis of ionic aggregation process influence on the existence of conductivity maximum on the concentration curve.

Thus, in this Chapter the detailed analysis of structural and transport properties of $SBPBF_4$ in AN solutions of seven different concentrations using classical molecular dynamics (MD) simulation is presented. The aggregate analysis was performed to analyze the ionic subsystem of the solutions. Additionally, the transport properties of the systems were obtained. The Chapter is organized as follows. In sec. 2 details of molecular dynamics simulation is provided as well as description of the cation force field development and validation. In sec. 3 the results of the simulation and their discussion are showed. In sec. 4 the main conclusions are presented.

4.2. Methodology

4.2.1. Details of molecular dynamics simulation

In the current work the series of classical MD simulations were performed. The simulated systems of $SBPBF_4$ in AN of different concentrations with a certain composition (Table 4.1.) were presented as a cubic box with periodic boundary conditions in all directions. Total number of ion pairs for each composition was always equal to 100.

To obtain the total number of ions and solvent molecules from the molarities the experimental density values were used.[31]

For the cation conformers analysis, the infinite diluted solution was simulated for 1 ns.

To validate the cation potential model the infinite diluted solutions (Table 4.1.) were simulated for 50 ns for 5 independent runs with a total statistic of 250 ns. For each run the ions and solvent molecules were put in the simulation box with a random seed.

All other simulations were performed as described in Chapter 2.

Table 4.1. The composition of the simulated systems of $SBPBF_4$ in AN.

$SBPBF_4$ concentration	**Number of SBP^+**	**Number of BF_4^-**	**Number of AN**	**ρ,[31] g/cm^3**
Infinite diluted solution	1	-	500	0.77
0.5 M			3483	0.82
1.0 M			1603	0.87
1.5 M			977	0.92
2.0 M	100	100	664	0.97
2.5 M			476	1.02
3.0 M			350	1.07
3.5 M			261	1.12

4.2.2. Potential model: development and validation

The structure of the cation, anion and solvent as well as labeling of the cation is shown at Figure 4.1.

The BF_4^- potential model was taken from.[32]

The acetonitrile model was taken from Koverga et al.[33]

The starting point in the development of the cation potential model under consideration was the quantum-chemical calculations of three SBP^+ conformers: E-E (Envelope-Envelope conformer, in which the N atom in both pyrrolidine rings is outside the plane of the ring), T-E (one ring in the Twist conformation, the other in the Envelope) and T-T (both pyrrolidine rings in a Twist conformation). The conformers are presented at Figure 4.2. All quantum-chemical calculations were performed using the Gaussian09 program[34] at the M06-2X/6-311++G(d,p) level; specific atomic charges were calculated by the Breneman method (ChelpG).[35, 36] The charges of conformers are shown in Table 4.2. The energies obtained for the equilibrium geometries E-E, E-T and T-T are in good agreement with the literature data: the E-E conformation has the

lowest energy, T-T is the highest, E-T occupies an intermediate position between the other two. The difference in energy between T-T and E-E conformers is equal to 14 kJ/mol, while E-T and E-E difference being on the order of 3-4 kJ/mol. The latter is comparable with the thermal energy *RT* equal to ~2.4 kJ/mol at 298.15 K. Thus, it can be possible for a cation to transit from E-T conformation to E-E and back during thermal motion in a liquid medium.

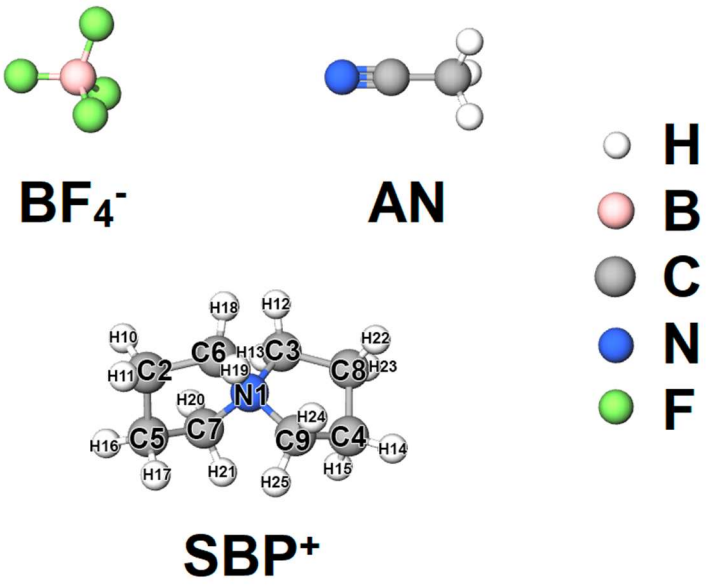

Figure 4.1. Structure of the SBP^+ cation, BF_4^- anion and AN. The labeling of cation used in potential model is also shown.

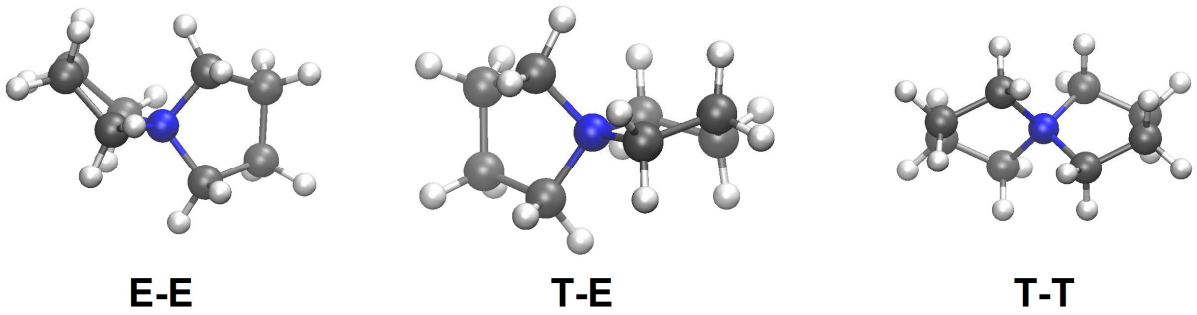

Figure 4.2. Structure of the SBP^+ cation conformers: Envelope-Envelope (left), Twist-Envelope (middle) and Twist-Twist (right).

Table 4.2. Partial charges of the SBP^+ E-E, T-E and T-T conformers as well as the unified charges after 2 iterations.

Atom	E-E	E-T	T-T	Unified
N^1	0.113039	0.119648	0.135923	0.1169112
C^2	-0.126957	-0.121679	-0.097901	-0.1236403
C^3	-0.131967	-0.034286	-0.04368	-0.0799324
C^4	-0.126957	-0.136825	-0.097901	-0.1314238
C^5	0.043744	-0.014057	-0.097896	0.0110940
C^6	-0.006476	0.006529	-0.043667	-0.0005663
C^7	-0.131967	-0.120269	-0.04368	-0.1241190
C^8	0.043744	-0.063084	-0.097896	-0.0141010
C^9	-0.006476	-0.067939	-0.043667	-0.0388354
H^{10}	0.079814	0.078743	0.068921	0.0856346
H^{11}	0.088551	0.09497	0.106933	0.0856346
H^{12}	0.109316	0.084141	0.087525	0.0948084
H^{13}	0.108487	0.080274	0.094215	0.0948084
H^{14}	0.088551	0.11117	0.106933	0.0915560
H^{15}	0.079814	0.085588	0.068921	0.0915560
H^{16}	0.070155	0.085205	0.068921	0.0561472
H^{17}	0.027229	0.038017	0.106933	0.0561472
H^{18}	0.094146	0.073641	0.087524	0.0846835
H^{19}	0.087439	0.084163	0.094211	0.0846835
H^{20}	0.109316	0.112409	0.094215	0.1114084
H^{21}	0.108487	0.11661	0.087525	0.1114084
H^{22}	0.070155	0.06509	0.068921	0.0666926
H^{23}	0.027229	0.099173	0.106933	0.0666926
H^{24}	0.087439	0.105045	0.094211	0.1013758
H^{25}	0.094146	0.117722	0.087524	0.1013758

The potential model was generated from the GROMOS54a7 force field.[37] For this force field potential models have the following functional form of the total potential energy:

$$U_{tot} = \sum_{ij}^{bonds} \frac{k_{r,ij}}{4}\left(r_{ij}^2 - r_{0,ij}^2\right)^2 + \sum_{ijk}^{angles} \frac{k_{\theta,ijk}}{2}\left(\cos\left(\theta_{ijk}\right) - \cos\left(\theta_{0,ijk}\right)\right)^2 + \\ + \sum_{ijkl}^{dihedral} k_{\phi,ijkl}\left(1 + \cos\left(n\phi_{ijkl} - \phi_{s,ijkl}\right)\right) + \sum_{ij}^{nonbonded}\left(\left(\frac{C12_{ij}}{r_{ij}^{12}} - \frac{C6_{ij}}{r_{ij}^{6}}\right) + \frac{q_i q_j}{4\pi\varepsilon_0 r_{ij}}\right), \tag{4.1}$$

where k is the force constant for bond stretching (r), angle bending (θ), proper and improper dihedral (ϕ), respectively, *C6* and *C12* are the Lennard-Jones parameters and q stands for the fractional charges of the interaction sites.

The first step in the unification of the data obtained for further creation of a potential model of the SBP^+ cation was the averaging of the partial charges of hydrogen atoms at a common carbon atom. It allowed to further unify all of three charge sets into one for all hydrogen atoms of SBP^+ in dependence with the number of conformers of different types that were observed in MD simulation in accordance with the equation 4.2:

$$\bar{q}_i = \sum_{n=1}^{3} P_n q_{in}, \tag{4.2}$$

where i is the atom in SBP^+ cation, n is the number of conformer (1-3), P_n is the probability to find the n^{th} conformer in the solution, q_{in} is the charge of the atom i in the SBP^+ cation of the n^{th} conformer.

The simulation for infinite diluted solution (Table 4.1.) was conducted. At each frame during the simulation the values of the C-C-C-C angles of both pyrrolidine rings were recorded. If the value was 0±10°, the conformation of the ring was considered as an Envelope; if the value was 45±10°, the conformation was considered as a Twist. Other variations were discarded. After the simulation the distribution of conformers was obtained: T-T – 0.08%, E-E – 8.06%, E-T – 91.86%. Due to the fact that E-T and E-E conformers can transform into one another as seen from the results of the quantum chemical calculations, the difference between their occurrence at more than 10 times seems unrealistic. It was decided to use the geometric parameters (bonds, angles, dihedrals) from the optimized geometry of lowest energy conformer (E-E) instead of the original from the GROMOS54a7 force field for further simulations.

The previous step (simulation of infinite diluted solution with recording of the conformers occurrence) was repeated. New results seemed more realistic, and

thus charges of hydrogen atoms were unified for this step (equation 4.2). After that, these unified charges were used for the new iteration of the unification.

After two such iterations of charge averaging the difference in occurring of different conformers seemed negligible. Final distribution of conformers for SBP^+ in AN was: T-T – 2.32%, E-E – 46.48%, E-T – 51.20%. These results seem realistic and prove the possible transition of SBP^+ from E-T conformation to E-E and vice versa during thermal motion. The charges obtained are presented in Table 4.2.

Using the charges after the two iterations of averaging the MD simulation for the same system but with long simulation time as described in previous section (infinite diluted solution, Table 4.1) was conducted. As a result, the diffusion coefficient of $1.64 \cdot 10^{-5}$ cm^2/s was obtained. Experimental value of SBP^+ cation in the infinite diluted solution was calculated from the experimental value of limiting conductance[38, 39] from the Nernst-Einstein equation. It is equal to $1.71 \cdot 10^{-5}$ cm^2/s which means that the results from the MD simulations are close to experimental value. The potential model parameters of SBP^+ are shown in the Table 4.3.

Table 4.3. Lennard-Jones parameters, *C*6 and *C*12 and intramolecular parameters, k_i, for SBP^+.

Atom	*C*6, $kJ \cdot nm^6/mol$	*C*12, $kJ \cdot nm^{12}/mol$
N^1	$2.4364096 \cdot 10^{-3}$	$2.319529 \cdot 10^{-6}$
C^{2-9}	$2.3406244 \cdot 10^{-3}$	$4.937284 \cdot 10^{-6}$
H^{10-25}	$8.464 \cdot 10^{-5}$	$1.5129 \cdot 10^{-8}$
Bond	r_0, nm	k_r, $kJ/(mol \cdot nm^4)$
N^1-$C^{6,9}$	0.151024	5430000
N^1-$C^{3,7}$	0.150106	5430000
C^2-C^5	0.155113	3081900
C^4-C^8	0.155113	3081900
C^2-C^6	0.153367	7150000
C^9-C^4	0.153367	7150000
C^3-C^8	0.152751	7150000
C^5-C^7	0.152751	7150000
C^2-H^{10-11}	0.109085	12300000
C^3-H^{12-13}	0.109085	12300000

Table 4.3 continued

C^4-H^{14-15}	0.109085	12300000
C^5-H^{16-17}	0.109085	12300000
C^6-H^{18-19}	0.109085	12300000
C^7-H^{20-21}	0.109085	12300000
C^8-H^{22-23}	0.109085	12300000
C^9-H^{24-25}	0.109085	12300000
Angle	θ_0, deg	k_θ, kJ/mol
N^1-C^3-C^8	104.2344	465.00
N^1-C^7-C^5	104.2344	465.00
N^1-C^6-C^2	104.5895	465.00
N^1-C^9-C^4	104.5895	465.00
N^1-C^3-H^{12}	109.2500	490.00
N^1-C^7-H^{20}	109.2500	490.00
N^1-C^3-H^{13}	106.4768	490.00
N^1-C^7-H^{21}	106.4768	490.00
N^1-C^6-H^{18}	106.4561	490.00
N^1-C^9-H^{25}	106.4561	490.00
N^1-C^6-H^{19}	109.3781	490.00
N^1-C^9-H^{24}	109.3781	490.00
C^3-N^1-C^7	114.5782	620.00
C^3-N^1-C^9	102.7900	620.00
C^6-N^1-C^7	102.7900	620.00
C^6-N^1-C^3	113.2590	620.00
C^7-N^1-C^9	113.2590	620.00
C^6-N^1-C^9	110.4723	620.00
C^2-C^5-C^7	104.8546	520.00
C^3-C^8-C^4	104.8546	520.00
C^5-C^2-C^6	105.4221	520.00
C^9-C^4-C^8	105.4221	520.00
C^2-C^5-H^{16}	112.5273	530.00
C^4-C^8-H^{22}	112.5273	530.00
C^2-C^5-H^{17}	110.9029	530.00
C^4-C^8-H^{23}	110.9029	530.00
C^3-C^8-H^{22}	110.6156	530.00
C^7-C^5-H^{16}	110.6156	530.00
C^3-C^8-H^{23}	110.6219	530.00
C^7-C^5-H^{17}	110.6219	530.00
C^5-C^2-H^{10}	111.0589	530.00
C^8-C^4-H^{15}	111.0589	530.00
C^5-C^2-H^{11}	112.1918	530.00
C^8-C^4-H^{14}	112.1918	530.00
C^6-C^2-H^{10}	111.1998	530.00
C^9-C^4-H^{15}	111.1998	530.00

Table 4.3 continued

C^6-C^2-H^{11}	109.8702	530.00	
C^9-C^4-H^{14}	109.8702	530.00	
C^2-C^6-H^{18}	111.9377	505.00	
C^4-C^9-H^{25}	111.9377	505.00	
C^2-C^6-H^{19}	114.9405	505.00	
C^4-C^9-H^{24}	114.9405	505.00	
C^5-C^7-H^{20}	115.3763	505.00	
C^8-C^3-H^{12}	115.3763	505.00	
C^5-C^7-H^{21}	111.8365	505.00	
C^8-C^3-H^{13}	111.8365	505.00	
H^{10}-C^2-H^{11}	107.1560	484.00	
H^{14}-C^4-H^{15}	107.1560	484.00	
H^{16}-C^5-H^{17}	107.3630	484.00	
H^{22}-C^8-H^{23}	107.3630	484.00	
H^{12}-C^3-H^{13}	109.1784	443.00	
H^{20}-C^7-H^{21}	109.1784	443.00	
H^{18}-C^6-H^{19}	109.1014	443.00	
H^{24}-C^9-H^{25}	109.1014	443.00	
Dihedral	ϕ_s , deg	$^k\phi$, kJ/mol	n
N^1-C^3-C^8-C^4	28.6529	1.00	3
N^1-C^7-C^5-C^2	28.6529	1.00	3
N^1-C^6-C^2-C^5	-21.3497	1.00	3
N^1-C^9-C^4-C^8	-21.3497	1.00	3
C^3-N^1-C^6-C^2	163.5471	1.05	3
C^3-N^1-C^7-C^5	-165.5924	1.05	3
C^3-N^1-C^9-C^4	39.3652	1.05	3
C^6-N^1-C^3-C^8	-42.0189	1.05	3
C^3-C^8-C^4-C^9	-4.3420	1.00	3
C^3-C^8-C^4-C^9	-4.3420	1.00	3

4.3. Results and discussion

4.3.1. Structural properties

Structural properties of $SBPBF_4$ in AN were analyzed in terms of radial distribution functions (RDF) and running coordination numbers (RCN). Because of quasispherical form of the ions their relative center atoms were chosen for the

analysis: N for SBP^+ and B for BF_4^-. The cation-anion RDFs for all systems are presented in Figure 4.3.

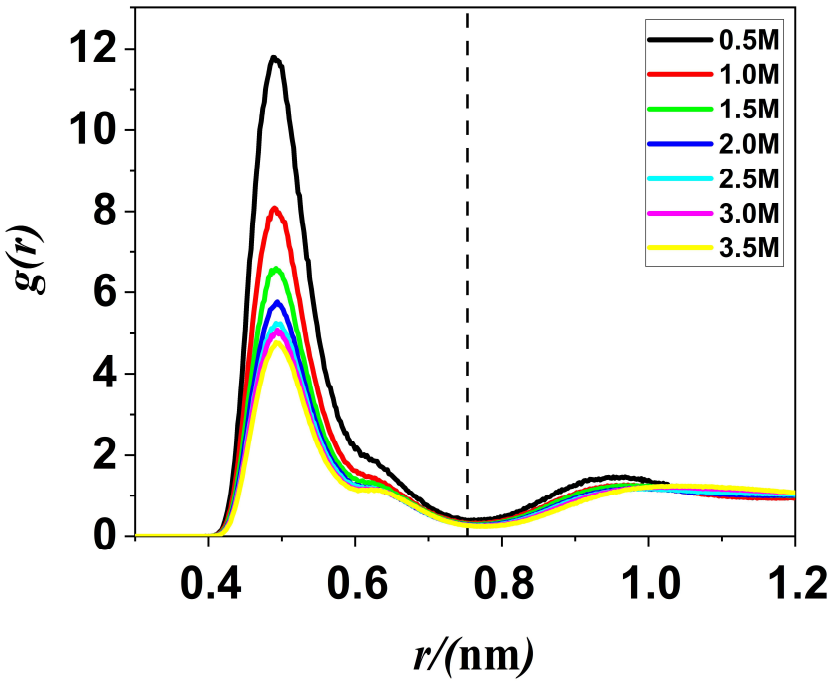

Figure 4.3. Cation-anion (N-B) radial distribution functions at various molar concentrations of $SBPBF_4$ in AN mixture. The vertical dashed line corresponds to the first coordination shell.

For all concentrations of the $SBPBF_4$ in AN similar behavior can be observed. The first maximum of RDF is constant for all simulated systems and is equal to approximately 0.50 nm. The RDF curve has some kind of shoulder (which more clearly resembles the local maximum for higher concentrations) with its peak at 0.63 nm. These values and RDF curve shape in these regions shows two possible configurations of cation-anion relative disposition near each other which was confirmed by analyzing GROMACS trajectory files from molecular dynamic simulations via VMD program package[40] (Figure 4.4). The maximum at 0.50 nm corresponds to axial relative position (BF_4^- is near nitrogen atom between pyrrolidinium rings) and the shoulder at 0.63 nm – to the equatorial relative position (BF_4^- is near one of the pyrrolidinium rings, in its plane). The minimum on RDF is at approximately 0.75 nm. This will be used later as the association

criteria because at this distance the cation can interact with anions in both position types described earlier. The heights of peaks are decreasing with the increasing of $SBPBF_4$ concentration. The similar results were obtained in other MD simulations.[31, 41]

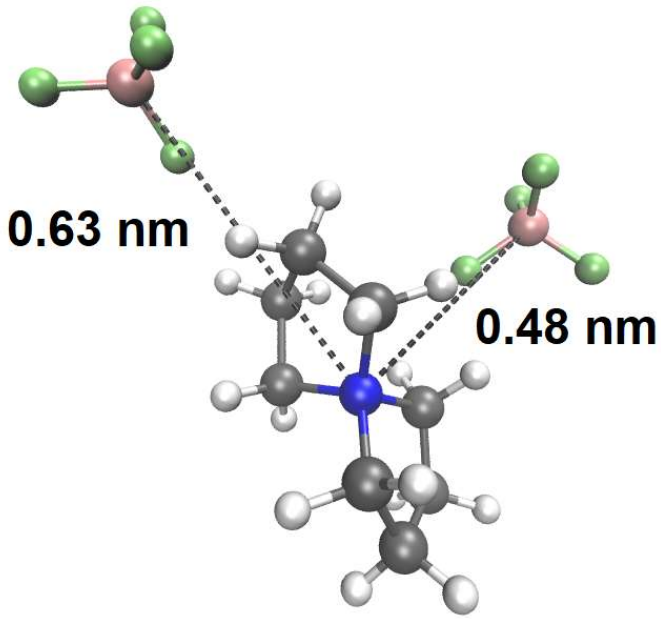

Figure 4.4. Example of $(SBP(BF_4)_2)^-$ associate with axial (0.48 nm) and equatorial (0.63 nm) relative positions of anions. The respective N-B distances are shown as well.

To study the solvation of the cation the RDF between the nitrogen atom of SBP^+ and the nitrogen atom of AN for all concentrations were obtained. According to Figure 4.5, the position of first maximum at 0.42 nm as well as small local maximum at 0.56 nm. These two peaks also can be explained in similar way as ones in cation-anion RDF: the axial (0.42 nm) and equatorial (0.56 nm) positions of solvent molecules regarding cation. The first minimum is at the 0.66 nm indicates the first solvation shell around the cation. The peaks heights are remaining almost the same with the concentration increase of $SBPBF_4$. Interesting to note that peak position as well as first minima on RDFs that indicate the

boundaries of the first solvation shells do not depend on the concentration of the electrolyte.

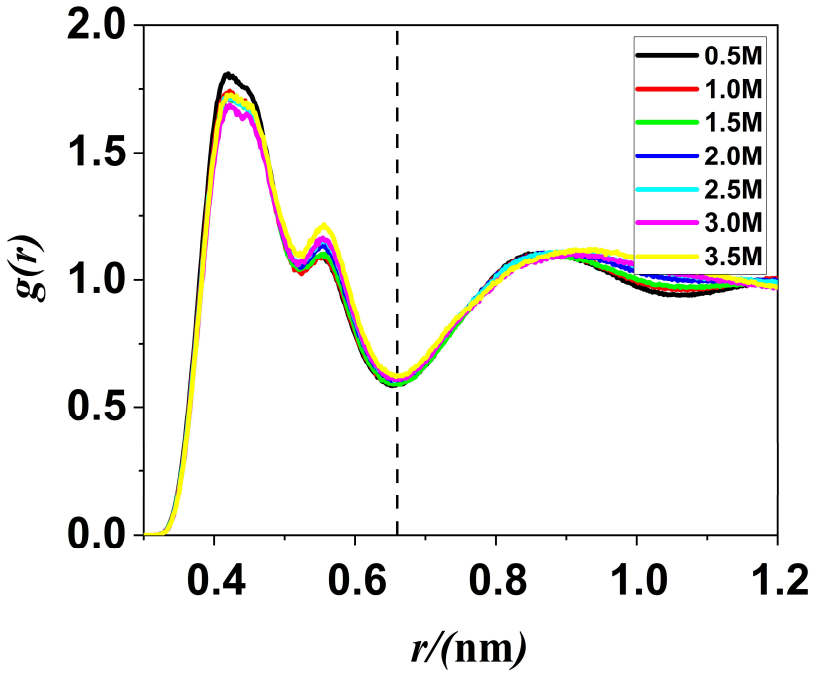

Figure 4.5. Cation-solvent (N-N_{AN}) radial distribution functions at various molar concentrations of $SBPBF_4$ in AN mixture. The vertical dashed line corresponds to the first solvation shell.

Respective cation-anion and cation-solvent RCNs for all concentrations of $SBPBF_4$ in an were obtained (Figure 4.6 and 4.7).

With the $SBPBF_4$ concentration increase the anions beginning to occupy space around the cation – and one can observe the increase of coordination numbers of anions to cation (Figure 4.6) from 1.4 to 4.2 occurs for first coordination shell, while the decrease of coordination numbers of solvents to cation (Figure 4.7) from 11.3 to 5.7 for the first solvation shell can be observed. Such a big difference in these numbers is due to the size of the solvent molecules versus anions. The PF_6^- anion is larger than the solvent molecule. Also, it cannot be packed as tightly as the AN molecule which has linear structure.

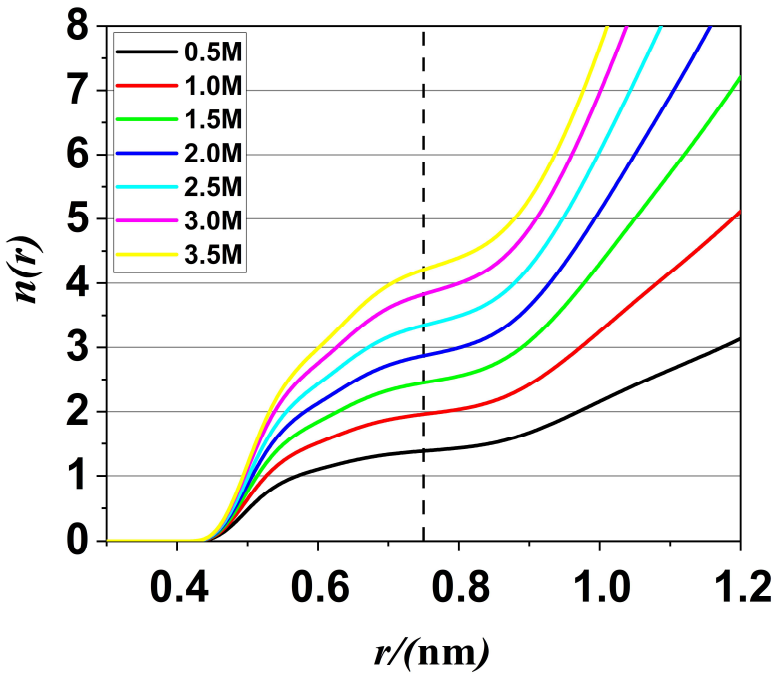

Figure 4.6. Cation-anion (N-B) running coordination numbers at various molar concentrations of $SBPBF_4$ in AN mixture. The vertical dashed line corresponds to the first coordination shell.

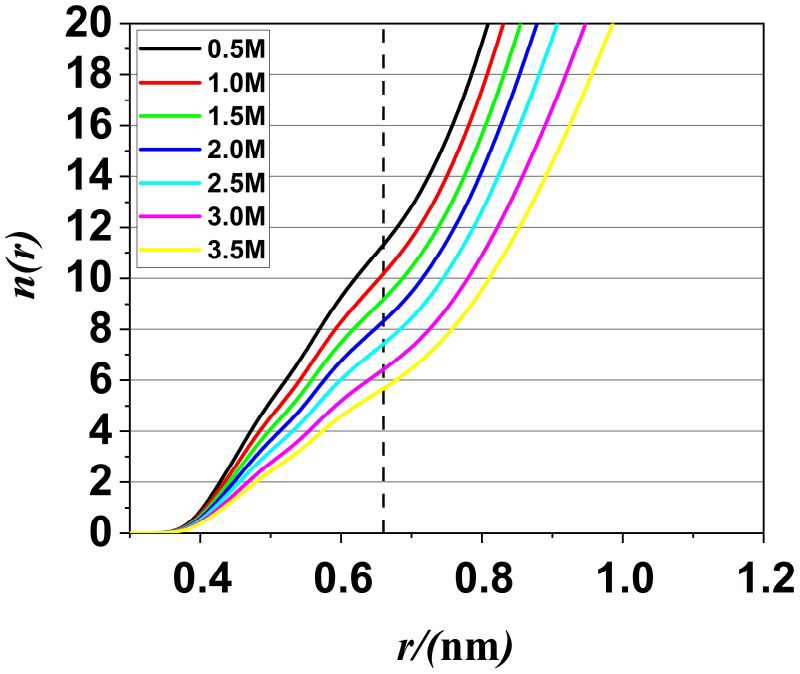

Figure 4.7. Cation-solvent ($N\text{-}N_{AN}$) running coordination numbers at various molar concentrations of $SBPBF_4$ in AN mixture. The vertical dashed line corresponds to the first solvation shell.

4.3.2. Aggregate analysis

To analyze the presence of ionic clusters two different distance criteria have been chosen. The first criterion is the first minimum on the interionic RDF (0.75 nm, Figure 4.2). In this case all anions in the first coordination sphere are involved, including those in equatorial position because they can form weak hydrogen bonds with the cation even if they do not interact with the nitrogen atom of SBP^+ directly.[41] The second criterion was determined from the second derivative of the cation-anion RCN that was discussed earlier (Figure 4.6). As can be seen in the Figure 4.8, the first minimum is approximately at 0.53 for all concentrations. This minimum indicates some region where RCN comes to the beginning of the plateau (or soft incline) on its curve. Also, it is strict criteria as it does not include the equatorial anions (see Figure 4.4) in the cluster determination.

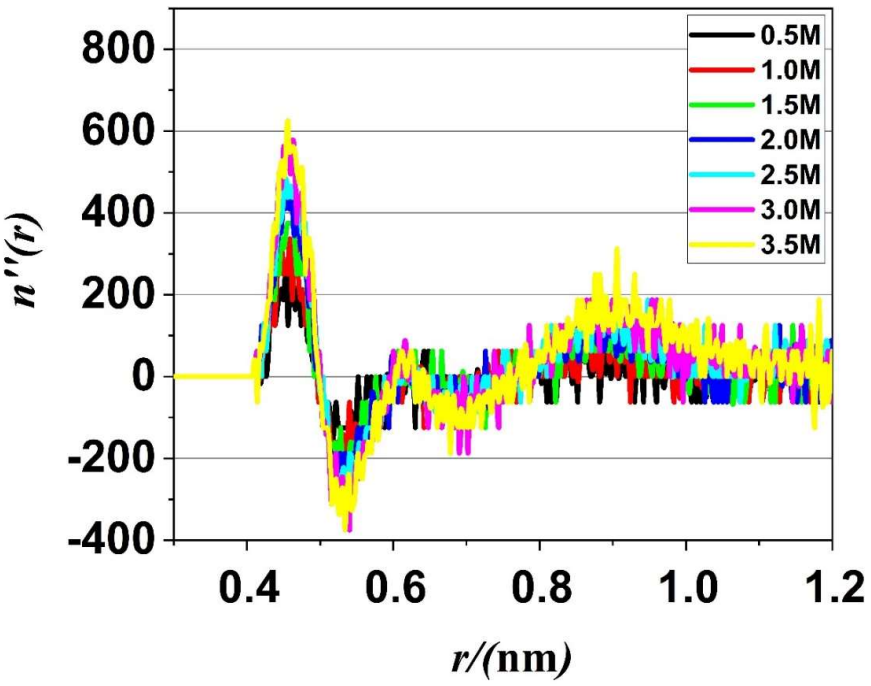

Figure 4.8. Second derivatives of cation-anion (N-B) running coordination numbers at various molar concentrations of $SBPBF_4$ in AN mixture.

The size distribution of the associates for both criteria can be found in Figures 4.9.

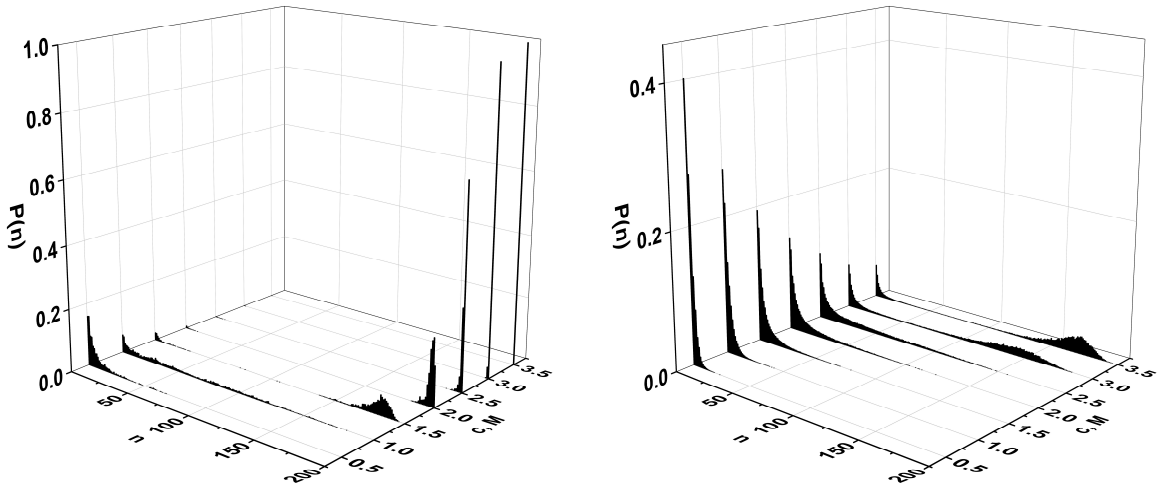

Figure 4.9. Probability distributions of aggregate sizes with first (left) and second (right) criterion at various molar concentrations of $SBPBF_4$ in AN mixture.

The first criterion (0.75 nm) shows that at 1.0 M the huge increase of number of different cluster types can be observed. At this concentration of the salt the system is in the transition state from free ions and small aggregates to large associates. Starting from the 1.5 M almost all of the ions in the system associated in large clusters. The most concentrated solution is considered the one large aggregate without free ions.

For the second criterion (0.53 nm) the most diluted system (0.5 M of $SBPBF_4$) contains mostly isolated ions and small aggregates. Up until 2.5 M the system looks similar, the aggregates sizes are increase. 3.0-3.5 M concentration represents transition state when large aggregates start to appear. In the highest concentration, although, a huge number of ions are forming big aggregates, are still forming relatively small associates and are temporary left out of the big cluster.

To better illustrate the results, the average numbers of association for all the criteria (Figure 4.10) were calculated.

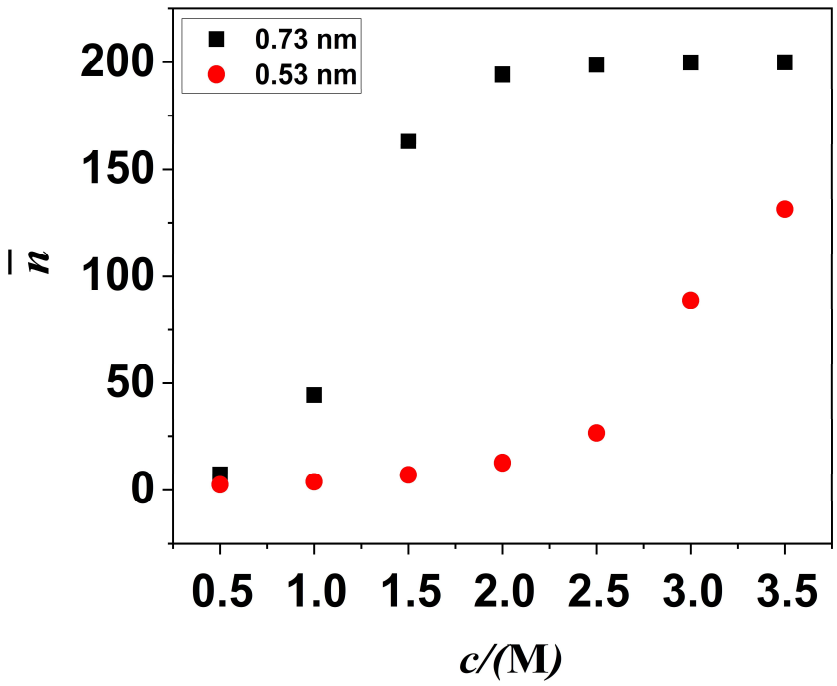

Figure 4.10. Average numbers of association for different criteria at various molar concentrations of $SBPBF_4$ in AN mixture.

According to the Nernst-Einstein relation,[42] the charge carrier concentration affects the conductivity value directly. The formation of the aggregates removes the ions (charge carriers) from the solution and, thus, should lower the electric conductivity. The rapid increasing of association process for $SBPBF_4$ in AN mixture is occurring at 1.0-1.5 M for first criterion and after that all of the ions are forming one large aggregate (Figure 4.10).[43] For the second criterion the size of aggregates starts to increase rapidly at 2.5 M, but even at 3.5 M the system is still not totally associated yet. In this case, the second criterion seems more correct. The first criterion seems to overvalues the aggregation as if all the ions are part of one large aggregate, the conductivity should be zero due to the charge carrier absence. The results for the second criterion correlate with the experimental conductivity for $SBPBF_4$ in AN which have the maximum that occurs at 2.0 M concentration of salt.[25, 28, 39]

4.3.3. Transport properties

The concentration dependence of the diffusion coefficients of the systems components and the shear viscosity of $SBPBF_4$ in AN solutions in comparison with experimental values are shown in Figure 4.11.

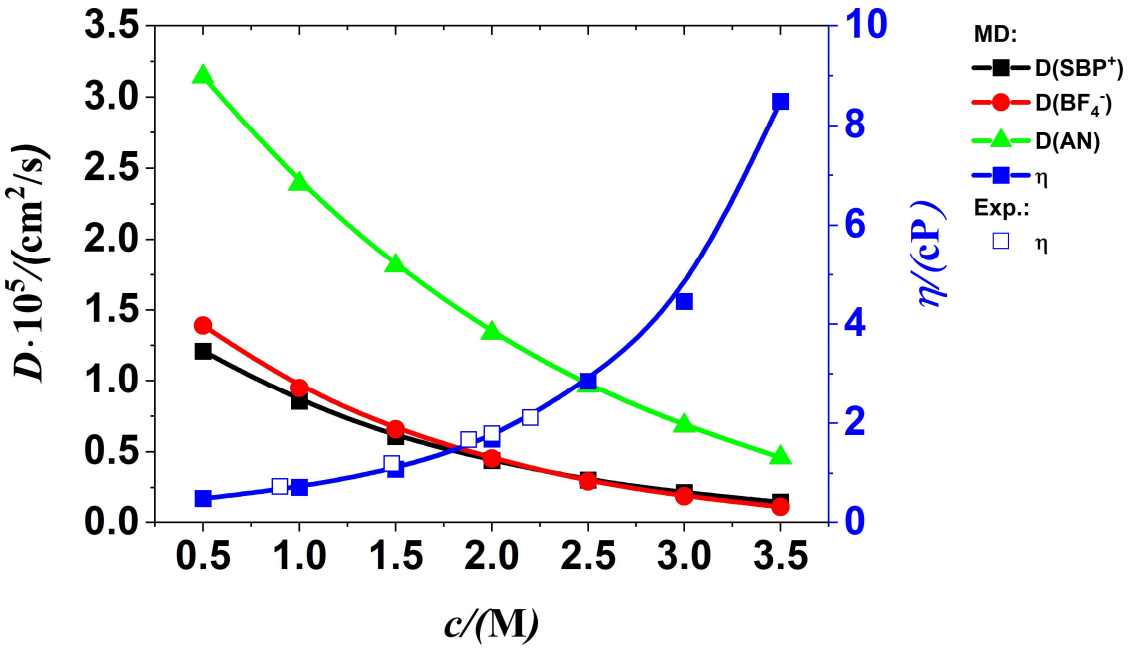

Figure 4.11. Diffusion coefficients for cation, anion and solvent molecule and viscosity values in comparison with the experimental data[31] at various molar concentrations of $SBPBF_4$ in AN mixture.

As can be seen from the figure, the diffusion coefficients of all ions and molecules with the increasing salt concentration become lower. Also, it can be noted that the diffusion coefficients of the relatively small and neutral molecules of AN are two times larger for those of SBP^+ and BF_4^- for almost all concentration range.

Viscosity perfectly fit the experimental data.[31] At concentration of approximately 2.0 M of $SBPBF_4$ the calculated viscosity increases drastically, indicating the inner processes of ionic aggregation that happen in the same concentration range.

The conductivity depends on the concentration of the charge carriers in the solution and diffusion coefficients of the ions according to the Nernst-Einstein equation.[42] Diffusion coefficients decrease and viscosity begin to drastically non-linearly increase at nearly 2.0 M of $SBPBF_4$ confirms the presence of the maximum of experimental electroconductivity at this concentration value.[25, 28, 39]

4.4 Conclusions

In the current work $SBPBF_4$ in AN solutions in a wide range of concentrations (0.5 M – 3.5 M) were investigated with classical MD simulation technique.

For this purpose, the cation full-atom potential model has been developed by authors. In order to account the existence of several conformers of the cation in the solution, the several iterations of MD simulations and charge unification for hydrogen atoms were performed. The final results after two iterations were taken into account. The SBP^+ cation diffusion coefficient is close to the one obtained from the experimental limiting molar conductivities.

The structure was studied in terms of RDFs and RCNs. The cation-anion (N-B) RDFs of mixtures of different concentrations shows the presence of two possible cation-anion relative disposition: axial and equatorial. As the concentration of $SBPBF_4$ rises the composition of the cations first coordination shell changes: PF_6^- anions (coordination number changes from 1.4 to 4.2) are replacing AN solvent molecules (coordination number changes from 11.3 to 5.7) in it.

Aggregate analysis was performed with the use of two different criteria. The second criterion is stricter, without considering the equatorial position of the anions relatively to the cations. As a result, the existence of ionic clusters in $SBPBF_4$ in AN systems was confirmed. For the first criterion the massive aggregation occurs at the concentration of $SBPBF_4$ in AN at 1.5 M while for the second criterion the average number of association begins to increase at the same

region where the experimental conductivity curve changes its behavior which indicates that this criterion is the correct choice for such an analysis.

The transport properties were investigated via diffusion coefficients of solution components and viscosity of simulated systems. Obtained viscosity values are matching the experimental ones. Diffusion coefficients of all components are decreasing while the viscosity of the system continuously increasing with the salt concentration increase. The obtained results show a good correlation with the association analysis and in accordance with the occurrence of the concentration conductivity maximum in the experiment.

4.4 References for Chapter 4

(1) Choi, N. S.; Chen, Z.; Freunberger, S. A.; Ji, X.; Sun, Y. K.; Amine, K.; Yushin, G.; Nazar, L. F.; Cho, J.; Bruce, P. G. Challenges Facing Lithium Batteries and Electrical Double-Layer Capacitors. *Angewandte Chemie International Edition* **2012**, *51*, 9994-10024.
(2) Abdel Maksoud, M. I. A.; Fahim, R. A.; Shalan, A. E.; Abd Elkodous, M.; Olojede, S. O.; Osman, A. I.; Farrell, C.; Al-Muhtaseb, A. a. H.; Awed, A. S.; Ashour, A. H.; et al. Advanced materials and technologies for supercapacitors used in energy conversion and storage: a review. *Environmental Chemistry Letters 2020 19:1* **2020**, *19*, 375-439.
(3) Simon, P.; Gogotsi, Y. Charge storage mechanism in nanoporous carbons and its consequence for electrical double layer capacitors. *Philosophical Transactions of the Royal Society A: Mathematical, Physical and Engineering Sciences* **2010**, *368*, 3457-3467.
(4) Najib, S.; Erdem, E. Current progress achieved in novel materials for supercapacitor electrodes: mini review. *Nanoscale Advances* **2019**, *1*, 2817-2827.
(5) Jiya, I. N.; Gurusinghe, N.; Gouws, R. Electrical Circuit Modelling of Double Layer Capacitors for Power Electronics and Energy Storage Applications: A Review. *Electronics 2018, Vol. 7, Page 268* **2018**, *7*, 268-268.
(6) Sharma, P.; Bhatti, T. S. A review on electrochemical double-layer capacitors. *Energy Conversion and Management* **2010**, *51*, 2901-2912.
(7) Horn, M.; MacLeod, J.; Liu, M.; Webb, J.; Motta, N. Supercapacitors: A new source of power for electric cars? *Economic Analysis and Policy* **2019**, *61*, 93-103.
(8) Nguyen, H. V. T.; Faheem, A. B.; Kwak, K.; Lee, K.-K. Propionitrile as a single organic solvent for high voltage electric double-layer capacitors. *Journal of Power Sources* **2020**, *463*, 228134-228134.
(9) Chu, A.; Braatz, P. Comparison of commercial supercapacitors and high-power lithium-ion batteries for power-assist applications in hybrid electric vehicles: I. Initial characterization. *Journal of Power Sources* **2002**, *112*, 236-246.
(10) Musolino, V.; Tironi, E. A comparison of supercapacitor and high-power lithium batteries. *International Conference on Electrical Systems for Aircraft, Railway and Ship Propulsion, ESARS 2010* **2010**.
(11) Lambert, S. M.; Pickert, V.; Holden, J.; He, X.; Li, W. Comparison of supercapacitor and lithium-ion capacitor technologies for power electronics applications. *IET Conference Publications* **2010**, *2010*.
(12) Ruch, P. W.; Cericola, D.; Foelske-Schmitz, A.; Kötz, R.; Wokaun, A. Aging of electrochemical double layer capacitors with acetonitrile-based electrolyte at elevated voltages. *Electrochimica Acta* **2010**, *55*, 4412-4420.
(13) Xu, J.; Zhao, L.; Xiong, D.; Zhang, Z.; Yu, J.; Cai, J.; Yang, Z. Density and viscosity behaviour of EBPBF4, TBPBF4 and HBPBF4 in acetonitrile solutions at different temperatures at T = (293.15–323.15) K. *The Journal of Chemical Thermodynamics* **2021**, *158*, 106467-106467.
(14) Kim, M.; Oh, I.; Kim, J. Effects of different electrolytes on the electrochemical and dynamic behavior of electric double layer capacitors based on a porous silicon carbide electrode. *Physical chemistry chemical physics : PCCP* **2015**, *17*, 16367-16374.
(15) Wang, H.; Liu, S.; Liu, S.; Liu, J.; Li, Y. Effect of tetraethylammonium tetrafluoroborate on the performance of super-capacitor battery. *Tianjin Daxue Xuebao (Ziran Kexue yu Gongcheng Jishu Ban)/Journal of Tianjin University Science and Technology* **2014**, *47*, 163-167.
(16) Jin, H.; Wang, X.; Gu, Z.; Anderson, G.; Muthukumarappan, K. Distillers dried grains with soluble (DDGS) bio-char based activated carbon for supercapacitors with organic electrolyte tetraethylammonium tetrafluoroborate. *Journal of Environmental Chemical Engineering* **2014**, *2*, 1404-1409.

(17) Chae, J. S.; Kwon, H. N.; Yoon, W. S.; Roh, K. C. Non-aqueous quasi-solid electrolyte for use in supercapacitors. *Journal of Industrial and Engineering Chemistry* **2018**, *59*, 192-195.
(18) Balducci, A.; Bardi, U.; Caporali, S.; Mastragostino, M.; Soavi, F. Ionic liquids for hybrid supercapacitors. *Electrochemistry Communications* **2004**, *6*, 566-570.
(19) Azaïs, P.; Duclaux, L.; Florian, P.; Massiot, D.; Lillo-Rodenas, M. A.; Linares-Solano, A.; Peres, J. P.; Jehoulet, C.; Béguin, F. Causes of supercapacitors ageing in organic electrolyte. *Journal of Power Sources* **2007**, *171*, 1046-1053.
(20) Yu, X.; Ruan, D.; Wu, C.; Wang, J.; Shi, Z. Spiro-(1,1′)-bipyrrolidinium tetrafluoroborate salt as high voltage electrolyte for electric double layer capacitors. *Journal of Power Sources* **2014**, *265*, 309-316.
(21) Perricone, E.; Chamas, M.; Leprêtre, J. C.; Judeinstein, P.; Azais, P.; Raymundo-Pinero, E.; Béguin, F.; Alloin, F. Safe and performant electrolytes for supercapacitor. Investigation of esters/carbonate mixtures. *Journal of Power Sources* **2013**, *239*, 217-224.
(22) Chiba, K.; Ueda, T.; Yamamoto, H. Performance of Electrolyte Composed of Spiro-type Quaternary Ammonium Salt and Electric Double-layer Capacitor Using It. *Electrochemistry* **2007**, *75*, 664-667.
(23) Nono, Y.; Kouzu, M.; Takei, K.; Chiba, K.; Sato, Y. EDLC performance of various activated carbons in spiro-type quaternary ammonium salt electrolyte solutions. *Electrochemistry* **2010**, *78*, 336-338.
(24) Perricone, E.; Chamas, M.; Cointeaux, L.; Leprêtre, J. C.; Judeinstein, P.; Azais, P.; Béguin, F.; Alloin, F. Investigation of methoxypropionitrile as co-solvent for ethylene carbonate based electrolyte in supercapacitors. A safe and wide temperature range electrolyte. *Electrochimica Acta* **2013**, *93*, 1-7.
(25) Higashiya, S.; Devarajan, T. S.; Rane-Fondacaro, M. V.; Dangler, C.; Snyder, J.; Haldar, P. Synthesis of Oxygen-Containing Spirobipyrrolidinium Salts for High Conductivity Room Temperature Ionic Liquids. *Helvetica Chimica Acta* **2009**, *92*, 1600-1609.
(26) Korenblit, Y.; Kajdos, A.; West, W. C.; Smart, M. C.; Brandon, E. J.; Kvit, A.; Jagiello, J.; Yushin, G. In Situ Studies of Ion Transport in Microporous Supercapacitor Electrodes at Ultralow Temperatures. *Advanced Functional Materials* **2012**, *22*, 1655-1662.
(27) Kalugin, O. N.; Voroshylova, I. V.; Riabchunova, A. V.; Lukinova, E. V.; Chaban, V. V. Conductometric study of binary systems based on ionic liquids and acetonitrile in a wide concentration range. *Electrochimica Acta* **2013**, *105*, 188-199.
(28) Jackson, N. M.; Payne, M. Functional Electrolytes for Use in Non-aqueous EDLCs. *ECS Transactions* **2008**, *16*, 139-149.
(29) Xu, K. Nonaqueous Liquid Electrolytes for Lithium-Based Rechargeable Batteries. *Chemical Reviews* **2004**, *104*, 4303-4418.
(30) Chaban, V. V.; Voroshylova, I. V.; Kalugin, O. N.; Prezhdo, O. V. Acetonitrile Boosts Conductivity of Imidazolium Ionic Liquids. *The Journal of Physical Chemistry B* **2012**, *116*, 7719-7727.
(31) Zhang, Q.-Y.; Xie, P.; Wang, X.; Yu, X.-W.; Shi, Z.-Q.; Zhao, S.-H. Thermodynamic and transport properties of spiro-(1,1')-bipyrrolidinium tetrafluoroborate and acetonitrile mixtures: A molecular dynamics study. *Chinese Physics B* **2016**, *25*, 066102-066102.
(32) Wu, X.; Liu, Z.; Huang, S.; Wang, W. Molecular dynamics simulation of room-temperature ionic liquid mixture of [bmim][BF_4] and acetonitrile by a refined force field. *Physical Chemistry Chemical Physics* **2005**, *7*, 2771-2771.
(33) Koverga, V. A.; Korsun, O. M.; Kalugin, O. N.; Marekha, B. A.; Idrissi, A. A new potential model for acetonitrile: Insight into the local structure organization. *Journal of Molecular Liquids* **2017**, *233*, 251-261.
(34) Frisch, M. J.; Trucks, G. W.; Schlegel, H. B.; Scuseria, G. E.; Robb, M. A.; Cheeseman, J. R.; Scalmani, G.; Barone, V.; Mennucci, B.; Petersson, G. A.; et al. Gaussian 09 Revision A.2. 2009.

(35) Mulliken, R. S. Electronic Population Analysis on LCAO–MO Molecular Wave Functions. I. *The Journal of Chemical Physics* **1955**, *23*, 1833-1840.
(36) Breneman, C. M.; Wiberg, K. B. Determining atom-centered monopoles from molecular electrostatic potentials. The need for high sampling density in formamide conformational analysis. *Journal of Computational Chemistry* **1990**, *11*, 361-373.
(37) Schmid, N.; Eichenberger, A. P.; Choutko, A.; Riniker, S.; Winger, M.; Mark, A. E.; van Gunsteren, W. F. Definition and testing of the GROMOS force-field versions 54A7 and 54B7. *European Biophysics Journal* **2011**, *40*, 843-856.
(38) Kalugin, O.; Lukinova, E.; Novikov, D. Electrical conductivity, ion-molecular and interionic interactions in solutions of some tetraalkylammonium salts in acetonitrile: the influence of the ion and temperature. *Kharkov University Bulletin Chemical Series* **2019**, 24-36.
(39) Pysmennyi, D. Conductometrical study of $SBPBF_4$ solutions in acetonitrile. V.N.Karazin Kharkin National University, 2018.
(40) Humphrey, W.; Dalke, A.; Schulten, K. VMD: Visual molecular dynamics. *Journal of Molecular Graphics* **1996**, *14*, 33-38.
(41) Vovchynskyi, I. S.; Kolesnik, Y. V.; Filatov, Y. I.; Kalugin, O. N. Molecular modelling on solutions of 1-1′-spirobipirrolidinium tetrafluoroborate in acetonitrile. *Journal of Molecular Liquids* **2017**, *235*, 60-67.
(42) France-Lanord, A.; Grossman, J. C. Correlations from Ion Pairing and the Nernst-Einstein Equation. *Phys Rev Lett* **2019**, *122*, 136001.
(43) Dudariev, D.; Lohachova, E.; Vovchynskyi, I.; Koverga, V.; Kalugin, O. Ion association and transport properties of highly concentrated ion-molecular systems: MD simulation. *Electrochemistry of Today: Achievements, Problems and Prospects. Collective monograph.* **2021**, 58-59.

Chapter 5. Microstructure and transport properties of imidazolium-based ionic liquids and molecular solvents from molecular dynamics simulations

Binary mixtures based on aprotic dipolar solvents like acetonitrile (AN, propylene carbonate (PC) or gamma butyrolactone (γ-BL) with room-temperature ionic liquids are widely used in the modern electrochemistry. These systems have maximum on the electroconductivity as well as other changes in diluted solutions confirmed by the nmR and vibration spectroscopic data, there is no such theory that can explain these phenomena. In current chapter twelve ILs (C_4mim^+ with BF_4^-, PF_6^-, TFO^- and $TFSI^-$) with molecular solvents (AN, PC and γ-BL) mixtures were studied by the molecular dynamics simulation technique. The local structure of the mixtures was studied in the framework of RDFs and RCNs that showed the particular behavior in AN and $TFSI^-$ systems. For $TFSI^-$ system the presence of two peaks on the RDFs with similar intensities were observed. The mutual arrangement of cation and anion corresponding to observed on the RDFs interatomic distances were investigated: they represent the position when the nitrogen atom of the anion is close to the imidazolium ring and when nitrogen atom of TFSI- not directly interacting with the ring, but instead the oxygen atoms do. The cation-anion coordination numbers changed for mixtures with AN from ~1.2 to ~3.6, for PC – from 0.6 to 3.0 and for γ-BL – from 0.8 to 3.1 with the increasing mole fraction of the ILs. Also, the association analysis with two different distance criteria have been performed. It showed the formation of the massive clusters at ~0.15, 0.20 and 0.25 IL mole fraction for AN, PC and for γ-BL respectively for the first criterium. These findings points out the overestimation of the aggregation process. With the second, stricter criterion the formation of big aggregates in the systems starting to occur at similar mole fractions of the ILs where the experimental conductivity curves have maximum. To analyze the transport properties the diffusion coefficients of all the components and shear viscosity for all binary mixtures were obtained. The diffusion coefficients show good agreement with experimental data. Although, the viscosity values didn't show any particular behavior.

5.1. Introduction

Ionic liquid (IL) mixtures with molecular solvents can be considered as electrolyte solutions, for which their structure and properties are determined by the balance of types of interactions between all particles in the solution (cation, anion and solvent), which determine the existence of ionic associates and high-order aggregates.[1-6] In this context, the main feature of binary systems based on IL is that the constituent ions are polyatomic and, as a rule, asymmetric. As a result, the interactions mentioned above should be considered as anisotropic, having a predominant localization around some molecular fragment (center of interaction).[7-9] Another important feature of these systems in comparison with ordinary solutions of electrolytes is the complete miscibility of IL with many molecular solvents, which makes it possible to obtain mixtures corresponding to either a solution of such a liquid in a molecular solvent or a solution of a molecular solvent in an ionic liquid.

Intermolecular interactions in mixtures of two liquids of different nature can be showed as a gradual transition from the “first pure liquid” to the “second pure liquid” through intermediate compositions. Thus, the task boils down to the following question: which ranges of composition correspond to the above-mentioned areas, and which intermolecular interactions are decisive.[10]

For pure ILs, there is currently no generally accepted picture of their structure due to the indirect nature of the methods used. It is widely believed that in the liquid state the structure of imidazolium ionic liquids is determined by strong interionic Coulomb interactions, which are relatively effectively shielded away from the central ion (i.e., are quite local). It is also assumed that a significant contribution is made by the three-dimensional network of hydrogen bonds between counterions.[11-15] The strength and structure of this network are determined by the nature (polarizability, polarizing action, size, etc.) of the anion.[16]

The above-mentioned considerations about the structure of pure components indicate the presence of two main phenomena in which a redistribution of the equilibrium between possible ion-ion, ion-molecular and intermolecular interactions can be manifested when the composition changes. These are ionic association and ionic solvation.[6, 17-20]

These phenomena can be understood as the gradual destruction of large ionic associates (the basic structural units of pure ionic liquids) into smaller ones, up to ion pairs. Subsequently, ion pairs completely dissociate into "free" ions in dilute solutions as a result of interaction with the solvent. Such an interaction can be both specific (localized ion-molecular interactions) and non-specific (the effect of the accumulation of a significant amount of solvent capable of forming an environment similar to a pure solvent).[21]

The phenomena of ionic association and solvation are manifested at the microscopic level in the redistribution of electron density in the corresponding areas of interaction and, therefore, in changes in the corresponding force constants. Among the currently known experimental methods that can detect such effects, NMR[17, 22-25] and vibrational (IR and Raman) spectroscopy[26-28] should be singled out. The first can reveal information about the change in the electronic microenvironment of each chemically non-equivalent nucleus and the relative location for some nuclei, while the second investigates changes in the constants of the dipole moment, polarizability, changes in the microenvironment of atoms participating in the studied vibrational mode.[17, 29]

The association and solvation are also reflected in the "statistical" microstructure of such binary mixtures. Currently, only various methods of diffraction of X-rays and neutrons can provide experimental data on the such microstructure in different time and size scales. Also, they are quite expensive and not always available, as well as difficult from the point of view of data processing. As well, usually there is only one IL-solvent system under investigation[30, 31] which means that the approach for studying such objects should be wider and more universal. Molecular dynamics (MD) simulation can help solve these problems,

and this method can also complete the picture with information not available from experiment.[32-34]

In this Chapter MD simulation of 12 mixtures of ILs (1-butyl-3-methylimidazolium C_4mim^+ cation coupled with BF_4^-, PF_6^-, TFO^- and $TFSI^-$ anions) with molecular solvents (AN, PC and γ-BL) of six IL mole fractions were performed. The molecular structures of the objects are presented at Figure 5.1. The microstructure, clusterization and, finally, the transport properties of the systems have been studied. The Chapter is organized as follows. In sec. 2 details of the system setup is provided. In sec. 3 the results of the simulation are showed and discussed. In sec. 4 the main conclusions of the study of this Chapter are summed up.

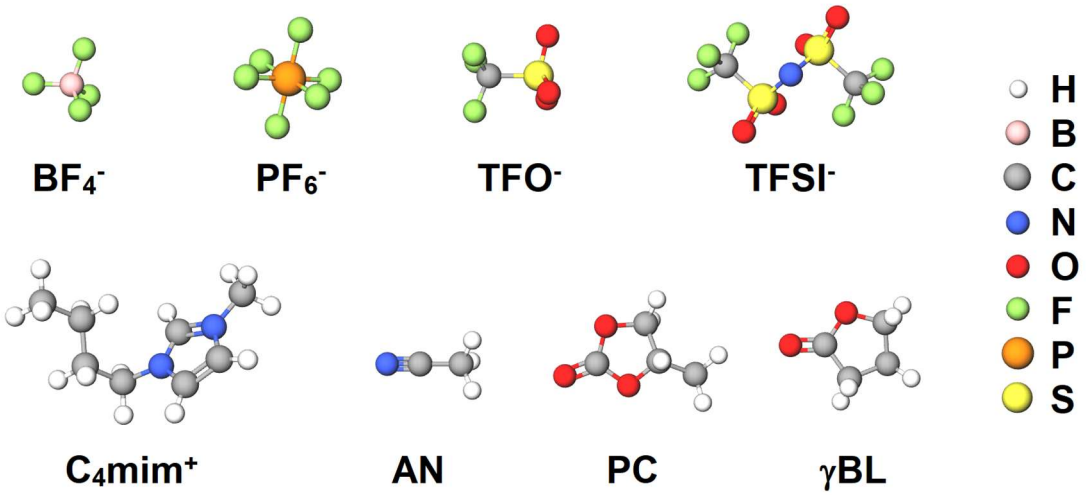

Figure 1. Structure of the ions and molecular solvents considered in this study.

5.2. Details of molecular dynamics simulation

The simulations of the binary mixtures (total of 12 systems) of four ILs of C_4mim^+ cation with different anions (BF_4^-, PF_6^-, TFO^- and $TFSI^-$) in three aprotic dipolar molecular solvents (AN, PC and γ-BL) have been performed. Six different compositions of the mole fraction of the ILs from 0.05 to 0.30 for each binary mixture were selected in a way that the total number of ion pairs for each

composition was always equal to 100. The number of the different particles of the ILs in the simulated systems are collected in Table 5.1.

Table 5.1. Composition of the systems simulated.

IL mole fraction	Number of cations	Number of anions	Number of solvent molecules
0.05	100	100	1900
0.10			900
0.15			566
0.20			400
0.25			300
0.30			232

The ILs have been described by the potential model of Mondal and Balasubramanian,[35, 36] while for the solvent molecules the potential model of Koverga et al.[37, 38] has been used. According to classical MD formalism, these potential models have the following functional form of the total potential energy:

$$U_{tot} = \sum_{ij}^{bonds} \frac{k_{r,ij}}{2}\left(r_{ij} - r_{0,ij}\right)^2 + \sum_{ijk}^{angles} \frac{k_{\theta,ijk}}{2}\left(\theta_{ijk} - \theta_{0,ijk}\right)^2 + \sum_{ijkl}^{dihedral} \sum_{n=0}^{5} C_n \left(\cos\left(\psi_{ijkl}\right)\right)^n + \\ + \sum_{ij}^{nonbonded} \left(4\varepsilon_{ij}\left[\left(\frac{\sigma_{ij}}{r_{ij}}\right)^{12} - \left(\frac{\sigma_{ij}}{r_{ij}}\right)^{6}\right] + \frac{q_i q_j}{4\pi\varepsilon_0 r_{ij}} \right), \tag{5.1}$$

where k is the force constant for bond stretching (r), angle bending (θ), torsion (ϕ), respectively, ε and σ are the Lennard-Jones energy and the distance parameters, respectively, and q stands for the fractional charges of the interaction sites. For torsion angle $\psi_{ijkl} = 180^o - \phi_{ijkl}$. Indices i, j, k and l run through the interaction sites of the particles, while the subscript '0' refers to the equilibrium value of the bond lengths and angles. The potential model of ILs can be regarded a refinement of the CLaP force field.[39-41] Thus, while the bond and angle

parameters have been retained, the torsional parameters have been adapted to the Ryckaert-Bellemans analytical expression.[42] Further, the charge distribution of the ions has been optimized in order to improve the agreement with the experimental thermodynamic and transport properties of the studied ILs. Thus, the ions of the IL carry a net charge that depends on the anion.[35, 36] The potential models used here were previously validated by their ability of reproducing the basic experimental physicochemical properties of the systems.[35, 36]

5.3. Results and discussion

5.3.1. Structural properties

With the aim to study the cation-anion interaction, the interionic RDFs and RCNs of IL-solvent binary mixtures were analyzed. To fully consider these interactions the respective atoms for cations and anions should be chosen. Also, these points in space need to take into consideration all the coordination centers of cations and anions at once. For the C_4mim^+ cation the most positive charge localized at the H-sites around imidazolium ring. Given this fact the center of the ring (CoR) is usually chosen as a reference point for the analysis.[43-45] Due to different structure, shape and symmetry of the anions their positions (X) for the analysis will be the follows: B atom in BF_4^-, P atom in PF_6^-, middle of the C-S bond in TFO^- (takes into account both O and F coordination sites) and N atom in $TFSI^-$ (takes into account N, O and F coordination sites).

The interionic RDFs for all IL-solvent binary mixtures for all simulated systems are shown in Figure 5.2.

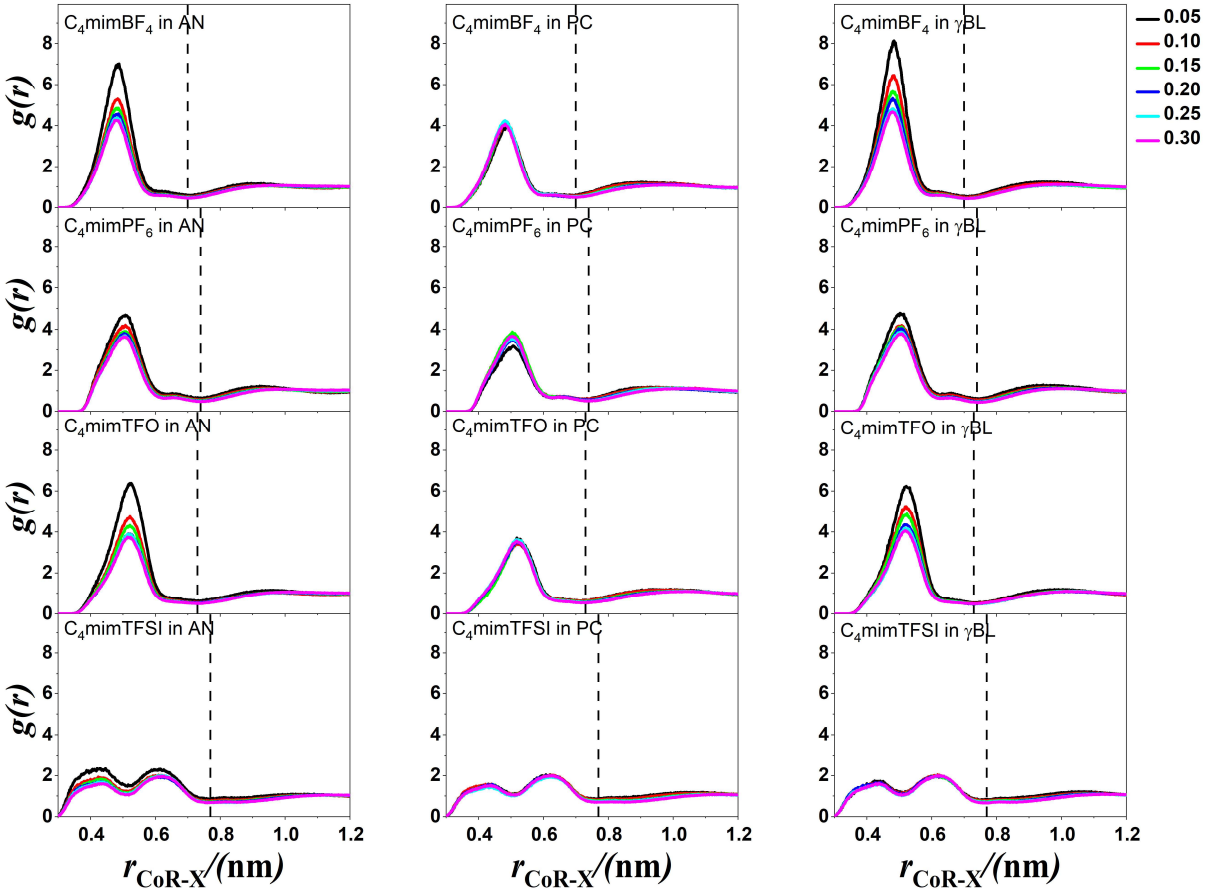

Figure 5.2. Cation-anion (CoR-X) radial distribution functions of the mixtures at various mole fraction of ionic liquid. The position of the cation is described with center of imidazolium ring. The positions of anions (X) are: B atom in BF_4^-, P atom in PF_6^-, middle of the C-S bond in TFO^- and N atom in $TFSI^-$. The vertical dashed line corresponds to the first coordination shell.

Here the similar curves were obtained for all IL mole fractions, meaning the positions of the peaks and minima do not depend on the concentration of the IL. Furthermore, their positions do not vary at all for the same IL in different solvents. The first maxima for various anions occur at 0.49 nm (BF_4^-), 0.51 nm (PF_6^-) and 0.52 nm (TFO^-). For the $TFSI^-$ anion the situation is more complicated as there are two peaks at relatively low distances, 0.44 nm and 0.62 nm respectively. Also, these peaks have lower intensity comparing to other ILs. The first maximum in this case corresponds to the CoR-N interaction when N atom is located directly near the center of the ring or the H-atoms of the ring (the distances in both cases are similar). At the same time the second peak indicates the CoR-N

interaction when N atom of $TFSI^-$ not directly interacting with the ring, but instead the oxygen atoms do. The example snapshot from the MD simulation trajectory files was obtained via VMD program package[46] (Figure 5.3). These findings prove the quantum chemical calculations from the literature data.[47] The first minima of RDFs for various anions are as follows: 0.70 nm (BF_4^-), 0.74 nm (PF_6^-), 0.73 nm (TFO^-) and 0.77 nm ($TFSI^-$). Also, for PF_6^-. The behavior of the intensities of the peaks also changes in different ILs-solvent combinations. For all systems with AN the intensity becomes lower with the increasing of the ILs mole fraction. Also, for $TFSI^-$ system these changes are the lowest. Similar situation can be observed for all PC-containing systems where peak intensity do not change with the mole fraction of the ILs.

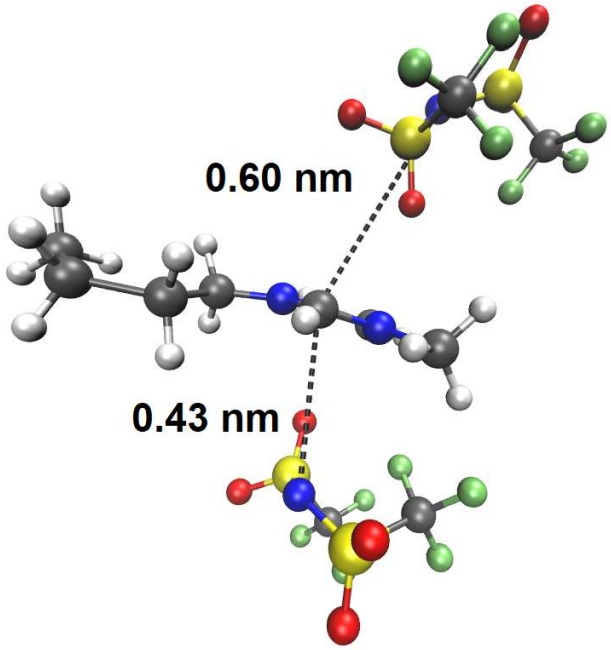

Figure 5.3. Example of $(C_4mim(TFSI)_2)^-$ associate in one of the C_4mimTFSI system.

The RCNs between cations and anions for all IL-solvent binary mixtures for all the systems simulated are presented in Figure 5.4.

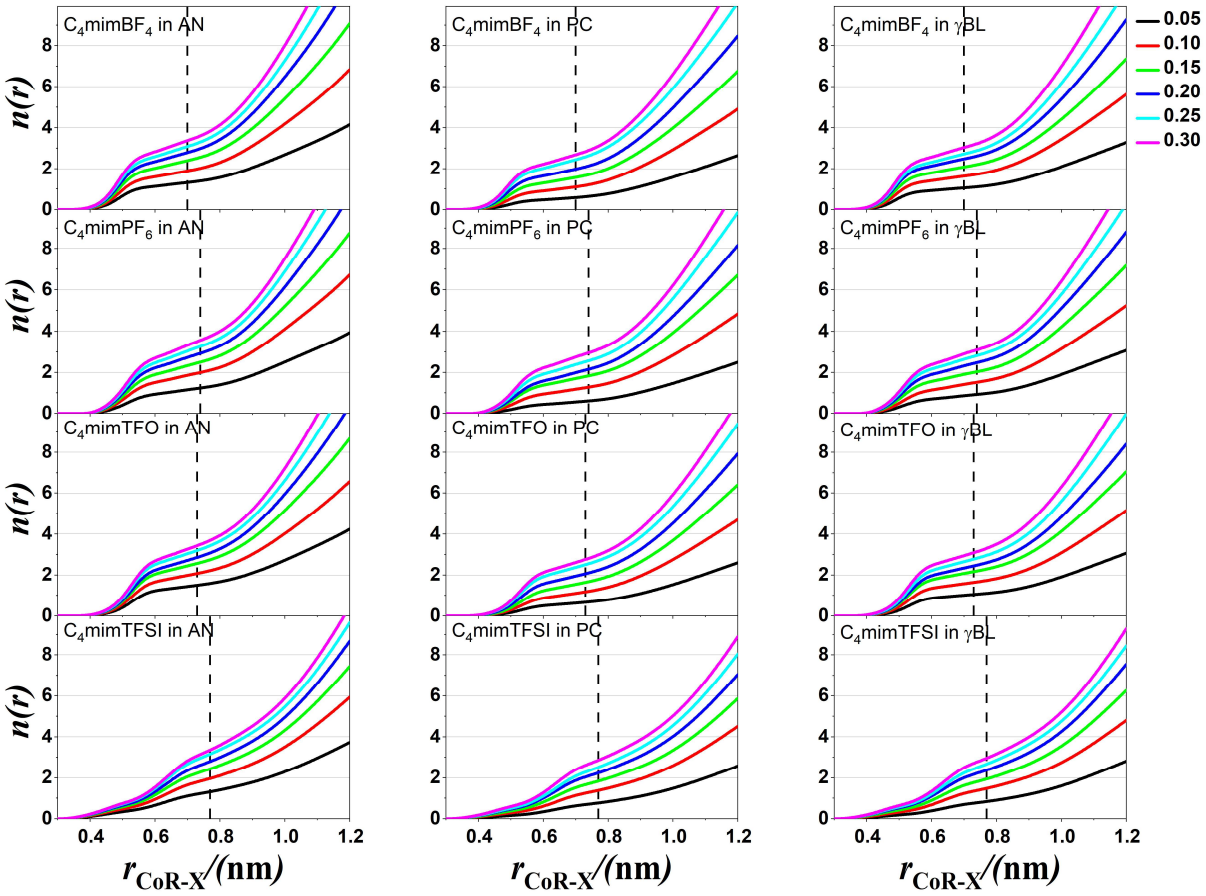

Figure 5.4. Cation-anion (CoR-X) running coordination numbers of the mixtures at various mole fraction of ionic liquid. The position of the cation is described with center of imidazolium ring. The positions of anions (X) are: B atom in BF_4^-, P atom in PF_6^-, middle of the C-S bond in TFO^- and N atom in $TFSI^-$. The vertical dashed line corresponds to the first coordination shell.

The expected increase of the coordination number of the anion around the cation with the IL mole fraction increase can be observed at all of the graphs. The values of the coordination numbers however depend on the solvent. E.g., for AN it varies from ~1.2 (0.05 mole fraction of IL) to ~3.6 (0.30 mole fraction of IL), for PC – from 0.6 to 3.0 and for γ-BL – from 0.8 to 3.1 for all ILs. The coordination numbers of AN system being the biggest indicate the lowest among other solvent molecules dipole moment and as a result the weakest ion-solvent interaction in these systems, meaning with the ILs fraction increase the AN molecules are actively replaced with the anions in the cation first coordination sphere. Also, in

the case of all $TFSI^-$ systems the curves values do not increase until at bigger distances.

5.3.2. Aggregate analysis

The ionic aggregates existence was analyzed via two different criteria. First criterion is the first minimum on the cation-anion RDF (Figure 5.2). This distance shows the border for the first coordination sphere where all of the anions are in strong interaction with the C_4mim^+ cation. The second criterion is the minimum on the second derivative of the RCN curve (Figure 5.5).

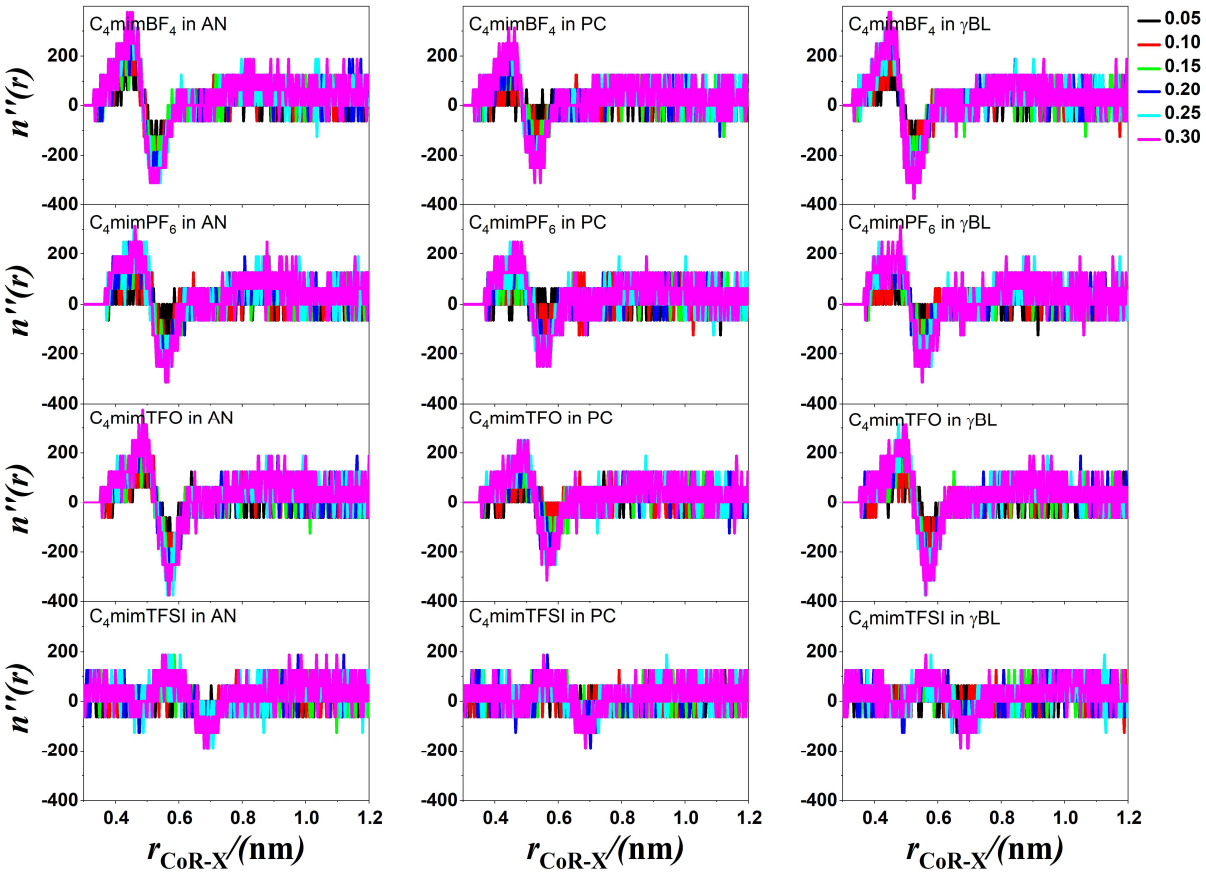

Figure 5.5. Second derivatives of the cation-anion (CoR-X) running coordination numbers of the mixtures at various mole fraction of ionic liquid. The position of the cation is described with center of imidazolium ring. The positions of anions are: B atom in BF_4^-, P atom in PF_6^-, middle of the C-S bond in TFO^- and N atom in $TFSI^-$.

This distance corresponds approximately to the area where the RCN curve starts to change its shape to the plateau after the initial rapid increase (first maximum on the RDF; second for the systems with $TFSI^-$ anion as described in the previous section). The values are next: 0.53 nm (BF_4^-), 0.56 nm (PF_6^-), 0.57 nm (TFO^-) and 0.69 nm ($TFSI^-$).

The results of the clusters formation probability for all mixtures of all mole fractions can be found in Figures 5.6-5.17 for the first and second criteria respectively.

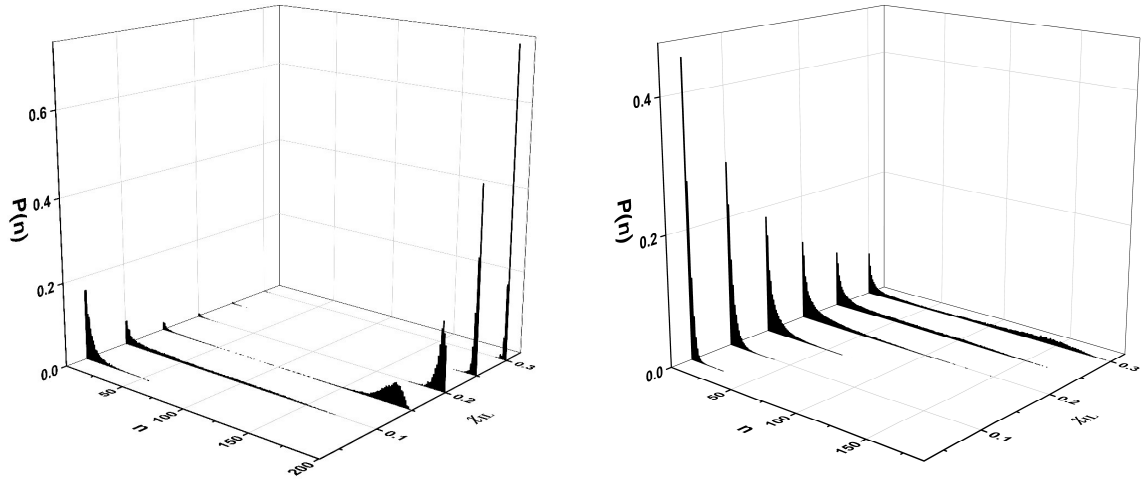

Figure 5.6. Probability distributions of aggregate sizes with first (left) and second (right) criterion of the C_4mimBF_4 in AN binary mixture at various mole fraction of ionic liquid.

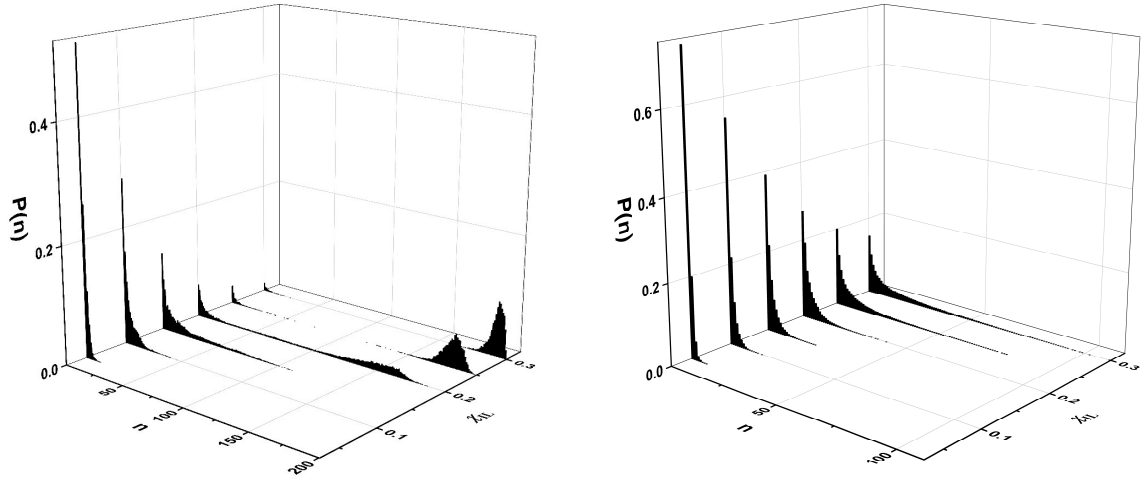

Figure 5.7. Probability distributions of aggregate sizes with first (left) and second (right) criterion of the C_4mimBF_4 in PC binary mixture at various mole fraction of ionic liquid.

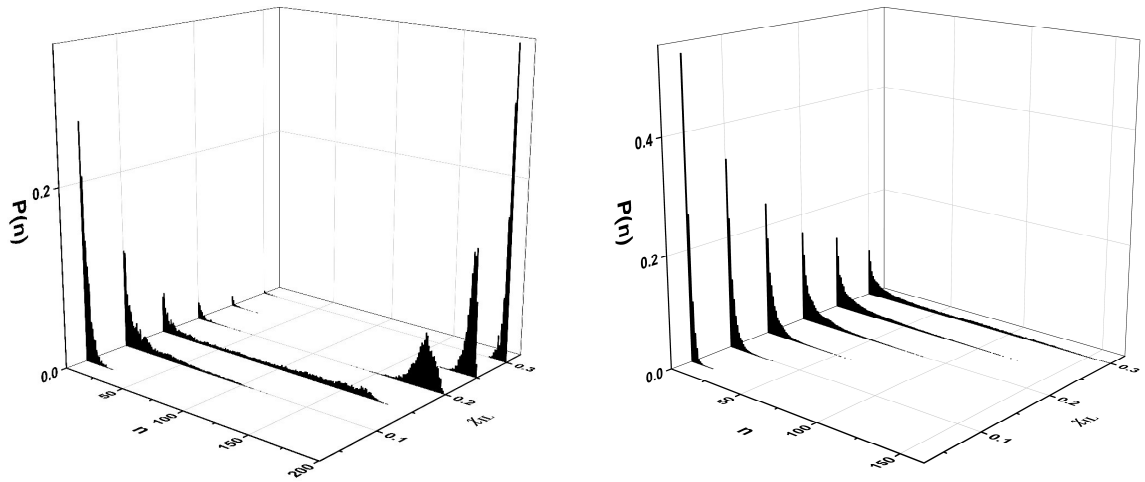

Figure 5.8. Probability distributions of aggregate sizes with first (left) and second (right) criterion of the C_4mimBF_4 in γ-BL binary mixture at various mole fraction of ionic liquid.

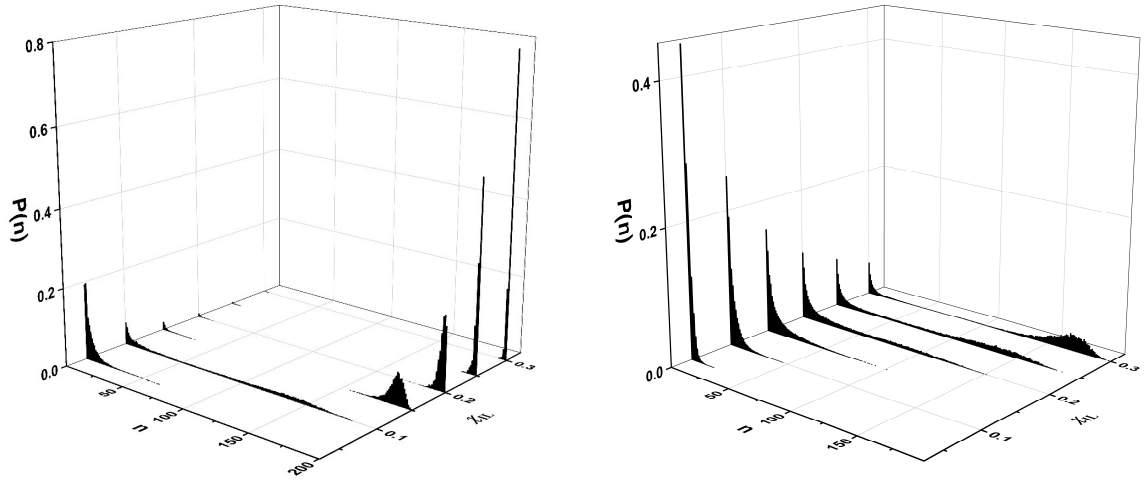

Figure 5.9. Probability distributions of aggregate sizes with first (left) and second (right) criterion of the C_4mimPF_6 in AN binary mixture at various mole fraction of ionic liquid.

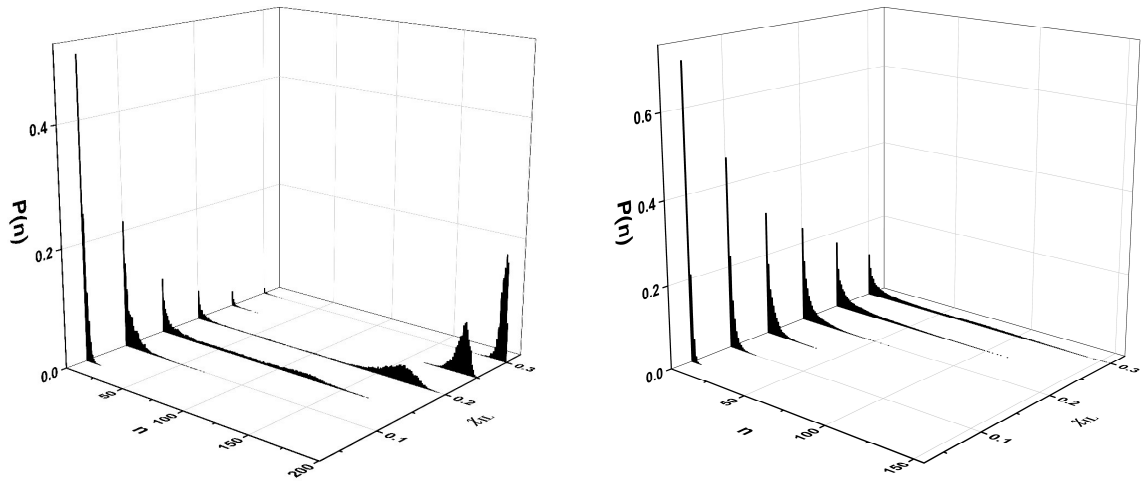

Figure 5.10. Probability distributions of aggregate sizes with first (left) and second (right) criterion of the C_4mimPF_6 in PC binary mixture at various mole fraction of ionic liquid.

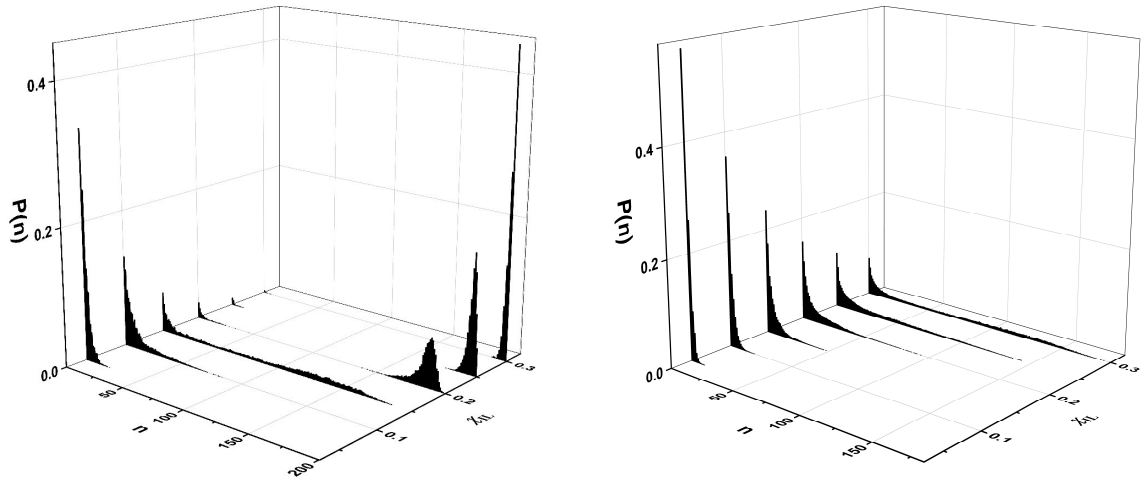

Figure 5.11. Probability distributions of aggregate sizes with first (left) and second (right) criterion of the C_4mimPF_6 in γ-BL binary mixture at various mole fraction of ionic liquid.

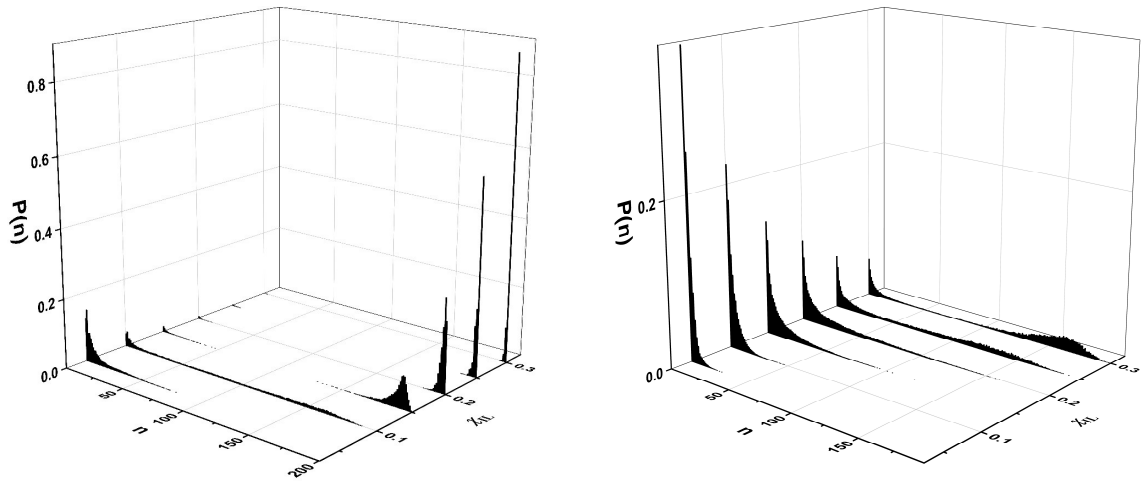

Figure 5.12. Probability distributions of aggregate sizes with first (left) and second (right) criterion of the C_4mimTFO in AN binary mixture at various mole fraction of ionic liquid.

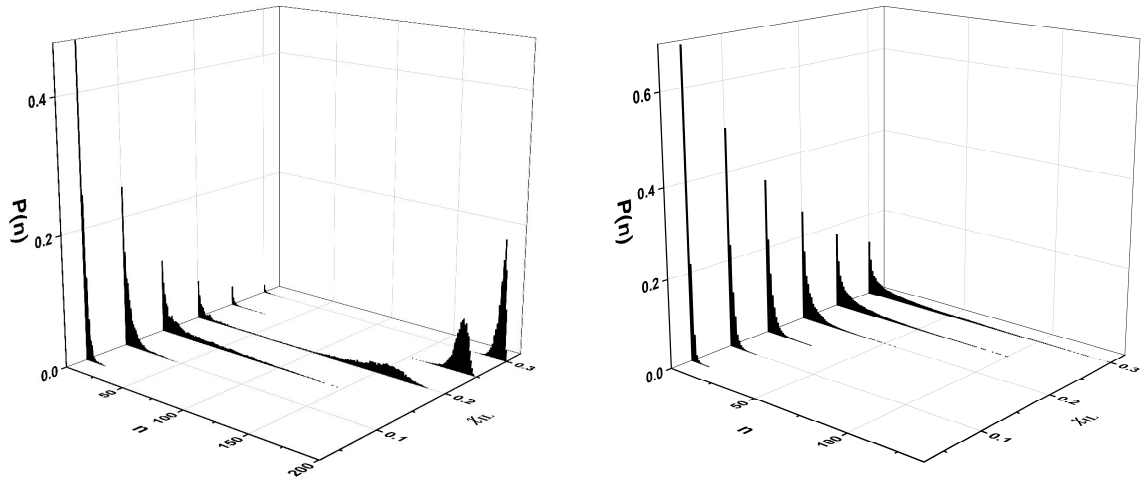

Figure 5.13. Probability distributions of aggregate sizes with first (left) and second (right) criterion of the C_4mimTFO in PC binary mixture at various mole fraction of ionic liquid.

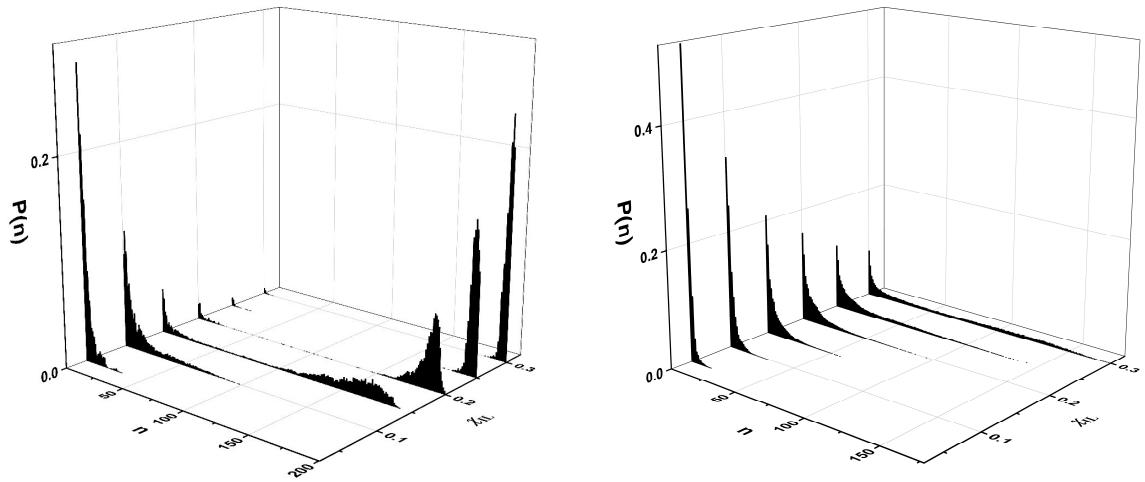

Figure 5.14. Probability distributions of aggregate sizes with first (left) and second (right) criterion of the C_4mimTFO in γ-BL binary mixture at various mole fraction of ionic liquid.

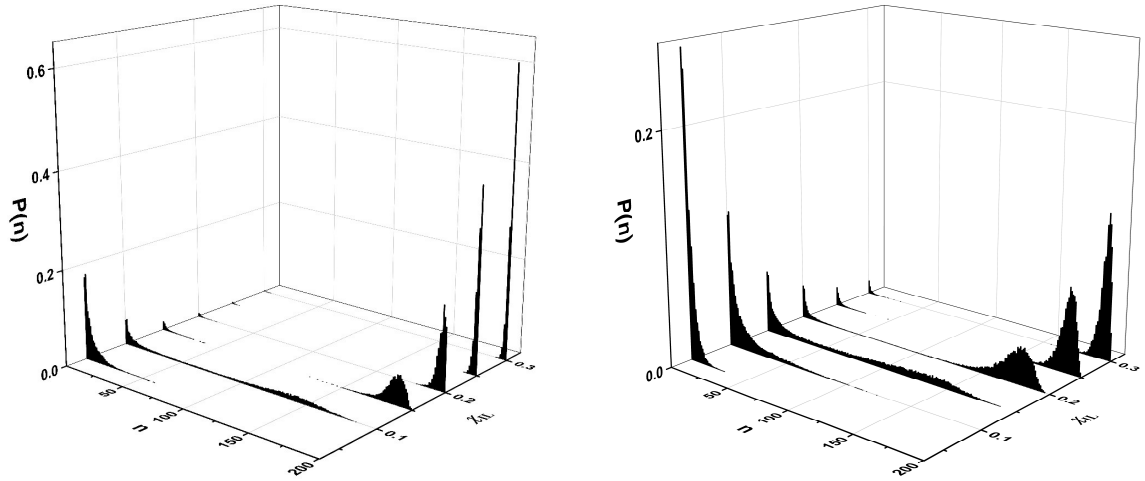

Figure 5.15. Probability distributions of aggregate sizes with first (left) and second (right) criterion of the C_4mimTFSI in AN binary mixture at various mole fraction of ionic liquid.

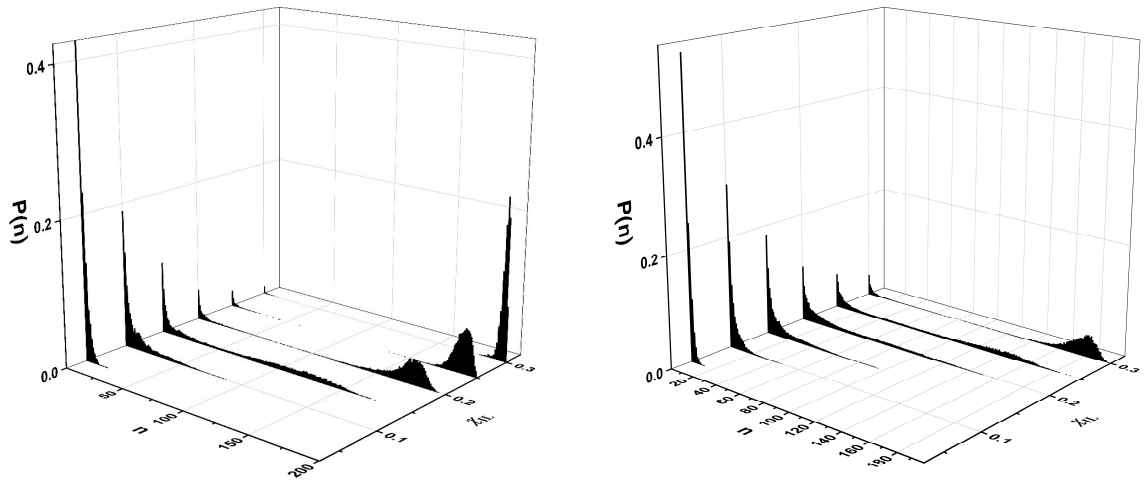

Figure 5.16. Probability distributions of aggregate sizes with first (left) and second (right) criterion of the C_4mimTFSI in PC binary mixture at various mole fraction of ionic liquid.

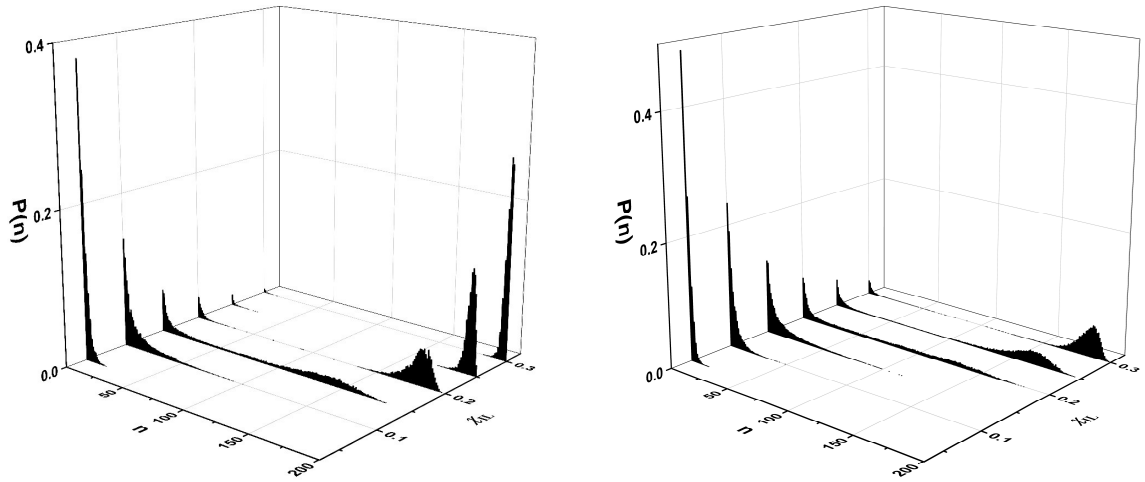

Figure 5.17. Probability distributions of aggregate sizes with first (left) and second (right) criterion of the C_4mimTFSI in γ-BL binary mixture at various mole fraction of ionic liquid.

The aggregates increase in size with the increasing of the IL mole fraction for each system. The small clusters are dominating in the most diluted systems when using the first criteria. With the increasing of the IL mole fraction up until 0.10 for AN mixtures, 0.15 for PC mixtures and 0.20 for γ-BL mixtures transition

systems formed where a large number of aggregates of different types are present. With the further increase of mole fraction of the ILs all the systems start to form large aggregates that include most of the ions in the mixture can be observed. The existence of such huge continuous polar network, however, still allows small clusters or even isolated ions to exist in systems. Most probably these small aggregates lose the connectivity with the huge cluster, but their low probabilities of formation prove that it is a temporary phenomenon. At the highest observed concentration, nevertheless, the ions are part of one massive associate.

It shows that at the first distance criterion (minimum on the interionic RDF) the aggregate formation is overestimated in the mixture as there are no charge carriers left in this case and thus there should be no conductivity at these mole fraction of the ILs. However, the experimental results show otherwise.[48-51]

As for the second criteria, it shows that transition to the massive association occurs only at the highest IL mole fraction of 0.30 (for $TFSI^-$ – at 0.20-0.25). However, for the binary mixtures with AN the tendency for larger clusters formation appears at lower IL mole fraction compared to PC and γ-BL mixtures. This shows that AN demonstrates a weaker ion-solvent interaction, allowing ions at lower concentration form a continuous polar network regardless of the chosen criteria.

To better illustrate the clusterization processes the average numbers of associations were obtained for all systems (Figure 5.18). The figure displays in more compact way the same results that were discussed earlier. Here for the first criterion ions in AN systems form massive aggregates at 0.15 mole fraction of ILs already, in γ-BL and PC mixtures – at 0.20 and 0.25 respectively. For the second criterion the ions in the systems are separated from each other or forming small aggregates until ~0.15-0.20 mole fraction of the ILs. After that mole fraction ILs in mixtures tend to form bigger aggregates. For the BF_4^-, PF_6^- and TFO^- in PC this trend is not so pronounced. The massive aggregation process occurs only in $TFSI^-$ systems for the second criterion and only at highest concentration of 0.30. The AN systems at this concentration at the transition stage, however for the

C_4mimTFSI in AN mixture almost all ions are part of the big associate even at the mole fraction of ILs of 0.25.

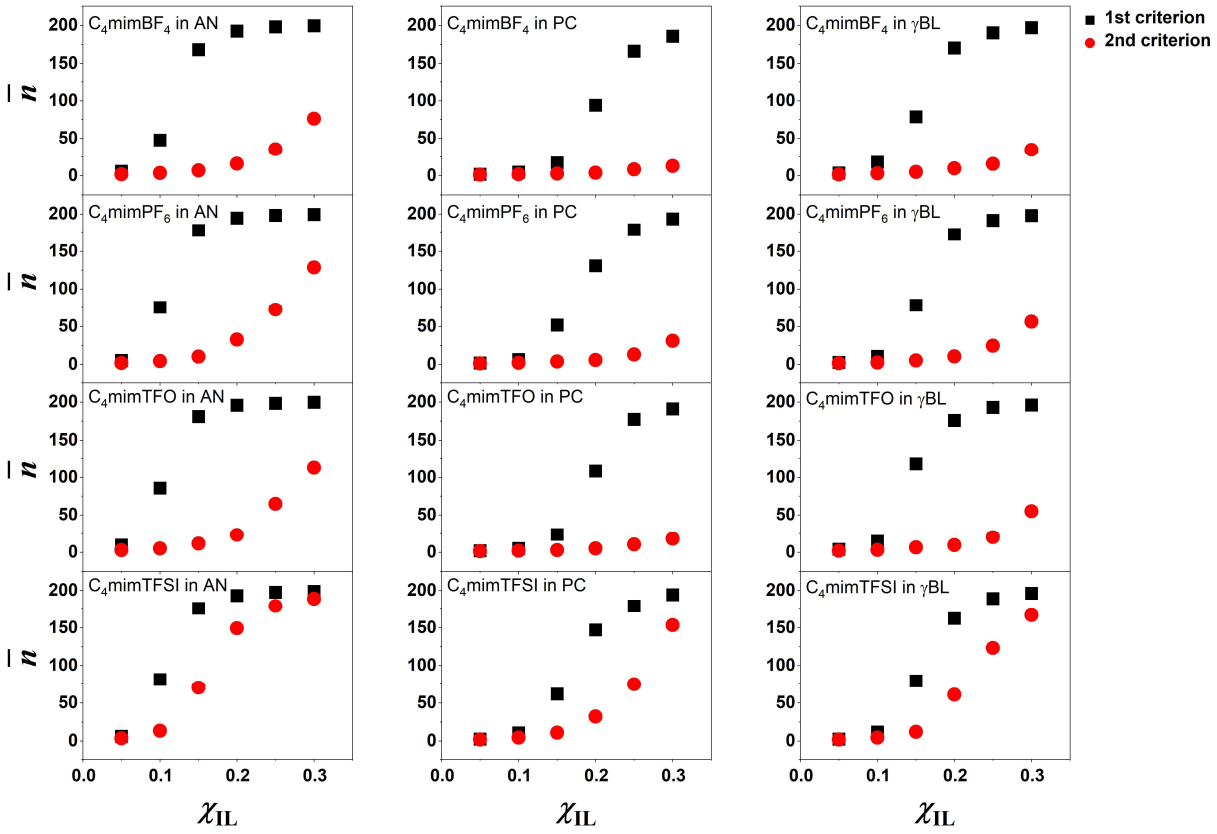

Figure 5.18. Average numbers of association with first minima on the RDFs (1st criteria) and with the minima on the second derivative on the RCN (2nd criteria) of the mixtures at various mole fraction of ionic liquid.

Nernst-Einstein relation postulates that conductivity depends on the concentration of the charge carriers in the solution.[52] Ionic aggregation reduces its concentration and effectively causes the drop in the conductivity value. As seen from the Figure 5.18, the mole fractions of rapid increase in the aggregates formation are the same as the conductivity maxima are located: at ~0.10 for AN systems and at ~0.20 for PC and γ-BL ones.[48-51]

5.3. Transport properties

The diffusion coefficients and shear viscosities were obtained for all the IL mole fractions for all systems. The results are presented at Figures 5.19 and 5.20 respectively.

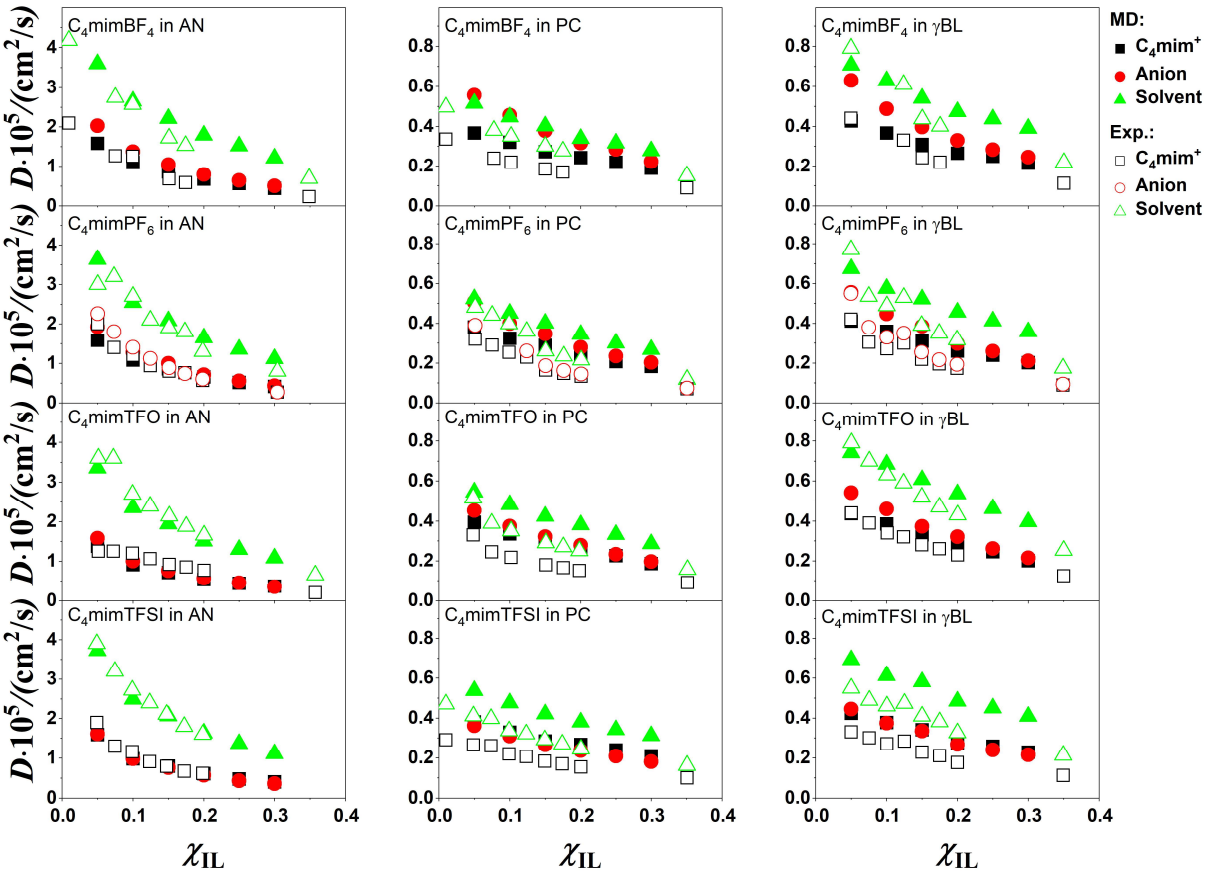

Figure 5.19. Diffusion coefficients for cation, anions and solvent molecules in comparison with the experimental data[53] of the mixtures at various mole fraction of ionic liquid.

The diffusion coefficients were compared to the experimental data for cations and solvent molecules (and also for anions for the systems with PF_6^-).[53] For the binary mixtures with AN the obtained coefficients are very close to the experimental ones for all of the components of the analysis. For the systems with PC and γ-BL the obtained diffusion coefficients have in general higher values comparing to the experiment by 20%, especially for the higher concentrations.

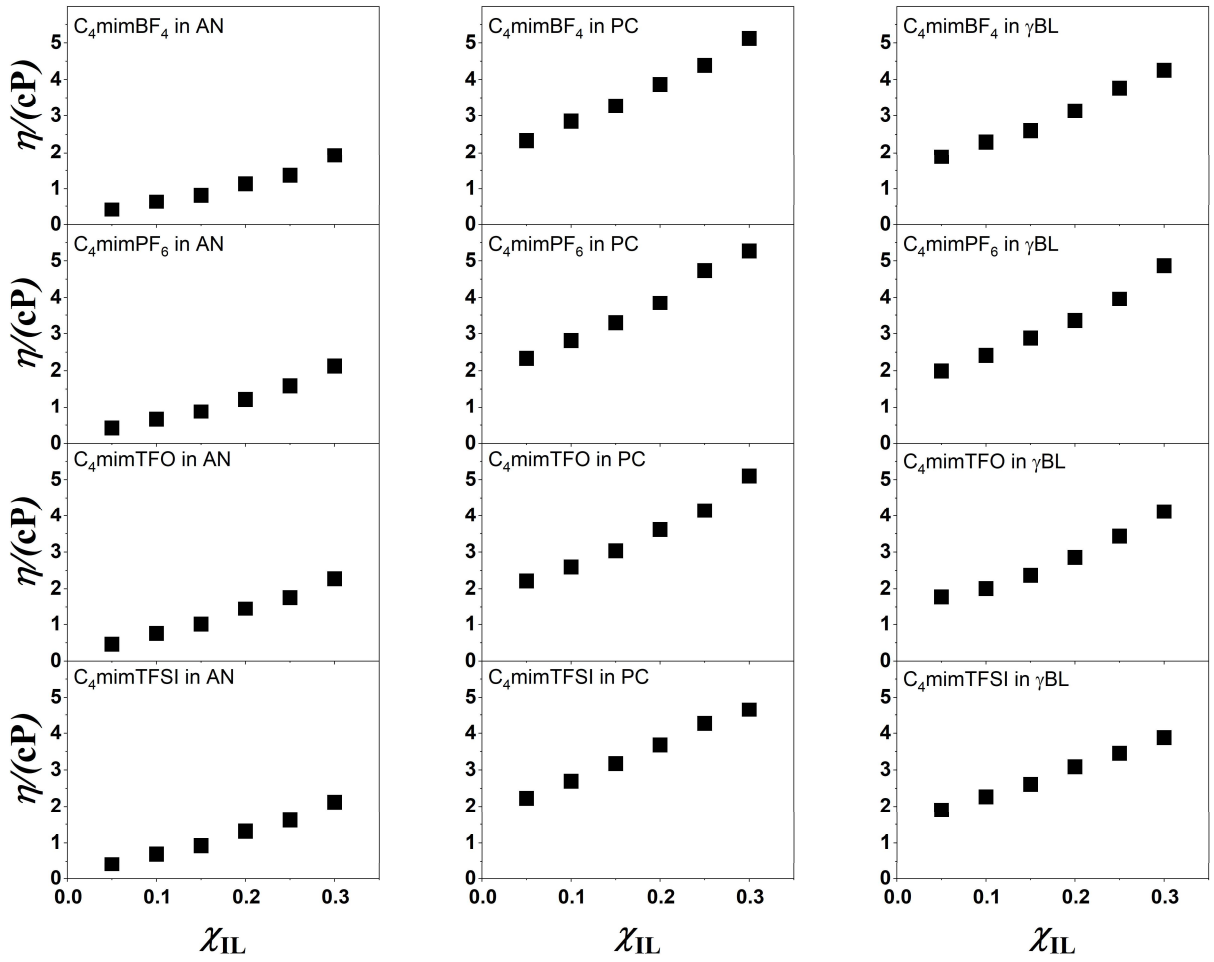

Figure 5.20. Viscosities of the mixtures at various mole fraction of ionic liquid.

For all systems the diffusion coefficients of the solvent molecules are higher than of the cation or anions, while the latter are close to each other for almost all systems and IL mole fractions. Also, the coefficients of the components in the systems with AN molecules are 3-5 times higher than with other two solvent molecules. For all PC systems the general trend is almost similar diffusion coefficient for anion and solvent molecule. For the C_4mimBF_4 in PC simulated system the anion diffusion coefficient is even higher in the most diluted solution. On the other hand, this behavior cannot be observed in the experimental data.

The viscosities at Figure 5.20 are increasing with the IL mole fraction increase by a non-linear dependance. Although, the values for all systems do not show any drastic changes at respective mole fractions where the experimental conductivity has maximum.

As the Nernst-Einstein relation shows, not only concentration of the charge carriers influence the conductivity but the diffusion coefficients as well.[52] The behavior of calculated diffusion coefficients from the simulation for ions is in agreement with this statement.

5.4. Conclusions

In current chapter twelve ILs (C_4mim^+ with BF_4^-, PF_6^-, TFO^- and $TFSI^-$) with molecular solvents (acetonitrile, propylene carbonate, and gamma butyrolactone) binary mixtures were studied by the molecular dynamics simulation technique.

The microstructure of the mixtures was studied in the framework of radial distribution functions and running coordination numbers. The RDFs and RCNs show the particular behavior in AN and $TFSI^-$ systems. For TFSI- system the cation-anion (CoR-N) RDFs curves showed two peaks with similar intensities. It was shown that they represent the position when the nitrogen atom of the anion is close to the imidazolium ring and when nitrogen atom of $TFSI^-$ not directly interacting with the ring, but instead the oxygen atoms do. The cation-anion coordination numbers changed in similar values for the same ionic liquids in different solvents: for AN it varies from ~1.2 to ~3.6, for PC – from 0.6 to 3.0 and for γ-BL – from 0.8 to 3.1 with the increasing mole fraction of the ILs. Also, data obtained were used to conduct a quantitative aggregate analysis with two different distance criteria (first minimum of RDF and minimum of the second derivative of the RCN respectively) to compare the results with each other. The analysis with the first criterion shows the formation of the massive cluster at ~0.15, 0.20 and 0.25 IL mole fraction for AN and for with γ-BL respectively. Thus, this criterion seems to overrate the aggregation process in the mixtures. With the second, stricter distance criteria the formation of big aggregates in the systems starting to occur at the same mole fractions of the ILs where the experimental conductivity curves change their behavior and the maximum occurs. It proves that the reason

of such drastic changes in the conductivity particular lies in the local structure of the ILs and solvent molecules.

To analyze the transport properties the diffusion coefficients of all the components and shear viscosity for all binary mixtures were obtained. The diffusion coefficients show good agreement with experimental data, especially for the systems with AN. The viscosity values didn’t show any particular behavior at the mole fraction of the ILs range where the experimental conductivity maximum occur.

5.5. References for Chapter 5

(1) Dorbritz, S.; Ruth, W.; Kragl, U. Investigation on Aggregate Formation of Ionic Liquids. *Advanced Synthesis & Catalysis* **2005**, *347*, 1273-1279.
(2) Andanson, J. M.; Traïkia, M.; Husson, P. Ionic association and interactions in aqueous methylsulfate alkyl-imidazolium-based ionic liquids. *The Journal of Chemical Thermodynamics* **2014**, *77*, 214-221.
(3) Bešter-Rogač, M.; Stoppa, A.; Hunger, J.; Hefter, G.; Buchner, R. Association of ionic liquids in solution: a combined dielectric and conductivity study of [bmim][Cl] in water and in acetonitrile. *Physical Chemistry Chemical Physics* **2011**, *13*, 17588-17588.
(4) Jan, R.; Rather, G. M.; Bhat, M. A. Association of ionic liquids in solution: Conductivity studies of [BMIM][Cl] and [BMIM][PF6] in binary mixtures of acetonitrile + methanol: Ion association in ionic liquid solutions. *J Solution Chem* **2013**, *42*, 738-745.
(5) Hou, J.; Zhang, Z.; Madsen, L. A. Cation/anion associations in ionic liquids modulated by hydration and ionic medium. *Journal of Physical Chemistry B* **2011**, *115*, 4576-4582.
(6) Boruń, A. Conductance and ionic association of selected imidazolium ionic liquids in various solvents: A review. *Journal of Molecular Liquids* **2019**, *276*, 214-224.
(7) Lovelock, K. R. J. Quantifying intermolecular interactions of ionic liquids using cohesive energy densities. *Royal Society Open Science* **2017**, *4*, 171223-171223.
(8) Fumino, K.; Reimann, S.; Ludwig, R. Probing molecular interaction in ionic liquids by low frequency spectroscopy: Coulomb energy, hydrogen bonding and dispersion forces. *Physical Chemistry Chemical Physics* **2014**, *16*, 21903-21929.
(9) Anderson, J. L.; Ding, J.; Welton, T.; Armstrong, D. W. Characterizing ionic liquids on the basis of multiple solvation interactions. *Journal of the American Chemical Society* **2002**, *124*, 14247-14254.
(10) Angenendt, K.; Johansson, P. Ionic Liquid Structures from Large Density Functional Theory Calculations Using Mindless Configurations. *The Journal of Physical Chemistry C* **2010**, *114*, 20577-20582.
(11) Xiong, Z.; Gao, J.; Zhang, D.; Liu, C. Hydrogen bond network of 1-alkyl-3-methylimidazolium ionic liquids: A network theory analysis. *Journal of Theoretical and Computational Chemistry* **2012**, *11*, 587-598.
(12) Niemann, T.; Strate, A.; Ludwig, R.; Zeng, H. J.; Menges, F. S.; Johnson, M. A. Cooperatively enhanced hydrogen bonds in ionic liquids: closing the loop with molecular mimics of hydroxy-functionalized cations. *Physical Chemistry Chemical Physics* **2019**, *21*, 18092-18098.
(13) Le Donne, A.; Adenusi, H.; Porcelli, F.; Bodo, E. Hydrogen Bonding as a Clustering Agent in Protic Ionic Liquids: Like-Charge vs Opposite-Charge Dimer Formation. *ACS Omega* **2018**, *3*, 10589-10600.
(14) Fumino, K.; Wulf, A.; Ludwig, R. Hydrogen Bonding in Protic Ionic Liquids: Reminiscent of Water. *Angewandte Chemie International Edition* **2009**, *48*, 3184-3186.
(15) Brela, M. Z.; Kubisiak, P.; Eilmes, A. Understanding the Structure of the Hydrogen Bond Network and Its Influence on Vibrational Spectra in a Prototypical Aprotic Ionic Liquid. *Journal of Physical Chemistry B* **2018**, *122*, 9527-9537.
(16) Avent, A. G.; Chaloner, P. A.; Day, M. P.; Seddon, K. R.; Welton, T. Evidence for hydrogen bonding in solutions of 1-ethyl-3-methylimidazolium halides, and its implications for room-temperature halogenoaluminate(III) ionic liquids. *Journal of the Chemical Society, Dalton Transactions* **1994**, 3405-3405.
(17) Marekha, B. A.; Kalugin, O. N.; Bria, M.; Idrissi, A. Probing structural patterns of ion association and solvation in mixtures of imidazolium ionic liquids with acetonitrile by means of relative ^{1}H and ^{13}C NMR chemical shifts. *Physical Chemistry Chemical Physics* **2015**, *17*, 23183-23194.

(18) Bester-Rogac, M.; Stoppa, A.; Buchner, R. Ion association of imidazolium ionic liquids in acetonitrile. *J Phys Chem B* **2014**, *118*, 1426-1435.
(19) Yalcin, D.; Drummond, C. J.; Greaves, T. L. Solvation properties of protic ionic liquids and molecular solvents. *Physical Chemistry Chemical Physics* **2019**, *22*, 114-128.
(20) Sadeghi, R.; Ebrahimi, N. Ionic association and solvation of the ionic liquid 1-hexyl-3-methylimidazolium chloride in molecular solvents revealed by vapor pressure osmometry, conductometry, volumetry, and acoustic measurements. *Journal of Physical Chemistry B* **2011**, *115*, 13227-13240.
(21) Dupont, J. On the solid, liquid and solution structural organization of imidazolium ionic liquids. *Journal of the Brazilian Chemical Society* **2004**, *15*, 341-350.
(22) Zhao, Y.; Gao, S.; Wang, J.; Tang, J. Aggregation of ionic liquids [Cnmim]Br (n = 4, 6, 8, 10, 12) in D2O: A NMR study. *Journal of Physical Chemistry B* **2008**, *112*, 2031-2039.
(23) Tokuda, H.; Baek, S. J.; Watanabe, M. Room-temperature ionic liquid-organic solvent mixtures: Conductivity and ionic association. *Electrochemistry* **2005**, *73*, 620-622.
(24) Richardson, P. M.; Voice, A. M.; Ward, I. M. Pulsed-Field gradient NMR self diffusion and ionic conductivity measurements for liquid electrolytes containing libf4 and propylene carbonate. *Electrochimica Acta* **2014**, *130*, 606-618.
(25) Burrell, G. L.; Burgar, I. M.; Gong, Q.; Dunlop, N. F.; Separovic, F. NMR relaxation and self-diffusion study at high and low magnetic fields of ionic association in protic ionic liquids. *Journal of Physical Chemistry B* **2010**, *114*, 11436-11443.
(26) Kundu, K.; Chandra, G. K.; Umapathy, S.; Kiefer, J. Spectroscopic and computational insights into the ion-solvent interactions in hydrated aprotic and protic ionic liquids. *Physical Chemistry Chemical Physics* **2019**, *21*, 20791-20804.
(27) Danten, Y.; Cabaço, M. I.; Besnard, M. Interaction of water diluted in 1-butyl-3-methyl imidazolium ionic liquids by vibrational spectroscopy modeling. *Journal of Molecular Liquids* **2010**, *153*, 57-66.
(28) Andanson, J. M.; Traïkia, M.; Husson, P. Ionic association and interactions in aqueous methylsulfate alkyl-imidazolium-based ionic liquids. *Journal of Chemical Thermodynamics* **2014**, *77*, 214-221.
(29) Marcus, Y.; Hefter, G. Ion Pairing. *Chemical Reviews* **2006**, *106*, 4585-4621.
(30) Shimomura, T.; Takamuku, T.; Yamaguchi, T. Clusters of Imidazolium-Based Ionic Liquid in Benzene Solutions. *The Journal of Physical Chemistry B* **2011**, *115*, 8518-8527.
(31) Russina, O.; Sferrazza, A.; Caminiti, R.; Triolo, A. Amphiphile Meets Amphiphile: Beyond the Polar–Apolar Dualism in Ionic Liquid/Alcohol Mixtures. *The Journal of Physical Chemistry Letters* **2014**, *5*, 1738-1742.
(32) Marekha, B. A.; Koverga, V. A.; Chesneau, E.; Kalugin, O. N.; Takamuku, T.; Jedlovszky, P.; Idrissi, A. Local Structure in Terms of Nearest-Neighbor Approach in 1-Butyl-3-methylimidazolium-Based Ionic Liquids: MD Simulations. *The Journal of Physical Chemistry B* **2016**, *120*, 5029-5041.
(33) Zahn, S.; Brehm, M.; Brüssel, M.; Hollóczki, O.; Kohagen, M.; Lehmann, S.; Malberg, F.; Pensado, A. S.; Schöppke, M.; Weber, H.; et al. Understanding ionic liquids from theoretical methods. *Journal of Molecular Liquids* **2014**, *192*, 71-76.
(34) Jan, R.; Rather, G. M.; Bhat, M. A. Association of Ionic Liquids in Solution: Conductivity Studies of [BMIM][Cl] and [BMIM][PF_6] in Binary Mixtures of Acetonitrile + Methanol. *J Solution Chem* **2013**, *42*, 738-745.
(35) Mondal, A.; Balasubramanian, S. Quantitative prediction of physical properties of imidazolium based room temperature ionic liquids through determination of condensed phase site charges: A refined force field. *Journal of Physical Chemistry B* **2014**, *118*, 3409-3422.
(36) Mondal, A.; Balasubramanian, S. A Refined All-Atom Potential for Imidazolium-Based Room Temperature Ionic Liquids: Acetate, Dicyanamide, and Thiocyanate Anions. *Journal of Physical Chemistry B* **2015**, *119*, 11041-11051.

(37) Koverga, V. A.; Korsun, O. M.; Kalugin, O. N.; Marekha, B. A.; Idrissi, A. A new potential model for acetonitrile: Insight into the local structure organization. *Journal of Molecular Liquids* **2017**, *233*, 251-261.
(38) Koverga, V. A.; Voroshylova, I. V.; Smortsova, Y.; Miannay, F. A.; Cordeiro, M. N. D. S.; Idrissi, A.; Kalugin, O. N. Local structure and hydrogen bonding in liquid γ-butyrolactone and propylene carbonate: A molecular dynamics simulation. *Journal of Molecular Liquids* **2019**, *287*, 110912-110912.
(39) Canongia Lopes, J. N.; Deschamps, J.; Pádua, A. A. H. Modeling Ionic Liquids Using a Systematic All-Atom Force Field. *The Journal of Physical Chemistry B* **2004**, *108*, 2038-2047.
(40) Canongia Lopes, J. N.; Pádua, A. A. H. Molecular Force Field for Ionic Liquids Composed of Triflate or Bistriflylimide Anions. *The Journal of Physical Chemistry B* **2004**, *108*, 16893-16898.
(41) Canongia Lopes, J. N.; Pádua, A. A. H. Molecular Force Field for Ionic Liquids III: Imidazolium, Pyridinium, and Phosphonium Cations; Chloride, Bromide, and Dicyanamide Anions. *The Journal of Physical Chemistry B* **2006**, *110*, 19586-19592.
(42) Ryckaert, J. P.; Bellemans, A. Molecular dynamics of liquid n-butane near its boiling point. *Chemical Physics Letters* **1975**, *30*, 123-125.
(43) Macchieraldo, R.; Esser, L.; Elfgen, R.; Voepel, P.; Zahn, S.; Smarsly, B. M.; Kirchner, B. Hydrophilic Ionic Liquid Mixtures of Weakly and Strongly Coordinating Anions with and without Water. *ACS Omega* **2018**, *3*, 8567-8582.
(44) Weber, H.; Hollóczki, O.; Pensado, A. S.; Kirchner, B. Side chain fluorination and anion effect on the structure of 1-butyl-3-methylimidazolium ionic liquids. *The Journal of Chemical Physics* **2013**, *139*, 084502-084502.
(45) Doherty, B.; Zhong, X.; Gathiaka, S.; Li, B.; Acevedo, O. Revisiting OPLS Force Field Parameters for Ionic Liquid Simulations. *Journal of Chemical Theory and Computation* **2017**, *13*, 6131-6145.
(46) Humphrey, W.; Dalke, A.; Schulten, K. VMD: Visual molecular dynamics. *Journal of Molecular Graphics* **1996**, *14*, 33-38.
(47) Marekha, B. A.; Kalugin, O. N.; Idrissi, A. Non-covalent interactions in ionic liquid ion pairs and ion pair dimers: a quantum chemical calculation analysis. *Physical Chemistry Chemical Physics* **2015**, *17*, 16846-16857.
(48) Kalugin, O. N.; Voroshylova, I. V.; Riabchunova, A. V.; Lukinova, E. V.; Chaban, V. V. Conductometric study of binary systems based on ionic liquids and acetonitrile in a wide concentration range. *Electrochimica Acta* **2013**, *105*, 188-199.
(49) Vraneš, M.; Papović, S.; Tot, A.; Zec, N.; Gadžurić, S. Density, excess properties, electrical conductivity and viscosity of 1-butyl-3-methylimidazolium bis(trifluoromethylsulfonyl)imide + γ-butyrolactone binary mixtures. *The Journal of Chemical Thermodynamics* **2014**, *76*, 161-171.
(50) Stoppa, A.; Hunger, J.; Buchner, R. Conductivities of Binary Mixtures of Ionic Liquids with Polar Solvents. *Journal of Chemical & Engineering Data* **2009**, *54*, 472-479.
(51) Fu, Y.; Cui, X.; Zhang, Y.; Feng, T.; He, J.; Zhang, X.; Bai, X.; Cheng, Q. Measurement and Correlation of the Electrical Conductivity of the Ionic Liquid [BMIM][TFSI] in Binary Organic Solvents. *Journal of Chemical & Engineering Data* **2018**, *63*, 1180-1189.
(52) France-Lanord, A.; Grossman, J. C. Correlations from Ion Pairing and the Nernst-Einstein Equation. *Phys Rev Lett* **2019**, *122*, 136001.
(53) Marekha, B. A.; Kalugin, O. N.; Bria, M.; Buchner, R.; Idrissi, A. Translational Diffusion in Mixtures of Imidazolium ILs with Polar Aprotic Molecular Solvents. *The Journal of Physical Chemistry B* **2014**, *118*, 5509-5517.

Chapter 6. Local Structure of Mixtures of Imidazolium-Based Ionic Liquids and Molecular Solvents from Molecular Dynamics Simulations and Voronoi Analysis

While the physicochemical properties as well as the nmR and vibration spectroscopic data of the mixtures of ionic liquids (ILs) with molecular solvents undergo a drastic change around the IL mole fraction of 0.2, the local structure of the mixtures pertaining to this behavior remains unclear. In this Chapter, the local structure of twelve mixtures of 1-butyl-3-methylimidazolium cation (C_4mim^+) combined with perfluorinated anions, such as tetrafluoroborate (BF_4^-), hexafluorophosphate (PF_6^-), trifluoromethylsulfonate (TFO^-), and bis(trifluoromethanesulfonyl)imide, ($TFSI^-$), and aprotic dipolar solvents, such as acetonitrile (AN), propylene carbonate (PC), and gamma butyrolactone (γ-BL) is studied by molecular dynamics simulations in the entire composition range, with an emphasize on the IL mole fractions around 0.2. Distributions of metric properties corresponding to the Voronoi polyhedra of the particles (volume assigned to the particles, local density, radius of spherical voids) are determined, using representative sites of the cations, anions and the solvent molecules, to characterize the changes in the local structure of these mixtures. By analyzing the mole fraction dependence of the average value, fluctuation, and skewness parameter of these distributions, the present study reveals that, around the IL mole fraction of 0.2, the local structure of the mixture undergoes a transition between that determined by the interionic interactions and that determined by the interactions between the ions and solvent molecules. It should be noted that the strength of the interactions between the ions and the solvent molecules, modulated by the change in the composition of the mixture, plays an important role in the occurrence of this transition. The signature of the change in the local structure is traced back to the nonlinear change of the mean values, fluctuations and skewness values of the metric Voronoi polyhedra distributions.

6.1. Introduction

The mixtures of room temperature ionic liquids (ILs), consisting of 1-butyl-3-methylimidazolium cations (C_4mim^+) and perfluorinated anions, such as tetrafluoroborate (BF_4^-), hexafluorophosphate (PF_6^-), trifluoromethylsulfonate (TFO^-), and bis(trifluoromethanesulfonyl)imide, ($TFSI^-$), with aprotic dipolar solvents, such as acetonitrile (AN), propylene carbonate (PC), or gamma butyrolactone (γ-BL), are adequate candidates to be used in electrochemical applications. As a consequence, these mixtures have been extensively studied by several experimental techniques in order to understand their macroscopic properties.[1-13] The existing array of experimental physicochemical data as well as spectroscopic results point out the significant changes occurring in the local structure of these mixtures at low IL mole fraction ($x_{IL} \sim 0.2$) values. Indeed, the conductivity values go through a maximum around this composition, with higher values in the mixtures of these ILs with AN. Furthermore, vibrational spectroscopic technics, such as IR, Raman, and nuclear magnetic resonance (NMR) spectroscopy were used to analyze the interionic and ion-solvent interactions in mixtures of imidazolium-based ILs with molecular solvents [14-26] The results show that significant changes in the C-H (or the cation ring) vibration modes as well as the ^1H chemical shift occur at low IL content. This was correlated with the modulation, by changing the mixture composition, of the balance between intercomponent interactions, such as interionic (dominating at very high IL mole fractions), ion-solvent, and solvent-solvent interactions in the mixtures. In accordance with these findings, molecular dynamics (MD) simulation results revealed that there is a crossover between the cation-anion, cation-solvent and anion-solvent average distances that occurs at low x_{IL} values, where cation-solvent interactions overcome those between the cations and anions.[27]

As a continuation of this analysis, to explain the composition dependence of the physicochemical properties, vibrational (i.e., IR and Raman) and NMR spectra of such mixtures, the changes of the local structure as a function of the

mixture composition are characterized. These structural changes may be captured using appropriate statistical functions that characterize the local environment of the components in more detail than what is provided by their radial distribution functions. The main idea is, therefore, to evaluate the distribution functions by averaging over part of the total three-dimensional space. Appropriate methods in this respect include statistical geometry approaches, where the local structure is characterized by the statistical analysis of the Voronoi polyhedra (VP) around the individual particles, obtained by a specific tessellation, such as the Voronoi tessellation, in three-dimensional space. This approach is free from any arbitrary parameter that is used in many other methods, such as, e.g., the lattice heterogeneity analysis of Wang et al.,[28] where the simulation space was divided into small cells the width of which was equal to the position of the minimum between the first and second peaks in the butyl-butyl radial distribution function. The Voronoi method was successfully applied to analyze the local structure of a number of different systems, such as hard sphere[29-33] and Lennard-Jones liquids,[34-38] molten salts[39, 40] and metals,[41, 42] water[43-49] under different thermodynamic conditions, including supercooled,[46, 49, 50] supercritical[47, 48, 51] and negative pressure ones,[44] other neat molecular liquids[43, 52] and their binary mixtures,[50, 53-57] ternary mixtures of spherical particles,[58] supercritical fluids,[47, 48, 59-61] polymers,[62, 63] hydrated salts,[64] amphiphiles,[65] peptides,[66] biomacromolecules,[67] lipid membranes[68-72] and also neat ILs[73-77] as well as their mixture with each other[78, 79] and with molecular solvents.[75, 78, 80-86]

In this chapter on the basis of molecular dynamics simulations, a detailed Voronoi analysis of the local structure around the hydrogen atoms of the C_4mim^+ cation in mixtures of ILs of this cation with four perfluorinated anions, such as BF_4^-, PF_6^-, TFO^- and $TFSI^-$, and three aprotic dipolar solvents, such AN, PC and γ-BL is presented. The structure of these molecules and molecular ions, along with the atomic labelling scheme, is shown in Figure 6.1. As the C_4mim^+ cation is large and asymmetric, different atoms of it are regarded as centers of the Voronoi polyhedra. Indeed, the formation of polar and non-polar domains around

the imidazolium ring and butyl chain of the cation gives a hint that there are specific local distributions around these groups of the cation.[75] In particular, in ILs bearing 1-alkyl-3-methlylimidazolium cations it is commonly accepted that H^2 and, to a less extent also H^4 and H^5 are the main hydrogen bonding sites of the cation.[87-90] Further, the literature data converges to show that these hydrogen atoms interact preferentially with the F (BF_4^- and PF_6^-) and O (TFO^- and $TFSI^-$) atoms of the anions.[13, 27, 91, 92]

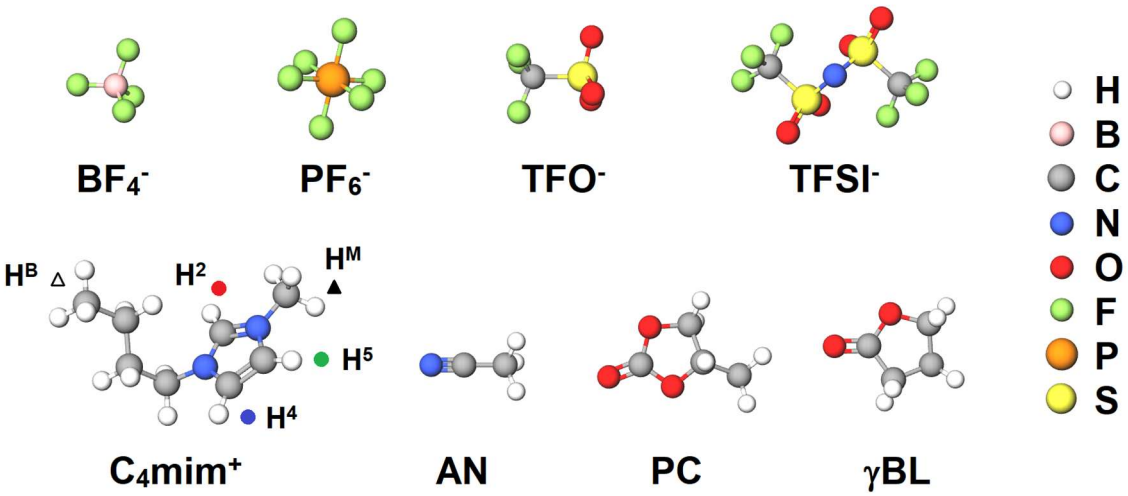

Figure 6.1. Structure of the ions and molecular solvents considered in this study. The labelling of the H atoms used to describe the position of the C_4mim^+ cation in the analyses is also shown.

6.2. Details of molecular dynamics simulation

MD simulations of the binary mixtures of four ILs, consisting of the C_4mim^+ cation and the BF_4^-, PF_6^-, TFO^-, or $TFSI^-$ anions, with three aprotic dipolar molecular solvents, i.e., AN, PC and γ-BL, have been performed for 13 different compositions, including the neat ionic and molecular liquids. The cubic basic box always consisted of 864 structural units (both ion pairs and solvent molecules). The number of the different particles and mole fraction of the IL in the simulated systems simulated are collected in Table 6.1.

Table 6.1. Composition of the systems simulated.

IL mole fraction	Number of cations	Number of anions	Number of solvent molecules
0.00	0	0	864
0.02	17	17	847
0.05	43	43	821
0.10	86	86	778
0.15	130	130	734
0.20	173	173	691
0.30	259	259	605
0.40	346	346	518
0.50	432	432	432
0.60	518	518	346
0.70	605	605	259
0.80	691	691	173
1.00	864	864	0

The ILs have been described by the potential model of Mondal and Balasubramanian,[93, 94] while for the solvent molecules the potential model of Koverga et al.[95, 96] has been used – the same potential models that were used and described in Chapter 5.

6.3. Results and discussion

6.3.1. Volume of the Voronoi polyhedra

The VP volume distributions considering all the components of the mixture, $P^T(V)$, are shown in Figures A1-A5 of the Supporting Information (SI), as obtained when describing the position of the C_4mim^+ cation by that of the H^2, H^4, H^5, H^B and H^M hydrogen atoms, respectively (for the labelling of the atoms, see Figure 6.1.). The obtained distributions, apart from those corresponding to neat molecular solvents, are not of Gaussian shape, but exhibit a slowly decaying tail at large volume values. With decreasing x_{IL}, the distributions shrink and shift to lower volumes, while the tail at large volumes progressively smears out and the

distributions become less asymmetric. Further, the extent of this asymmetry is higher when the $TFSI^-$ anion is present in the mixture, independently from the chosen molecular solvent. In order to quantify the shift and asymmetry of these distribution, the composition dependence of the mean value and skewness parameter (see equation 6.2) of the $P^T(V)$ distributions are presented in Figures 6.2 and 6.3, respectively, as obtained in all systems simulated.

As is seen from Figure 6.2, with decreasing mole fraction of the IL, the mean volume of the VP, $\langle V^T \rangle$, shifts to lower values, and it does not depend on which H atom is chosen to represent the position of the cation. The extent of this shift is the largest in the presence of the $TFSI^-$ anion and AN, while it is the smallest in the mixture of C_4mimBF_4 and PC. Of note is that the rate of the shift is somewhat lower in the x_{IL} range between 1 and 0.2 than below $x_{IL} = 0.2$. This change of the rate of decrease of the mean volume value is a signature of changes occurring in the local structure around the components of the mixture.

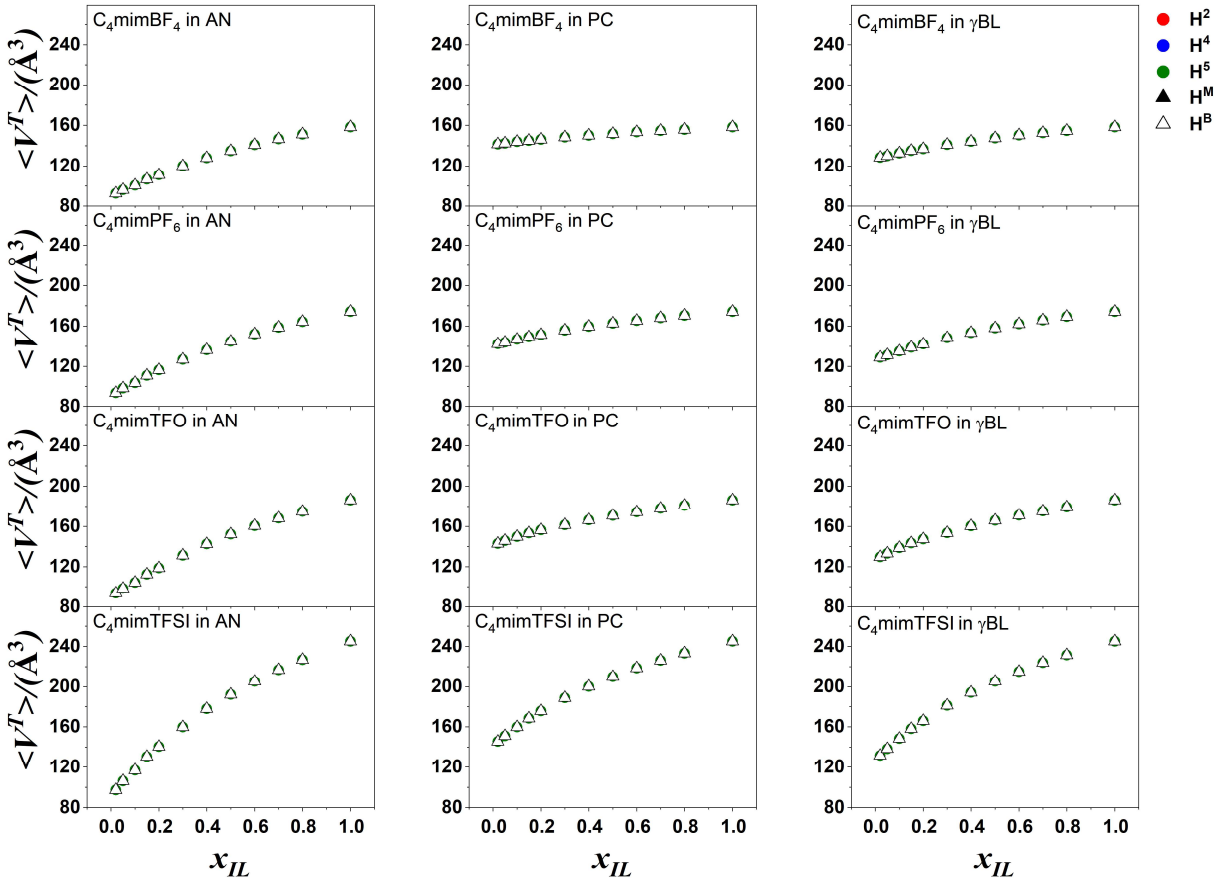

Figure 6.2. IL mole fraction dependence of the average value of the VP volume, $\langle V^T \rangle$, obtained considering all the ions and molecules in the analysis.

Concerning the asymmetry of the $P^T(V)$ distributions, it is seen from Figure 6.3 that the values of $m_{3/2}$ are larger than 1 in every case, being close to unity only in the neat molecular solvents. In neat ILs, the large positive values of $m_{3/2}$ indicate that the $P^T(V)$ distributions extend considerably longer at the high than at the low volume side of their peak (see also Figs. B1-B5 of the SI).

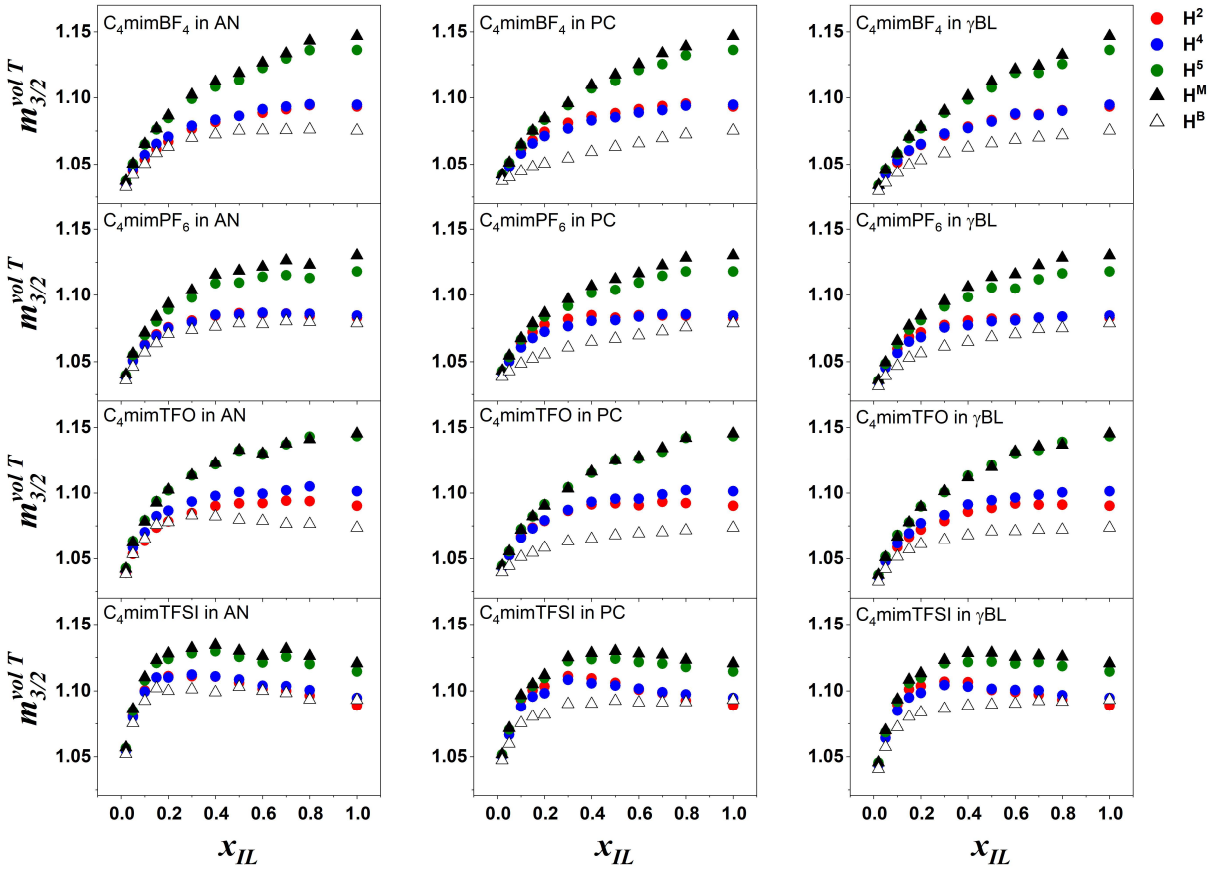

Figure 6.3. IL mole fraction dependence of the skewness parameter of the VP volume distributions, $m_{3/2}^T$, obtained considering all the ions and molecules in the analysis.

Small VP volume values are associated with closely packed domains, while large volume values (contributing to the long tail of the $P^T(V)$ distributions, better seen on logarithmic scale) are associated with loosely packed domains. It is also apparent that the $m_{3/2}$ values are higher when the H^M or H^5 atom is chosen to represent the position of the cation than when the other H atoms are considered. This finding indicates that in neat ILs the local structure is more packed around

the latter sites than around the former ones. When adding the solvent to the ILs, the $m_{3/2}$ value decreases non-linearly, and the decay occurs with considerably lower rate in the x_{IL} range between 1 and 0.2 than for further dilution of the IL. In dilute mixtures of the ILs, the rate of decrease is similar for all the sites chosen to represent the position of the cation. Of note is that in the presence of the $TFSI^-$ anion, a maximum of $m_{3/2}$ occurs around the x_{IL} value of 0.2.

In principle, the value of $m_{3/2}$ is determined by the shape of the $P^T(V)$ distribution at large and small volume values. The decrease of the $m_{3/2}$ is thus correlated with the decrease of the dominant, long decaying tail of the $P^T(V)$ distribution at the large volume side of the peak, and the concomitant increase of the contributions to small VP volume values. However, when the $m_{3/2}$ value goes through a maximum, not only the large volume tail of the overall $P^T(V)$ distribution is decreasing (see Figs. A1-A5), but the contributions to the small volume part of the distribution (closely packed local structures) also have to decrease, and this latter decrease overweighs that at the large volume side (loosely packed local structures). For further dilution of ILs, the $m_{3/2}$ values decrease and infer that these distributions are shaped by the local structure of the solvent molecules, which is more packed than that of the ILs.

To go further in the investigation of the effect of composition on the local structure in IL-solvent mixtures, the $P^{CA}(V)$ and $P^S(V)$ distributions by taking into account only the ions and only the solvent molecules, respectively, in the analysis were calculated. The $P^{CA}(V)$ distributions, obtained by describing the position of the cation by that of the H^2, H^4, H^5, H^B and H^M hydrogen atoms, are shown in Figures A6-A10, respectively, while the $P^S(V)$ distributions are shown in Figure A11. The distributions broaden drastically and become progressively more asymmetric with increasing mole fraction of the disregarded component, developing an exponentially decaying tail (transformed to a line by the logarithmic scale) at large volume values. The occurrence of this exponentially

decaying tail is a clear sign of the self-association behavior of both the ions and the solvent molecules.[53, 97]

To quantify the development of this tail, the skewness parameter of the $P^{CA}(V)$ and $P^{S}(V)$ distributions as a function of the IL mole fraction were plotted in Figures 6.4 and 6.5, respectively.

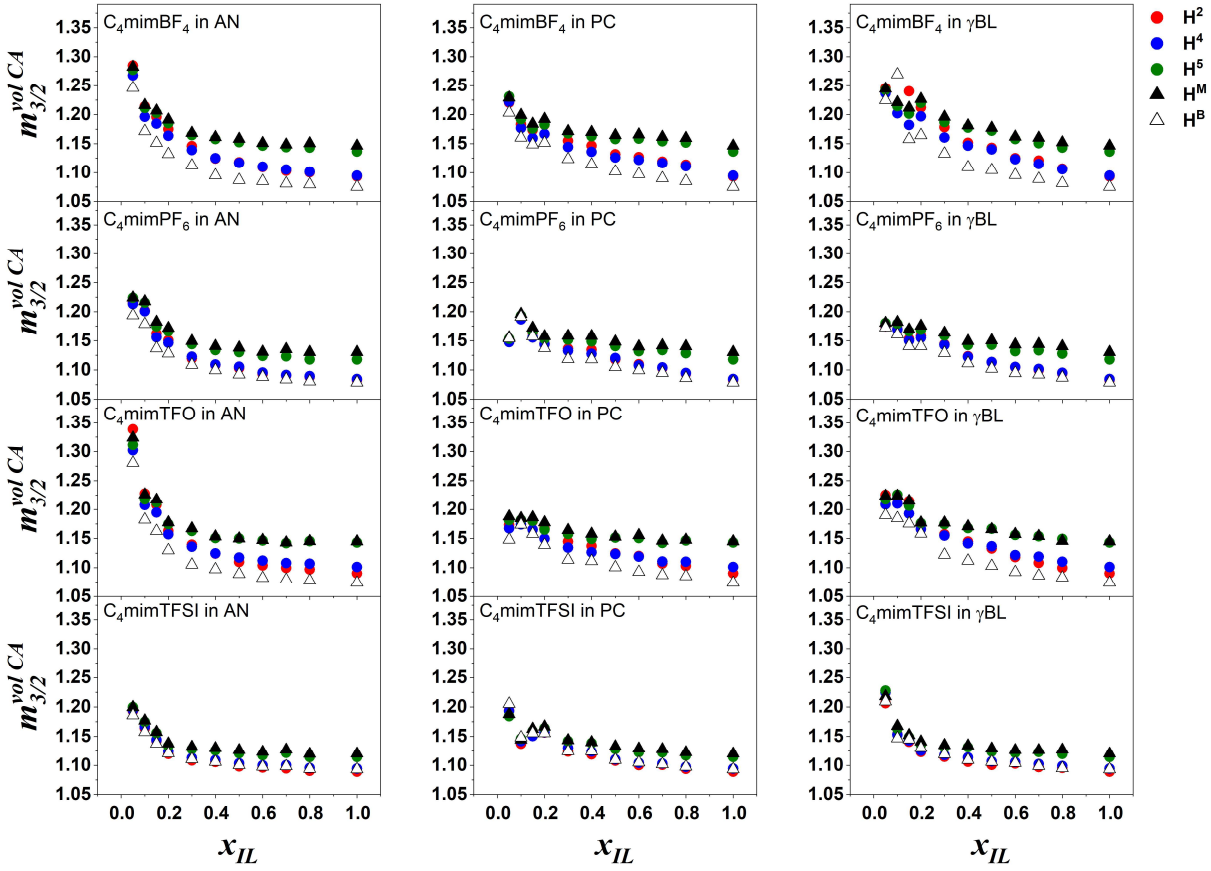

Figure 6.4. IL mole fraction dependence of the skewness parameter of the VP volume distributions, $m_{3/2}^{CA}$, obtained considering only the ions, while disregarding the solvent molecules in the analysis.

In the case of the $P^{CA}(V)$, the skewness parameter decreases with increasing x_{IL} (Figure 6.4.). This decrease occurs with two markedly different rates, a low one at high IL mole fractions (i.e., between 1 and 0.2), inferring that the local structure of the ions corresponding to the neat ILs is not altered strongly by the solvents molecules in this composition range, and a high one for lower IL

content. This strong decrease of the skewness parameter at $x_{IL} < 0.2$ is noticeably steeper when the IL is mixed with AN than with the other solvents. This difference is related to the different extent of self-association of the solvent molecules. Thus, the weak interaction between the ions and AN favors the self-association of the AN molecules, while the strong interactions between the PC or γ-BL molecules and the ions reduces the extent of self-association of the molecular solvent. Further, the difference between the rate of decrease observed with different anions reflects the different strength of the interaction of these anions with the C_4mim^+ cation (mainly visible in the mixture in AN).

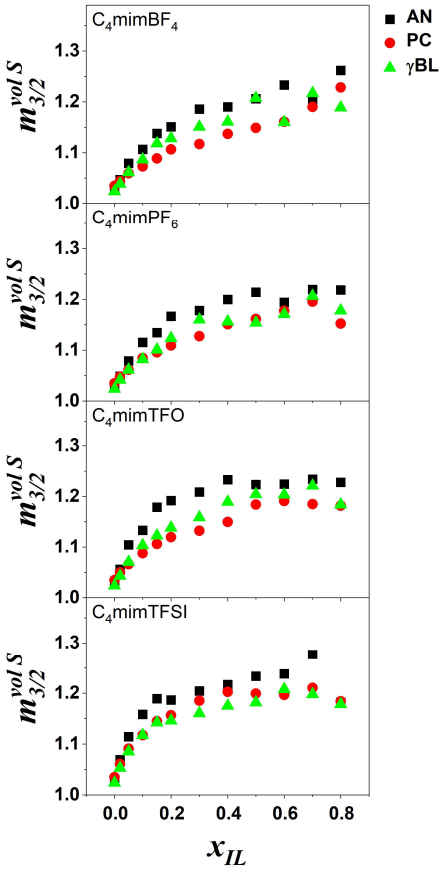

Figure 6.5. IL mole fraction dependence of the skewness parameter of the VP volume distributions, $m_{3/2}^{S}$, obtained considering only the solvent molecules, while disregarding the ions in the analysis.

The skewness parameter of the $P^S(V)$ distributions, obtained by disregarding the ions and taking only the solvent molecules into account in the

analysis, increases with increasing IL mole fraction (see Figure 6.5.), and this increase occurs again with two different rates, a high one in the x_{IL} range between about 0 and 0.2, and a low one for further dilution of the solvent. Again, the differences observed in the rate of this increase when considering different anions or solvent molecules reflect the competition between the anion-cation and solvent-cation interactions.

6.3.2. Local density

Complementary information on the local structure around the components can be obtained by analyzing the distributions of the local density (or reciprocal volume), $P^T(\rho)$. The distributions obtained by representing the position of the C_4mim^+ cation with that of the H^2, H^4, H^5, H^B and H^M hydrogen atoms are shown in Figures A12-A16, respectively. Upon dilution of the ILs, these distributions shift to higher values, reflecting simply the fact that the number density of the molecular solvents is higher than that of the ILs. It is also seen that, among the molecular solvents considered, AN, while among the anions considered, $TFSI^-$ corresponds to the largest shift, although the choice of the anion has a smaller effect in this respect. This trend is also seen from Figure 6.6, showing the IL mole fraction dependence of the mean value of the $P^T(\rho)$ distribution in all systems simulated. Again, the rate of decrease of $\langle\rho^T\rangle$ with increasing x_{IL} is considerably larger below the IL mole fraction of about 0.2 than above this value.

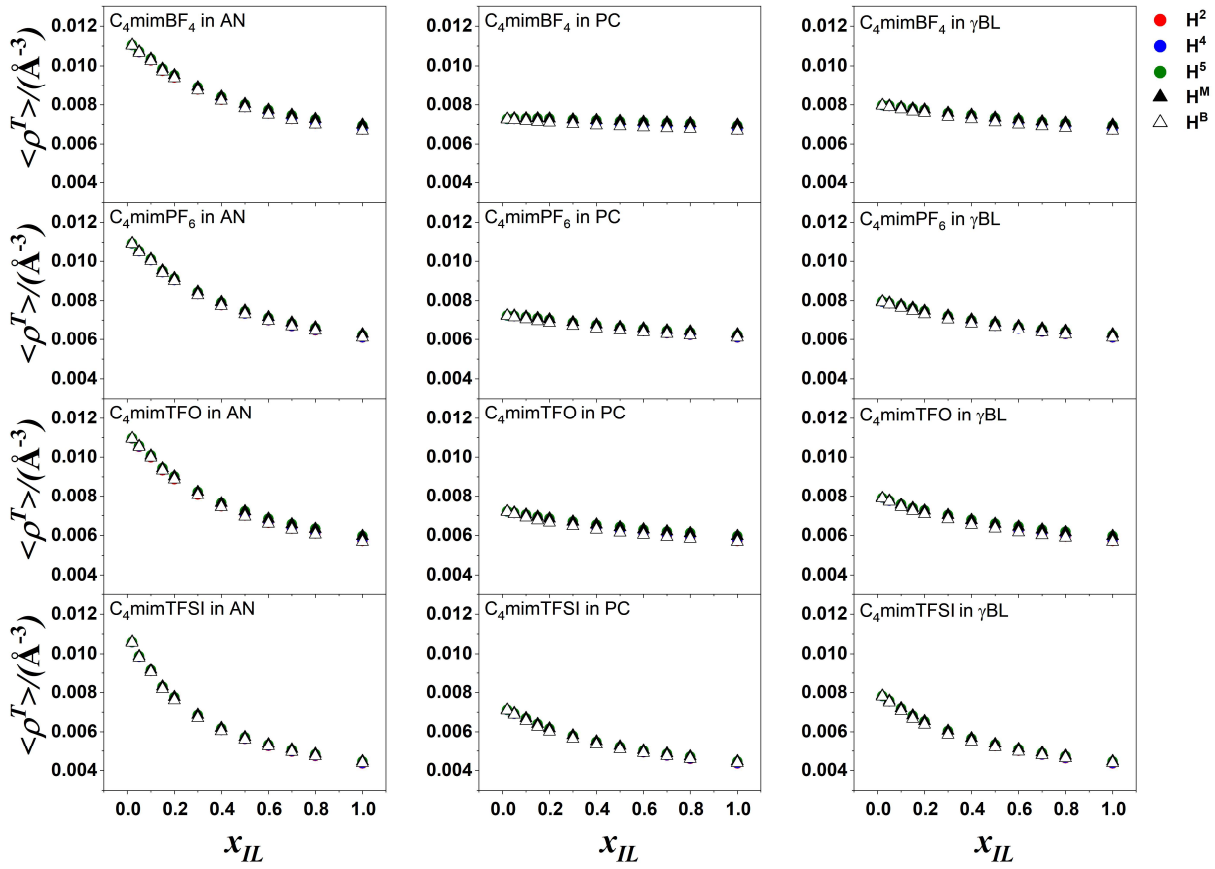

Figure 6.6. IL mole fraction dependence of the average value of the reciprocal VP volume, characterizing the local density, $\langle \rho^T \rangle$, obtained considering all the ions and molecules in the analysis.

A deeper insight into the composition dependence of the local density can be gained by analyzing the standard deviation of these distributions, $\Delta\rho^T$. The change of $\Delta\rho^T$ with x_{IL} is plotted in Figure 6.7 as obtained in the different systems simulated. As is seen, in mixtures where the rate of decrease of $\langle \rho^T \rangle$ as a function of x_{IL} exhibits a sharp change around $x_{\mathrm{IL}} = 0.2$, this is translated to the occurrence of a maximum of the local density fluctuation at this composition. The occurrence of such a maximum is a signature of the inhomogeneous distribution of the components in the system. In the other mixtures, such as those of BmimTFO and $BmimBF_4$ with PC and γ-BL, the $\Delta\rho^T$ values are almost constant in the x_{IL} range between 0.2 and 1, but decrease sharply for further dilution of the IL.

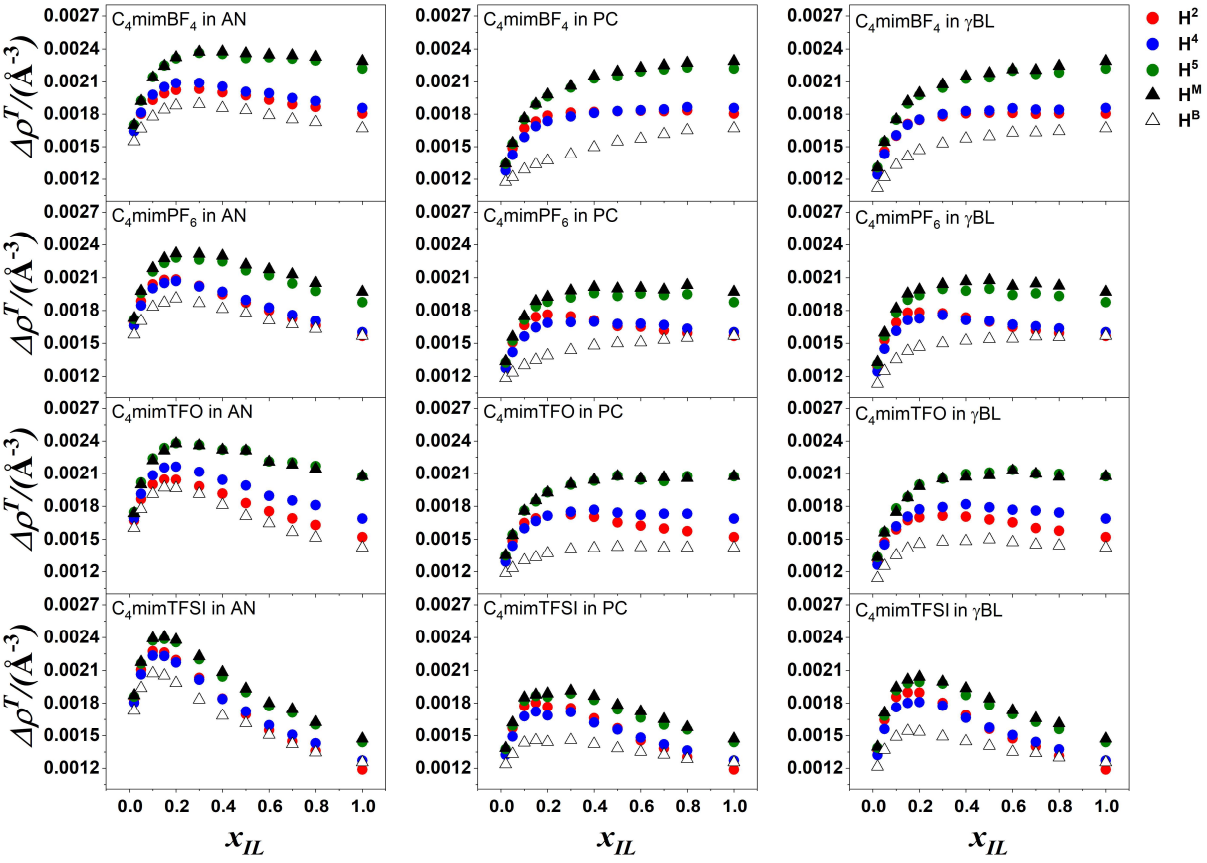

Figure 6.7. IL mole fraction dependence of the standard deviation of the reciprocal VP volume distribution, $\Delta\rho^T$, obtained considering all the ions and molecules in the analysis.

To go further in understanding the origin of the observed maximum of density fluctuations around $x_{\mathrm{IL}} = 0.2$, the $P^{CA}(\rho)$ and $P^{S}(\rho)$ local density distributions by taking into account only the ions and only the solvent molecules, respectively, in the analysis were calculated. The $P^{CA}(\rho)$ distributions obtained by representing the position of the cation by that of the H^2, H^4, H^5, H^B and H^M hydrogen atoms are shown in Figures A17-A21, respectively, while the $P^{S}(\rho)$ distributions in Figure A22. Further, the mean values corresponding to these distributions, $\langle\rho^{CA}\rangle$ and $\langle\rho^{S}\rangle$, are shown in Figures 6.8 and 6.9, while the standard deviations, $\Delta\rho^{CA}$ and $\Delta\rho^{S}$, in Figures 6.10 and 6.11, respectively, as a function of the IL mole fraction.

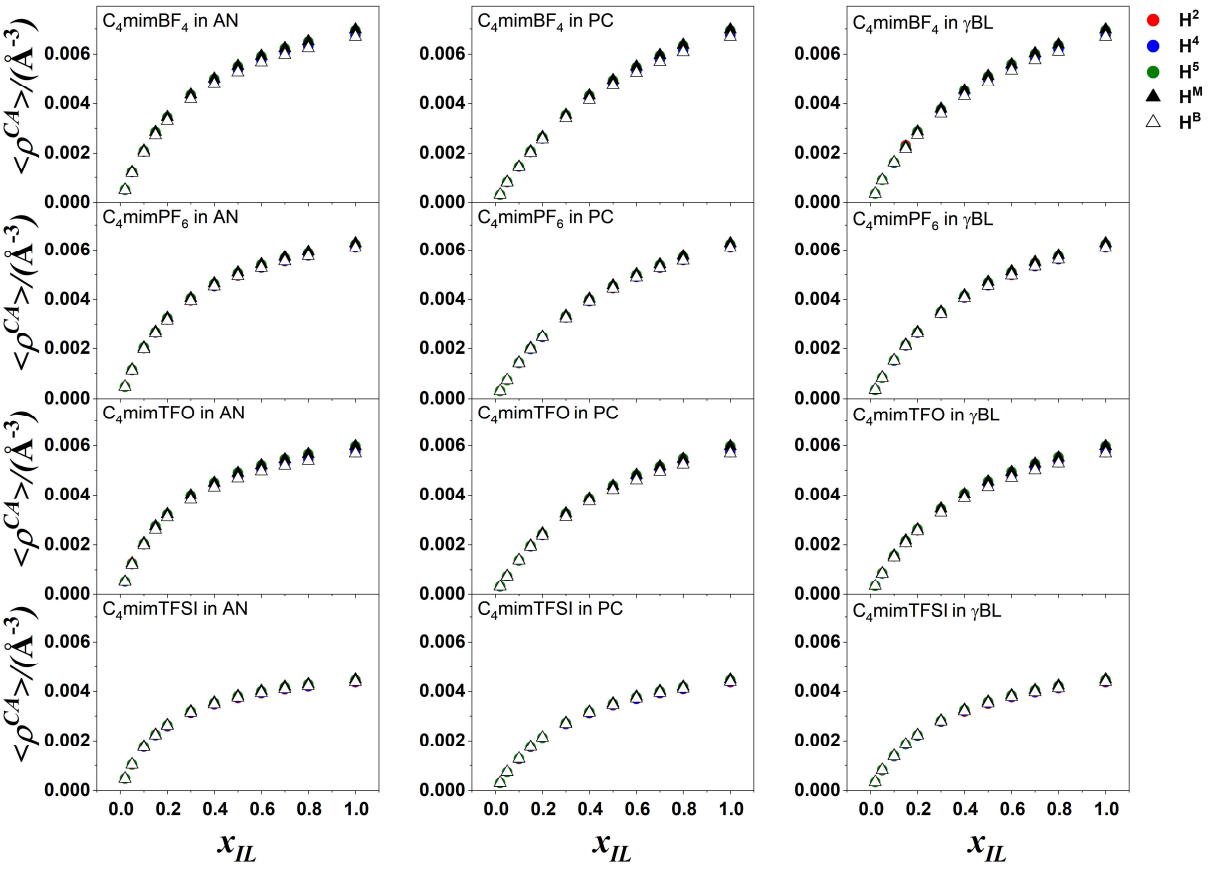

Figure 6.8. IL mole fraction dependence of the average value of the reciprocal VP volume, characterizing the local density, $\langle \rho^{CA} \rangle$, obtained considering only the ions, while disregarding the solvent molecules in the analysis.

Figure 6.8 and 6.9 show that the rate of the density change with the composition is again considerably larger below the x_{IL} value of 0.2 than at higher IL mole fractions. Such a rapid change of the density suggests the presence of large density fluctuations in the system (in a clear analogy with critical phenomena). This point can be clarified by analyzing the corresponding density fluctuations.

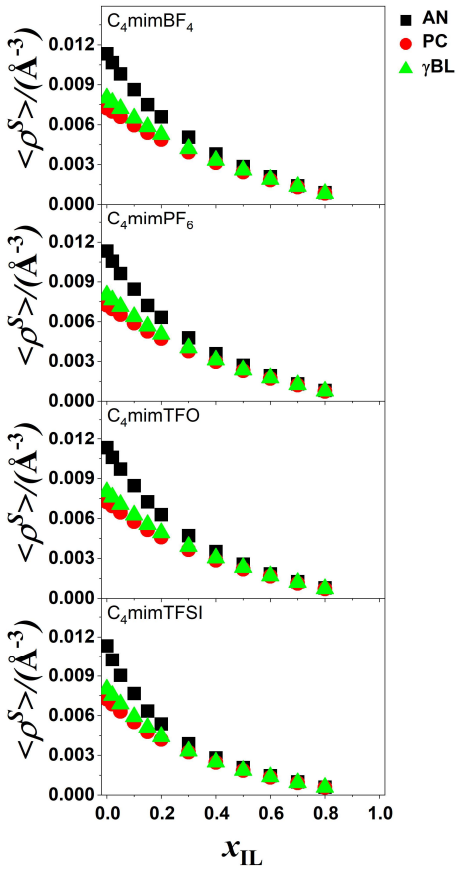

Figure 6.9. IL mole fraction dependence of the average value of the reciprocal VP volume, characterizing the local density, $\langle \rho^S \rangle$, obtained considering only the solvent molecules, while disregarding the ions in the analysis.

As is seen from Figure 6.10, in the x_{IL} range between 1 and 0.2, the density fluctuation of the ions, $\Delta\rho^{CA}$, decreases with a considerably smaller rate than below $x_{IL} = 0.2$. This finding is in a clear accordance with the behavior of the skewness parameter of the VP volume, and indicates that at $x_{IL} > 0.2$ the disregarded solvent molecules are more or less randomly distributed in the mixture, but below this IL mole fraction it is no longer the case. It should be noted that in this low x_{IL} composition range, where already the ions are the minor component, the solvation of the cations and anions can be very different. In particular, the solvation depends on the balance between the interionic interactions and those between the ions and solvent molecules. The finding that $\Delta\rho^{CA}$ decreases rapidly below $x_{IL} = 0.2$ indicates that in this composition range the former interaction is noticeably reduced in favor of the latter. This suggests

that here the cations and anions are progressively better solvated by the solvent molecules, and hence the local environment of the ions becomes progressively homogeneous, resulting in a marked decrease of the density fluctuation values with decreasing x_{IL}.

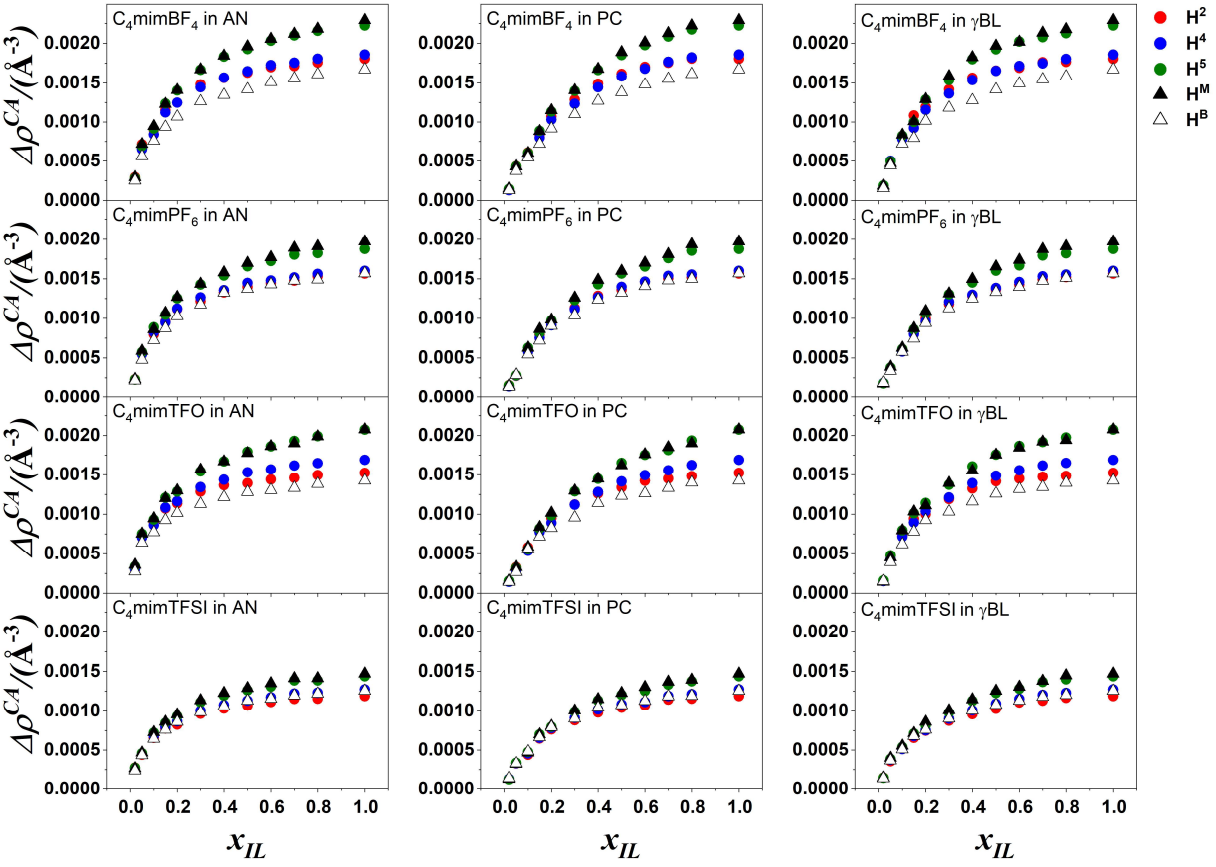

Figure 6.10. IL mole fraction dependence of the standard deviation of the reciprocal VP volume distribution, $\Delta\rho^{CA}$, obtained considering only the ions, while disregarding the solvent molecules in the analysis.

It is also seen that the difference between the density fluctuation values calculated considering the different H atoms of the cation is rather small in the presence of PF_6^- and $TFSI^-$, while it is considerably larger in the presence of BF_4^- and TFO^- anions. This finding clearly indicates that the distribution of the solvent molecules around these sites depends on the interaction between the cations and the anions. The persistence of this difference even at low IL mole fractions (in particular, in systems consisting of BF_4^- and TFO^- anions) indicates that the

solvent is still not completely solvating the ions, and the interaction of the oppositely charged ions, although strongly weakened with respect to that in neat IL, is still not negligible.

This physical picture can be further refined by analyzing the composition dependence of the density fluctuation considering only the solvent molecules in the analysis, $\Delta\rho^S$ (Figure 6.11).

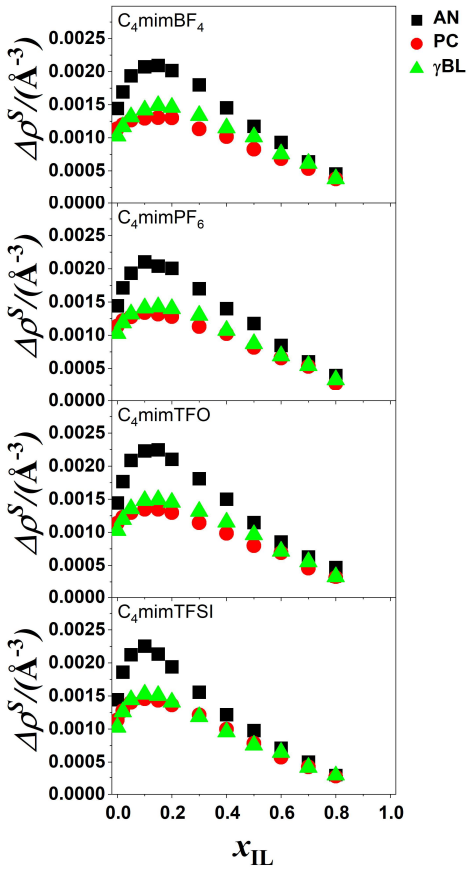

Figure 6.11. IL mole fraction dependence of the standard deviation of the reciprocal VP volume distribution, $\Delta\rho^S$, obtained considering only the solvent molecules, while disregarding the ions in the analysis.

As is seen, the values of this parameter go through a maximum at $x_{IL} \sim 0.2$, and this maximum is the highest when AN is the solvent, independently from the choice of the anion. Clearly, when disregarding the cations and anions in the analysis, the ions are transformed to empty holes, the size of which is depending on the extent of solvation of the disregarded ions by the solvent molecules. This

solvation is modulated by the balance between the interionic, ion-solvent, and solvent-solvent interactions. Thus, the increasing solvent density fluctuation observed upon addition of IL to the neat solvent indicates different extent of solvation of the oppositely charged ions, while the maximum of the $\Delta\rho^S$ values corresponds to the maximum difference between the solvation of the cations and anions by the solvent molecules. Above this composition, the interaction between cations and anions becomes dominant over that between the ions and solvent molecules. Thus, further dilution of the solvent leads to stronger interionic interaction, and hence the disregarding of the ions in the analysis creates more and more regular holes, leading eventually to the observed decrease of the density fluctuation of the solvent molecules.

Finally, the fact that the $\Delta\rho^S$ values are higher for AN than for the other solvents indicates that the interaction of AN with the ions is weaker than that of the other two solvents considered here, presumably because of the smaller dipole moment of AN than that of PC and γ-BL.[98, 99] As a consequence, in AN the importance of the interionic interaction relative to the ion-solvent interactions is larger than in the other two solvents, leading to the expulsion of the AN molecules, to a certain extent, from the vicinity of the ions, and eventually to the formation of self-associates of the AN molecules. This larger self-association leads then to larger density fluctuations in AN than in the other two molecular solvents considered.

6.3.3. Radius of the voids

The analysis of the distribution of the radius of spherical voids between the particles can provide some additional insight into the local environment of the components in these mixtures. The $P^T(R)$ and $P^{CA}(R)$ distributions, obtained by considering all particles and only the ions, respectively, in the analysis, describing the position of the cation by that of the H^2, H^4, H^5, H^B and H^M hydrogen atoms are shown in Figures A23-A27 and Figures A28-A32, respectively, while the

$P^S(R)$ distributions, obtained by considering only the solvent molecules and disregarding the ions are shown in Figure A33.

The analysis of the $P^T(R)$ distributions (Figures A23-A27) shows that the size of the voids is larger in the neat ILs than in the molecular solvents, reflecting both the different size of the ions and solvent molecules, and also the fact that the solvent molecules are more closely packed in their neat liquid than the ions. The shape of the $P^T(R)$ distribution is Gaussian in both neat systems, the fluctuation being larger in the neat ILs. When diluting the ILs, the $P^T(R)$ distributions retain their Gaussian shape and shift slightly towards smaller R values in the x_{IL} range between 1 and 0.2. In some of the mixtures, the peak position shifts smoothly towards that in the pure solvent, while the Gaussian-like shape of the distribution is retained in the entire composition range. However, in mixtures consisting of either AN molecules or $TFSI^-$ anions, a shoulder emerges at the low R side of the peak and turns gradually to a separate peak upon further dilution. Of note is that, simultaneously with the turning of this shoulder to the main peak, occurring roughly at the same position as that in the neat solvent, the previous peak gradually turns to a shoulder at the high R side of the distribution. The occurrence of these shoulders indicates self-association of the components, as the local environment around a certain fraction of the voids is markedly different than that around other voids.[100] In particular, the fact that the shoulder at low R values occurs roughly at the same position as the peak in the neat solvent indicates that a certain fraction of the voids in the mixtures are in a local environment that is very similar to that in the neat solvent. On the other hand, the shoulder at the high R side occurs at markedly different position than the peak in the neat IL, indicating the lack of a considerable number of voids that are in a neat IL-like local environment. Thus, our findings reveal stronger self-association of the solvent molecules than that of the ions. Considering that, among the three molecular solvents considered, this behavior is only seen in AN, the present result clearly confirms our previous finding concerning larger density fluctuations of AN than that of the other solvents (see sec. 6.3.2), and stresses that, due to its somewhat

weaker interaction with the ions, AN self-associates more than the other two molecular solvents considered.

Additional information in this respect can be gained again when one of the components is discarded in the analysis. Thus, the self-association of the solvent molecules can be further addresses by analyzing the $P^{CA}(R)$ distributions, calculated by taking only the ions into account while disregarding the solvent molecules in the calculation. These distributions (Figures A28-A32) shift to higher R values with decreasing x_{IL}, simply because the volume occupied by the increasing amount of solvent molecules is turned into increasingly large voids in the analysis. However, it is interesting to note that, consistently with the behavior of $P^{T}(R)$, the $P^{CA}(R)$ distributions shift to only slightly larger void radii when the ILs are diluted to about x_{IL} = 0.2, while further dilution leads to a drastic shift and expansion of the distribution. To quantify this effect, the $\langle R^{CA} \rangle$ and ΔR^{CA} values were calculated, the composition dependence of which are shown in Figures 6.12 and 6.13, respectively. Both parameters remain almost unaffected when the ILs are diluted from their neat liquid to their mole fraction of about 0.2, while their values increase drastically for further dilution. Of note is that these values are independent from the choice of the representative atom that describes the position of the cation.

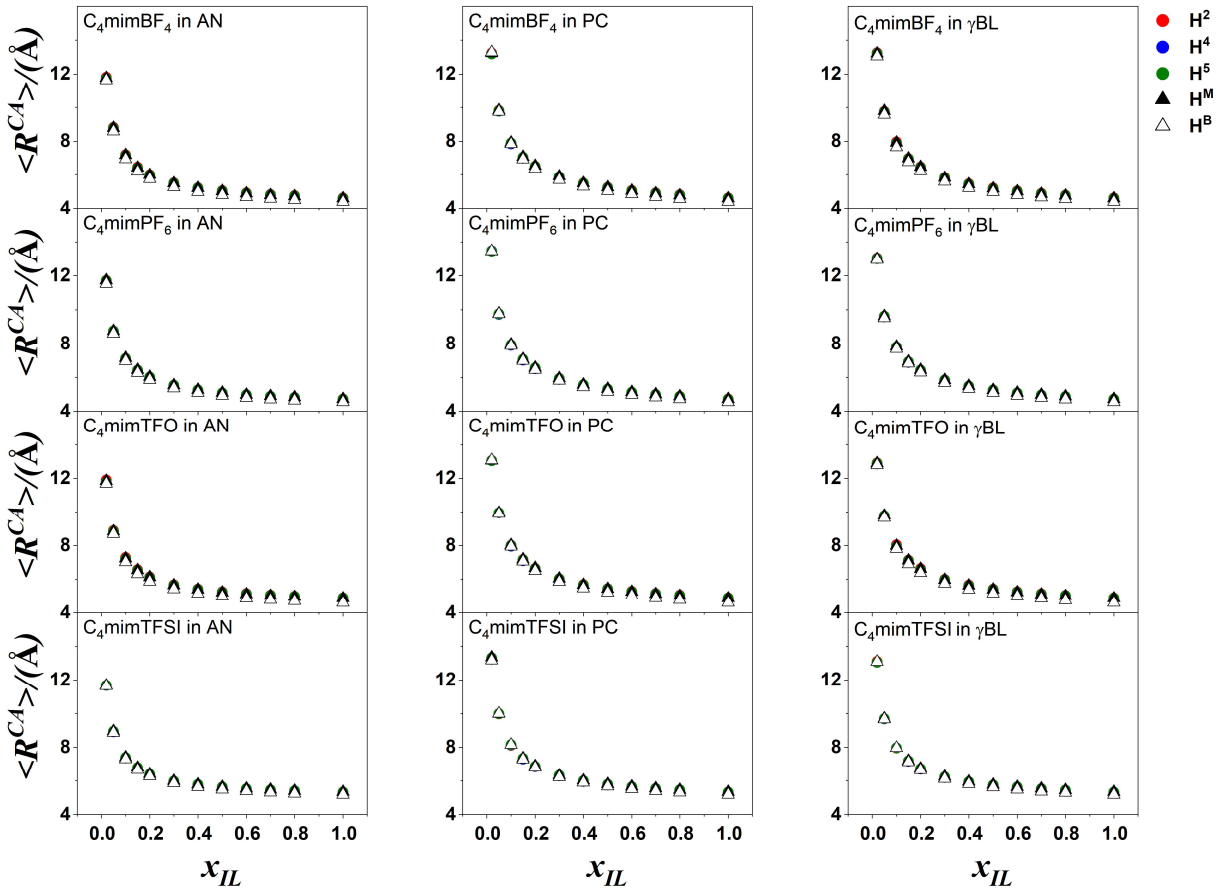

Figures 6.12. IL mole fraction dependence of the average value of the spherical voids' radius distribution, calculated as the distance of the VP vertices from the center of the polyhedra, $\langle R^{CA} \rangle$, obtained considering only the ions, while disregarding the solvent molecules in the analysis.

The $P^S(R)$ distributions, obtained by taking only the solvent molecules into account in the analysis (Figure A33) show an overall shift to higher R values with increasing x_{IL}, reflecting again the trivial effect of dilution. More importantly, upon dilution of the solvent, the $P^S(R)$ distribution turns out to be bimodal, exhibiting a second peak the intensity and position of which are mole fraction dependent. In the low mole fraction range of the discarded ions, this second peak emerges as a shoulder in the high R side of the main peak, while at higher IL mole fractions it gradually turns to a broad peak, located at large void radius values. Simultaneously, the height of the first peak gradually decreases, and ultimately it turns to a shoulder of the large R peak, however, unlike the other peak, it always appears at the same position. This peak (or shoulder) is thus given by voids that

are surrounded by solvent molecules in all direction, and its presence even at high dilution of the solvent molecules indicates the persistence of solvent domains (inside which the voids are in the same local environment as in the neat solvent), and hence self-association of the solvent molecules up to relatively large IL mole fractions. On the other hand, the peak at large R values is given by voids that are in a mixed local environment, i.e., surrounded both by solvent molecules and ions, and the shift of its position to larger values with increasing IL mole fraction marks the increasing mole fraction of the ions even in their mixed local environment.

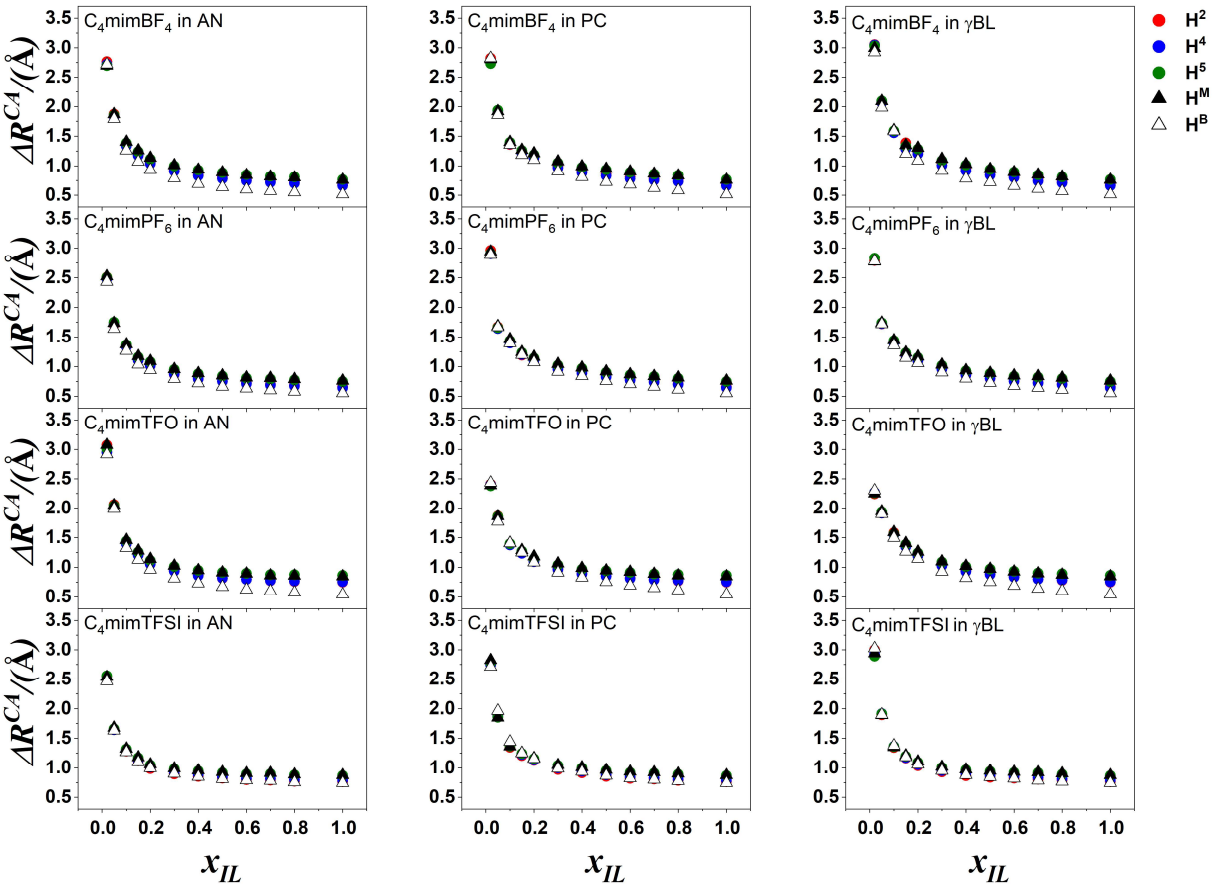

Figures 6.13. IL mole fraction dependence of the standard deviation of the spherical voids' radius distribution, calculated as the distance of the VP vertices from the center of the polyhedra, ΔR^{CA}, obtained considering only the ions, while disregarding the solvent molecules in the analysis.

6.4. Conclusions

The local structure in mixtures of ILs consisting of the C_4mim^+ cation and four different perfluorinated anions with three aprotic dipolar solvents, i.e., acetonitrile, propylene carbonate, and gamma butyrolactone were studied by molecular dynamics simulation technique. Distributions of several metric characteristics (i.e., volume, reciprocal volume, characteristic of the local density, and vertex distance, marking the radius of the largest spherical void) of the Voronoi polyhedra of the particles have been used as statistical observables to characterize the local structure around the components of the mixtures. Since both the change of several physicochemical properties of these mixtures as well as nmR and vibrational spectroscopy data show that important changes occur around the IL mole fraction of 0.2 in these systems, several simulations at the vicinity of this composition were performed. A drastic change in the behavior of the calculated properties at this composition have been found, confirming that these changes concern the local structure around the particles. The picture that emerges from the present results shows that below the IL mole fraction of about 0.2, the ions are well solvated by the solvent molecules, but above this mole fraction they start to form contact pairs, while the solvent molecules, expelled from the vicinity of the ions, form self-associates. This self-association is stronger in the case of AN than of the other solvents considered, because, due to its smaller dipole moment, AN has a weaker interaction with the ions than the other ones. Similarly, this solvent self-association is stronger in the presence of $TFSI^-$ than of the other anions considered. All these results stress that the local structure, and thus also the physicochemical properties of the IL-solvent mixtures are eventually governed by the delicate interplay of the interionic and solvent-ion interactions.

6.5. References for Chapter 6

(1) Stoppa, A.; Hunger, J.; Buchner, R. Conductivities of Binary Mixtures of Ionic Liquids with Polar Solvents. *Journal of Chemical & Engineering Data* **2009**, *54*, 472-479.
(2) Zafarani-Moattar, M. T.; Shekaari, H. Volumetric and Speed of Sound of Ionic Liquid, 1-Butyl-3-methylimidazolium Hexafluorophosphate with Acetonitrile and Methanol at T = (298.15 to 318.15) K. *Journal of Chemical & Engineering Data* **2005**, *50*, 1694-1699.
(3) Huo, Y.; Xia, S.; Ma, P. Densities of Ionic Liquids, 1-Butyl-3-methylimidazolium Hexafluorophosphate and 1-Butyl-3-methylimidazolium Tetrafluoroborate, with Benzene, Acetonitrile, and 1-Propanol at T = (293.15 to 343.15) K. *Journal of Chemical & Engineering Data* **2007**, *52*, 2077-2082.
(4) Zhu, A.; Wang, J.; Han, L.; Fan, M. Measurements and correlation of viscosities and conductivities for the mixtures of imidazolium ionic liquids with molecular solutes. *Chemical Engineering Journal* **2009**, *147*, 27-35.
(5) Vraneš, M.; Zec, N.; Tot, A.; Papović, S.; Dožić, S.; Gadžurić, S. Density, electrical conductivity, viscosity and excess properties of 1-butyl-3-methylimidazolium bis(trifluoromethylsulfonyl)imide + propylene carbonate binary mixtures. *The Journal of Chemical Thermodynamics* **2014**, *68*, 98-108.
(6) Zarrougui, R.; Dhahbi, M.; Lemordant, D. Volumetric Properties of Ethylammonium Nitrate + γ-Butyrolactone Binary Systems: Solvation Phenomena from Density and Raman Spectroscopy. *J Solution Chem* **2010**, *39*, 1531-1548.
(7) Jarosik, A.; Krajewski, S. R.; Lewandowski, A.; Radzimski, P. Conductivity of ionic liquids in mixtures. *Journal of Molecular Liquids* **2006**, *123*, 43-50.
(8) Canongia Lopes, J. N.; Costa Gomes, M. F.; Husson, P.; Pádua, A. l. A. H.; Rebelo, L. P. N.; Sarraute, S.; Tariq, M. Polarity, Viscosity, and Ionic Conductivity of Liquid Mixtures Containing $[C_4C_1im][Ntf_2]$ and a Molecular Component. *The Journal of Physical Chemistry B* **2011**, *115*, 6088-6099.
(9) Kalugin, O. N.; Voroshylova, I. V.; Riabchunova, A. V.; Lukinova, E. V.; Chaban, V. V. Conductometric study of binary systems based on ionic liquids and acetonitrile in a wide concentration range. *Electrochimica Acta* **2013**, *105*, 188-199.
(10) Rizzuto, A. M.; Pennington, R. L.; Sienerth, K. D. Study of the BMIM-PF_6: Acetonitrile binary mixture as a solvent for electrochemical studies involving CO_2. *Electrochimica Acta* **2011**, *56*, 5003-5009.
(11) Li, W.; Zhang, Z.; Han, B.; Hu, S.; Xie, Y.; Yang, G. Effect of Water and Organic Solvents on the Ionic Dissociation of Ionic Liquids. *The Journal of Physical Chemistry B* **2007**, *111*, 6452-6456.
(12) Zafarani-Moattar, M. T.; Majdan-Cegincara, R. Viscosity, Density, Speed of Sound, and Refractive Index of Binary Mixtures of Organic Solvent + Ionic Liquid, 1-Butyl-3-Methylimidazolium Hexafluorophosphate at 298.15 K. *Journal of Chemical & Engineering Data* **2007**, *52*, 2359-2364.
(13) Marekha, B. A.; Koverga, V. A.; Chesneau, E.; Kalugin, O. N.; Takamuku, T.; Jedlovszky, P.; Idrissi, A. Local Structure in Terms of Nearest-Neighbor Approach in 1-Butyl-3-methylimidazolium-Based Ionic Liquids: MD Simulations. *The Journal of Physical Chemistry B* **2016**, *120*, 5029-5041.
(14) Kiefer, J. Vibrational Spectroscopy for Studying Hydrogen Bonding in Imidazolium Ionic Liquids and their Mixtures with Cosolvents. In *Hydrogen Bonding and Transfer in the Excited State*, John Wiley & Sons, Ltd, 2010; pp 341-352.
(15) Cha, S.; Ao, M.; Sung, W.; Moon, B.; Ahlstrom, B.; Johansson, P.; Ouchi, Y.; Kim, D. Structures of ionic liquid-water mixtures investigated by IR and NMR spectroscopy. *Physical Chemistry Chemical Physics* **2014**, *16*, 9591-9601.

(16) Takamuku, T.; Kyoshoin, Y.; Shimomura, T.; Kittaka, S.; Yamaguchi, T. Effect of Water on Structure of Hydrophilic Imidazolium-Based Ionic Liquid. *The Journal of Physical Chemistry B* **2009**, *113*, 10817-10824.
(17) Wang, H.; Wang, J.; Zhang, L. Temperature dependence of the microstructure of 1-butyl-3-methylimidazolium tetrafluoroborate in aqueous solution. *Vibrational Spectroscopy* **2013**, *68*, 20-28.
(18) Zhang, Q.-G.; Wang, N.-N.; Wang, S.-L.; Yu, Z.-W. Hydrogen Bonding Behaviors of Binary Systems Containing the Ionic Liquid 1-Butyl-3-methylimidazolium Trifluoroacetate and Water/Methanol. *The Journal of Physical Chemistry B* **2011**, *115*, 11127-11136.
(19) Zhang, Q.-G.; Wang, N.-N.; Yu, Z.-W. The Hydrogen Bonding Interactions between the Ionic Liquid 1-Ethyl-3-Methylimidazolium Ethyl Sulfate and Water. *The Journal of Physical Chemistry B* **2010**, *114*, 4747-4754.
(20) Zhang, L.; Xu, Z.; Wang, Y.; Li, H. Prediction of the solvation and structural properties of ionic liquids in water by two-dimensional correlation spectroscopy. *The Journal of Physical Chemistry B* **2008**, *112*, 6411-6419.
(21) Jeon, Y.; Sung, J.; Kim, D.; Seo, C.; Cheong, H.; Ouchi, Y.; Ozawa, R.; Hamaguchi, H.-o. Structural Change of 1-Butyl-3-methylimidazolium Tetrafluoroborate + Water Mixtures Studied by Infrared Vibrational Spectroscopy. *The Journal of Physical Chemistry B* **2008**, *112*, 923-928.
(22) Jeon, Y.; Sung, J.; Seo, C.; Lim, H.; Cheong, H.; Kang, M.; Moon, B.; Ouchi, Y.; Kim, D. Structures of Ionic Liquids with Different Anions Studied by Infrared Vibration Spectroscopy. *The Journal of Physical Chemistry B* **2008**, *112*, 4735-4740.
(23) Fazio, B.; Triolo, A.; Di Marco, G. Local organization of water and its effect on the structural heterogeneities in room-temperature ionic liquid/H_2O mixtures. *Journal of Raman Spectroscopy* **2008**, *39*, 233-237.
(24) Holomb, R.; Martinelli, A.; Albinsson, I.; Lassègues, J. C.; Johansson, P.; Jacobsson, P. Ionic liquid structure: the conformational isomerism in 1-butyl-3-methyl-imidazolium tetrafluoroborate ([bmim][BF_4]). *Journal of Raman Spectroscopy* **2008**, *39*, 793-805.
(25) Hatano, N.; Watanabe, M.; Takekiyo, T.; Abe, H.; Yoshimura, Y. Anomalous Conformational Change in 1-Butyl-3-methylimidazolium Tetrafluoroborate–D_2O Mixtures. *The Journal of Physical Chemistry A* **2012**, *116*, 1208-1212.
(26) Andanson, J. M.; Traïkia, M.; Husson, P. Ionic association and interactions in aqueous methylsulfate alkyl-imidazolium-based ionic liquids. *The Journal of Chemical Thermodynamics* **2014**, *77*, 214-221.
(27) Koverga, V. A.; Smortsova, Y.; Miannay, F. A.; Kalugin, O. N.; Takamuku, T.; Jedlovszky, P.; Marekha, B.; Cordeiro, M. N. D. S.; Idrissi, A. Distance Angle Descriptors of the Interionic and Ion–Solvent Interactions in Imidazolium-Based Ionic Liquid Mixtures with Aprotic Solvents: A Molecular Dynamics Simulation Study. *The Journal of Physical Chemistry B* **2019**, *123*, 6065-6075.
(28) Wang, Y.; Voth, G. A. Tail Aggregation and Domain Diffusion in Ionic Liquids. *The Journal of Physical Chemistry B* **2006**, *110*, 18601-18608.
(29) Finney, J. L. Random Packings and the Structure of Simple Liquids. I. The Geometry of Random Close Packing. *Proceedings of the Royal Society of London. A. Mathematical and Physical Sciences* **1970**, *319*, 479-493.
(30) Sastry, S.; Truskett, T. M.; Debenedetti, P. G.; Torquato, S.; Stillinger, F. H. Free volume in the hard sphere liquid. *Molecular Physics* **1998**, *95*, 289-297.
(31) Lavrik, N. L.; Voloshin, V. P. Calculation of mean distances between the randomly distributed particles in the model of points and hard spheres (the method of Voronoi polyhedra). *The Journal of Chemical Physics* **2001**, *114*, 9489-9491.
(32) Yi, L. Y.; Dong, K. J.; Zou, R. P.; Yu, A. B. Radical tessellation of the packing of ternary mixtures of spheres. *Powder Technology* **2012**, *224*, 129-137.

(33) Zhou, W.; Wu, W.; Ma, G.; Ng, T. t.; Chang, X. Undrained behavior of binary granular mixtures with different fines contents. *Powder Technology* **2018**, *340*, 139-153.
(34) Ruff, I.; Baranyai, A.; Pálinkás, G.; Heinzinger, K. Grand canonical Monte Carlo simulation of liquid argon. *The Journal of Chemical Physics* **1986**, *85*, 2169-2177.
(35) Hsu, T.-J.; Mou, C.-Y. Molecular dynamics study of liquid-solid transition of dense Lennard-Jones liquid. *Molecular Physics* **1992**, *75*, 1329-1344.
(36) Montoro, J. C. G.; Abascal, J. L. F. The Voronoi polyhedra as tools for structure determination in simple disordered systems. *The Journal of Physical Chemistry* **1993**, *97*, 4211-4215.
(37) Voloshin, V. P.; Naberukhin, Y. I.; Medvedev, N. N.; Jhon, M. S. Investigation of free volume percolation under the liquid–glass phase transition. *The Journal of Chemical Physics* **1995**, *102*, 4981-4986.
(38) Voloshin, V. P.; Beaufils, S.; Medvedev, N. N. Void space analysis of the structure of liquids. *Journal of Molecular Liquids* **2002**, *96–97*, 101-112.
(39) Baranyai, A.; Ruff, I. Statistical geometry of molten alkali halides. *The Journal of Chemical Physics* **1986**, *85*, 365-373.
(40) Pusztai, L.; Baranyai, A.; Ruff, I. Vacancies in molten salts: a characteristic feature of the structure. *Journal of Physics C: Solid State Physics* **1988**, *21*, 3687.
(41) Luchnikov, V. A.; Medvedev, N. N.; Appelhagen, A.; Geiger, A. Medium-range structure of amorphous silicon studied by the Voronoi—Delaunay method. *Molecular Physics* **1996**, *88*, 1337-1348.
(42) Brostow, W.; Chybicki, M.; Laskowski, R.; Rybicki, J. Voronoi polyhedra and Delaunay simplexes in the structural analysis of molecular-dynamics-simulated materials. *Physical Review B* **1998**, *57*, 13448-13458.
(43) Ruocco, G.; Sampoli, M.; Vallauri, R. Analysis of the network topology in liquid water and hydrogen sulphide by computer simulation. *The Journal of Chemical Physics* **1992**, *96*, 6167-6176.
(44) Ruocco, G.; Sampoli, M.; Torcini, A.; Vallauri, R. Molecular dynamics results for stretched water. *The Journal of Chemical Physics* **1993**, *99*, 8095-8104.
(45) Shih, J. P.; Sheu, S. Y.; Mou, C. Y. A Voronoi polyhedra analysis of structures of liquid water. *The Journal of Chemical Physics* **1994**, *100*, 2202-2212.
(46) Yeh, Y.-l.; Mou, C.-Y. Orientational Relaxation Dynamics of Liquid Water Studied by Molecular Dynamics Simulation. *The Journal of Physical Chemistry B* **1999**, *103*, 3699-3705.
(47) Mountain, R. D. Voids and clusters in expanded water. *The Journal of Chemical Physics* **1999**, *110*, 2109-2115.
(48) Jedlovszky, P. Voronoi polyhedra analysis of the local structure of water from ambient to supercritical conditions. *The Journal of Chemical Physics* **1999**, *111*, 5975-5985.
(49) Jedlovszky, P.; Pártay, L. B.; Bartók, A. P.; Voloshin, V. P.; Medvedev, N. N.; Garberoglio, G.; Vallauri, R. Structural and thermodynamic properties of different phases of supercooled liquid water. *The Journal of Chemical Physics* **2008**, *128*, 164512.
(50) Coslovich, D.; Pastore, G. Understanding fragility in supercooled Lennard-Jones mixtures. I. Locally preferred structures. *Journal of Chemical Physics* **2007**, *127*, 124504
(51) Yoon, T. J.; Ha, M. Y.; Lee, W. B.; Lee, Y. W. Monte Carlo simulations on the local density inhomogeneities of sub- and supercritical carbon dioxide: Statistical analysis based on the Voronoi tessellation. *The Journal of Supercritical Fluids* **2017**, *119*, 36-43.
(52) Jedlovszky, P. The local structure of various hydrogen bonded liquids: Voronoi polyhedra analysis of water, methanol, and HF. *The Journal of Chemical Physics* **2000**, *113*, 9113-9121.
(53) Idrissi, A.; Damay, P.; Yukichi, K.; Jedlovszky, P. Self-association of urea in aqueous solutions: A Voronoi polyhedron analysis study. *The Journal of Chemical Physics* **2008**, *129*, 164512.
(54) Idrissi, A.; Polok, K.; Gadomski, W.; Vyalov, I.; Agapov, A.; Kiselev, M.; Barj, M.; Jedlovszky, P. Detailed Insight into the Hydrogen Bonding Interactions in Acetone-Methanol

Mixtures. A Molecular Dynamics Simulation and Voronoi Polyhedra Analysis Study. *Phys. Chem. Chem. Phys.* **2012**, *14*, 5979-5987.
(55) Fábián, B.; Idrissi, A.; Marekha, B.; Jedlovszky, P. Local lateral environment of the molecules at the surface of DMSO-water mixtures. *Journal of Physics: Condensed Matter* **2016**, *28*, 404002.
(56) Koverga, V.; Juhász, Á.; Dudariev, D.; Lebedev, M.; Idrissi, A.; Jedlovszky, P. Local Structure of DMF-Water Mixtures, as Seen from Computer Simulations and Voronoi Analysis. *Journal of Physical Chemistry B* **2022**, *126*, 6964-6978.
(57) Luning Prak, D. J.; Morrow, B. H.; Cowart, J. S.; Trulove, P. C.; Harrison, J. A. Thermophysical Properties of Binary Mixtures of n-Dodecane with n-Alkylcyclohexanes: Experimental Measurements and Molecular Dynamics Simulations. *Journal of Chemical and Engineering Data* **2019**, *64*, 1550-1568.
(58) Zharbossyn, A.; Berkinova, Z.; Boribayeva, A.; Yermukhambetova, A.; Golman, B. Analysis of Tortuosity in Compacts of Ternary Mixtures of Spherical Particles. *Materials (Basel, Switzerland)* **2020**, *13*, 1-14.
(59) Idrissi, A.; Vyalov, I.; Damay, P.; Kiselev, M.; Puhovski, Y. P.; Jedlovszky, P. Local structure in sub- and supercritical CO_2: A Voronoi polyhedra analysis study. *Journal of Molecular Liquids* **2010**, *153*, 20-24.
(60) Idrissi, A.; Vyalov, I.; Kiselev, M.; Fedorov, M. V.; Jedlovszky, P. Heterogeneity of the Local Structure in Sub- and Supercritical Ammonia: A Voronoi Polyhedra Analysis. *The Journal of Physical Chemistry B* **2011**, *115*, 9646-9652.
(61) Chakraborty, D.; Chandra, A. An analysis of voids and necks in supercritical water. *Journal of Molecular Liquids* **2011**, *163*, 1-6.
(62) Tokita, N.; Hirabayashi, M.; Azuma, C.; Dotera, T. Voronoi space division of a polymer: Topological effects, free volume, and surface end segregation. *The Journal of Chemical Physics* **2004**, *120*, 496-505.
(63) Sega, M.; Jedlovszky, P.; Medvedev, N. N.; Vallauri, R. Free volume properties of a linear soft polymer: A computer simulation study. *The Journal of Chemical Physics* **2004**, *121*, 2422-2427.
(64) Gil Montoro, J. C.; Bresme, F.; Abascal, J. L. F. Ionic association in electrolyte solutions: A Voronoi polyhedra analysis. *The Journal of Chemical Physics* **1994**, *101*, 10892-10898.
(65) Kim, A. V.; Medvedev, N. N.; Geiger, A. Molecular dynamics study of the volumetric and hydrophobic properties of the amphiphilic molecule C8E6. *Journal of Molecular Liquids* **2014**, *189*, 74-80.
(66) Voloshin, V. P.; Medvedev, N. N.; Andrews, M. N.; Burri, R. R.; Winter, R.; Geiger, A. Volumetric Properties of Hydrated Peptides: Voronoi–Delaunay Analysis of Molecular Simulation Runs. *The Journal of Physical Chemistry B* **2011**, *115*, 14217-14228.
(67) Voloshin, V. P.; Kim, A. V.; Medvedev, N. N.; Winter, R.; Geiger, A. Calculation of the volumetric characteristics of biomacromolecules in solution by the Voronoi–Delaunay technique. *Biophysical Chemistry* **2014**, *192*, 1-9.
(68) Shinoda, W.; Okazaki, S. A Voronoi analysis of lipid area fluctuation in a bilayer. *The Journal of Chemical Physics* **1998**, *109*, 1517-1521.
(69) Jedlovszky, P.; Medvedev, N. N.; Mezei, M. Effect of Cholesterol on the Properties of Phospholipid Membranes. 3. Local Lateral Structure. *The Journal of Physical Chemistry B* **2004**, *108*, 465-472.
(70) Alinchenko, M. G.; Anikeenko, A. V.; Medvedev, N. N.; Voloshin, V. P.; Mezei, M.; Jedlovszky, P. Morphology of Voids in Molecular Systems. A Voronoi−Delaunay Analysis of a Simulated DMPC Membrane. *The Journal of Physical Chemistry B* **2004**, *108*, 19056-19067.
(71) Alinchenko, M. G.; Voloshin, V. P.; Medvedev, N. N.; Mezei, M.; Pártay, L.; Jedlovszky, P. Effect of Cholesterol on the Properties of Phospholipid Membranes. 4. Interatomic Voids. *The Journal of Physical Chemistry B* **2005**, *109*, 16490-16502.

(72) Rabinovich, A. L.; Balabaev, N. K.; Alinchenko, M. G.; Voloshin, V. P.; Medvedev, N. N.; Jedlovszky, P. Computer simulation study of intermolecular voids in unsaturated phosphatidylcholine lipid bilayers. *The Journal of Chemical Physics* **2005**, *122*, 084906.
(73) Brehm, M.; Weber, H.; Thomas, M.; Hollõczki, O.; Kirchner, B. Domain Analysis in Nanostructured Liquids: A Post-Molecular Dynamics Study at the Example of Ionic Liquids. *ChemPhysChem* **2015**, *16*, 3271-3277.
(74) Jedlovszky, P.; Idrissi, A.; Koverga, V.; Maity, N.; Miannay, F. A.; Kalugin, O. N.; Juhasz, A.; Swiątek, A.; Polok, K.; Takamuku, T. Voronoi polyhedra as a tool for the characterization of inhomogeneous distribution in 1-butyl-3-methylimidazolium cation-based ionic liquids. *Journal of Physical Chemistry B* **2020**, *124*, 10419-10434.
(75) Macchieraldo, R.; Esser, L.; Elfgen, R.; Voepel, P.; Zahn, S.; Smarsly, B. M.; Kirchner, B. Hydrophilic Ionic Liquid Mixtures of Weakly and Strongly Coordinating Anions with and without Water. *ACS Omega* **2018**, *3*, 8567-8582.
(76) Reddy, T. D. N.; Mallik, B. S. Heterogeneity in the microstructure and dynamics of tetraalkylammonium hydroxide ionic liquids: insight from classical molecular dynamics simulations and Voronoi tessellation analysis. *Physical Chemistry Chemical Physics* **2020**, *22*, 3466-3480.
(77) Shelepova, E. A.; Medvedev, N. N. Investigation of the intermolecular voids at the dissolution of CO_2 in ionic liquids. *Journal of Molecular Liquids* **2022**, *349*, 118127.
(78) Esser, L.; Macchieraldo, R.; Elfgen, R.; Sieland, M.; Smarsly, B. M.; Kirchner, B. $TiCl_4$ Dissolved in Ionic Liquid Mixtures from Ab Initio Molecular Dynamics Simulations. *Molecules* **2020**, *26*, 79.
(79) Shelepova, E. A.; Ludwig, R.; Paschek, D.; Medvedev, N. N. Structural similarity of an ionic liquid and the mixture of the neutral molecules. *Journal of Molecular Liquids* **2021**, *329*, 115589.
(80) Sharma, A.; Zhang, Y.; Gohndrone, T.; Oh, S.; Brennecke, J. F.; McCready, M. J.; Maginn, E. J. How mixing tetraglyme with the ionic liquid 1-n-hexyl-3-methylimidazolium bis(trifluoromethylsulfonyl)imide changes volumetric and transport properties: An experimental and computational study. *Chemical Engineering Science* **2017**, *159*, 43-57.
(81) Sharma, A.; Ghorai, P. K. Effect of water on structure and dynamics of [BMIM][PF_6] ionic liquid: An all-atom molecular dynamics simulation investigation. *J Chem Phys* **2016**, *144*, 114505.
(82) Sharma, A.; Ghorai, P. K. Effect of alcohols on the structure and dynamics of [BMIM][PF_6] ionic liquid: A combined molecular dynamics simulation and Voronoi tessellation investigation. *Journal of Chemical Physics* **2018**, *148*, 204514.
(83) Schröder, C.; Neumayr, G.; Steinhauser, O. On the collective network of ionic liquid/water mixtures. III. Structural analysis of ionic liquids on the basis of Voronoi decomposition. *The Journal of Chemical Physics* **2009**, *130*, 194503.
(84) Biswas, A.; Mallik, B. S. Microheterogeneity-Induced Vibrational Spectral Dynamics of Aqueous 1-Alkyl-3-methylimidazolium Tetrafluoroborate Ionic Liquids of Different Cationic Chain Lengths. *Journal of Physical Chemistry B* **2022**, *126*, 5523-5533.
(85) Haberler, M.; Schröder, C.; Steinhauser, O. Hydrated ionic liquids with and without solute: The influence of water content and protein solutes. *Journal of Chemical Theory and Computation* **2012**, *8*, 3911-3928.
(86) Rajbangshi, J.; Banerjee, S.; Ghorai, P. K.; Biswas, R. Cosolvent polarity dependence of solution structure in [BMIM] [PF_6] + acetonitrile/1, 4-dioxane/hexane binary mixtures: Insights from composition dependent Voronoi polyhedra analyses, iso-surfaces and radial distribution functions. *Journal of Molecular Liquids* **2020**, *317*, 113746.
(87) Tsuzuki, S.; Tokuda, H.; Mikami, M. Theoretical analysis of the hydrogen bond of imidazolium C_2–H with anions. *Physical Chemistry Chemical Physics* **2007**, *9*, 4780.

(88) Tsuzuki, S.; Tokuda, H.; Hayamizu, K.; Watanabe, M. Magnitude and Directionality of Interaction in Ion Pairs of Ionic Liquids: Relationship with Ionic Conductivity. *The Journal of Physical Chemistry B* **2005**, *109*, 16474-16481.
(89) Hunt, P. A.; Ashworth, C. R.; Matthews, R. P. Hydrogen bonding in ionic liquids. *Chemical Society Reviews* **2015**, *44*, 1257-1288.
(90) Hunt, P. A.; Gould, I. R. Structural characterization of the 1-butyl-3-methylimidazolium chloride ion pair using ab initio methods. *The Journal of Physical Chemistry A* **2006**, *110*, 2269-2282.
(91) Fujii, K.; Kanzaki, R.; Takamuku, T.; Kameda, Y.; Kohara, S.; Kanakubo, M.; Shibayama, M.; Ishiguro, S.; Umebayashi, Y. Experimental evidences for molecular origin of low-Q peak in neutron/x-ray scattering of 1-alkyl-3-methylimidazolium bis(trifluoromethanesulfonyl)amide ionic liquids. *J Chem Phys* **2011**, *135*, 244502.
(92) Fujii, K.; Soejima, Y.; Kyoshoin, Y.; Fukuda, S.; Kanzaki, R.; Umebayashi, Y.; Yamaguchi, T.; Ishiguro, S.-i.; Takamuku, T. Liquid Structure of Room-Temperature Ionic Liquid, 1-Ethyl-3-methylimidazolium Bis-(trifluoromethanesulfonyl) Imide. *The Journal of Physical Chemistry B* **2008**, *112*, 4329-4336.
(93) Mondal, A.; Balasubramanian, S. Quantitative prediction of physical properties of imidazolium based room temperature ionic liquids through determination of condensed phase site charges: A refined force field. *Journal of Physical Chemistry B* **2014**, *118*, 3409-3422.
(94) Mondal, A.; Balasubramanian, S. A Refined All-Atom Potential for Imidazolium-Based Room Temperature Ionic Liquids: Acetate, Dicyanamide, and Thiocyanate Anions. *Journal of Physical Chemistry B* **2015**, *119*, 11041-11051.
(95) Koverga, V. A.; Korsun, O. M.; Kalugin, O. N.; Marekha, B. A.; Idrissi, A. A new potential model for acetonitrile: Insight into the local structure organization. *Journal of Molecular Liquids* **2017**, *233*, 251-261.
(96) Koverga, V. A.; Voroshylova, I. V.; Smortsova, Y.; Miannay, F. A.; Cordeiro, M. N. D. S.; Idrissi, A.; Kalugin, O. N. Local structure and hydrogen bonding in liquid γ-butyrolactone and propylene carbonate: A molecular dynamics simulation. *Journal of Molecular Liquids* **2019**, *287*, 110912-110912.
(97) Zaninetti, L. The Voronoi tessellation generated from different distributions of seeds. *Physics Letters A* **1992**, *165*, 143-147.
(98) Reichardt, C.; Welton, T. *Solvents and Solvent Effects in Organic Chemistry*; Wiley-VCH Verlag GmbH & Co. KGaA, 2011.
(99) Fornefeld-Schwarz, U. M.; Svejda, P. Refractive Indices and Relative Permittivities of Liquid Mixtures of γ-Butyrolactone, γ-Valerolactone, δ-Valerolactone, or ε-Caprolactone + Benzene, + Toluene, or + Ethylbenzene at 293.15 K and 313.15 K and Atmospheric Pressure. *Journal of Chemical and Engineering Data* **1999**, *44*, 597-604.
(100) Idrissi, A.; Marekha, B.; Kiselev, M.; Jedlovszky, P. The local environment of the molecules in water-DMSO mixtures, as seen from computer simulations and Voronoi polyhedra analysis. *Physical chemistry chemical physics : PCCP* **2015**, *17*, 3470-3481.

Conclusions and perspectives

This thesis presents a molecular dynamics description of the transport properties and the local structure in three different type of systems (with lithium salts, alkylammonium salts and solutions with ionic liquids) that can be used as advanced electrochemical systems for energy store devices. All of these systems have maximum at the electroconductivity-concentration curve but as for today there is still no constant theory or quantitative approach to investigate the reasoning behind these phenomena. Understanding the undergoing processes that cause such behavior is crucial task on the way of successful use of such solutions and their analogues in practical aspects.

Three different types of systems of different concentrations were investigated: $LiPF_6$ in dimethyl carbonate (DMC) / ethylene carbonate (EC) binary mixture, 1-1'-spirobipyrrolidinium tetrafluoroborate ($SBPBF_4$) in acetonitrile (AN) and 1-butyl-3-methylimidazolium-based (C_4mim^+) ILs with perfluorinated anions (BF_4^-, PF_6^-, TFO^-, $TFSI^-$) and dipolar aprotic solvents such as AN, γ-butyrolactone (γ-BL) and propylene carbonate (PC).

First, the $LiPF_6$ salt in DMC/EC (1:1) binary mixture solutions of five different concentrations have been studied with classical MD simulation technique. The potential models for DMC and EC molecules were optimized in this work from the combination of two different force fields: OPLS-AA and GAFF in order to properly reproduce the transport properties of these solvents. The structure has been analyzed in terms of cation-anion and cation-solvent RDFs and RCNs. The snapshot from the trajectory files of the simulation confirmed the RDF and RCN data and shoved that Li^+ cations tend to form contact ion pairs (CIP) as well as solvent-shared ion pairs (SSIP). The RCNs showed that total coordination number of the cation for the first coordination sphere remains 5.5-6.0 for all concentrations. For the ionic aggregate analysis two set of criteria were proposed (based on the fact of formation of CIPs and SSIPs). For them two different distances were used: minima on the RDFs and the minima on the second

derivative of the RCNs. As with the first set of criteria only small aggregates were spotted in the system, the previous statement was confirmed that $LiPF_6$ give preference to formation of SSIPs in DMC/EC (1:1) binary mixtures. The massive aggregation for the second set of criteria was spotted beginning from the concentration of 1.0 M for both criteria. The results for distances of minimum on the RDFs or minimum on the second derivative on the RCNs are not differ significantly. Also, the distances taken for the second set of criteria seem to overestimate the aggregation. Lastly, the transport properties of simulated systems were obtained. The diffusion coefficients for all components are decreasing and viscosity values are non-linearly increasing with the salt concentration increase. The drastic non-linear increase of the viscosity from nearly 1.0 M and for higher concentrations of $LiPF_6$ also occurs. These findings are consistent with the maximum of experimental electroconductivity at this concentration value.

$SBPBF_4$ in AN solutions in a wide range of concentrations were also investigated via classical MD simulation. The cation full-atom potential model has been developed by authors. In order to account the existence of several conformers of the cation in the solution, the several iterations of MD simulations and charge unification for hydrogen atoms were performed. The final results after two iterations were taken into account. The SBP^+ cation diffusion coefficient is close to the one obtained from the experimental limiting molar conductivities. The structure was studied in terms of RDFs and RCNs. The cation-anion (N-B) RDFs of mixtures of different concentrations shows the presence of two possible cation-anion relative disposition: axial and equatorial. As the concentration of $SBPBF_4$ rises the composition of the cations first coordination shell changes: PF_6^- anions (coordination number changes from 1.4 to 4.2) are replacing AN solvent molecules (coordination number changes from 11.3 to 5.7) in it. Aggregate analysis was performed with the use of two different criteria. The second criterion is stricter, without considering the equatorial position of the anions relatively to the cations. For the first criterion the massive aggregation occurs at the

concentration of $SBPBF_4$ in AN at 1.5 M while for the second criterion the average number of association begins to increase at the same region where the experimental conductivity curve changes its behavior which indicates that this criterion is the correct choice for such an analysis. The transport properties were investigated via diffusion coefficients of solution components and viscosity of simulated systems. Obtained viscosity values are matching the experimental ones. Diffusion coefficients of all components are decreasing while the viscosity of the system continuously increasing with the salt concentration increase. The obtained results show a good correlation with the association analysis and in accordance with the occurrence of the concentration conductivity maximum in the experiment.

Next, twelve ILs (C_4mim^+ with BF_4^-, PF_6^-, TFO^- and $TFSI^-$) with molecular solvents (AN, PC, and γ-BLF) binary mixtures were studied by the molecular dynamics simulation technique. The microstructure of the mixtures was studied in the framework of radial distribution functions and running coordination numbers. The RDFs and RCNs show the particular behavior in AN and $TFSI^-$ systems. For TFSI- system the cation-anion (CoR-N) RDFs curves showed two peaks with similar intensities that represent the position when the nitrogen atom of the anion is close to the imidazolium ring and when nitrogen atom of $TFSI^-$ not directly interacting with the ring, but instead the oxygen atoms do. The cation-anion coordination numbers changed in similar values for the same ionic liquids in different solvents: for AN it varies from ~1.2 to ~3.6, for PC – from 0.6 to 3.0 and for γ-BL – from 0.8 to 3.1 with the increasing mole fraction of the ILs. Also, data obtained were used to conduct a quantitative aggregate analysis with two different distance criteria (first minimum of RDF and minimum of the second derivative of the RCN respectively). The analysis with the first criterion shows the formation of the massive cluster at ~0.15, 0.20 and 0.25 IL mole fraction for AN and for with γ-BL respectively. Thus, this criterion seems to overrate the aggregation process in the mixtures. With the second, stricter distance criteria the formation of big aggregates in the systems starting to occur at the same mole

fractions of the ILs where the experimental conductivity curves change their behavior and the maximum occurs. To analyze the transport properties the diffusion coefficients of all the components and shear viscosity for all binary mixtures were obtained. The diffusion coefficients show good agreement with experimental data, especially for the systems with AN. The viscosity values didn't show any particular behavior at the mole fraction of the ILs range where the experimental conductivity maximum occur.

Finally, the local structure in twelve mixtures of ILs was also studied via distributions of several metric characteristics (i.e., volume, reciprocal volume, characteristic of the local density, and vertex distance, marking the radius of the largest spherical void) of the Voronoi polyhedra. A drastic change in the behavior of the calculated properties at this composition was found, proving that these changes concern the local structure around the particles. The results show that below the IL mole fraction of about 0.2, the ions are well solvated by the solvent molecules, but above this mole fraction they start to form contact pairs, while the solvent molecules, expelled from the vicinity of the ions, form self-associates. This self-association is stronger in the case of AN than of the other solvents considered, because, due to its smaller dipole moment, AN has a weaker interaction with the ions than the other ones. Similarly, this solvent self-association is stronger in the presence of $TFSI^-$ than of the other anions considered. All these results stress that the local structure, and thus also the physicochemical properties of the IL-solvent mixtures are eventually governed by the delicate interplay of the interionic and solvent-ion interactions.

As for the general results, both of the approaches – association analysis via distance criterion of cluster formation and Voronoi polyhedral analysis – allow to investigate the local structure of the simulated systems of different types. Also, the crucial role of the processes that occur in the microenvironment of ions and solvent molecules were confirmed.

Appendices

Appendix A: Voronoi polyhedra analysis

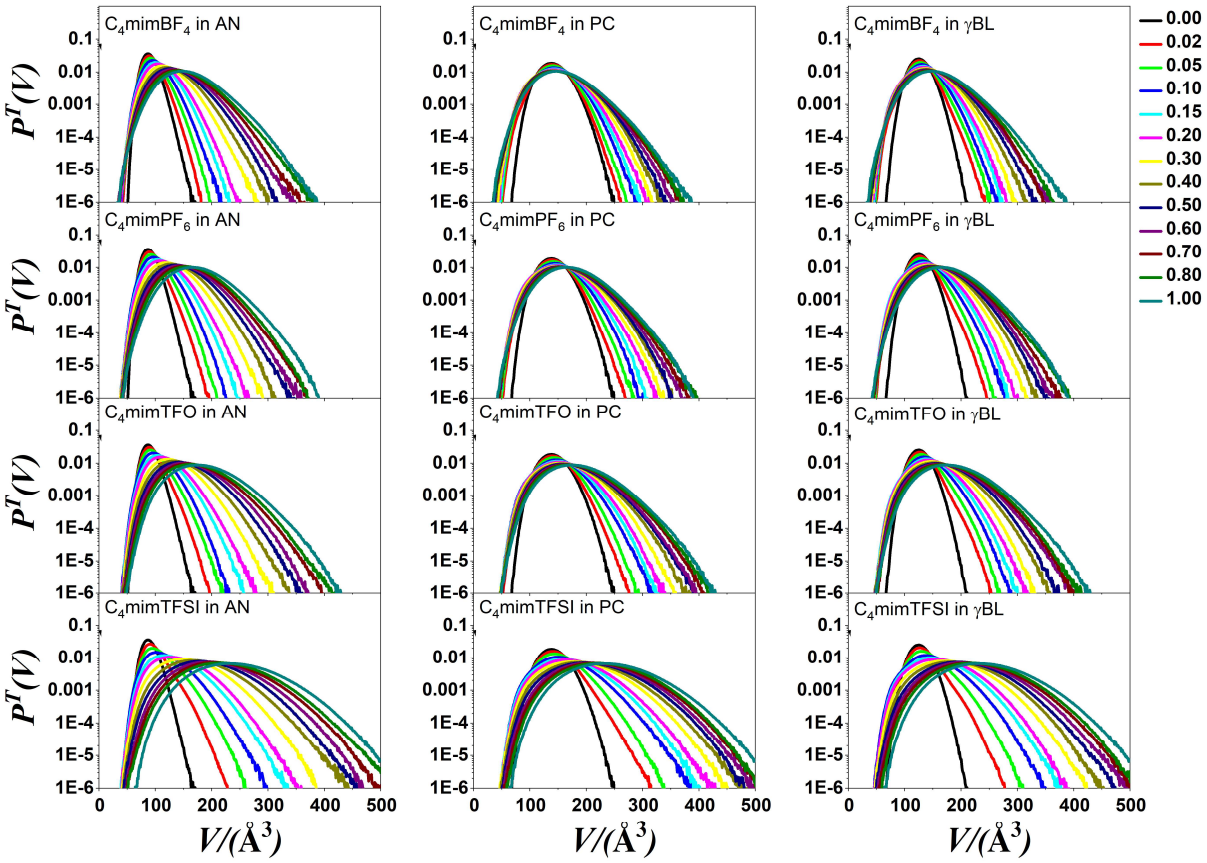

Figure A1. Volume distributions of the Voronoi polyhedra of the components of the mixtures at various mole fraction of ionic liquid, when all components are taken into account in the analysis. The position of the cation is described with ring H^2 hydrogen of C_4mim^+. The F ($BF_4^-$and PF_6^-) and the O (TFO^- and $TFSI^-$) atoms describe position of the anion while the N and O atoms describe the position of the AN, PC and γ-BL, respectively.

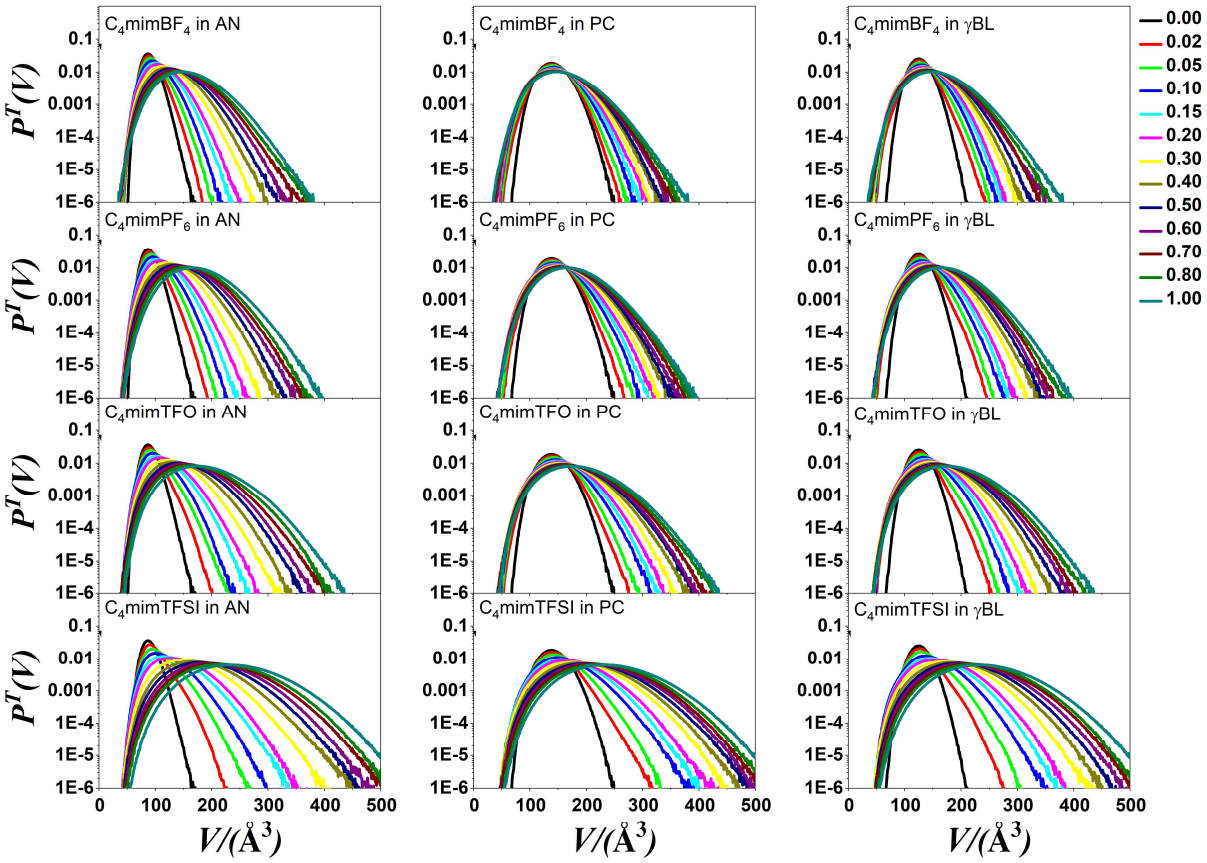

Figure A2. Volume distributions of the Voronoi polyhedra of the components of the mixtures at various mole fraction of ionic liquid, when all components are taken into account in the analysis. The position of the cation is described with ring H^4 hydrogen of C_4mim^+. The F ($BF_4^-$and PF_6^-) and the O (TFO^- and $TFSI^-$) atoms describe position of the anion while the N and O atoms describe the position of the AN, PC and γ-BL, respectively.

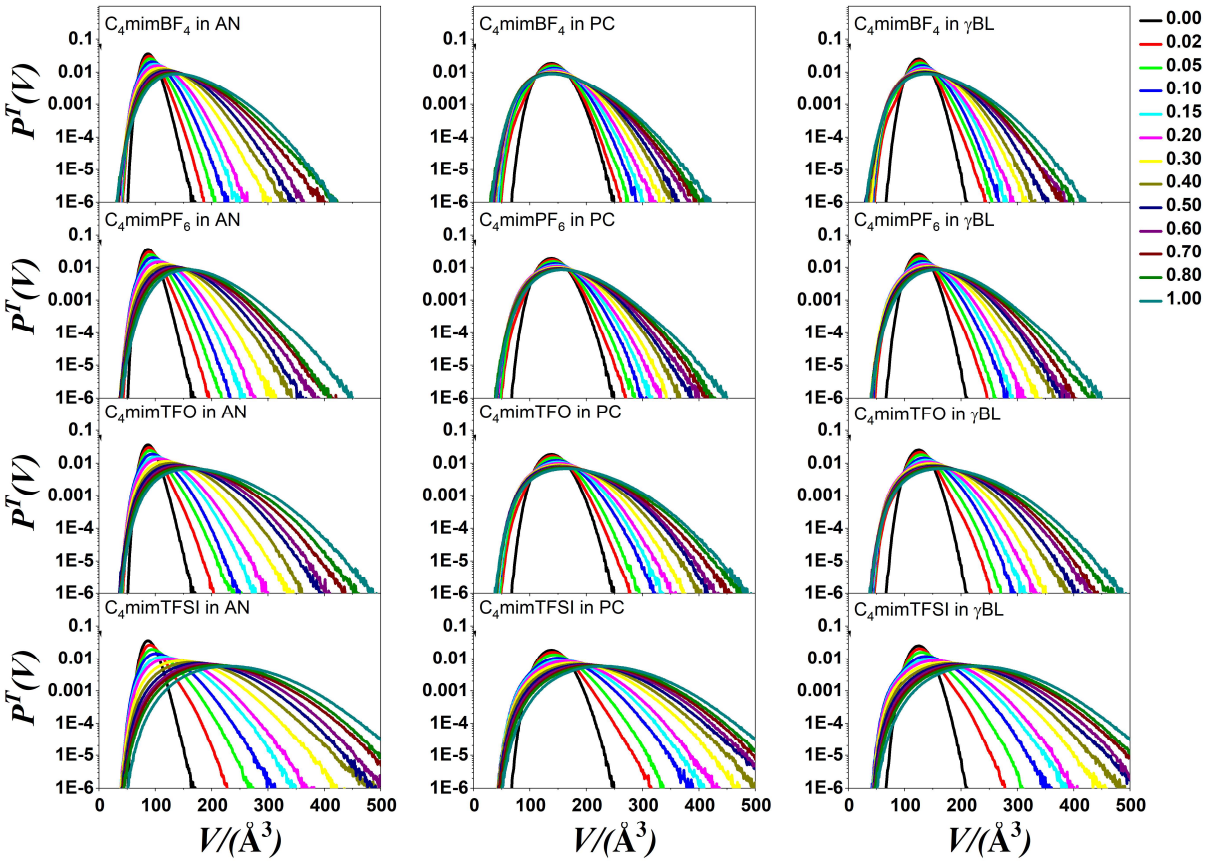

Figure A3. Volume distributions of the Voronoi polyhedra of the components of the mixtures at various mole fraction of ionic liquid, when all components are taken into account in the analysis. The position of the cation is described with ring H^5 hydrogen of C_4mim^+. The F ($BF_4^-$and PF_6^-) and the O (TFO^- and $TFSI^-$) atoms describe position of the anion while the N and O atoms describe the position of the AN, PC and γ-BL, respectively.

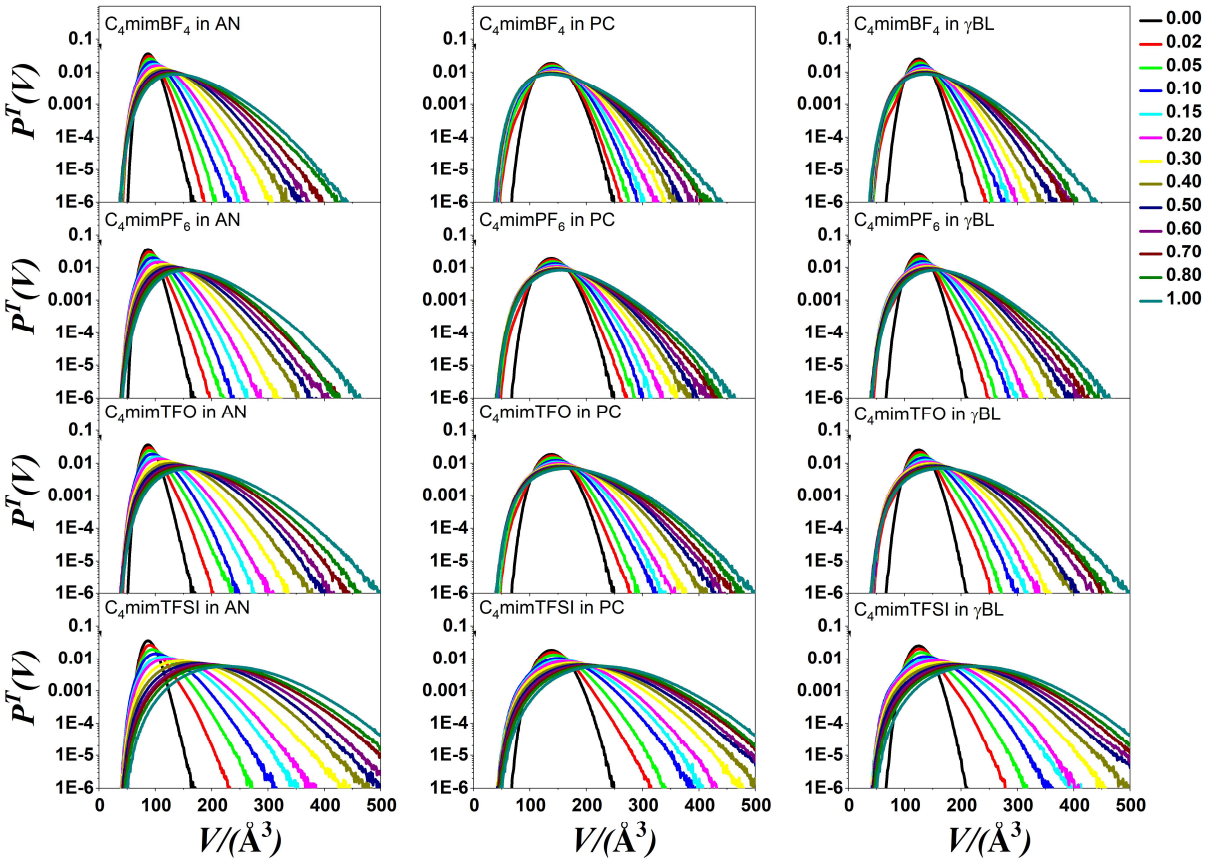

Figure A4. Volume distributions of the Voronoi polyhedra of the components of the mixtures at various mole fraction of ionic liquid, when all components are taken into account in the analysis. The position of the cation is described with alkyl H^M hydrogen of C_4mim^+. The F ($BF_4^-$and PF_6^-) and the O (TFO^- and $TFSI^-$) atoms describe position of the anion while the N and O atoms describe the position of the AN, PC and γ-BL, respectively.

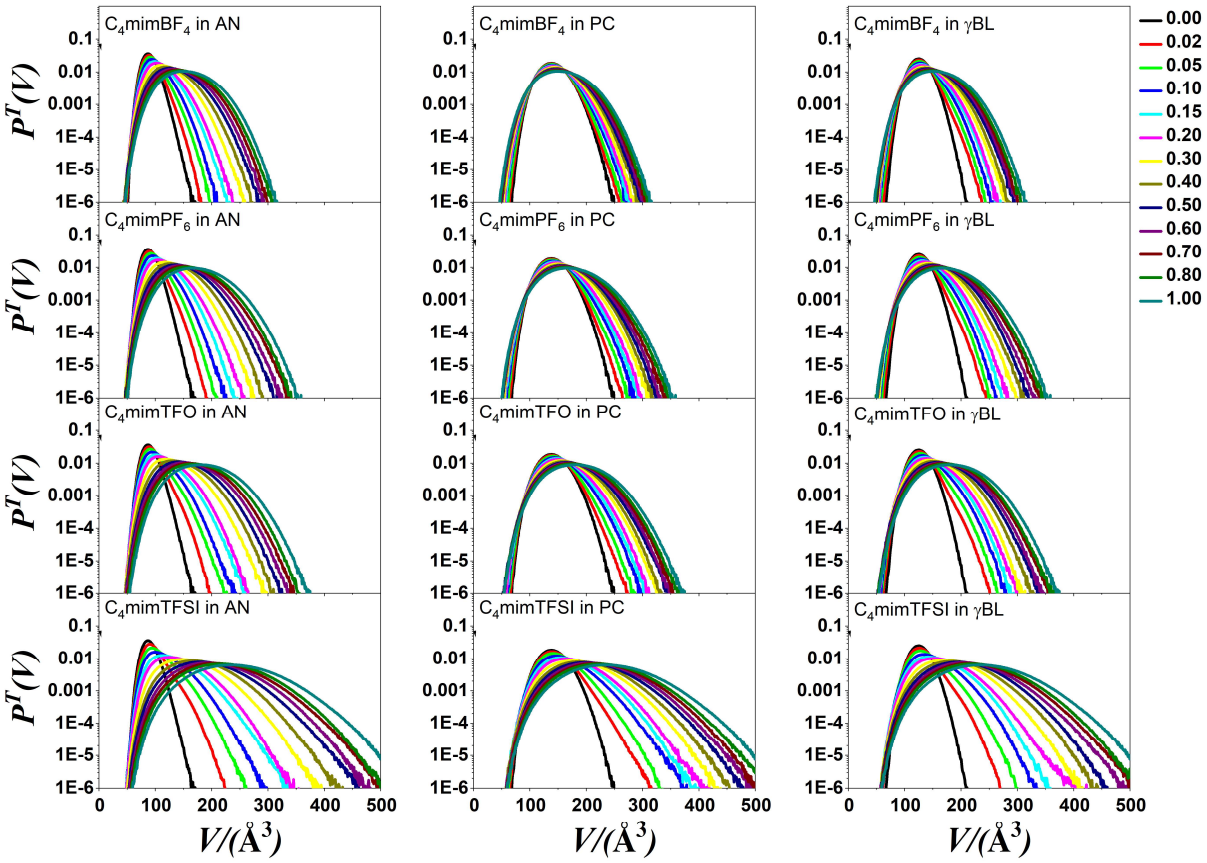

Figure A5. Volume distributions of the Voronoi polyhedra of the components of the mixtures at various mole fraction of ionic liquid, when all components are taken into account in the analysis. The position of the cation is described with alkyl H^B hydrogen of C_4mim^+. The F ($BF_4^-$and PF_6^-) and the O (TFO^- and $TFSI^-$) atoms describe position of the anion while the N and O atoms describe the position of the AN, PC and γ-BL, respectively.

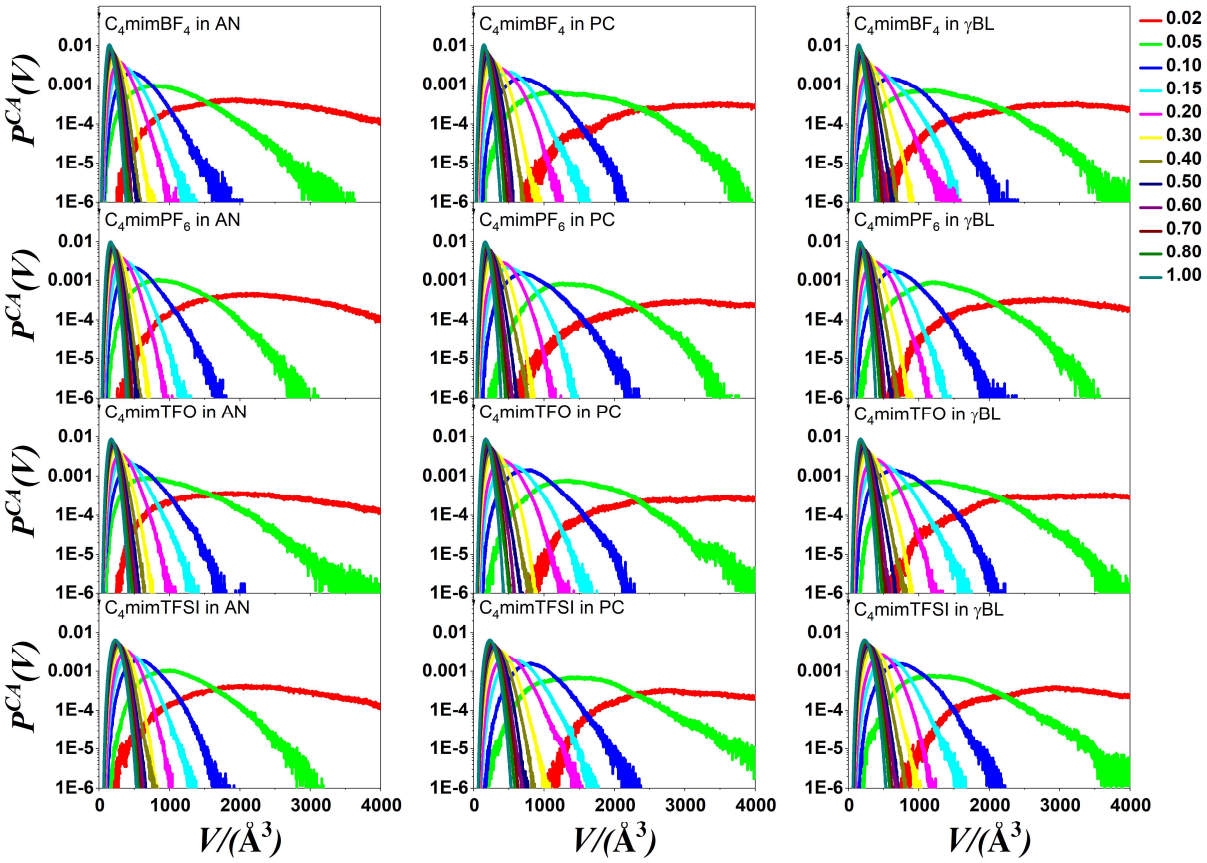

Figures A6. Volume distributions of the Voronoi polyhedra of the components of the mixtures at various mole fraction of ionic liquid, when only the ions are taken into account, and the solvent molecules are disregarded. The position of the cation is described with ring H^2 hydrogen of C_4mim^+. The F ($BF_4^-$and PF_6^-) and the O (TFO^- and $TFSI^-$) atoms describe position of the anion while the N and O atoms describe the position of the AN, PC and γ-BL, respectively.

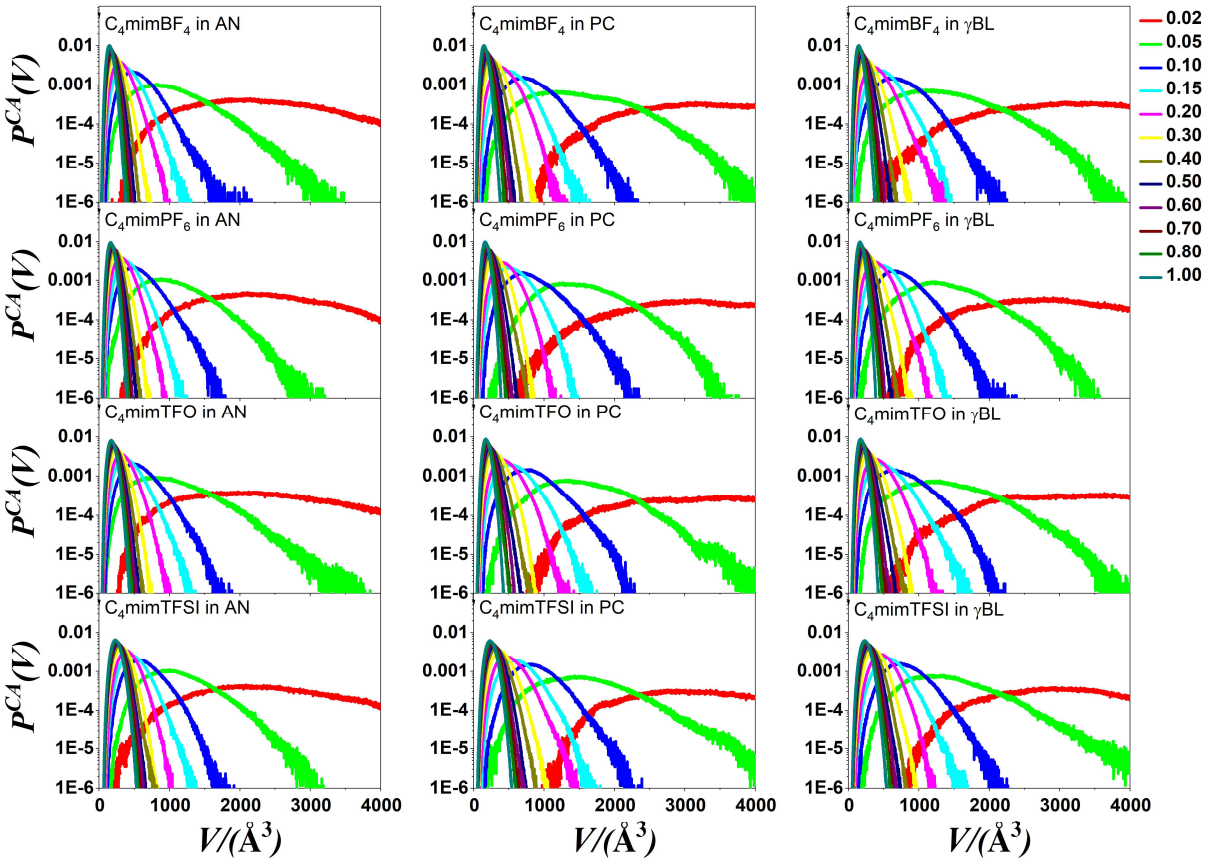

Figures A7. Volume distributions of the Voronoi polyhedra of the components of the mixtures at various mole fraction of ionic liquid, when only the ions are taken into account, and the solvent molecules are disregarded. The position of the cation is described with ring H^4 hydrogen of C_4mim^+. The F ($BF_4^-$and PF_6^-) and the O (TFO^- and $TFSI^-$) atoms describe position of the anion while the N and O atoms describe the position of the AN, PC and γ-BL, respectively.

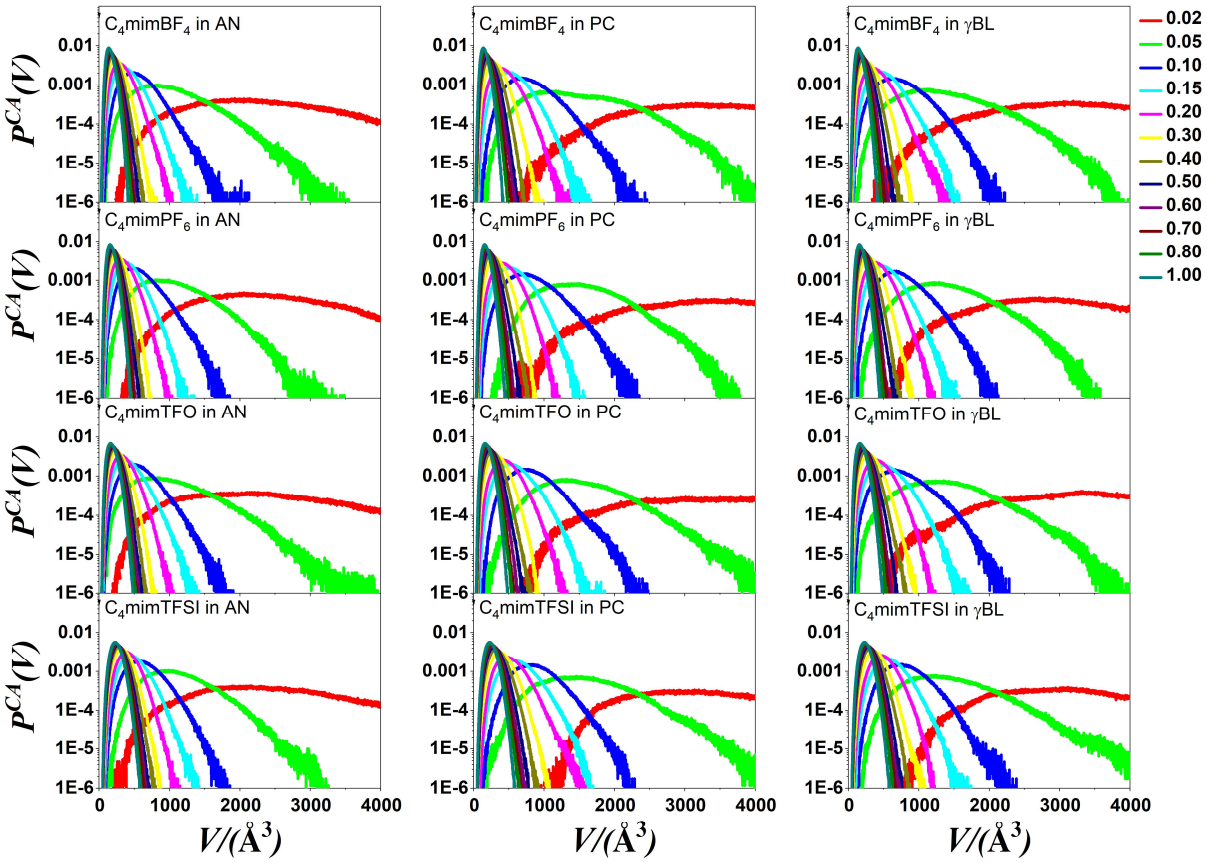

Figures A8. Volume distributions of the Voronoi polyhedra of the components of the mixtures at various mole fraction of ionic liquid, when only the ions are taken into account, and the solvent molecules are disregarded. The position of the cation is described with ring H^5 hydrogen of C_4mim^+. The F ($BF_4^-$and PF_6^-) and the O (TFO^- and $TFSI^-$) atoms describe position of the anion while the N and O atoms describe the position of the AN, PC and γ-BL, respectively.

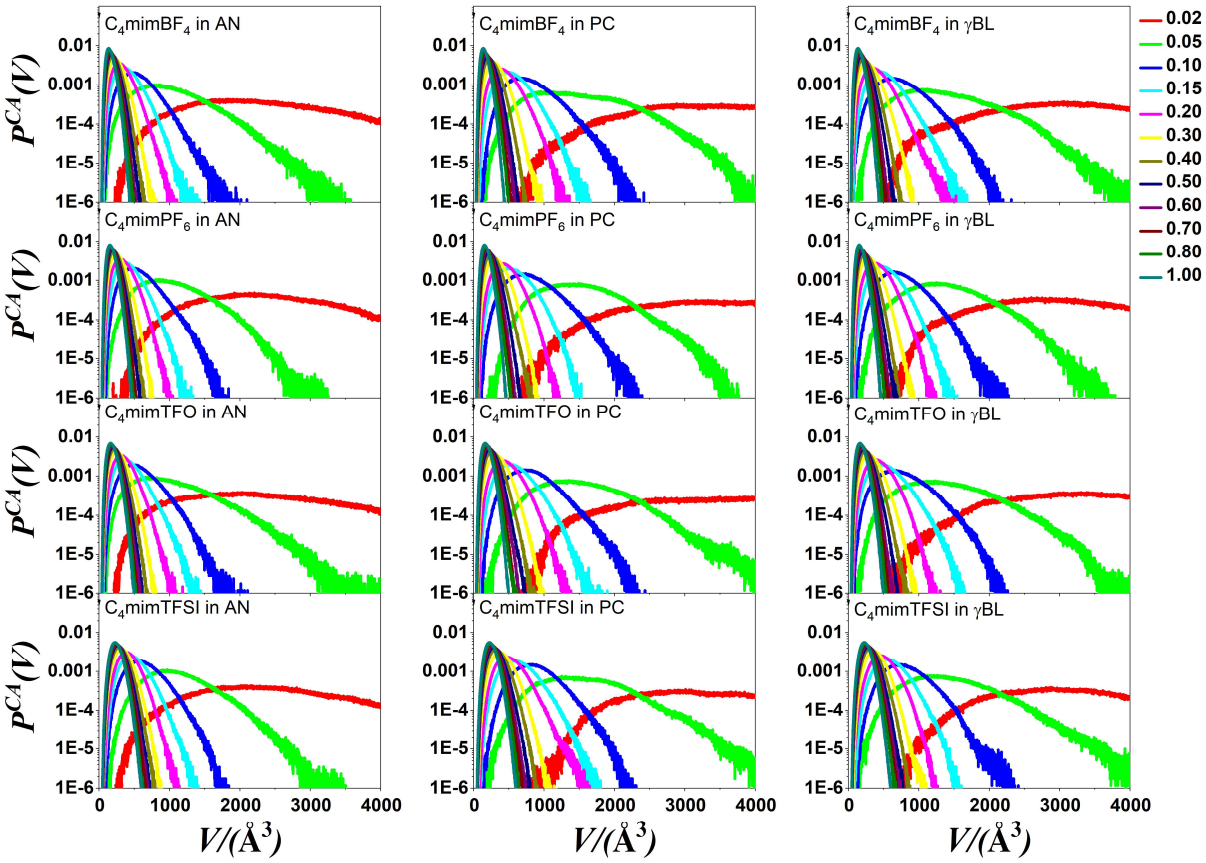

Figures A9. Volume distributions of the Voronoi polyhedra of the components of the mixtures at various mole fraction of ionic liquid, when only the ions are taken into account, and the solvent molecules are disregarded. The position of the cation is described with alkyl H^M hydrogen of C_4mim^+. The F ($BF_4^-$and PF_6^-) and the O (TFO^- and $TFSI^-$) atoms describe position of the anion while the N and O atoms describe the position of the AN, PC and γ-BL, respectively.

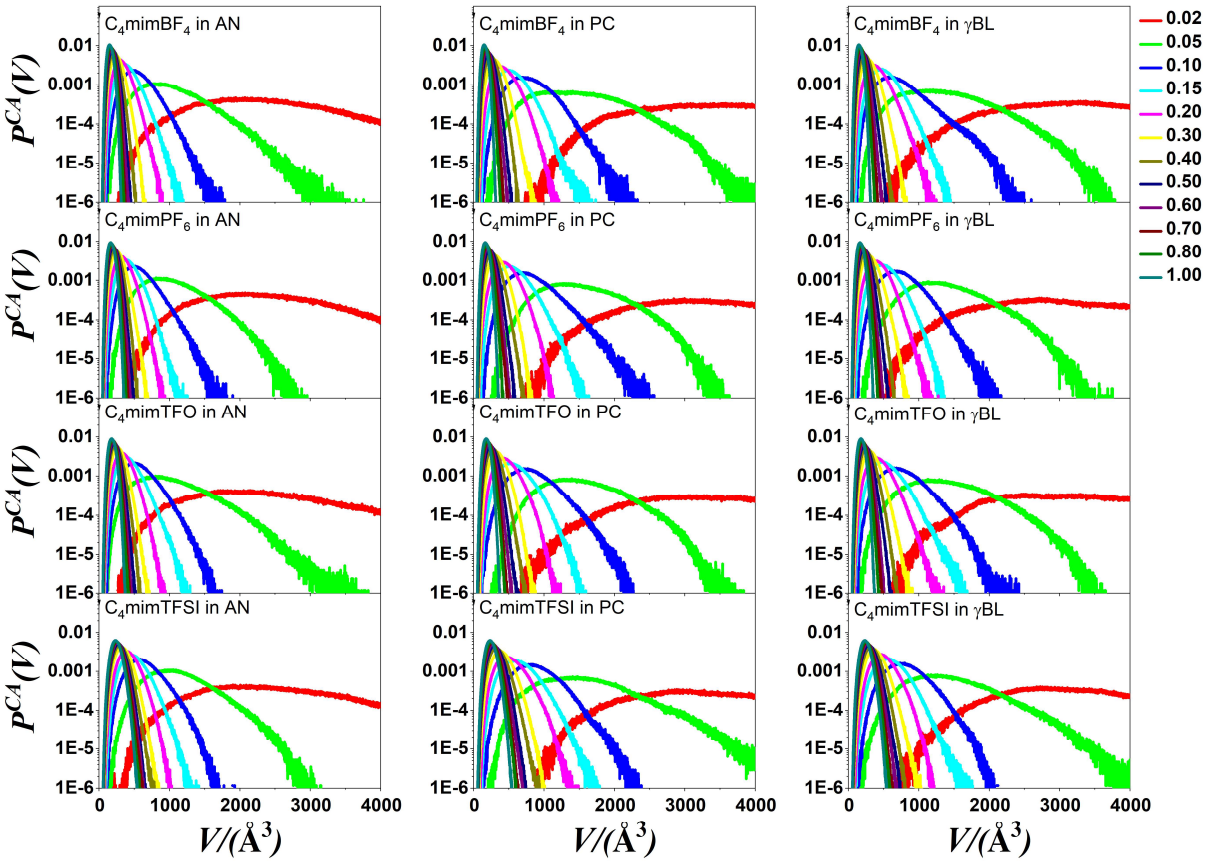

Figures A10. Volume distributions of the Voronoi polyhedra of the components of the mixtures at various mole fraction of ionic liquid, when only the ions are taken into account, and the solvent molecules are disregarded. The position of the cation is described with alkyl H^B hydrogen of C_4mim^+. The F ($BF_4^-$and PF_6^-) and the O (TFO^- and $TFSI^-$) atoms describe position of the anion while the N and O atoms describe the position of the AN, PC and γ-BL, respectively.

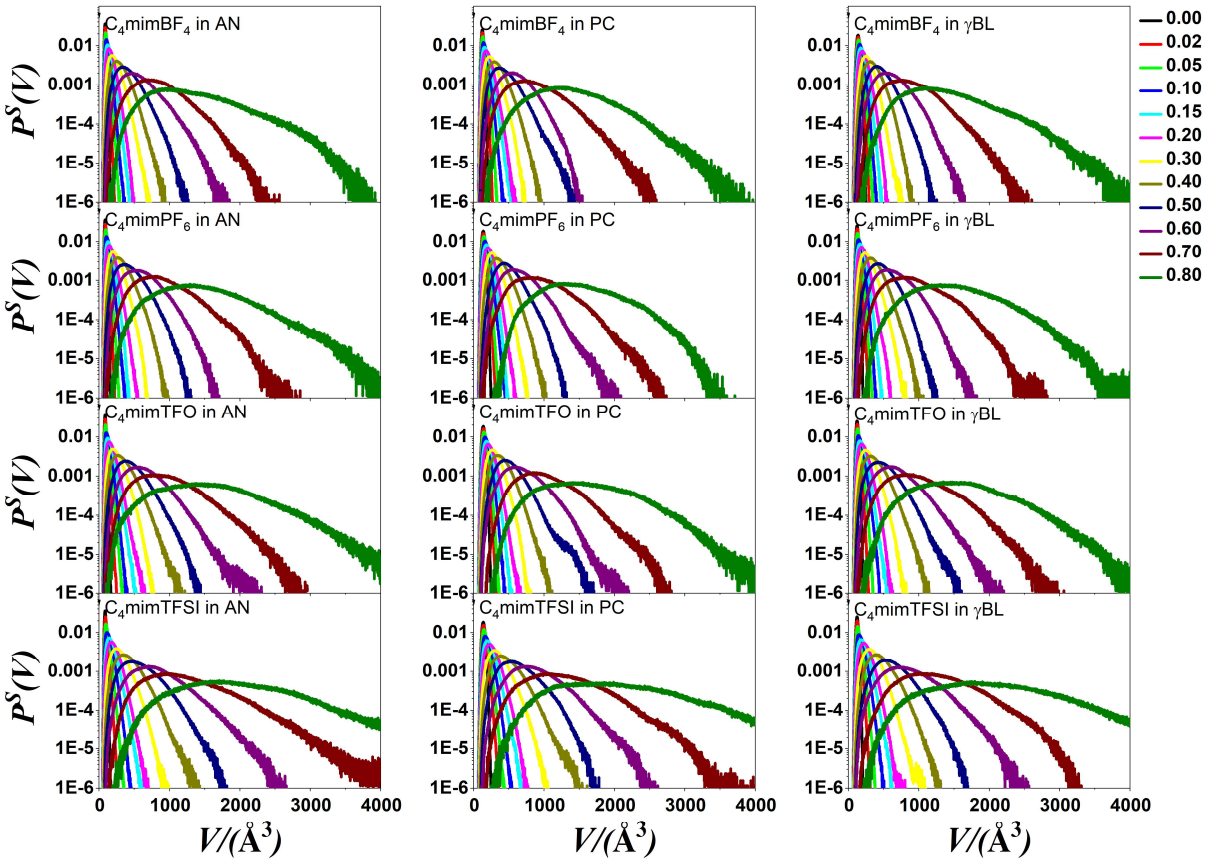

Figures A11. Volume distributions of the Voronoi polyhedra of the components of the mixtures at various mole fraction of ionic liquid, when only the solvent molecules are taken into account. The N and O atoms describe the position of the AN, PC and γ-BL, respectively.

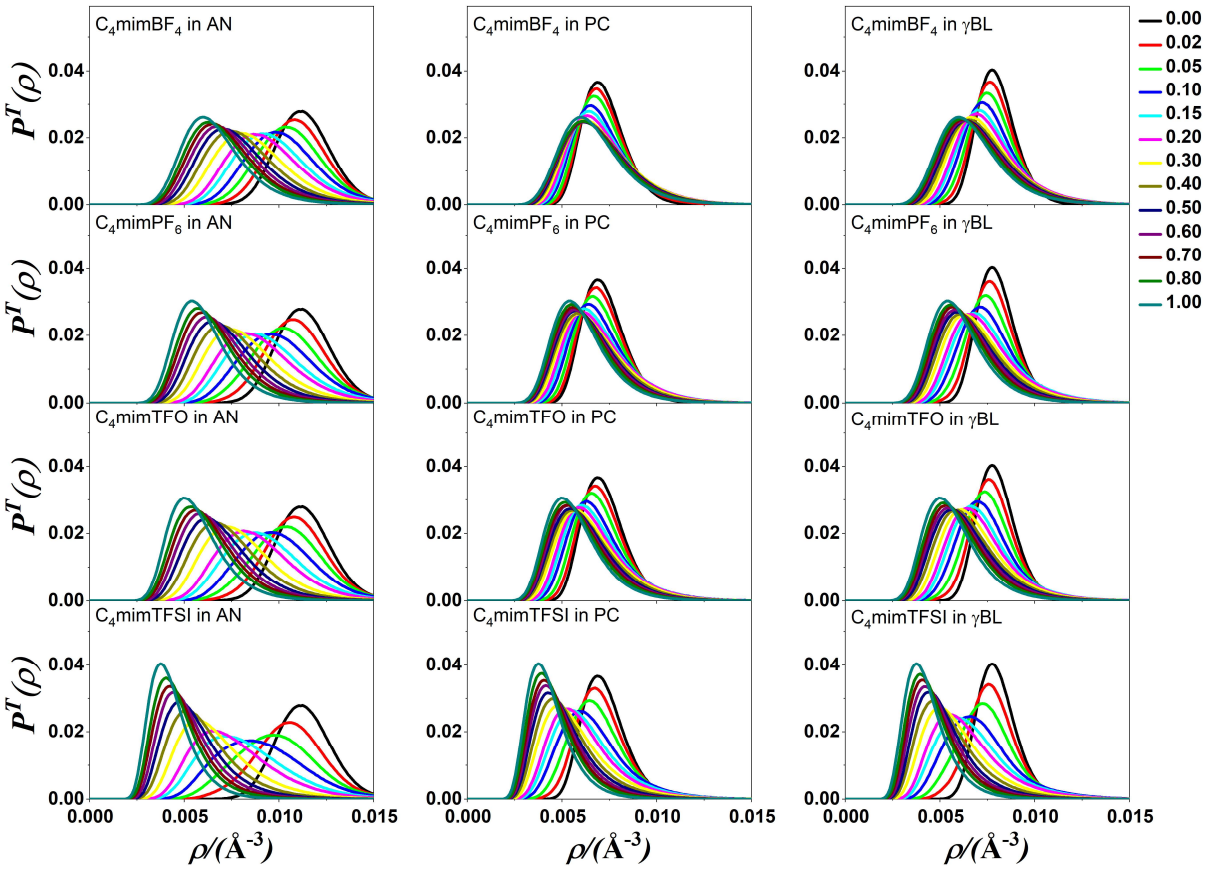

Figure A12. Reciprocal volume distributions of the Voronoi polyhedra of the components of the mixtures at various mole fraction of ionic liquid, when all components are taken into account in the analysis. The position of the cation is described with ring H^2 hydrogen of C_4mim^+. The F ($BF_4^-$and PF_6^-) and the O (TFO^- and $TFSI^-$) atoms describe position of the anion while the N and O atoms describe the position of the AN, PC and γ-BL, respectively.

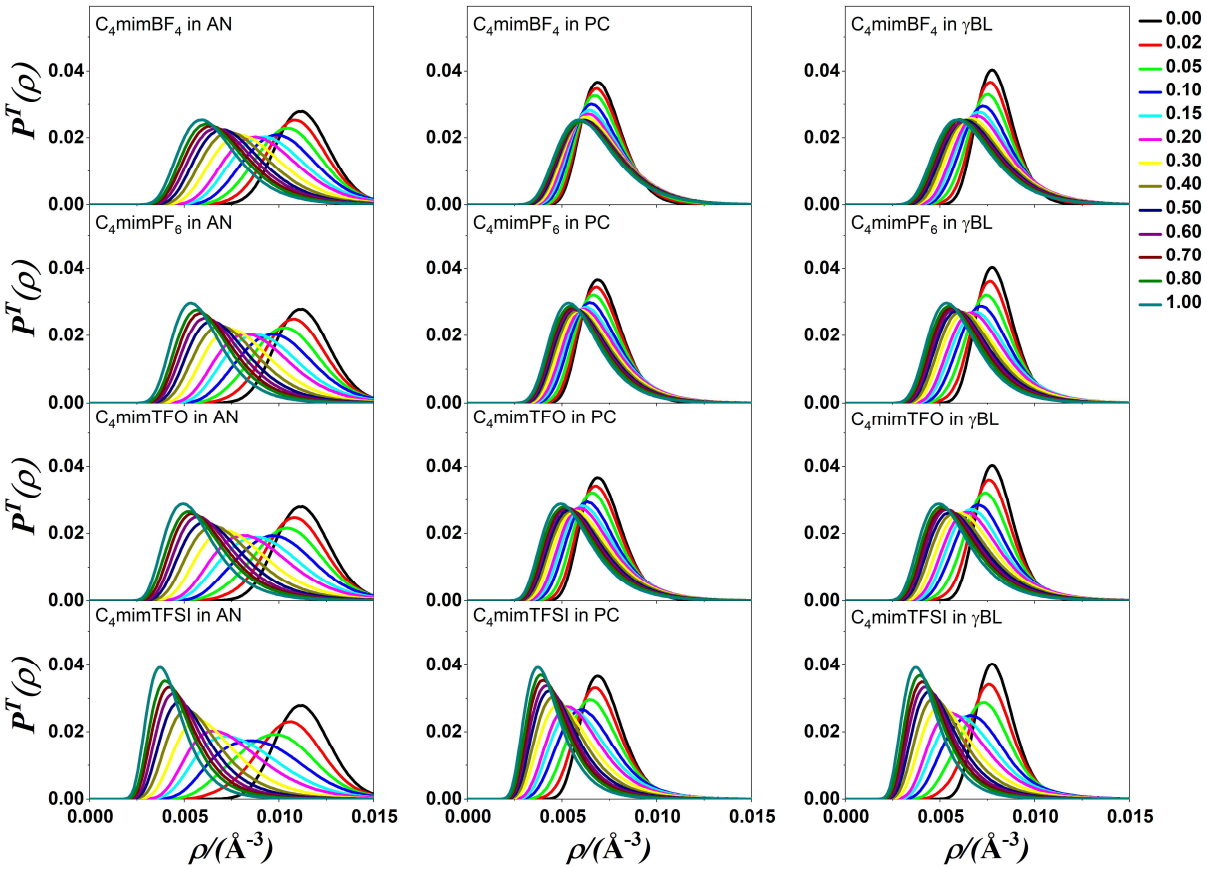

Figure A13. Reciprocal volume distributions of the Voronoi polyhedra of the components of the mixtures at various mole fraction of ionic liquid, when all components are taken into account in the analysis. The position of the cation is described with ring H^4 hydrogen of C_4mim^+. The F ($BF_4^-$and PF_6^-) and the O (TFO^- and $TFSI^-$) atoms describe position of the anion while the N and O atoms describe the position of the AN, PC and γ-BL, respectively.

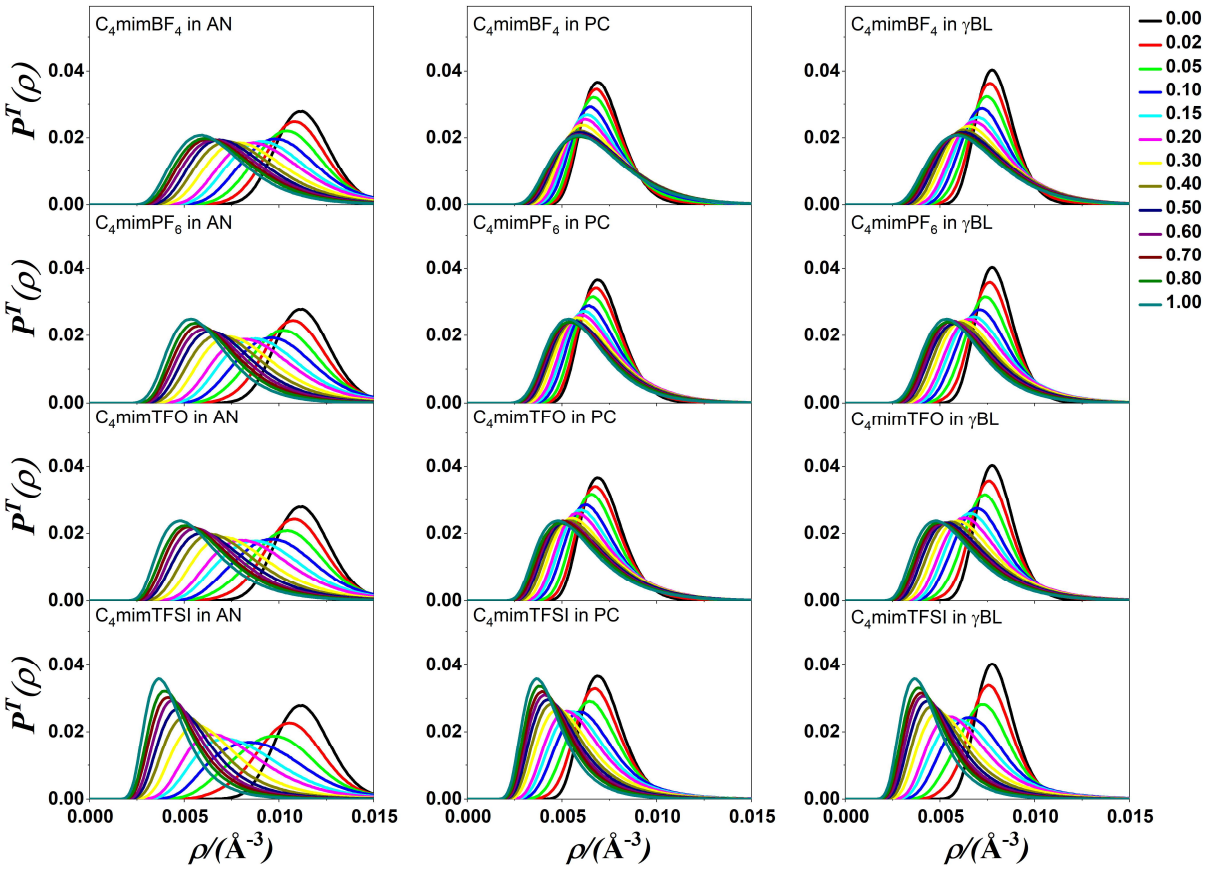

Figure A14. Reciprocal volume distributions of the Voronoi polyhedra of the components of the mixtures at various mole fraction of ionic liquid, when all components are taken into account in the analysis. The position of the cation is described with ring H^5 hydrogen of C_4mim^+. The F ($BF_4^-$and PF_6^-) and the O (TFO^- and $TFSI^-$) atoms describe position of the anion while the N and O atoms describe the position of the AN, PC and γ-BL, respectively.

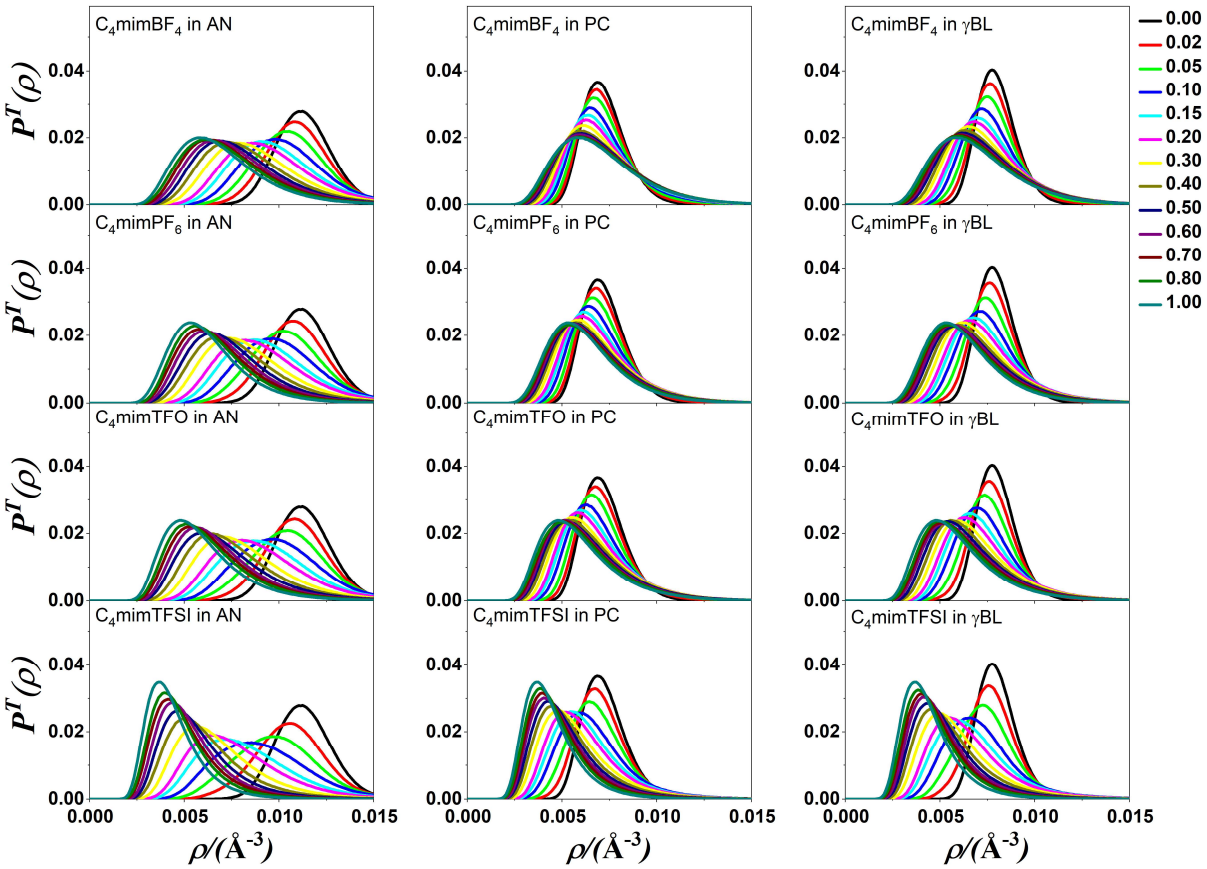

Figure A15. Reciprocal volume distributions of the Voronoi polyhedra of the components of the mixtures at various mole fraction of ionic liquid, when all components are taken into account in the analysis. The position of the cation is described with alkyl H^M hydrogen of C_4mim^+. The F ($BF_4^-$and PF_6^-) and the O (TFO^- and $TFSI^-$) atoms describe position of the anion while the N and O atoms describe the position of the AN, PC and γ-BL, respectively.

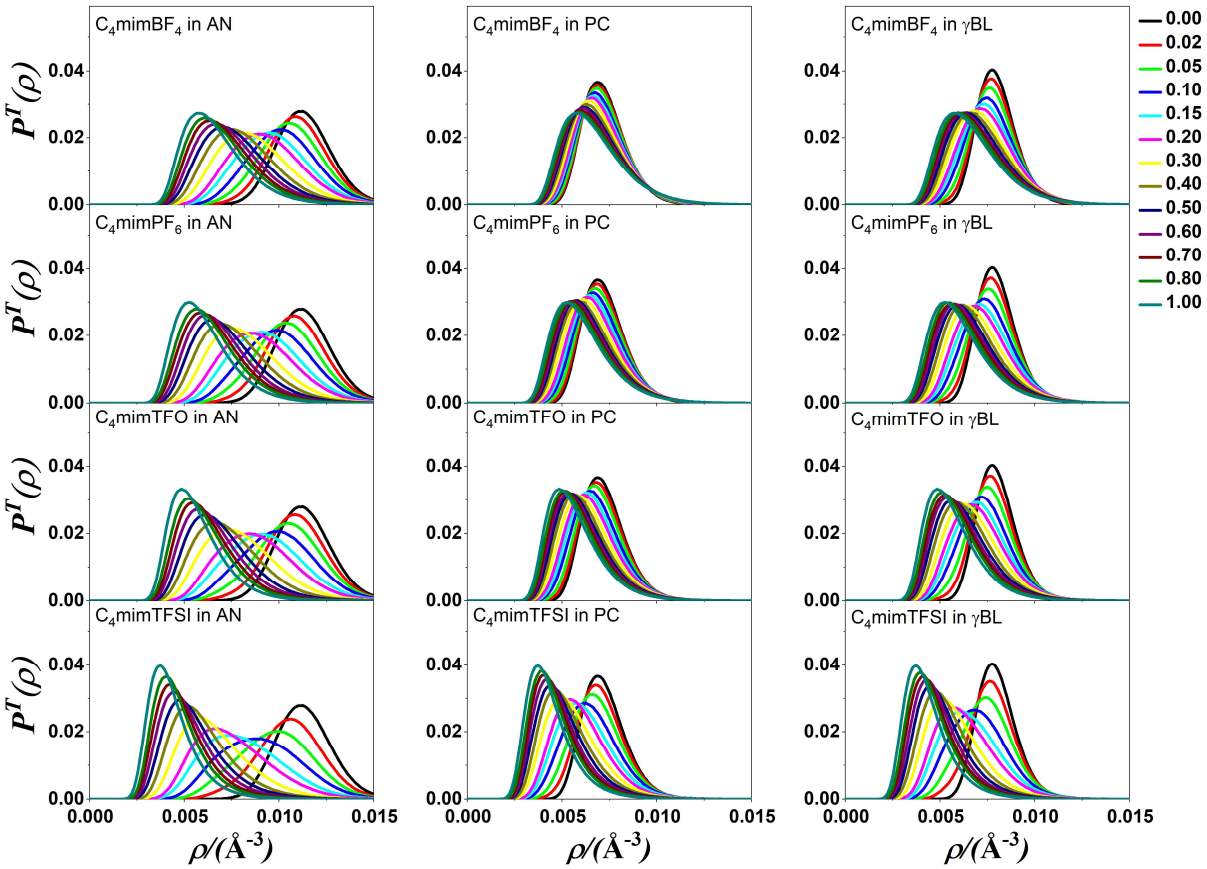

Figure A16. Reciprocal volume distributions of the Voronoi polyhedra of the components of the mixtures at various mole fraction of ionic liquid, when all components are taken into account in the analysis. The position of the cation is described with alkyl H^B hydrogen of C_4mim^+. The F ($BF_4^-$and PF_6^-) and the O (TFO^- and $TFSI^-$) atoms describe position of the anion while the N and O atoms describe the position of the AN, PC and γ-BL, respectively.

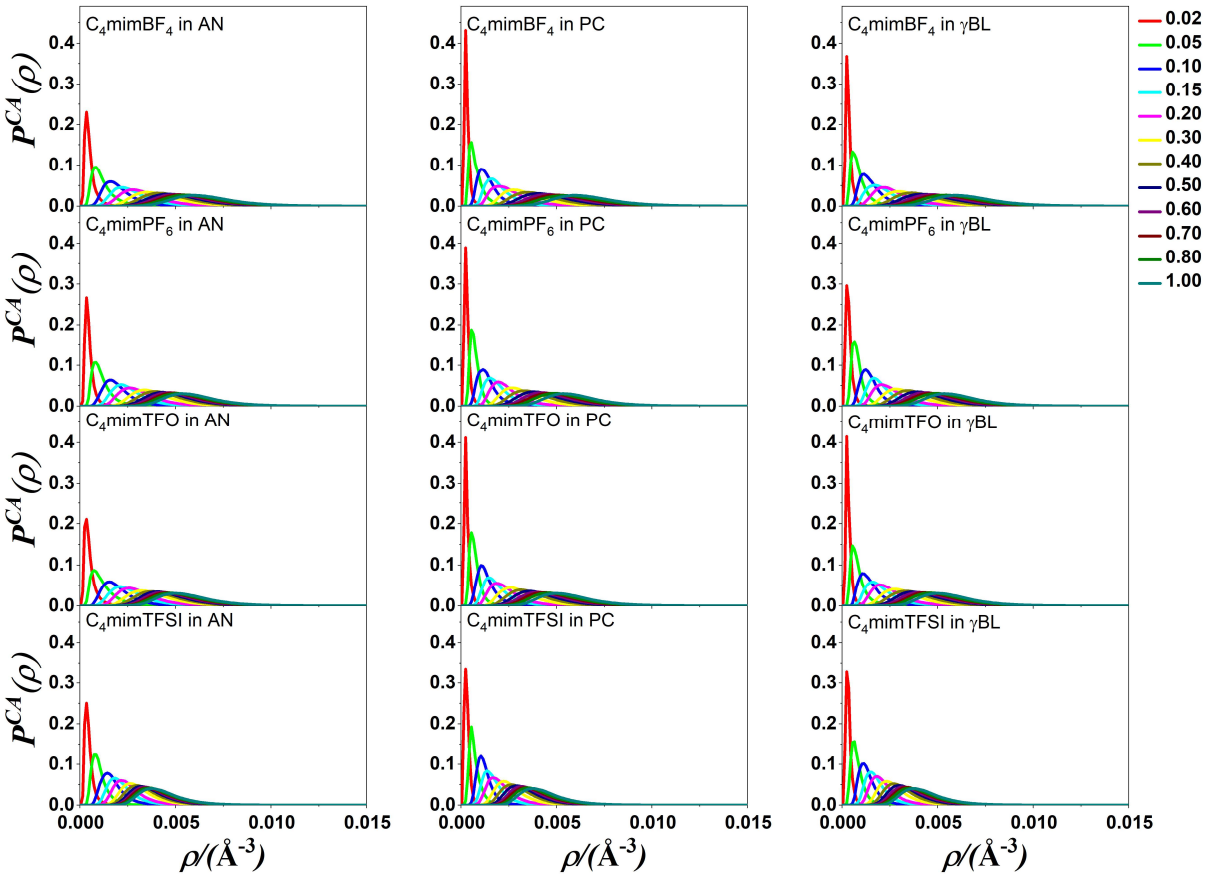

Figures A17. Reciprocal volume distributions of the Voronoi polyhedra of the components of the mixtures at various mole fraction of ionic liquid, when only the ions are taken into account, and the solvent molecules are disregarded. The position of the cation is described with ring H^2 hydrogen of C_4mim^+. The F (BF_4^- and PF_6^-) and the O (TFO^- and $TFSI^-$) atoms describe position of the anion while the N and O atoms describe the position of the AN, PC and γ-BL, respectively.

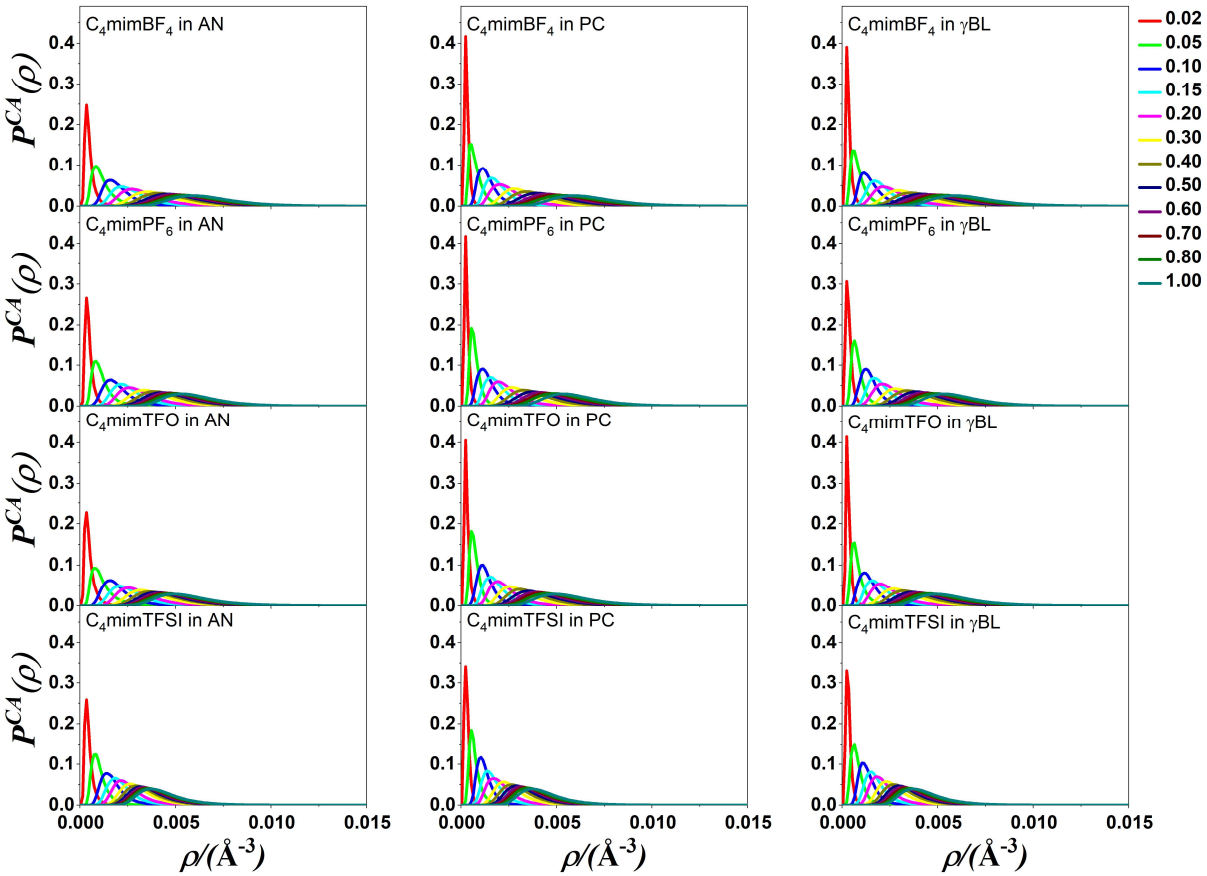

Figures A18. Reciprocal volume distributions of the Voronoi polyhedra of the components of the mixtures at various mole fraction of ionic liquid, when only the ions are taken into account, and the solvent molecules are disregarded. The position of the cation is described with ring H^4 hydrogen of C_4mim^+. The F (BF_4^- and PF_6^-) and the O (TFO^- and $TFSI^-$) atoms describe position of the anion while the N and O atoms describe the position of the AN, PC and γ-BL, respectively.

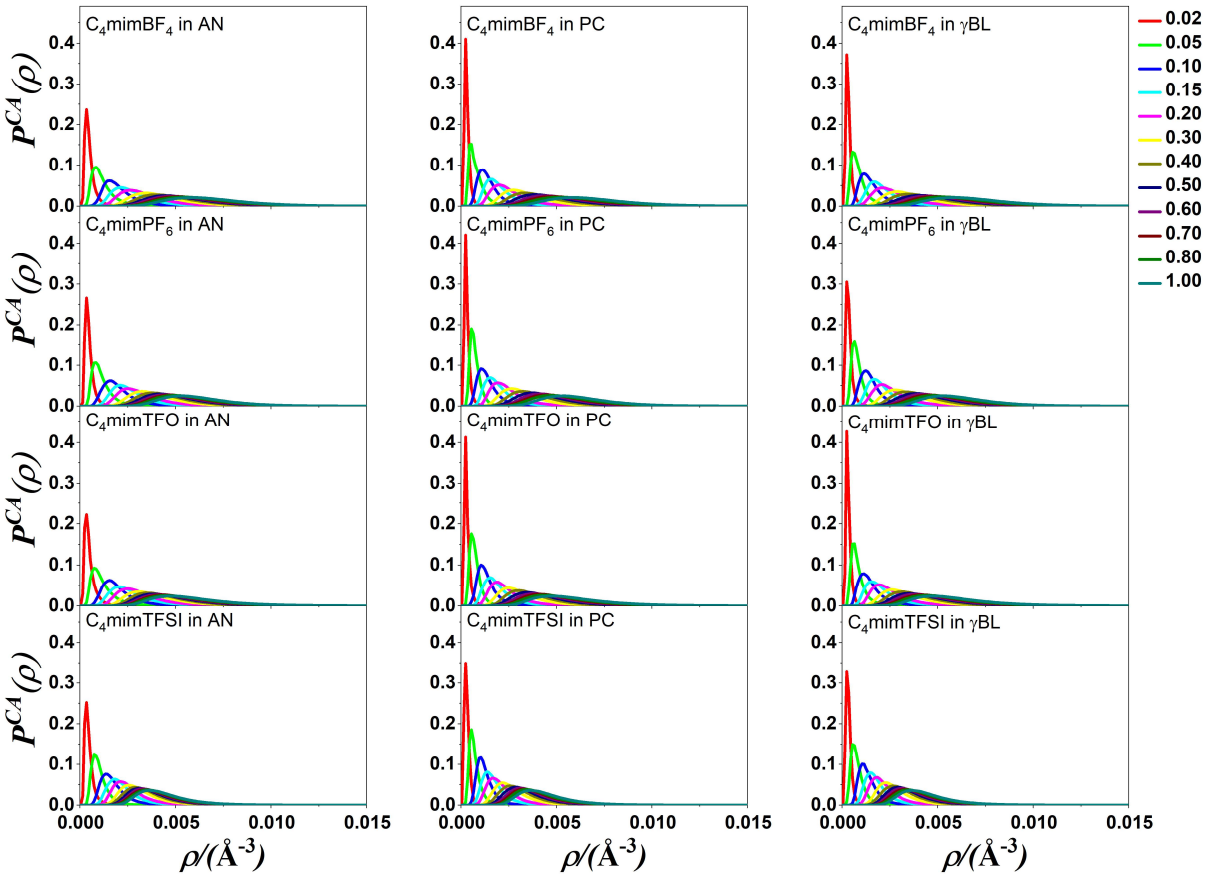

Figures A19. Reciprocal volume distributions of the Voronoi polyhedra of the components of the mixtures at various mole fraction of ionic liquid, when only the ions are taken into account, and the solvent molecules are disregarded. The position of the cation is described with ring H^5 hydrogen of C_4mim^+. The F (BF_4^- and PF_6^-) and the O (TFO^- and $TFSI^-$) atoms describe position of the anion while the N and O atoms describe the position of the AN, PC and γ-BL, respectively.

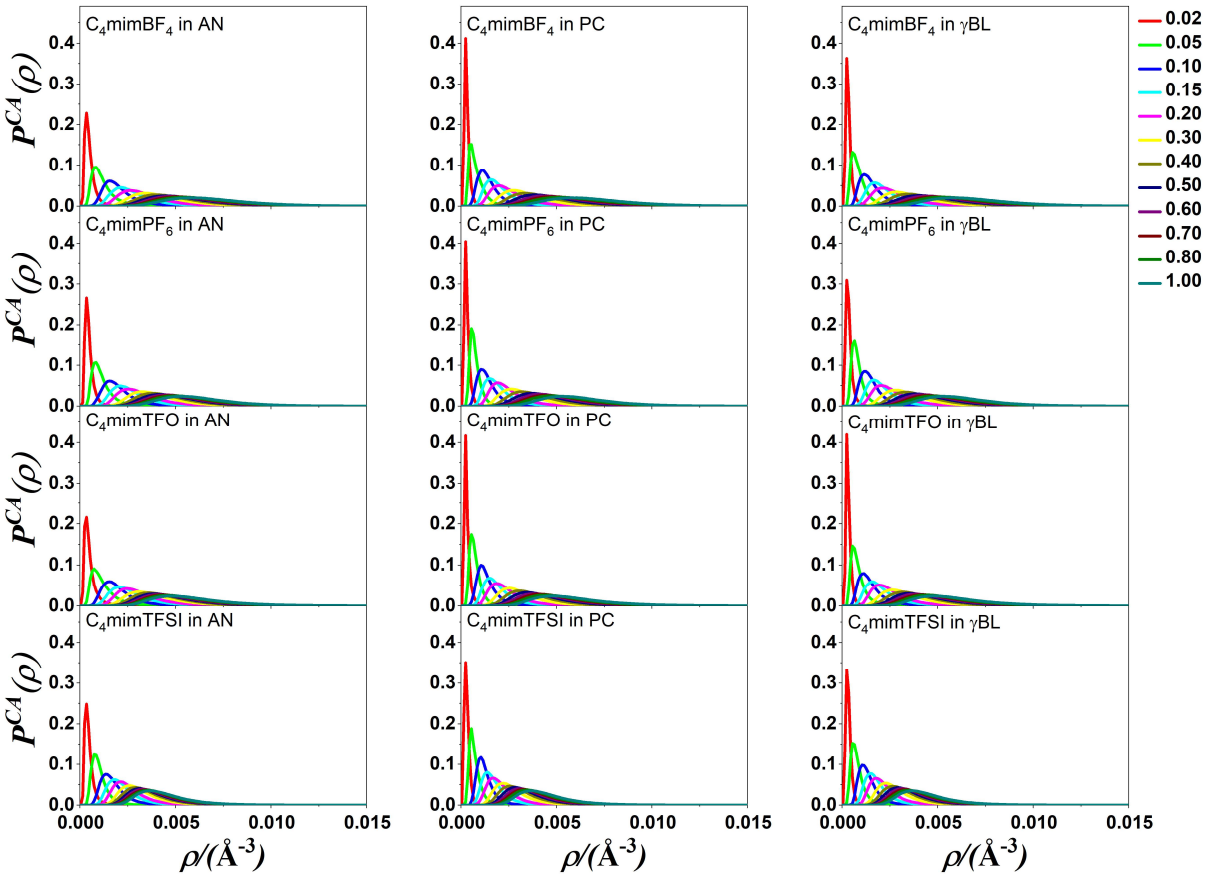

Figures A20. Reciprocal volume distributions of the Voronoi polyhedra of the components of the mixtures at various mole fraction of ionic liquid, when only the ions are taken into account, and the solvent molecules are disregarded. The position of the cation is described with alkyl H^M hydrogen of C_4mim^+. The F (BF_4^- and PF_6^-) and the O (TFO^- and $TFSI^-$) atoms describe position of the anion while the N and O atoms describe the position of the AN, PC and γ-BL, respectively.

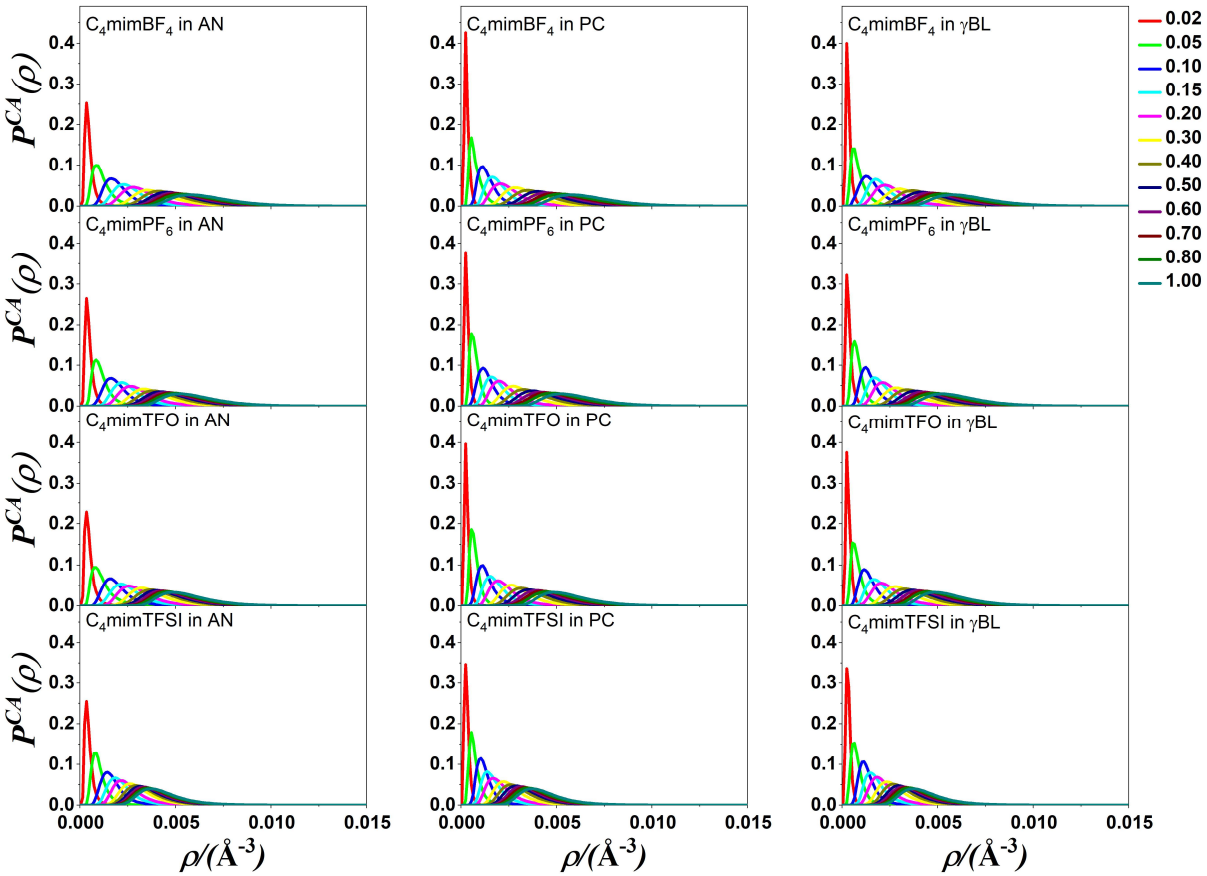

Figures A21. Reciprocal volume distributions of the Voronoi polyhedra of the components of the mixtures at various mole fraction of ionic liquid, when only the ions are taken into account, and the solvent molecules are disregarded. The position of the cation is described with alkyl H^B hydrogen of C_4mim^+. The F (BF_4^- and PF_6^-) and the O (TFO^- and $TFSI^-$) atoms describe position of the anion while the N and O atoms describe the position of the AN, PC and γ-BL, respectively.

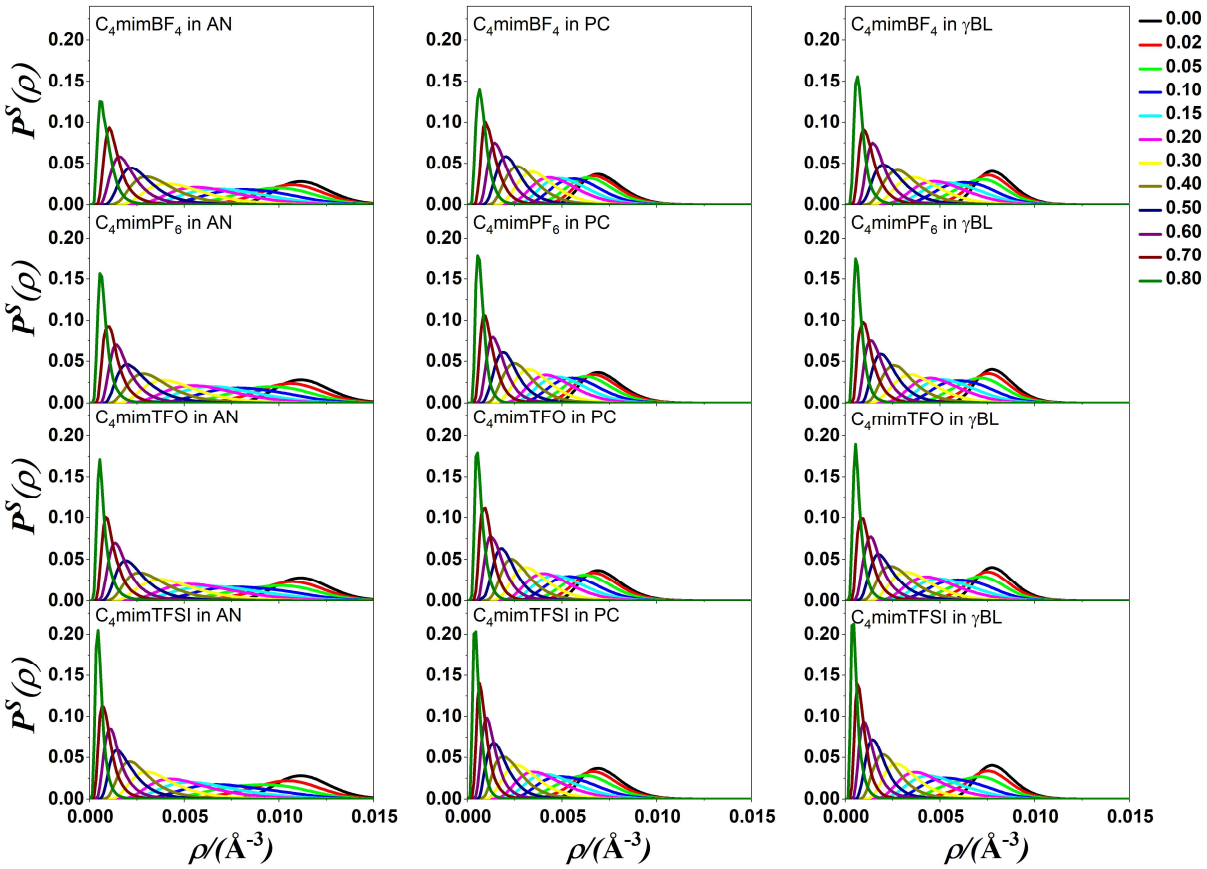

Figures A22. Reciprocal volume distributions of the Voronoi polyhedra of the components of the mixtures at various mole fraction of ionic liquid, when only the solvent molecules are taken into account. The N and O atoms describe the position of the AN, PC and γ-BL, respectively.

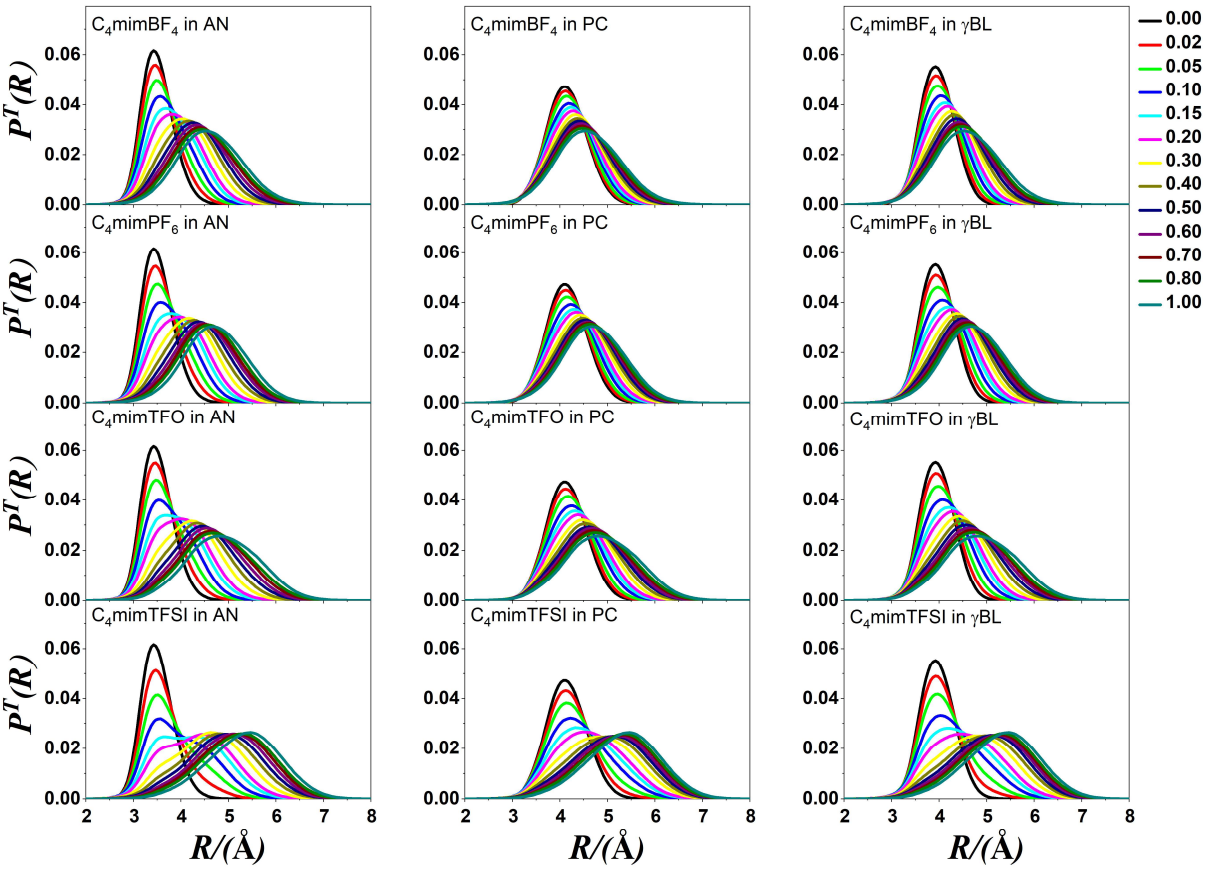

Figure A23. Vertex radius distributions of the Voronoi polyhedra of the components of the mixtures at various mole fraction of ionic liquid, when all components are taken into account in the analysis. The position of the cation is described with ring H^2 hydrogen of C_4mim^+. The F ($BF_4^-$and PF_6^-) and the O (TFO^- and $TFSI^-$) atoms describe position of the anion while the N and O atoms describe the position of the AN, PC and γ-BL, respectively.

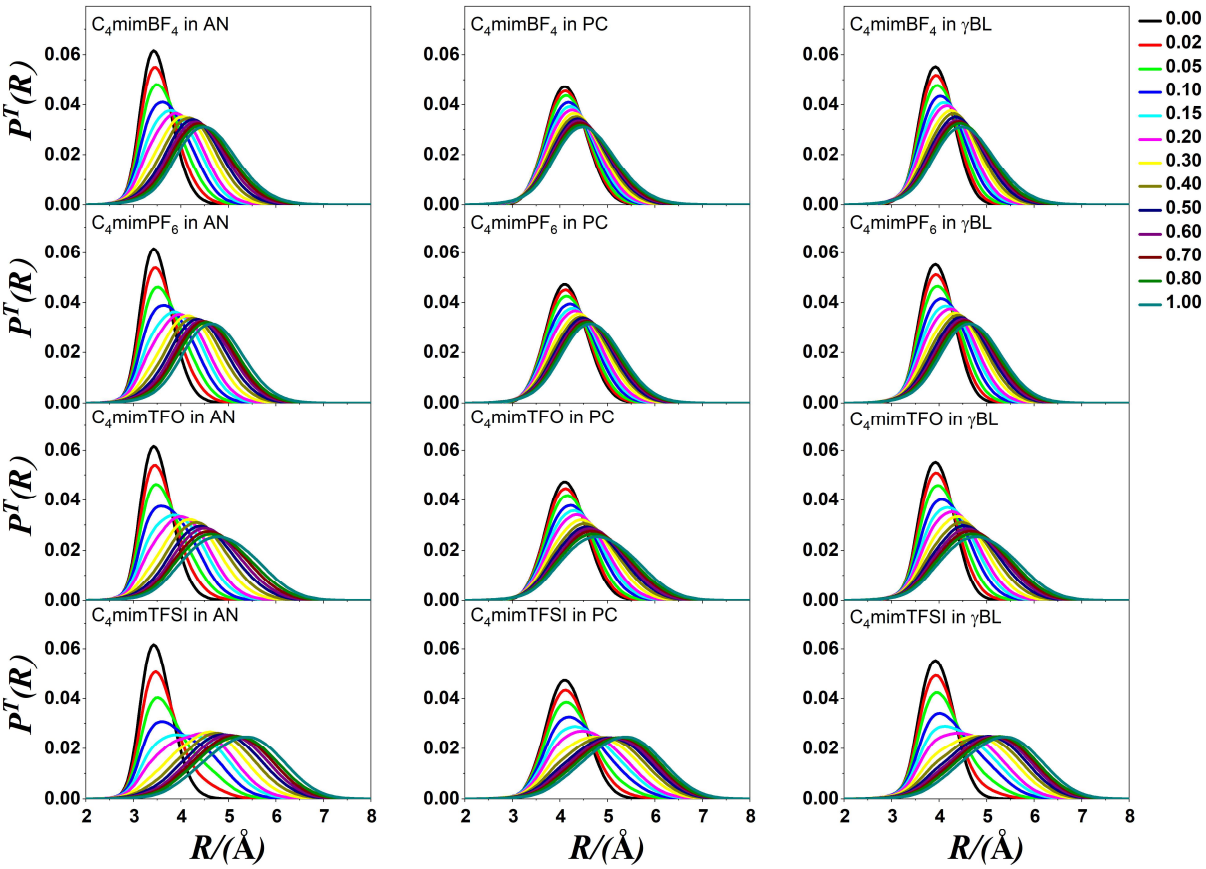

Figure A24. Vertex radius distributions of the Voronoi polyhedra of the components of the mixtures at various mole fraction of ionic liquid, when all components are taken into account in the analysis. The position of the cation is described with ring H^4 hydrogen of C_4mim^+. The F ($BF_4^-$and PF_6^-) and the O (TFO^- and $TFSI^-$) atoms describe position of the anion while the N and O atoms describe the position of the AN, PC and γ-BL, respectively.

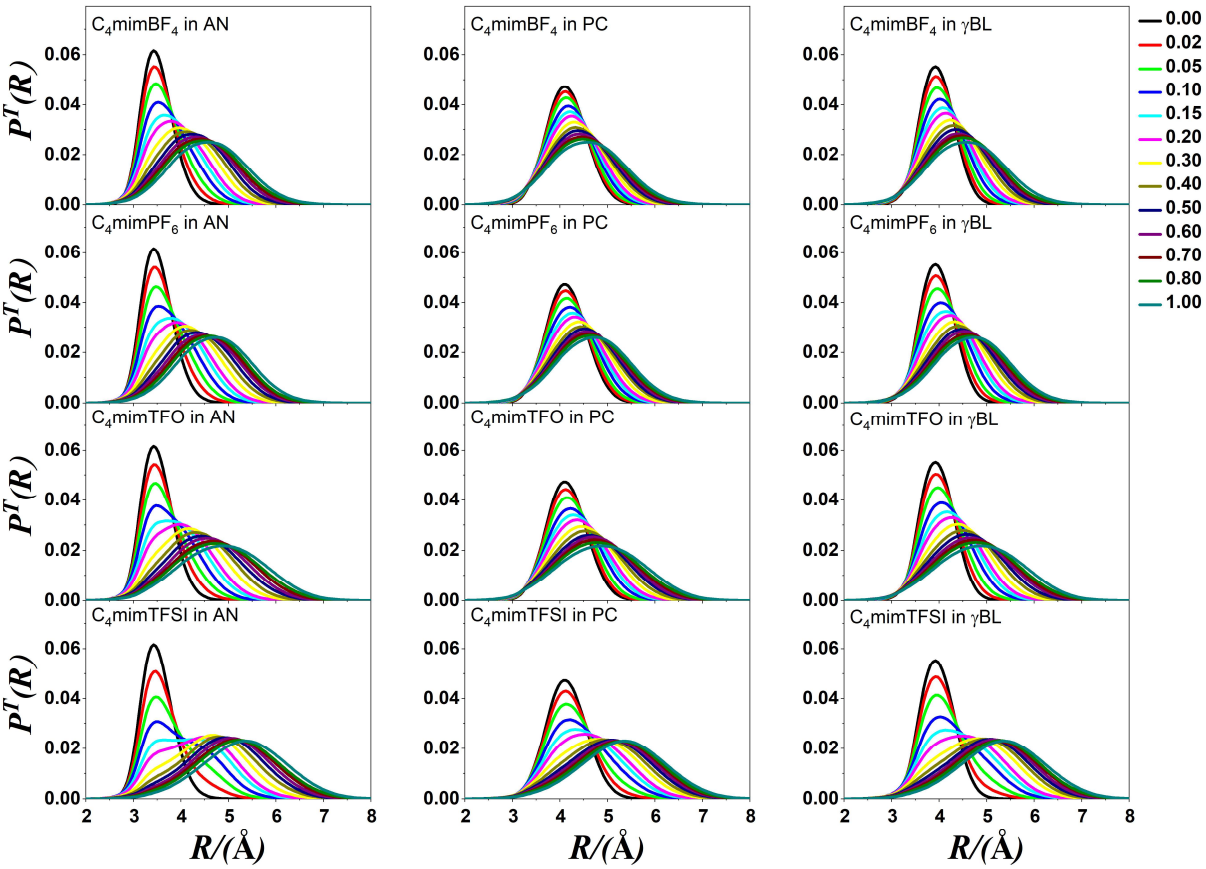

Figure A25. Vertex radius distributions of the Voronoi polyhedra of the components of the mixtures at various mole fraction of ionic liquid, when all components are taken into account in the analysis. The position of the cation is described with ring H^5 hydrogen of C_4mim^+. The F ($BF_4^-$and PF_6^-) and the O (TFO^- and $TFSI^-$) atoms describe position of the anion while the N and O atoms describe the position of the AN, PC and γ-BL, respectively.

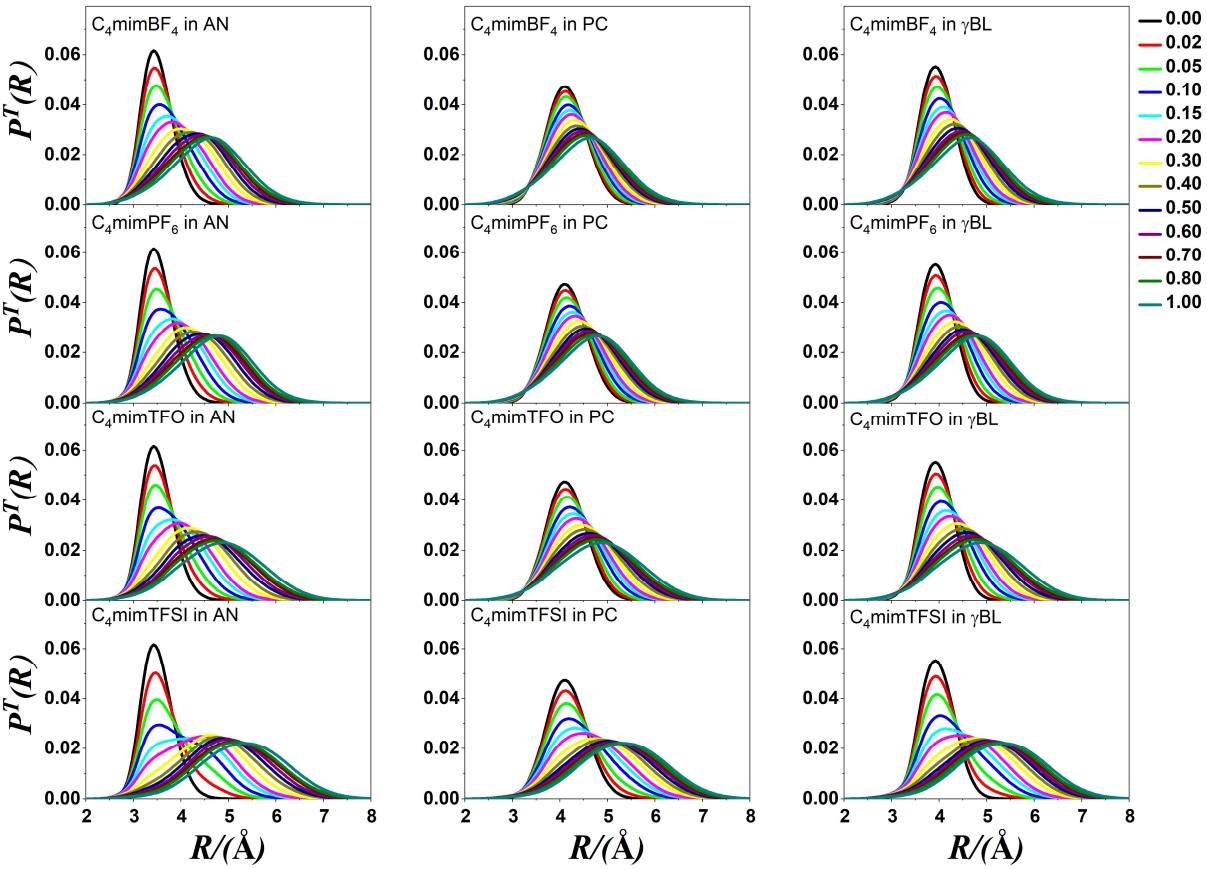

Figure A26. Vertex radius distributions of the Voronoi polyhedra of the components of the mixtures at various mole fraction of ionic liquid, when all components are taken into account in the analysis. The position of the cation is described with alkyl H^M hydrogen of C_4mim^+. The F ($BF_4^-$and PF_6^-) and the O (TFO^- and $TFSI^-$) atoms describe position of the anion while the N and O atoms describe the position of the AN, PC and γ-BL, respectively.

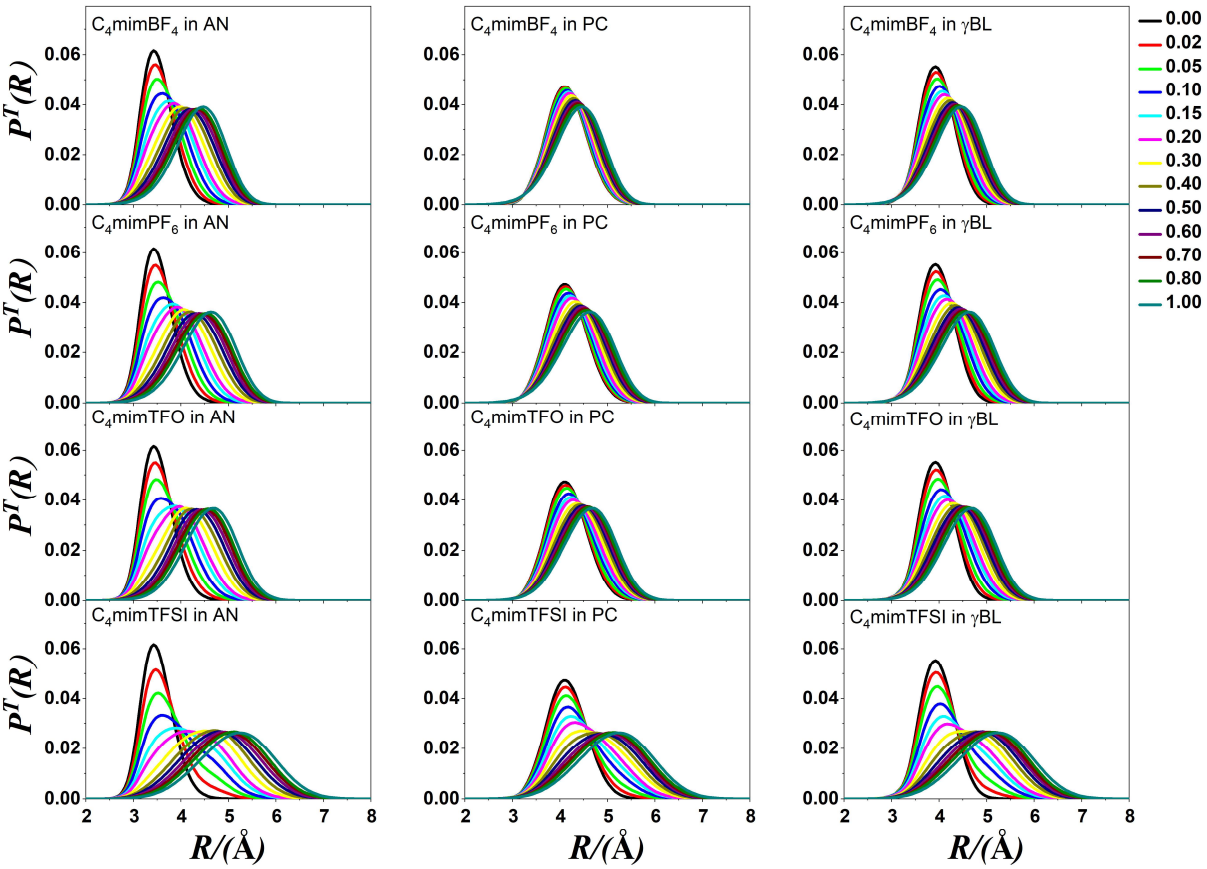

Figure A27. Vertex radius distributions of the Voronoi polyhedra of the components of the mixtures at various mole fraction of ionic liquid, when all components are taken into account in the analysis. The position of the cation is described with alkyl H^B hydrogen of C_4mim^+. The F ($BF_4^-$and PF_6^-) and the O (TFO^- and $TFSI^-$) atoms describe position of the anion while the N and O atoms describe the position of the AN, PC and γ-BL, respectively.

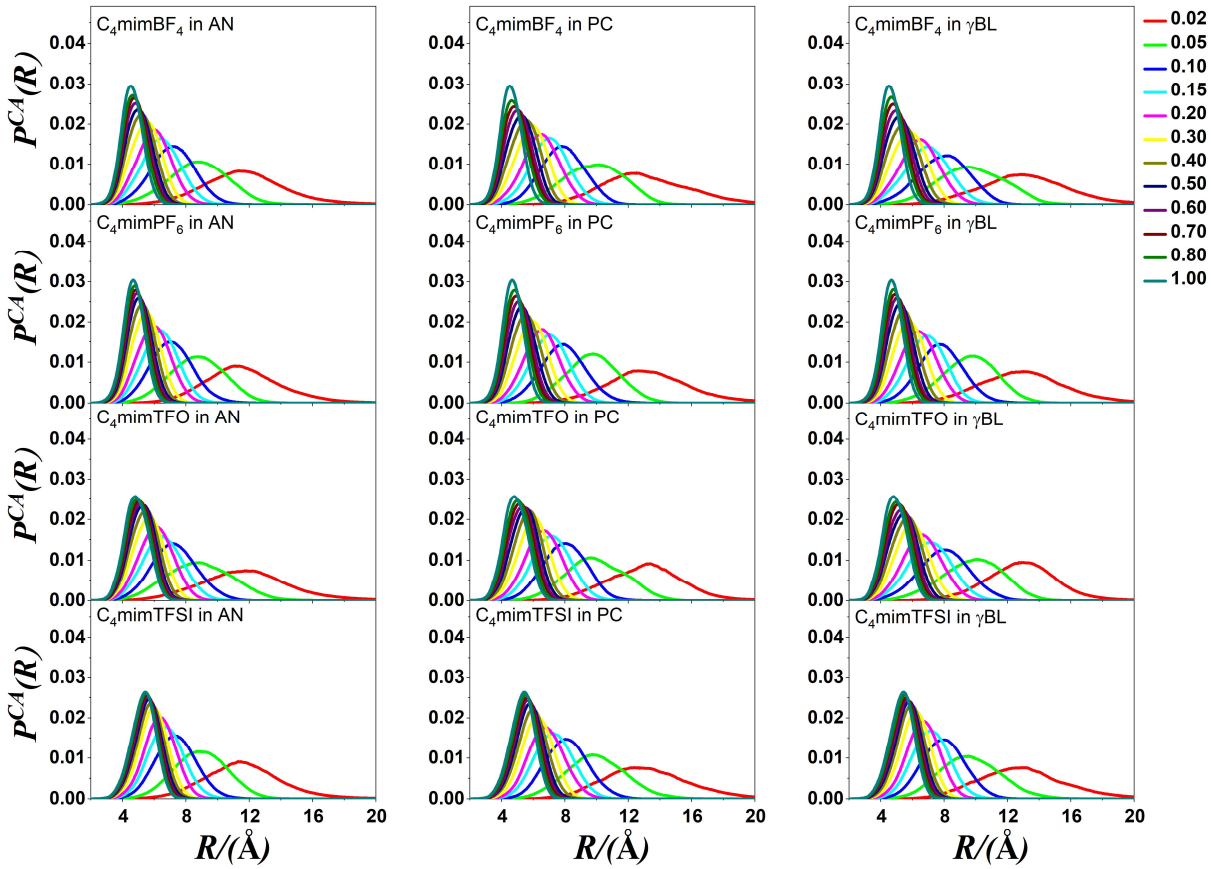

Figures A28. Vertex radius distributions of the Voronoi polyhedra of the components of the mixtures at various mole fraction of ionic liquid, when only the ions are taken into account, and the solvent molecules are disregarded. The position of the cation is described with ring H^2 hydrogen of C_4mim^+. The F (BF_4^- and PF_6^-) and the O (TFO^- and $TFSI^-$) atoms describe position of the anion while the N and O atoms describe the position of the AN, PC and γ-BL, respectively.

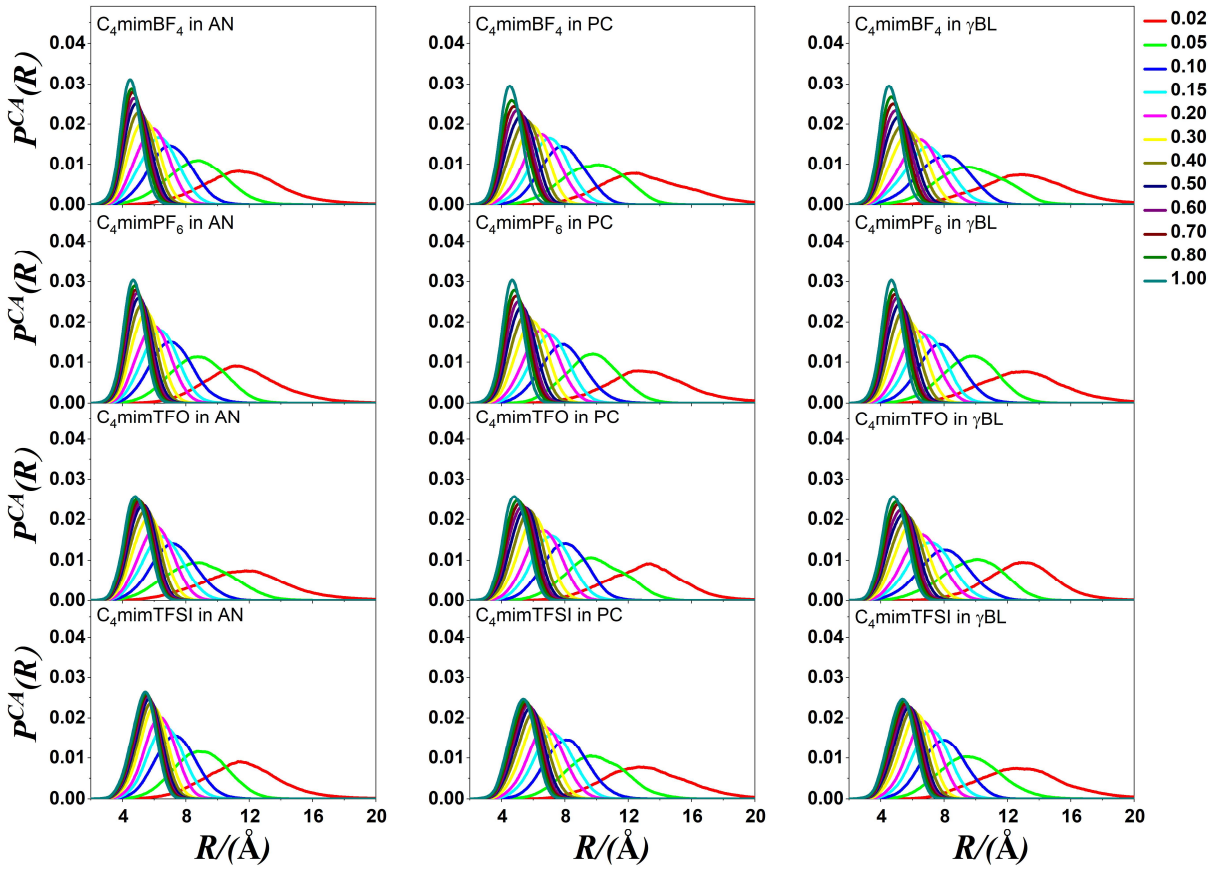

Figures A29. Vertex radius distributions of the Voronoi polyhedra of the components of the mixtures at various mole fraction of ionic liquid, when only the ions are taken into account, and the solvent molecules are disregarded. The position of the cation is described with ring H^4 hydrogen of C_4mim^+. The F (BF_4^- and PF_6^-) and the O (TFO^- and $TFSI^-$) atoms describe position of the anion while the N and O atoms describe the position of the AN, PC and γ-BL, respectively.

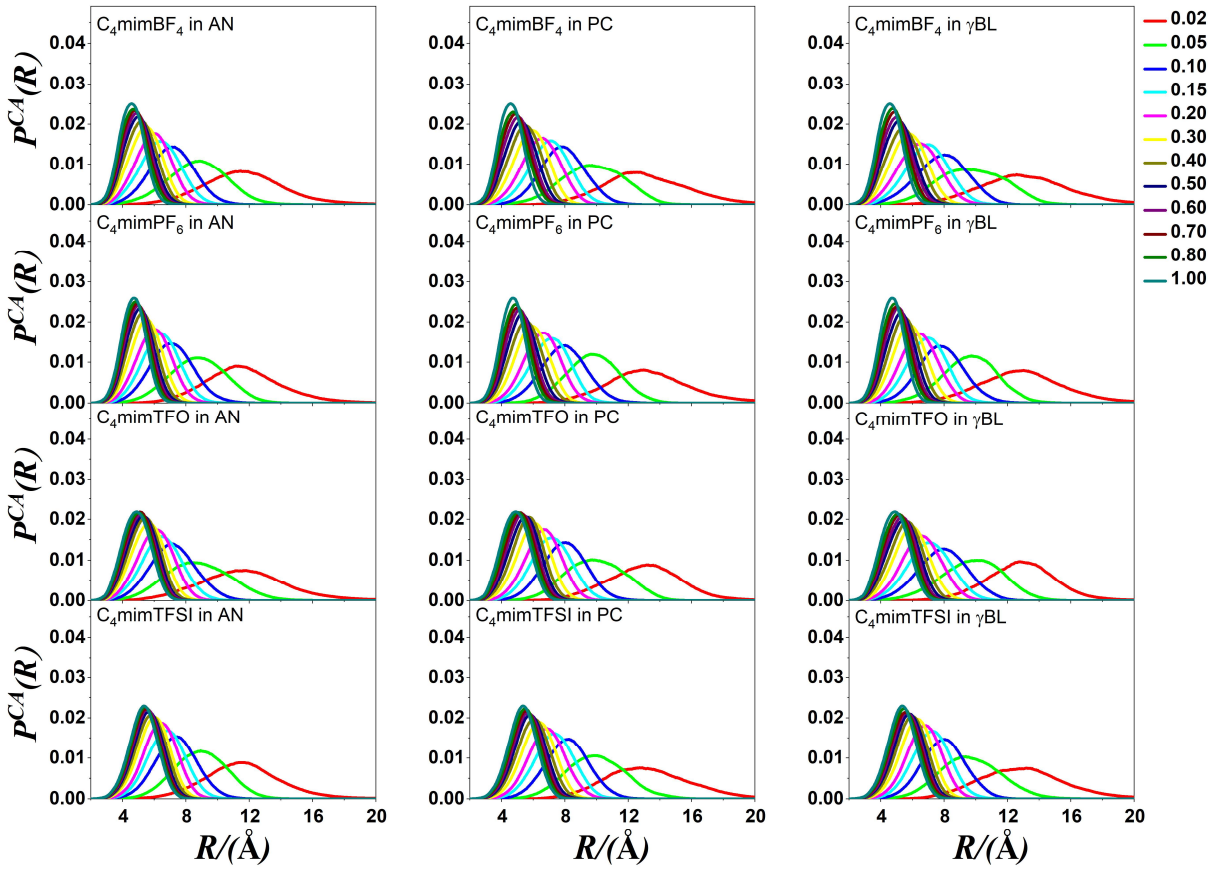

Figures A30. Vertex radius distributions of the Voronoi polyhedra of the components of the mixtures at various mole fraction of ionic liquid, when only the ions are taken into account, and the solvent molecules are disregarded. The position of the cation is described with ring H^5 hydrogen of C_4mim^+. The F (BF_4^- and PF_6^-) and the O (TFO^- and $TFSI^-$) atoms describe position of the anion while the N and O atoms describe the position of the AN, PC and γ-BL, respectively.

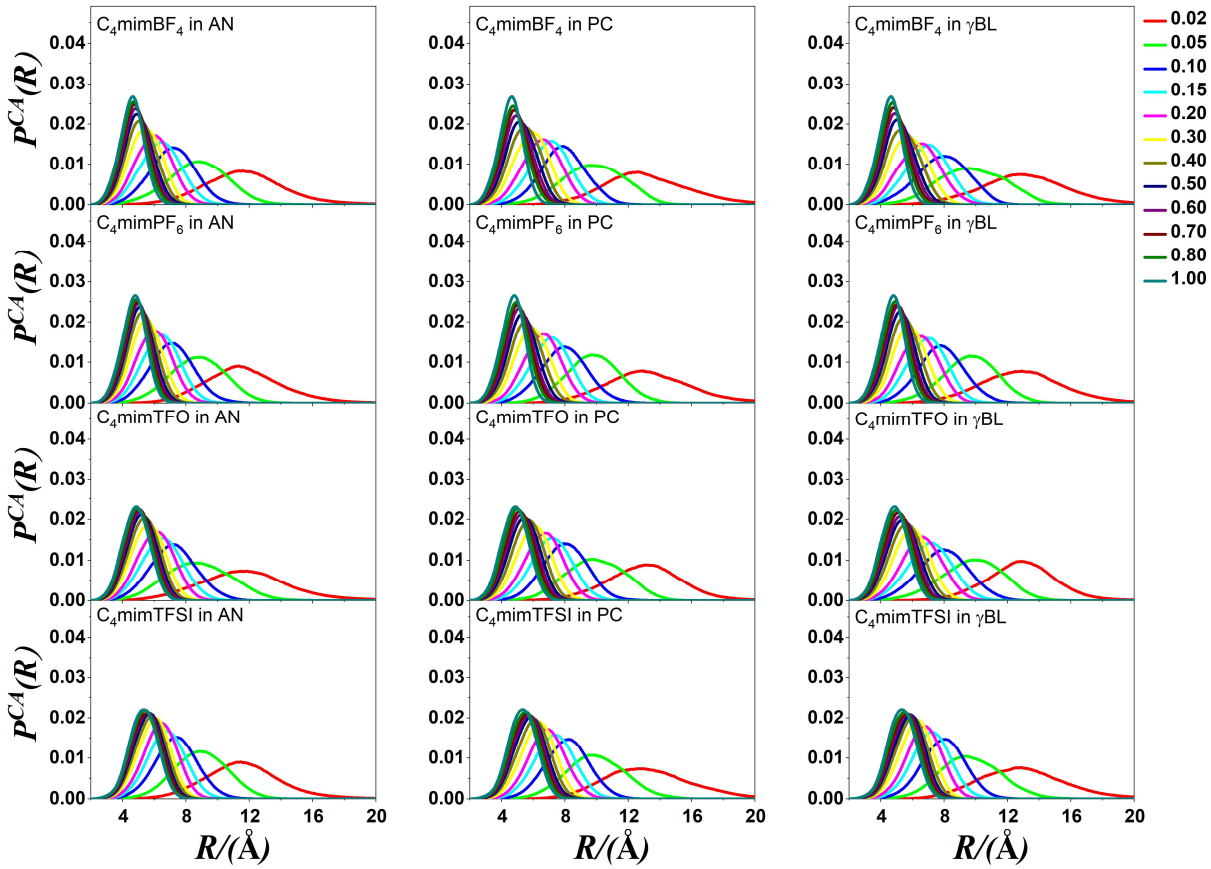

Figures A31. Vertex radius distributions of the Voronoi polyhedra of the components of the mixtures at various mole fraction of ionic liquid, when only the ions are taken into account, and the solvent molecules are disregarded. The position of the cation is described with alkyl H^M hydrogen of C_4mim^+. The F (BF_4^- and PF_6^-) and the O (TFO^- and $TFSI^-$) atoms describe position of the anion while the N and O atoms describe the position of the AN, PC and γ-BL, respectively.

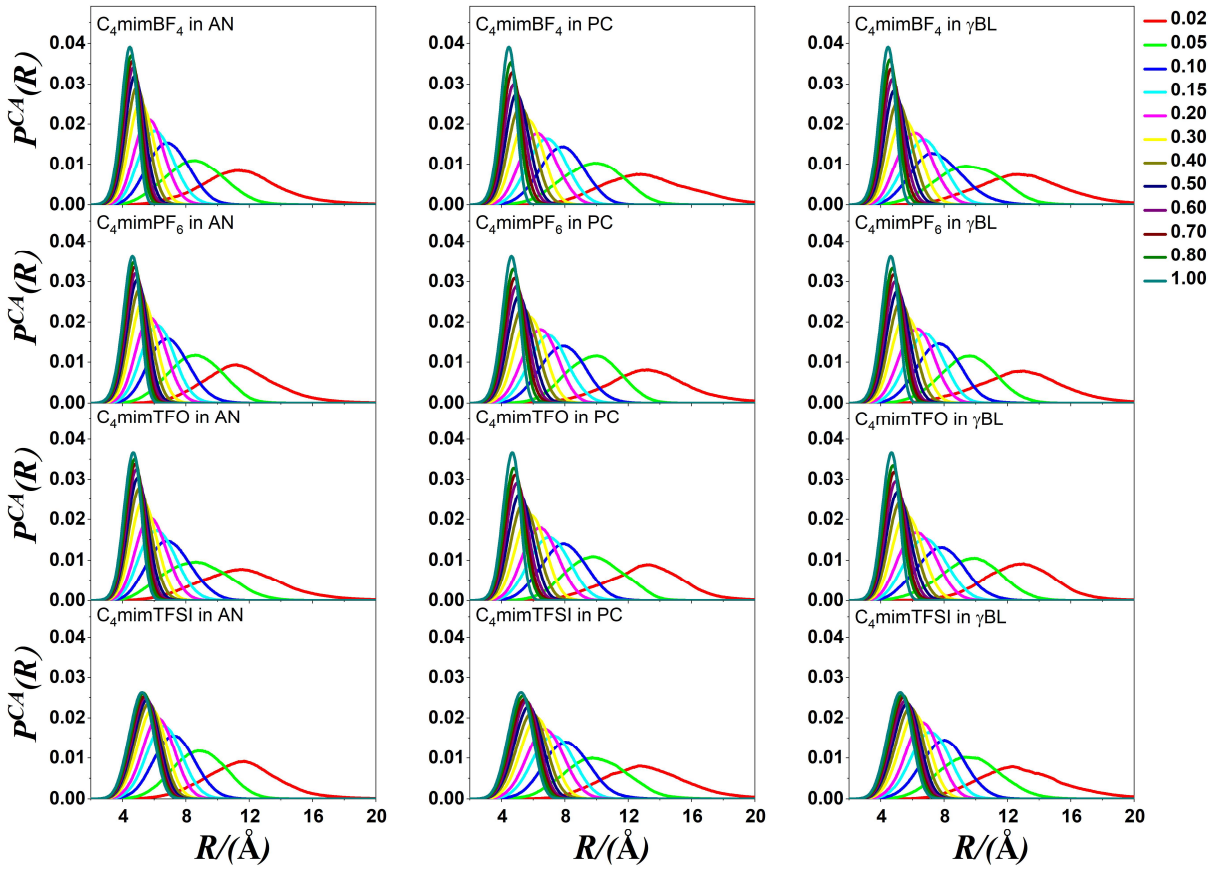

Figures A32. Vertex radius distributions of the Voronoi polyhedra of the components of the mixtures at various mole fraction of ionic liquid, when only the ions are taken into account, and the solvent molecules are disregarded. The position of the cation is described with alkyl H^B hydrogen of C_4mim^+. The F (BF_4^- and PF_6^-) and the O (TFO^- and $TFSI^-$) atoms describe position of the anion while the N and O atoms describe the position of the AN, PC and γ-BL, respectively.

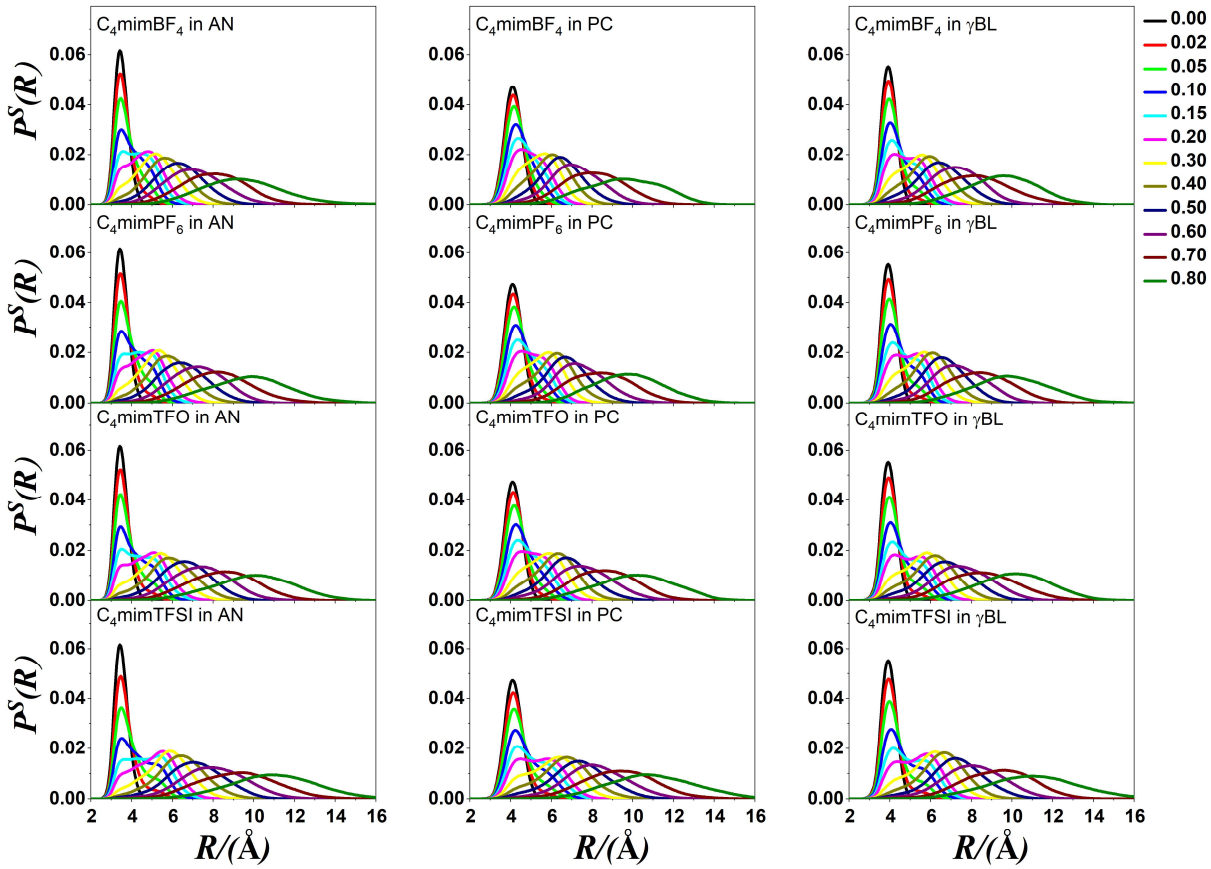

Figures A33. Vertex radius distributions of the Voronoi polyhedra of the components of the mixtures at various mole fraction of ionic liquid, when only the solvent molecules are taken into account. The N and O atoms describe the position of the AN, PC and γ-BL, respectively.